

AD-A076 204

MASSACHUSETTS INST OF TECH CAMBRIDGE GAS TURBINE AND--ETC F/G 21/5
BOUNDARY LAYER AND WAKE MODIFICATIONS TO COMPRESSOR DESIGN SYST--ETC(U)
MAR 79 A K SEHRA F33615-76-C-2118

UNCLASSIFIED

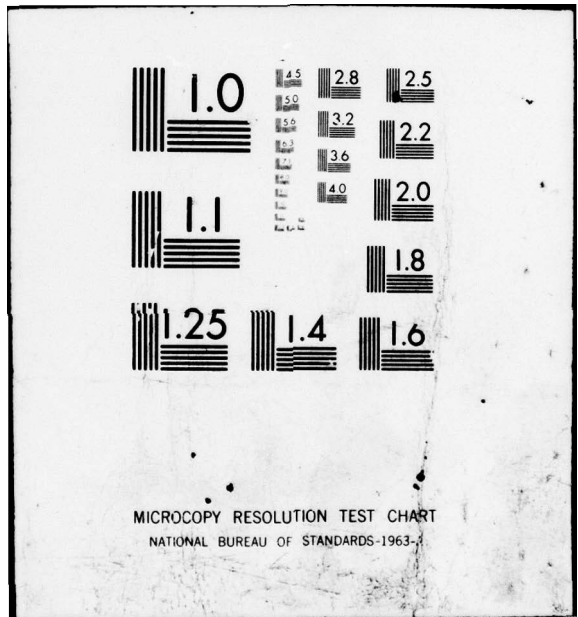
GT/PDL-144

AFAPL-TR-79-2010

NL

1 OF 3
AD
A076204





AFAPL-TR-79-2010

LEVEL II

2

AD A 076204

BOUNDARY LAYER AND WAKE MODIFICATIONS
TO COMPRESSOR DESIGN SYSTEMS:

THE EFFECT OF BLADE-TO-BLADE FLOW VARIATIONS
ON THE MEAN FLOW FIELD OF A TRANSONIC ROTOR

ARUN K. SEHRA

DDC
NOV 7 1979
E

GAS TURBINE AND PLASMA DYNAMICS LABORATORY
MASSACHUSETTS INSTITUTE OF TECHNOLOGY
CAMBRIDGE, MASSACHUSETTS 02139

MARCH 1979

DDC FILE COPY

FINAL REPORT

01 SEPTEMBER 1976 - 31 AUGUST 1978

Approved for public release; distribution unlimited

AIR FORCE AERO PROPULSION LABORATORY
AIR FORCE WRIGHT AERONAUTICAL LABORATORIES
AIR FORCE SYSTEMS COMMAND
WRIGHT-PATTERSON AIR FORCE BASE, OHIO 45433

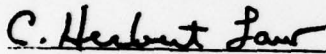
79 11-05 005

NOTICE

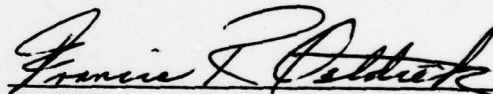
When Government drawings, specifications, or other data are used for any purpose other than in connection with a definitely related Government procurement operation, the United States Government thereby incurs no responsibility nor any obligation whatsoever; and the fact that the government may have formulated, furnished, or in any way supplied the said drawings, specifications, or other data, is not to be regarded by implication or otherwise as in any manner licensing the holder or any other person or corporation, or conveying any rights or permission to manufacture, use, or sell any patented invention that may in any way be related thereto.

This report has been reviewed by the Information Office (OI) and is releasable to the National Technical Information Service (NTIS). At NTIS, it will be available to the general public, including foreign nations.

This technical report has been reviewed and is approved for publication.



C. HERBERT LAW
Project Engineer



FRANCIS R. OSTDIEK
Acting Chief, Technology Branch

FOR THE COMMANDER



H. I. BUSH
Deputy Director
Turbine Engine Division

If your address has changed, if you wish to be removed from our mailing list, or if the addressee is no longer employed by your organization please notify AFAPL/TBX , W-PAFB, OH 45433 to help us maintain a current mailing list.

Copies of this report should not be returned unless return is required by security considerations, contractual obligations, or notice on a specific document.

UNCLASSIFIED

SECURITY CLASSIFICATION OF THIS PAGE (When Data Entered)

19 REPORT DOCUMENTATION PAGE		READ INSTRUCTIONS BEFORE COMPLETING FORM
1. REPORT NUMBER AFAPL-TR-79-2010	2. GOVT ACCESSION NO.	3. RECIPIENT'S CATALOG NUMBER 9
4. TITLE (and Subtitle) BOUNDARY LAYER AND WAKE MODIFICATIONS TO COMPRESSOR DESIGN SYSTEMS: The Effect of Blade- To-Blade Flow Variations On The Mean Flow Field of a Transonic Rotor,	5. TYPE OF REPORT & PERIOD COVERED FINAL REPORT 1 Sept 1976 - 31 Aug 1978	
	6. PERFORMING ORG. REPORT NUMBER GT&PDL Report No. 144	
7. AUTHOR(s) ARUN K./SEHRA	8. CONTRACT OR GRANT NUMBER(s) F33615-76-C-2118	
9. PERFORMING ORGANIZATION NAME AND ADDRESS MASSACHUSETTS INSTITUTE OF TECHNOLOGY GAS TURBINE & PLASMA DYNAMICS LABORATORY CAMBRIDGE, MA 02139	10. PROGRAM ELEMENT, PROJECT, TASK AREA & WORK UNIT NUMBERS 2307-4S1-32	
	11. CONTROLLING OFFICE NAME AND ADDRESS AIR FORCE AERO PROPULSION LABORATORY (TBX) WRIGHT-PATTERSON AIR FORCE BASE, OH 45433	
14. MONITORING AGENCY NAME & ADDRESS (if different from Controlling Office) 218	12. REPORT DATE March 1979	
	13. NUMBER OF PAGES 222	
15. SECURITY CLASS. (of this report) UNCLASSIFIED		15a. DECLASSIFICATION/DOWNGRADING SCHEDULE
16. DISTRIBUTION STATEMENT (of this Report) Approved for public release; distribution unlimited. 14 GT/PDL-144		
17. DISTRIBUTION STATEMENT (of the abstract entered in Block 20, if different from Report)		
18. SUPPLEMENTARY NOTES		
19. KEY WORDS (Continue on reverse side if necessary and identify by block number) TRANSONIC COMPRESSOR BOUNDARY LAYER FLOW VARIATIONS WAKES		
20. ABSTRACT (Continue on reverse side if necessary and identify by block number) The effect of blade-to-blade flow variations on the mean flow field of a highly loaded transonic axial flow compressor was investigated. The theoretical approach centered around modeling of three important phenomena associated with blade-to-blade flow fluctuations, which control the mean momentum and energy transfer processes. Apparent stresses were introduced into the mean flow momentum equations by pitchwise averaging. Loss concept of mean relative total pressure, due to conversion of mean flow kinetic energy to the energy of fluctuations, was introduced. Based on this concept, mean rothalpy and the production of apparent		

DD FORM 1 JAN 73 1473

UNCLASSIFIED

SECURITY CLASSIFICATION OF THIS PAGE (When Data Entered)

410 554

LB

UNCLASSIFIED

SECURITY CLASSIFICATION OF THIS PAGE(When Data Entered)

20. (cont'd)

entropy were defined. An expression for mean rothalpy variation along the streamline was derived by pitchwise averaging of the energy equation. Mean flow equations suitable for the streamline curvature computational scheme were developed which include these three effects. Apparent stresses, mean rothalpy and apparent entropy variations were calculated from measured velocity fluctuations. The revised streamline curvature procedure was then used to predict the axisymmetric (peripheral mean) flow. The agreement of rotor outlet tangential velocity is excellent reproducing an unusual peak which is not explainable by usual techniques. The results showed that 3-D inviscid effects do not significantly modify the mean flow, and that the direct effect of apparent stresses on the mean flow is also small. Major deviations of the actual flow field from the inviscid flow field are due to the variations of mean rothalpy and production of apparent entropy due to flow fluctuations, both effects which are introduced here for the first time.

UNCLASSIFIED

SECURITY CLASSIFICATION OF THIS PAGE(When Data Entered)

FOREWORD

This Final Scientific Report was prepared by the Gas Turbine and Plasma Dynamics Laboratory of the Department of Aeronautics and Astronautics, Massachusetts Institute of Technology, under contract F33615-76-C-2118 to the United States Air Force Aero Propulsion Laboratory of the Aeronautical Systems Division, Air Force Systems Command. C. Herbert Law was the AFAPL Project Engineer. Professor Jack L. Kerrebrock directed the work with the assistance of Arun K. Sehra.

This Final Report describes the entire study accomplished during the period 01 September 1976 - 31 August 1978.

Accession For	
NTIS GMA&I	<input checked="" type="checkbox"/>
DIC TAB	<input type="checkbox"/>
Unannounced	<input type="checkbox"/>
Justification	
By _____	
Distribution/	
Availability Codes	
Dist	Avail and/or special
A	

TABLE OF CONTENTS

Section	Page
I INTRODUCTION	1
1.1 General Statement of the Problem	1
1.2 Objectives of the Present Investigation	3
1.3 Phenomena Treated	4
1.4 Method of Investigation	4
II LITERATURE SURVEY	11
2.1 Methods of Predicting the Flow Field	12
2.1.1 Analytical Methods	12
2.1.2 Computational Methods	16
2.2 Blade Boundary Layer and Wakes	19
III MEAN FLOW EQUATIONS OF MOTION, ROTHALPY VARIATION, AND ENTROPY PRODUCTION	25
3.1 Apparent Stresses	25
3.2 Mean Flow Equations of Motion	26
3.2.1 Non-Bladed Region	26
3.2.2 Bladed Region	29
3.3 Mean Flow Equation for Rothalpy Variation Along the Streamline	32
3.4 Mean Flow Equation for Entropy Production	40
3.4.1 Entropy Production Associated with Flow Fluctuations	43
3.4.2 Entropy Production in the Rotor	45
3.4.3 Entropy Production due to Blade Passage Shock	47
IV MEAN FLOW EQUATIONS FOR STREAMLINE CURVATURE COMPUTATIONAL METHOD	49
4.1 Basic Equation of Motion in l-Direction	50
4.2 Equation of Motion for Computer Program	54
4.2.1 Blade Forces	54
4.2.2 Equation for Meridional Velocity Gradient	58
4.2.3 Analysis Type Momentum Equation for Computer Program	60

TABLE OF CONTENTS (cont'd)

Section		Page
V	CRITICAL ANALYSIS OF THE EXPERIMENTAL DATA	65
	5.1 Mean Velocities	67
	5.2 Apparent Stresses	69
	5.2.1 Apparent Stresses, $z/c = 0.1$	69
	5.2.2 Apparent Stresses, $z/c = 1.0$	71
	5.3 Static Pressure	71
	5.4 Entropy Distribution	72
VI	COMPUTER PROGRAM	73
	6.1 General Description of Computing Routine for the Analysis Program	73
	6.2 Modified Streamline Curvature Program	79
	6.3 Computation of Mean Flow Quantities and the Apparent Stresses from the Experimental Data	82
VII	RESULTS OF NUMERICAL CALCULATIONS AND DISCUSSION	85
	7.1 Computational Mesh and Basic Input Data	86
	7.2 Mean Flow Field	88
	7.2.1 Computed Flow with Cascade Losses	88
	7.2.2 Computed Flow with Cascade Losses and Apparent Stresses	89
	7.2.3 Computed Flow with Cascade Losses and Apparent Entropy Production	90
	7.2.4 Computed Flow with Cascade Losses and Rothalpy Variation Along the Streamline	91
	7.2.5 Computed Flow with Cascade Losses, Rothalpy Variation, and Apparent Entropy Production Along the Streamline	91
	7.2.6 Computed Flow with Cascade Losses, Rothalpy Variation, Apparent Entropy Production, and Apparent Stresses	92
	7.2.7 Computed Flow with Experimental Losses	93
VIII	CONCLUSIONS	95
	REFERENCES	99

TABLE OF CONTENTS (cont'd)

Appendix		Page
A	DERIVATION OF RADIAL, TANGENTIAL AND AXIAL EQUATIONS OF MOTION	103
B	PITCHWISE AVERAGING	113
C	MEAN FLOW ENERGY EQUATION	119
D	DERIVATION OF MEAN FLOW EQUATIONS FOR MOTION FOR STREAMLINE CURVATURE TECHNIQUE	125

LIST OF ILLUSTRATIONS

Figure		Page
1	Rotor section cut a $z = \text{constant}$ plane.	139
2	Passage shock-wave configuration.	140
3	Meridional plane picture of a passage.	141
4	Blade forces.	142
5	Experimental distribution of mean pitch-wise velocity, 0.1 chord downstream of the rotor.	143
6	Experimental \bar{V}_z and \bar{V}_r , 0.1 chord downstream of the rotor.	144
7	Experimental distribution of mean pitch-wise velocity, 1.0 chord downstream of the rotor.	145
8	Experimental \bar{V}_z and \bar{V}_r , 1.0 chord downstream of the rotor.	146
9	Apparent shear stress $\overline{V_z'V_r'}$, 0.1 chord downstream of the rotor.	147
10	Apparent shear stress $\overline{V_z'V_\theta'}$, 0.1 chord downstream of the rotor.	148
11	Apparent shear stress $\overline{V_r'V_\theta'}$, 0.1 chord downstream of the rotor.	149
12	$\overline{V_r'^2}$, 0.1 chord downstream of the rotor.	150
12a	$\frac{\partial \overline{V_r'^2}}{\partial r} / \frac{V_\theta^2}{r}$, 0.1 chord downstream of the rotor.	151
13	Apparent normal stress $\overline{V_\theta'^2}$, 0.1 chord downstream of the rotor.	152
14	Apparent normal stress $\overline{V_z'^2}$, 0.1 chord downstream of the rotor.	153
15	Apparent shear stress $\overline{V_r'V_z'}$, 1.0 chord downstream of the rotor.	154

LIST OF ILLUSTRATIONS (cont'd)

Figure		Page
16	Apparent shear stress $\overline{V'_z V'_\theta}$, 1.0 chord downstream of the rotor.	155
17	Apparent shear stress $\overline{V'_r V'_\theta}$, 1.0 chord downstream of the rotor.	156
18	Apparent normal stress $\overline{V'_r{}^2}$, 1.0 chord downstream of the rotor.	157
19	Apparent normal stress $\overline{V'_\theta{}^2}$, 1.0 chord downstream of the rotor.	158
20	Apparent normal stress $\overline{V'_z{}^2}$, 1.0 chord downstream of the rotor.	159
21	$\overline{P}_{s_2} / \overline{P}_{t_1}$, 0.1 chord downstream of the rotor.	160
22	Mean experimental entropy, 0.1 chord downstream of the rotor.	161
23	Mean experimental entropy, 1.0 chord downstream of the rotor.	162
24	Overall logic of the original streamline-curvature program.	163
25	Interaction of subroutines CORDTA, SPLINE, ROEN1, ROEN2, and WATRAN with the main program.	164
26	Adjusted experimental entropy, 0.1 chord downstream of the rotor.	165
27	Layout of the computational mesh.	166
28a	Basic input data for computation.	167
28b	Apparent stress data.	168
29	Mean pitchwise velocity, 0.1 chord downstream of the rotor.	169
30	Mean axial and radial velocities, 0.1 chord downstream of the rotor.	170

LIST OF ILLUSTRATIONS (cont'd)

Figure		Page
31	Mean pitchwise velocity, 1.0 chord downstream of the rotor.	171
32	Mean axial and radial velocities, 1.0 chord downstream of the rotor.	172
33	Mean pitchwise velocity, 0.1 chord downstream of the rotor.	173
34	Mean axial and radial velocities, 0.1 chord downstream of the rotor.	174
35	Mean pitchwise velocity, 1.0 chord downstream of the rotor.	175
36	Mean axial and radial velocities, 1.0 chord downstream of the rotor.	176
37	Apparent stresses (\bar{V}_θ^2/r), 0.1 chord downstream of the rotor.	177
38	Computed $\frac{\partial \bar{I}}{\partial m}$ and $T(\frac{\partial S}{\partial m})_{app}$, station 4.	178
39	Calculated distribution of $\partial I/\partial m$ and $T \partial S/\partial m$, station 5.	179
40	Apparent entropy rise across the rotor.	180
41	Mean pitchwise velocity, 0.1 chord downstream of the rotor.	181
42	Mean axial and radial velocities, 0.1 chord downstream of the rotor.	182
43	Mean pitchwise velocity, 1.0 chord downstream of the rotor.	183
44	Mean axial and radial velocities, 1.0 chord downstream of the rotor.	184
45	Calculated mean rothalpy change across the rotor.	185
46	Mean pitchwise velocity, 0.1 chord downstream of the rotor.	186

LIST OF ILLUSTRATIONS (cont'd)

Figure		Page
47	Mean axial and radial velocities, 0.1 chord downstream of the rotor.	187
48	Mean pitchwise velocity, 1.0 chord downstream of the rotor.	188
49	Mean axial velocity, 1.0 chord downstream of the rotor.	189
50	Mean radial velocity, 1.0 chord downstream of the rotor.	190
51	Equivalent entropy rise across the rotor.	191
52	Mean pitchwise velocity, 0.1 chord downstream of the rotor.	192
53	Mean axial and radial velocities, 0.1 chord downstream of the rotor.	193
54	Mean pitchwise velocity, 1.0 chord downstream of the rotor.	194
55	Mean axial velocity, 1.0 chord downstream of the rotor.	195
56	Mean radial velocity, 1.0 chord downstream of the rotor.	196
57	Mean pitchwise velocity, 0.1 chord downstream of the rotor.	197
58	Mean axial and radial velocities, 0.1 chord downstream of the rotor.	198
59	Mean pitchwise velocity, 1.0 chord downstream of the rotor.	199
60	Mean axial velocity, 1.0 chord downstream of the rotor.	200
61	Mean radial velocity, 1.0 chord downstream of the rotor.	201

LIST OF ILLUSTRATIONS (cont'd)

Figure		Page
62	Mean pitchwise velocity, 0.1 chord downstream of the rotor.	202
63	Mean pitchwise velocity, 0.1 chord downstream of the rotor.	203
64	Mean axial velocity, 0.1 chord downstream of the rotor.	204
65	Mean radial velocity, 0.1 chord downstream of the rotor.	205
66	Mean pitchwise velocity, 1.0 chord downstream of the rotor.	206
67	Mean axial velocity, 1.0 chord downstream of the rotor.	207
68	Mean radial velocity, 1.0 chord downstream of the rotor.	208

LIST OF SYMBOLS

r, θ, z	radial, pitchwise and axial directions
v	absolute velocity
w	relative velocity
\bar{v}, \bar{w}	time average of velocity with respect to the absolute frame of reference, or pitchwise average with respect to the frame of reference fixed to the blades
$\langle v \rangle, \langle w \rangle$	ensemble average with respect to the absolute frame of reference, or time average with respect to the frame of reference fixed to the blades
v', w', p'	fluctuating part of velocity, pressure
$\rho, \bar{\rho}$	density
p_s, p_t	static and total pressures
p_o	reference pressure
T, T_s	static temperature
T_t	total temperature
t	time
$\beta, \bar{\beta}$	Mean relative flow angle defined by $\tan \beta = \frac{\bar{w}_\theta}{\bar{v}_m}$
β_m	Mean blade surface angle defined by the mean value of $(r \frac{\partial \theta}{\partial z})$ for the suction and pressure surfaces of a blade
ξ	blade lean angle in $r-\theta$ plane
ξ_m	Mean blade surface angle defined by the mean value of $(r \frac{\partial \theta}{\partial z})$ for the suction and pitchwise surfaces of the blade
m	meridional streamline direction
l	direction of computation in the meridional plane - outward from the hub

LIST OF SYMBOLS (cont'd)

I	rothalpy defined by $I \equiv h + \frac{w^2}{2} - \frac{r^2 \Omega^2}{2}$
h	static enthalpy
H	total enthalpy
Ω	angular velocity of the rotor
q	total absolute velocity defined by $q = \sqrt{u_x^2 + u_\theta^2 + u_z^2}$
F	blade force
$F_{r\theta}, F_{\theta z}, F_{zr}$	viscous body force components per unit mass in the r, θ and z directions
r_c	radius of curvature
$\phi, \bar{\phi}$	angle between the meridional and axial directions
γ	angle between the direction of computation (1) and the radial direction, or ratio of specific heats
n	direction normal to m -direction in the meridional plane
S	entropy
a	velocity of sound
$\Sigma_{r\lambda}, \Sigma_{\theta\lambda}, \Sigma_{z\lambda}$ $\Sigma_r, \Sigma_\theta, \Sigma_z$	apparent stress terms appearing in the radial, pitchwise and axial momentum equations $\Sigma_{r\lambda} = \frac{1}{r\lambda} \left(\frac{\partial(r\lambda w_r)}{\partial r} + \frac{\partial(r\lambda w_\theta w_\theta)}{\partial z} - \frac{w_\theta^2}{r} \right)$; $\Sigma_z = \frac{\partial w_r^2}{\partial r} + \frac{\partial w_\theta^2 w_\theta^2}{\partial z} - \frac{w_\theta^2}{r}$ etc.
<u>Subscripts</u>	
r, θ, z	radial, pitchwise and axial components
m	meridional component, mean value
l	component in the direction of computation
n	component perpendicular to m -direction
i	inviscid component
v	viscous component
s	pertaining to suction surface
p	pertaining to pressure surface

SECTION I

INTRODUCTION

1.1 General Statement of the Problem

One of the basic problems in achieving efficient designs of high work compressor stages is the lack of an adequate technique for predicting the flow field and losses through a turbomachine stage. Current design systems are based on the assumption that the flow can be adequately modeled by a combination of axisymmetric through flow and two-dimensional cascade flow.^{1,14,25} Whereas this procedure has proved quite satisfactory for lightly loaded compressor stages, it is found to give a considerably different flow field from that observed in highly loaded stages.² The deviation is attributed to three-dimensional effects which become significant in a highly loaded system. Some of the important phenomena responsible for three-dimensional effects are blade passage shocks, the inviscid pressure field of the blades resulting in the distortion of stream surface, span-wise flows in the blade boundary layer and wakes, secondary flows due to the end wall boundary layer, and shock boundary layer interaction. The first two are inviscid effects and their proper treatment would require a full three-dimensional transonic inviscid computation. The last three effects are intrinsically viscous in origin, as they involve boundary layer growth on the blade surfaces and the end walls. The evolution of wakes and their subsequent interaction with the adjacent blade row makes the problem of

predicting the flow field more complex. Further complexities are introduced by the three-dimensional nature of the rotor blade boundary layer coupled with shock boundary layer interaction, and secondary flow arising from the end wall boundary layer and tip leakage. An accurate estimate of viscous effects would require a detailed computation of the three-dimensional blade surface boundary layer and end wall flow.

Current analytical and computational methods for prediction of the flow field are not advanced enough to account for all the coupled three-dimensional effects present in a highly loaded system. At best one can account for each individual effect by isolating it from the other three-dimensional effects. Although recent advances in 3-D inviscid² and multi 2-D³ computational schemes are encouraging, their use is restricted to lightly loaded systems since no capability exists to account for the above mentioned viscous effects. It will be shown later in this report that 3-D inviscid effects alone do not produce significant changes in the mean flow field of the compressor, rather 3-D viscous effects are mainly responsible for deviation of the mean flow field from that predicted by the usual axisymmetric theories.

One important step in prediction of the flow field of a compressor is inclusion of the effect of blade to blade (or pitch-wise) flow variations on mean (tangentially averaged) flow field of the compressor. This is the goal of this investigation.

1.2 Objectives of the Present Investigation

More specifically, the present investigation has the following objectives:

- a) To determine the effect of pitchwise flow variations on the mean flow field of an axial compressor. In particular, to determine how pitchwise flow variations effect the circumferential mean momentum and energy transport processes.
- b) To derive the equations of mean flow for the streamline curvature computational scheme implemented in the computer program of Reference (1), including the effects of blade to blade flow variations.
- c) To carry out a critical analysis of the time resolved experimental data of the MIT Blowdown Compressor, the purpose being to assess the magnitudes of various three-dimensional effects (discussed in Section 1.1 of this chapter) in a highly loaded transonic compressor.
- d) To modify the computer program of Reference (1) in order to account for the effects of pitchwise flow variations on the mean flow field and then to compute the mean flow field using the velocity correlations as estimated from the experimental data.

1.3 Phenomena Treated

In order to introduce the nonaxisymmetric effects into the axisymmetric computation, the following phenomena are treated:

- a) Apparent stresses introduced in the mean flow field due to pitchwise averaging of the equations of motion.
- b) Streamwise variation of mean Rothalpy due to energy transfer across the stream surfaces by apparent stresses, and by conversion of mean flow kinetic energy to energy of fluctuations.
- c) Apparent entropy production due to dissipation associated with apparent stresses, and due to the production of fluctuation energy.

1.4 Method of Investigation

It is well known that the blade surface boundary layer and wakes are primarily responsible for the pitchwise flow variations within and downstream of a rotor blade row. One way of accounting for the pitchwise or blade to blade flow variations is to treat them as flow fluctuations around the circumferentially averaged flow. With respect to an absolute frame of reference these will be temporal fluctuations around the mean which is a time mean. These fluctuations can therefore be treated as analogous to turbulent flow fluctuations and a quasi-steady approximation can be applied

to the flow field downstream of a blade row. However, if the frame of reference is fixed to the blades, as is the normal practice for flow analysis within the blade row, these blade to blade flow variations represent spatial fluctuations around the mean which is a spatial mean or mean in $r\theta$. By analogy to turbulent stresses (Reynolds stresses) these large scale fluctuations will also introduce apparent stresses, and the momentum and energy transfer associated with these stresses will modify the mean flow field of the compressor.

Following the above mentioned concept, mean flow equations of motion for a frame of reference fixed to the blades are first derived (Section 3.2). This is achieved by carrying out a pitchwise average from the pressure surface of one blade to the suction surface of the adjacent blade. An integral representation for averaging any quantity is given by

$$\bar{f} = \frac{1}{\theta_s - \theta_p} \int_{\theta_p}^{\theta_s} f d\theta$$

where θ_s and θ_p represent the angular positions of the suction and pressure surfaces of the two adjacent blades. The averaging procedure which uses Liebnitz rule for finding the pitchwise average of derivatives has been discussed by Smith⁴ and Fujii⁵. Pitchwise averaging of the equations of motion introduces two types of additional terms into the mean flow

equations of motion. One type of term represents the inviscid blade forces while the other type contains velocity correlations which can be considered as apparent stresses in the mean flow. It may be mentioned here that existing axisymmetric through flow theories do include inviscid blade force terms but assume that velocity correlation terms are small. A detailed derivation of the pitchwise averaged equations is given in Appendix A.

For the purpose of flow field computation, the pitchwise averaged equations of motion are derived for the Streamline Curvature Computational method. Normal practice for the Streamline Curvature Scheme is to derive the radial equilibrium equation (40) in which the axial derivative terms are replaced by the meridional and radial derivatives, and the pressure gradient is replaced by the enthalpy and entropy gradients as in Crocco's equation. However, for a more general case where a computing station need not be along a radial direction, the method suggested by Wennerstrom⁷ is more suitable. Streamline Curvature equations based on the Wennerstrom procedure have the advantage over the usual type that a computing station can be placed along the blade leading or trailing edge. The equation of motion in apparent stress format and along an arbitrary direction in the meridional plane, is suitably modified for application to the computer program of Reference (1).

The general problem of prediction of the loss distribution is important because in the Crocco form of momentum equation, the distributions of entropy and rothalpy represent the pressure gradient, and therefore these have an important effect on the flow field. The losses can be viewed as consisting of a viscous part and an inviscid part. Here viscous losses refer to the blade surface friction losses and can be approximated from the two-dimensional cascade data. Because of the gradual variation of viscous losses in the spanwise direction, these losses primarily effect the compressor efficiency but have little influence on the spanwise flow distribution. The concept of inviscid losses is not as straightforward as the viscous losses, and in fact is introduced to the turbomachinery context here for the first time. It refers to the conversion of mean flow kinetic energy to the energy of fluctuations. In the case of turbulent flow, such a conversion is normally known as "loss to fluctuations" and it implies that the energy of fluctuations is an unavailable form of energy as far as the mean flow is concerned. These losses can be termed "apparent losses" and their effect is felt through the reduction of mean relative total pressure along the streamline. For the particular case of the Crocco form of mean flow momentum equation, these losses will alter the mean rothalpy and mean entropy gradient terms. It may be mentioned here that the energy of fluctuations is eventually converted to thermal energy by viscous dissipation at the

molecular level, resulting in the increase of real entropy. Here it is assumed that the presence of fluctuations creates an apparent increase in entropy equivalent to that resulting from the viscous dissipation of the energy of fluctuations to heat.

Modeling of inviscid losses (Section III) is achieved by defining a mean rothalpy \bar{I} and an apparent entropy production along the streamline.

As will be discussed in Section III, the pitchwise averaged rothalpy is defined as

$$\bar{I} \equiv \bar{h} + \frac{\bar{W}^2}{2} - \frac{r^2 \Omega^2}{2} \quad (1)$$

and not

$$\bar{I} = \bar{h} + \frac{\bar{W}^2}{2} + \frac{\overline{W'^2}}{2} - \frac{r^2 \Omega^2}{2} \quad (2)$$

which would result from the averaging procedure discussed earlier.

The production of apparent entropy along a streamline is defined as

$$\frac{DS_{app}}{Dt} = \dot{I} + \frac{D}{Dt} \left(\overline{W'^2} / 2 \right) \quad (3)$$

where $\bar{\phi}$ represents dissipation associated with apparent stresses, and $\frac{D(\overline{w'^2/2})}{Dt}$ represents the production of fluctuation energy along the streamline. The concepts used in arriving at the above definition are discussed in Section III.

An equation for the rate of change of mean rothalpy along the streamline is derived by carrying out pitchwise averaging of the energy equation using equation (1).

The estimation of spanwise distribution of mean rothalpy (or apparent entropy) at any axial station is achieved by numerically integrating the equations for $\frac{\partial \bar{I}}{\partial m}$ and $\frac{\partial S_{app}}{\partial m}$ along the meridional streamline, the constant of integration being evaluated from the known value of mean rothalpy (or apparent entropy) at the upstream station. This completes the theoretical formulation for "apparent stress correction" to the mean flow model based on the combination of axisymmetric through flow and two-dimensional cascade flow. A detailed derivation of the equations for the mean rothalpy and apparent entropy gradients along the meridional streamline is given in Section III.

Experimental data from the MIT Blowdown Compressor is used to estimate distributions of mean flow properties such as velocities, apparent stresses (velocity correlations), and mean entropy. All the flow parameters were reduced to correspond to standard conditions at the inlet with air as the fluid. Velocity correlations are calculated for use in

the theoretical formulation for the prediction of flow field using Streamline Curvature Computational technique.

Finally, the Streamline Curvature program of Reference (1) is modified to account for the effect of blade to blade flow variations. A splinefit approximation is adopted for interpolating the experimentally estimated mean quantities. Inputs to the modified streamline curvature program are the hub and casing geometry, relative flow angle distribution at the blade exit, viscous loss distribution from the two-dimensional cascade data, mass flow, and apparent stress distribution.

SECTION II
LITERATURE SURVEY

Past work being reviewed in this section has been divided into two parts, one dealing with the methods of predicting the flow field of an axial compressor, and the other dealing with blade boundary layers and wakes. The latter are responsible for the large pitchwise flow variations, spanwise flow and large spanwise gradients of losses.

The problem of predicting the flow field through a turbomachine stage can be approached either as a design (indirect) problem or as an analysis (direct) problem. In the design problem, the distribution of angular momentum change $\Delta(rv_\theta)$ (or total enthalpy change) across the blade row is assumed to be known. The blade profiles have to be chosen to give the desired angular momentum change, with the aid of experimental cascade data. The analysis problem deals with prediction of the flow field from the known blade exit flow angles and the losses through the blade row. This problem is considerably more complex than the design problem, but is more versatile since it can be applied to all operating conditions of the turbomachine. The success of analytical methods has been mainly restricted to solving design problems. For solving an analysis problem one has normally to resort to a computational method.

The blade surface boundary layer and wakes seem to have received very little attention from turbomachine analysts. A few semi-empirical efforts to predict the nature of blade boundary layers and wakes have not proven good enough for any realistic application.

2.1 Methods of Predicting the Flow Field

2.1.1 Analytical Methods

During the past four decades considerable effort has gone into the methods of flow analysis. Early efforts were concentrated on the flow analysis for simplified flows. Starting with pitchline analysis⁸, the flow analysis techniques were soon extended to simple radial equilibrium⁹. In the radial equilibrium theory one looks only at the flow upstream and downstream of the blade row where the radial velocity is assumed to be zero. The theory also assumes a completely axially symmetric flow. The drawback of this theory is that it gives no account of how the changes in velocity distribution take place across a blade row. A major breakthrough in the flow analysis resulted from the concept of 'Actuator disc' with the aid of which not only the velocity distribution across a blade row could be predicted but mutual interaction between the blade rows could also be accounted for. In the actuator disc theory, it is imagined that the blade row, moving or stationary, is replaced by a disc of infinitely small axial thickness, across which a sudden change in tangential velocity and vorticity takes place. Radial equilibrium exists far upstream and far downstream of the actuator disc, but not necessarily in between these stations. The parallel assumption of axial symmetry is also made, as in the radial equilibrium theory. Analytical studies of the actuator disc model have been made by several turbomachine designers^{10,11,12} but perhaps the most complete account

employing the concept of actuator disc was presented by Marble¹³. Although this theory has been classified as three-dimensional since it allows for velocities in the radial, azimuthal and axial directions, it really permits flow variations in two directions only, axial and radial. In this sense, it is really a two-dimensional theory. In this pseudo three-dimensional theory which has come to be known as "axisymmetric through flow theory", the effect of blades is represented by distributed forces having the same integrated effect as the blades in the radial, azimuthal and axial directions. Marble's success in getting analytical solutions for several types of circulation distributions (indirect problem) resulted from the fact that he was able to linearize the problem by considering the three-dimensional aspect of the flow as a perturbation on the upstream flow. However, the assumption of small perturbation on the upstream flow restricted the application of this theory to lightly loaded systems only. For highly loaded systems it was not possible to linearize the problem and therefore computational techniques were required for analyzing the flow field.

The above mentioned analytical methods for the prediction of turbomachine flow have no provision for estimating losses and flow deviation angles. This necessitated a parallel effort for obtaining the loss distribution and deviation angles with the aid of experimental studies since the theoretical methods failed to give realistic results.

These experimental studies¹⁴ could be generalized only for two-dimensional cascade flows in which the characteristics of through flow are represented by the entering and leaving flow angles, by a mean stream surface slope along which the cascade lies, and by the change of axial mass flow density between the inlet and outlet. Thus a combination of axisymmetric through flow and two-dimensional cascade flow became an attractive technique for predicting the mean flow field of an axial compressor. This concept was generalized by Marble¹³ for lightly loaded systems and was considered a major breakthrough in solving a design problem. However, with the introduction of highly loaded compressor stages for modern high thrust/weight ratio aircraft engines, this linearized theory was not considered very attractive for designing an axial compressor.

An inviscid 3-D flow model was achieved by McCune and Hawthorne in 1976. In the case of axisymmetric through flow one visualizes the trailing vorticity arising from the nonuniformity of blade loading to be smeared uniformly in the pitchwise direction. On the other hand, if it is assumed that the trailing vorticity is concentrated in discrete sheets, it is possible to evaluate the pitchwise flow variation from the induced velocity field of the trailing vortex sheets. McCune and Hawthorne¹⁵ succeeded in using this concept in their three-dimensional inviscid, incompressible theory for a

rectilinear cascade. They replaced the blade row with a set of lifting lines of bound vorticity, and assumed that sheets of vorticity from the trailing edge of each blade are convected approximately by the mean flow (Beltrami Flow). In order to apply this theory to a highly loaded blade row, mean flow equations of motion were not linearized and the solution for mean flow was obtained by using an iterative scheme. Several subsequent improvements were introduced in this theory to make it more versatile in its application. Morton¹⁶ applied this theory to compressible flow through a highly loaded, rectilinear cascade. Cheng¹⁷ applied this theory to incompressible flow through a highly loaded annular cascade. All the above cases were restricted to nearly free vortex flow for which the spanwise variation in loading is not large. This restriction was removed by Adebayo¹⁸ and the theory was made applicable to a highly loaded blade row with arbitrary spanwise load distribution. The theory was made possible by the concept of treating the three-dimensional aspect of the mean flow field as perturbation about the axisymmetric mean flow instead of about the upstream flow, as is the case with other linearized theories. Therefore, this theory though still "linearized" is linearized about the fully nonlinear mean flow. Tan¹⁹ extended McCune's three-dimensional theory to vorticity arising from viscous wakes. These three-dimensional theories for predicting pitchwise

flow variations downstream of a rotor are a major step forward in the analytical methods. However, since the knowledge of mean U_e distribution is required a priori, these theories are restricted to 'design problem'.

2.1.2 Computational Methods

With the advent of high speed digital computers, the possibility of predicting the mean flow field of a highly loaded compressor stage appeared bright. Wu²⁰ was probably first to formulate equations for computing the complete three-dimensional flow. In his general theory the equations of fluid flow are satisfied on intersecting families of streamsurfaces, the complete three-dimensional flow being obtained by an iterative process between the solutions for the flow on the two sets of surfaces. The two sets of streamsurfaces are S_1 blade to blade surfaces and S_2 surfaces which pass through the blade row. However, Wu's general theory did not find much application and axisymmetric counterpart of this theory (Wu's through flow theory) was considered more suitable for computing the flow field. Wu's through flow theory is similar to the general theory, but the equations of flow are solved for the mean S_2 streamsurfaces on which the flow and fluid state are regarded as average values for the flow within the blade passage. For a multistage machine, the time dependence of the flow is removed by treating the through flow solution as an axially symmetric flow for the duct region between each pair of blade rows.

During the past decade two numerical methods based on the combination of axisymmetric through flow and two-dimensional cascade flow became the guidelines for most of the computer programs. These methods have come to be known as the Streamline Curvature technique^{4,21,22} and the Matrix through flow method²³. In the streamline curvature computational procedure, a radial equilibrium equation is solved simultaneously with mass conservation in the meridional plane. The equations are written in terms of the meridional streamline slope and curvature, which are fixed initially by assuming uniform flow through the duct, and are iteratively revised after solving the flow equations. The Matrix through flow method solves the flow equations on the S_2 surface of Wu's through flow theory. Here the governing equation is transformed into a Poisson equation for the stream function. The resulting matrix equation is solved by using a suitable iterative scheme.

More recently at the MIT Gas Turbine Laboratory, Oliver and Sparis²⁴, and Thompkins² have successfully developed and applied a fully three-dimensional inviscid scheme to a transonic compressor rotor. Although this scheme is a big step in evaluation of three-dimensional flow of a highly loaded system, its utility is limited because it does not include viscous effects. Novak and Hearsey²⁵ have developed a multi two-dimensional technique for computing the three-

dimensional flow field. The method is based on the iterative coupling of streamline curvature solutions on Wu's S_1 and S_2 surfaces where S_1 is a concentric blade to blade surface and the S_2 surface represents a mean stream sheet defined by stream function $\psi = 0.5$. The main limitation of this method is that it cannot be applied to a system where large blade to blade flow variations exist as is the case in the blade surface boundary layer.

Most of the well known computational schemes use finite difference methods for computing the flow field. Efforts are being made by a few workers to apply finite element computational methods to the turbomachine flow field but it is difficult to assess their effectiveness at this early stage. A computational scheme based on the finite element method which examines the contributions of pitchwise flow variations on the axisymmetric through flow, was proposed by Hirsch in 1975²⁶. The basic approach adopted by Hirsch for pitchwise averaging of the equation of motion was similar to the one undertaken for this investigation, but his apparent stress model is unrealistic because he used the 2-D isolated wake model of Silverstein et al.²⁷ for a wake structure which is highly three-dimensional. In addition, his model did not include the concept of mean rothalpy and apparent entropy, which will be seen to be of major impact.

It may be mentioned here that all the computational schemes discussed here depend on external sources (such as cascade data) for loss distribution through the blade row.

2.2 Blade Boundary Layer and Wakes

As mentioned earlier, the viscous effects are mainly responsible for the large blade to blade or pitchwise flow variation in a highly loaded blade row. Due to the combined action of increased centrifugal force in the blade boundary layer and coriolis forces arising from the blade surface curvature, large spanwise flows are set up in the blade boundary layer. This makes more complex the problem of estimating the pitchwise flow variation. Further, since the spanwise loss distribution is significantly altered due to the spanwise flows in the blade boundary layer, a detailed computation of three-dimensional boundary layer is needed. But the existing knowledge of the computational methods suitable for the present day computer hardware, are not advanced enough to handle such a problem. Therefore, a virtual vacuum seems to prevail as far as the theoretical modeling of blade boundary layer is concerned.

The first systematic effort for computing the three-dimensional boundary layer to a turbomachine blade row seems to have been by Mager²⁸ in 1954, who adopted Gruschwitz²⁹ type of coordinate system for the three-dimensional integral momentum boundary layer prediction. He, however, assumed the

blade surface to be plane and introduced several other simplifications to achieve the integral momentum solution. Subsequent effort by several workers resulted in many improvements and more recently Hules³⁰ was able to formulate integral momentum equations for a three-dimensional compressible boundary layer in a rotating variable-pitch helical coordinate system, ideal for describing arbitrary shaped turbomachine blades. He computed the boundary layer characteristic parameters for a turbine rotor without any streamwise pressure gradient. Application of this technique to an axial compressor rotor with large adverse pressure gradient is still to be tried.

With respect to the blade wakes, the major effort in the past has been restricted to study of the wake structure of isolated airfoils. Silverstein, Katzoff, and Bullevant²⁷ were the first to investigate the near and far wakes of an isolated airfoil in 1939. They used a theoretical treatment put forth by Prandtl to generalize their experimental results to predict the important wake parameters in terms of the distance behind the trailing edge and the profile drag coefficient. Preston and Sweeting³¹ in 1945 carried out a systematic investigation of the characteristics of the wake behind an isolated airfoil and observed that a similarity in mean velocity profile exists close behind the airfoil and that the wake centerline velocity recovered to about 80% of the free stream velocity in a quarter chord length from the

trailing edge. These observations led Spence³² in 1953 to give a general expression for the wake centerline velocity as a function of distance behind the trailing edge of the airfoil and the wake edge velocity. No attempt, however, seems to have been made to arrive at a generalized theoretical formulation of wake structure as a function of the physical characteristics of an airfoil or its loading. Very recently analytical and experimental investigations of the characteristics of 3-D turbulent wakes downstream of a turbomachine rotor have been carried out by Raj and Lakshminarayana³². By introducing the Reynolds stress terms in the equations of motion expressed in streamwise orthogonal coordinate system, they tried to develop an approximate quasi-three-dimensional turbulent wake model for a turbomachine rotor. Their conclusion that the wake velocity defect almost completely vanishes very near the blade trailing edge, does not agree with the experimental data from MIT Blowdown Compressor² which indicates that the velocity defect can even grow with distance downstream of the blade trailing edge. Since the rotor used by Raj and Lakshminarayana was a non-lifting type, the validity of their model for a highly loaded compressor rotor has still to be confirmed. During the past few years, the MIT Gas Turbine Laboratory has been conducting systematic experimental and theoretical studies of the behavior of wakes behind a highly loaded compressor rotor. By application of a general small disturbance theory,

Kerrebrock³⁴ has shown that the wakes are not purely convected in a strongly swirling flow, but can exhibit wave like propagating behavior. Kerrebrock and Mikolajczak³⁵ carried out a kinematic analysis of the interaction of rotor wakes with stator and predicted the pitchwise distribution of stagnation temperature and pressure at stator exit by using the two-dimensional wake model of Silverstein et al.,²⁷ in the generalized form as given by Kemp and Seers³⁶. By using a fast response strain gauge probe, Thompkins and Kerrebrock³⁷ successfully obtained wake velocity distributions at two axial locations downstream of a highly loaded transonic compressor. As mentioned earlier, one of the important findings was the persistence of wake velocity defect downstream of the rotor. Measurements made at a distance of 1.0 chord behind the trailing edge indicated an increased velocity defect at certain radial locations.

Hence, it is seen that most of the previous investigations on the flow modeling for axial compressors have neglected the effect of pitchwise flow variations while estimating the mean flow field. The only attempt by Hirsch²⁶ in trying to assess the effect of pitchwise flow variations was inconclusive since an unrealistic two-dimensional wake model was adopted for modeling the velocity correlations. The author has not come across any publication which examines the possibility of the existence of inviscid or apparent

losses. These losses may have greater effect on the mean flow than the viscous losses.

It is further seen that a virtual vacuum appears to exist as far as the study of three-dimensional blade boundary layer and wakes is concerned. The only detailed investigation of three-dimensional blade boundary layer³⁰ has been restricted to integral momentum methods for turbomachine blades without any pressure gradient. Similarly, the only known flow model³³ for three-dimensional wakes does not appear to be useful in its present form for a highly loaded compressor blade row.

It may be concluded from the study of literature presented in this chapter that the existing knowledge of analytical and computational techniques is not advanced enough to solve the problem of predicting the flow field of a highly loaded transonic axial flow compressor. However, the past work is very useful in understanding several important concepts and the limitations of various analytical and computational techniques. The availability of the time resolved experimental data downstream of the MIT Blowdown Compressor rotor is an opportunity to assess the order of magnitude of various three-dimensional effects (discussed in Section I). This data is of vital importance in studying the effect of pitchwise flow variations on the mean flow of an axial compressor, which is the objective of this investigation.

SECTION III

MEAN FLOW EQUATIONS OF MOTION, ROTHALPY VARIATION AND ENTROPY PRODUCTION

3.1 Apparent Stresses

It is well known that temporal fluctuations in the velocity field of a flow with spatial gradients influence the mean motion in such a way that the mean flow exhibits an apparent increase in resistance to deformation. In other words these fluctuations introduce "apparent stresses", thus augmenting the viscous stresses. For turbulent flow these apparent stresses are commonly known as Reynolds Stresses. The direct application of this idea to the flow field behind a turbomachine blade row would consist in time averaging the three-dimensional equations of motion written in a coordinate system fixed to the blade row (stationary for a stator and rotating for a rotor), whereupon Reynolds stresses arise as a result of turbulent fluctuations (or temporal fluctuations) in that coordinate system. This approach has been followed by Raj and Lakshminarayana³³ in their attempt to study the characteristic behavior of three-dimensional wakes downstream of a rotor.

Here the concept of apparent stresses is used in a different way. In order to account for the effect of blade to blade or pitchwise flow variations, it is proposed to consider them as flow fluctuations around the mean defined as

axisymmetric mean. With respect to the absolute frame of reference, these pitchwise fluctuations would become temporal fluctuations around the mean which is a time mean, and analogous to the turbulent flow, these fluctuations would introduce apparent stresses in the mean flow field. However, if the frame of reference is fixed to the blade row, these pitchwise flow variations represent spatial fluctuations around the mean which is a spatial mean or mean in $r\theta$. Here the apparent stresses would appear in the equations of motion as a result of pitchwise averaging and can play a significant role in the transfer of mean momentum and energy.

3.2 Mean Flow Equations of Motion

3.2.1 Non-Bladed Region

Normally, the procedure for arriving at the governing equations in Reynolds stress format is for a rotor exit flow field, identical to the classical procedure described in Reference (38) for unsteady turbulent flows.

It consists in:

- a) Combining the continuity equation with the momentum equation.
- b) Expressing each variable as the sum of a mean plus a fluctuating part, for example the velocity.

$$\underline{v} = \underline{\bar{v}} + \underline{v}'$$

where

$$\underline{\bar{v}} = \lim_{T \rightarrow \infty} \frac{1}{T} \int_0^T \underline{v} dt$$

and T is large enough so that \bar{u} is independent of T .

- c) Averaging the momentum equations in time over the interval T , thus eliminating all terms linear in the disturbance quantities, while retaining those which are quadratic.

It should be noted at this point that if the rotor exit flow is fully periodic in blade passing, then T need be only one blade passing period. But the procedure admits the possibility of dealing with flows which are unsteady in rotor coordinates by simply increasing T to average out such fluctuations.

If density fluctuations are neglected, the mass conservation equation for the mean flow remains unchanged but the equations of motion and energy will have additional terms containing correlations of fluctuating quantities. However, if density fluctuations are not small, mean mass conservation equation will also have additional terms containing correlations of fluctuating quantities.

The present analysis will be restricted to the case of small density fluctuations. It is further assumed that the rotor exit flow is periodic in blade passing, which means in the absence of turbulent fluctuations the temporal average of unsteady flow with respect to the absolute frame of reference is the same as the pitchwise average with

respect to the moving frame of reference. We can thus represent the effect of pitchwise flow variations in the non-bladed region by time averaging the equations of motion written in the absolute frame of reference. Mean mass and momentum conservation equations in the absolute cylindrical frame of reference are:

Mass Conservation

$$\frac{1}{r} \frac{\partial (r \bar{v}_r)}{\partial r} + \frac{\partial (\bar{v}_z)}{\partial z} = 0 \quad (4)$$

Momentum Conservation

r-direction

$$\bar{v}_r \frac{\partial \bar{v}_r}{\partial r} + \bar{v}_z \frac{\partial \bar{v}_r}{\partial z} - \frac{\bar{v}_\theta^2}{r} = -\frac{1}{\rho} \frac{\partial \bar{p}}{\partial r} - \left\{ \frac{\partial (\overline{v_r' v_r'})}{\partial r} + \frac{\partial (\overline{v_r' v_z'})}{\partial z} + \frac{\rho \overline{v_r'^2}}{r} - \frac{\rho \overline{v_\theta'^2}}{r} \right\} + \bar{F}_{rv} \quad (5)$$

\theta-direction

$$\bar{v}_r \frac{\partial \bar{v}_\theta}{\partial r} + \bar{v}_z \frac{\partial \bar{v}_\theta}{\partial z} + \frac{\bar{v}_r \bar{v}_\theta}{r} = -\left\{ \frac{\partial (\overline{v_r' v_\theta'})}{\partial r} + \frac{\partial (\overline{v_\theta' v_z'})}{\partial z} + \frac{\partial (\overline{v_r' v_\theta'})}{\partial r} \right\} + \bar{F}_{\theta v} \quad (6)$$

z-direction

$$\bar{v}_r \frac{\partial \bar{v}_z}{\partial r} + \bar{v}_z \frac{\partial \bar{v}_z}{\partial z} = -\frac{1}{\rho} \frac{\partial \bar{p}}{\partial z} - \left\{ \frac{\partial (\overline{v_r' v_z'})}{\partial r} + \frac{\partial (\overline{v_z'^2})}{\partial z} + \frac{\overline{v_r' v_z'}}{r} \right\} + \bar{F}_{zv} \quad (7)$$

Here the correlations of fluctuating velocities represent the effect of pitchwise flow variations on the axisymmetric mean flow and should not be confused with turbulent fluctuations. Analogous to Reynold Stresses, these correlations can be considered as apparent normal and shear stresses. For example, $-\rho \overline{v_r'^2}$ can be considered an apparent radial

normal stress since it represents the transport of radial momentum in the radial direction due to the above mentioned fluctuations. Similarly, a term such as $-\rho \overline{v'_\theta v'_r}$ can be considered an apparent shear stress and represents the transport of pitchwise momentum through a surface normal to the radial direction. $\overline{F_{rv}}$, $\overline{F_{\theta v}}$ and $\overline{F_{zv}}$ are the average viscous forces per unit mass in the r, θ , and z directions.

3.2.2 Bladed Region

The method of Reference (38) for deriving mean flow equations of motion is not applicable within the blade row because of the presence of blades across which a jump in flow properties takes place. The correct procedure for the bladed region is to write down the equations of motion in the relative frame of reference and carry out spatial averaging in the circumferential direction from the pressure surface of one blade to the suction surface of the adjacent blade. Ruden³⁹ appears to have been first to discuss the use of pitchwise averaged equations in turbomachine aerodynamics. The subject was treated in greater detail by Smith⁴, Horlock⁴⁰ and Fujii⁵. This averaging procedure introduces two types of additional terms in the mean flow equations of motion. First, there are those which contain the effect of pressure jump across the blade, while the second are the correlations of the fluctuating quantities. The former can be interpreted to represent inviscid blade forces which can be expressed

in terms of the gradients of angular momentum by using the procedure of Reference (7). It may be mentioned here that axisymmetric through flow theory does include inviscid blade force terms but assumes that velocity correlation terms are small.

The pitchwise or circumferential average of any quantity

$$\bar{f}(r, \theta, z) \text{ is given by the integral}$$

$$\bar{f} = \frac{1}{\theta_s - \theta_p} \int_{\theta_p}^{\theta_s} f(r, \theta, z) d\theta \quad (8)$$

where θ_s and θ_p represent the angular positions of the suction and pressure surfaces of the adjacent blades.

It is also known from Leibnitz Rule that integral of a derivative is given by

$$\int_{\theta_p}^{\theta_s} \frac{\partial f}{\partial x} d\theta = \frac{\partial}{\partial x} \int_{\theta_p}^{\theta_s} f d\theta + \int_p \frac{\partial \theta_p}{\partial x} - \int_s \frac{\partial \theta_s}{\partial x} \quad (9)$$

Using equations (8) and (9), pitchwise averages of the derivatives of pressure and the products of velocities can be evaluated. For example, pitchwise averages of $\frac{\partial p}{\partial r}$ and $\frac{\partial (w_r w_z)}{\partial r}$ are approximately given by the following relations

$$\overline{\frac{\partial p}{\partial r}} = \frac{\partial \bar{p}}{\partial r} + \frac{(p_s - p_p)}{(2\pi \lambda N)} \frac{\tan \epsilon_m}{r} \quad (10)$$

and

$$\overline{\frac{\partial (W_r W_z)}{\partial t}} = \frac{\partial \overline{W_r W_z}}{\partial t} + \frac{\overline{W_r W_z}}{\lambda} \frac{\partial \lambda}{\partial z} + \frac{\partial \overline{W_r' W_z'}}{\partial z} + \frac{\overline{W_r' W_z'}}{\lambda} \frac{\partial \lambda}{\partial z} \quad (11)$$

where ϵ_m is the blade lean angle and $2\pi\lambda/N = (\theta_s - \theta_p)$

The term $\frac{(P_s - P_p)}{(2\pi\lambda/N)} \frac{\tan \epsilon_m}{r}$ represents the radial component of inviscid blade force. A detailed derivation of equations (10) and (11) is given in Appendix B.

It is now possible to obtain mean flow equations of motion with the aid of equations (10) and (11). These are r-direction momentum equation

$$\begin{aligned} \overline{W_r} \frac{\partial \overline{W_r}}{\partial t} + \overline{W_z} \frac{\partial \overline{W_r}}{\partial z} - \frac{\overline{W_\theta}^2}{r} - 2\overline{W_\theta} \Omega - \Omega^2 r \\ = -\frac{1}{s} \frac{\partial \overline{p}}{\partial r} - \frac{1}{\lambda} \left\{ \frac{\partial (\lambda \overline{W_r'^2})}{\partial z} + \frac{\partial (\lambda \overline{W_r' W_z'})}{\partial z} - \frac{\lambda \overline{W_\theta'^2}}{r} \right\} + F_{ri} + \overline{F_{r\theta}} \end{aligned} \quad (12)$$

θ -direction

$$\begin{aligned} \overline{W_r} \frac{\partial \overline{W_\theta}}{\partial t} + \overline{W_z} \frac{\partial \overline{W_\theta}}{\partial z} + \frac{\overline{W_\theta} \overline{W_r}}{r} + 2\Omega \overline{W_r} \\ = -\frac{1}{\lambda} \left\{ \frac{\partial (\lambda \overline{W_r' W_\theta'})}{\partial z} + \frac{\partial (\lambda \overline{W_z' W_\theta'})}{\partial z} + \frac{2\lambda \overline{W_r' W_\theta'}}{r} \right\} + F_{\theta i} + \overline{F_{\theta r}} \end{aligned} \quad (13)$$

z -direction

$$\begin{aligned} \overline{W_r} \frac{\partial \overline{W_z}}{\partial t} + \overline{W_z} \frac{\partial \overline{W_z}}{\partial z} = -\frac{1}{s} \frac{\partial \overline{p}}{\partial z} + F_{zi} + F_{z\theta} \\ - \frac{1}{\lambda} \left\{ \frac{\partial (\lambda \overline{W_r' W_z'})}{\partial z} + \frac{\partial (\lambda \overline{W_z'^2})}{\partial z} + \frac{\lambda \overline{W_z' W_r'}}{r} \right\} \end{aligned} \quad (14)$$

Here F_{ri} , $F_{\theta i}$ and F_{zi} are the r, θ , and z components of inviscid blade force.

It may be mentioned here that it is possible to represent the effect of turbulence explicitly in the above equations by first taking the time average of the flow at various pitchwise locations and then carrying out a pitchwise average of the time averaged equations of motion. Appendix A gives the details of this procedure.

Equations (12), (13), and (14) can be transformed to the absolute frame of reference by putting $\overline{W_r} = \overline{U_r}$, $\overline{W_z} = \overline{U_z}$, $\overline{W_\theta} = \overline{U_\theta} - r\Omega$. The change in the frame of reference does not effect the magnitudes of the apparent stresses. $\overline{W_r'^2} = \overline{U_r'^2}$, $\overline{W_r'W_\theta'} = \overline{U_r'U_\theta'}$ etc.

3.3 Mean Flow Equation for Rothalpy Variation Along the Streamline

An important assumption in the existing numerical methods is that rothalpy remains constant along the streamline. The Euler Turbine equation $\frac{DI}{Dt} = 0$, which represents the conservation of rothalpy along the streamline is applicable only when the flow is steady and viscous effects are not significant. It was indicated in Section 1.3 of this thesis that the conversion of mean flow kinetic energy to energy of fluctuations will result in the decrease of mean relative total pressure. In order to better understand this concept and the correct meaning of the mean relative total pressure, it is assumed that the flow is

incompressible so that the relative total pressure can be defined as

$$P_{tr} = p + \frac{\rho W^2}{2} \quad (15)$$

Pitchwise averaging of this equation as per the procedure outlined in Appendix B gives

$$\overline{P_{tr}} = \overline{p} + \frac{\rho \overline{W}^2}{2} + \frac{\rho \overline{W'^2}}{2} \quad (16)$$

Here it has been assumed that the pitchwise variation of density is small and the region is outside the blade row.

Equation (16) indicates that conversion of the mean flow kinetic energy ($\frac{\rho \overline{W}^2}{2}$) to the energy of fluctuations ($\frac{\rho \overline{W'^2}}{2}$) does not change the value of the mean relative total pressure. This, however, assumes that the energy of fluctuations is recoverable when the fluid is stagnated. In keeping with the physical postulate that the energy of fluctuations is not recoverable by the mean flow, we define the mean relative stagnation pressure $\overline{P_{tr}}$ by

$$\overline{P_{tr}} \equiv \overline{p} + \frac{\rho \overline{W}^2}{2} \quad (17)$$

In this example it is assumed that the energy fed into fluctuations comes from the mean flow kinetic energy and not from the heat energy or the energy related to the pressure work.

Consistent with the concept of mean total pressure, the mean total rothalpy is defined as

$$\bar{I} \equiv \bar{h} + \frac{\bar{W}^2}{2} - \frac{r^2 \Omega^2}{2} \quad (18)$$

In order to derive an expression for the rate of change of mean rothalpy along the mean streamline, pitchwise averaging of the energy equation is carried out with mean rothalpy defined by the above expression. The procedure involves equating the mean rate of gain of internal and kinetic energy to the mean rate of work from the pressure forces, centrifugal force, and the apparent stresses. A detailed derivation of $\frac{\overline{D\bar{I}}}{Dt}$ in terms of the fluctuating quantities is given in Appendix C. Equation (C-22) from the appendix is reproduced here

$$\begin{aligned} \frac{\overline{D\bar{I}}}{Dt} = & - \left[\left\{ \overline{W_r} \left(\Sigma_r + \frac{W_\theta'^2}{r} \right) + \overline{W_\theta} \Sigma_\theta + \overline{W_z} \Sigma_z \right\} - \overline{\Phi}_{app} + \frac{\overline{D W'^2/2}}{Dt} \right] \\ & + \frac{1}{\rho} \left\{ - \frac{\overline{D p'}}{Dt} + \frac{\overline{p' W_r'}}{\rho} \frac{\partial \rho}{\partial r} + \frac{\overline{p' W_z'}}{\rho} \frac{\partial \rho}{\partial z} \right\} \\ & + \left\{ \frac{\overline{D W'^2/2}}{Dt} + \frac{\overline{D'(\overline{W W'})}}{Dt} \right\} \end{aligned} \quad (C-22)$$

In deriving this equation, the work associated with viscous stresses has been assumed to be small as compared to that due to the apparent stresses. Such an assumption is justified in the non-bladed region, but within the blade row where the viscous effects due to the blade surface friction are significant, it will be more realistic to include the work associated with viscous stresses. Equation (C-22) for viscous flow will become

$$\begin{aligned}
 \frac{\overline{D I}}{Dt} = & - \left[\underbrace{\left\{ \overline{W_r} \left(\Sigma_r + \frac{\overline{W_\theta^2}}{r} \right) + \overline{W_\theta} \Sigma_\theta + \overline{W_z} \Sigma_z \right\}}_I - \underbrace{\phi_{app} + \frac{\overline{D W'^2}}{Dt}}_{II} \right] \\
 & + \frac{1}{s} \left\{ \underbrace{- \frac{\overline{D' p'}}{Dt}}_{III} + \underbrace{\frac{\overline{p' W_r'}}{s} \frac{\partial s}{\partial r}}_{IV} + \underbrace{\frac{\overline{p' W_z'}}{s} \frac{\partial s}{\partial z}}_V \right\} \\
 & + \left\{ \underbrace{\frac{\overline{D' W'^2}}{Dt}}_{VI} + \underbrace{\frac{\overline{D' (\overline{W W'})}}{Dt}}_{VII} \right\} + \underbrace{\tau_{vis}}_{VIII} \quad (19)
 \end{aligned}$$

where

$$\begin{aligned}
 \tau_{vis} = & \left[\frac{\partial \{ \overline{\tau_{rz} W_z} + \overline{\tau_{r\theta} W_\theta} \}}{\partial r} + \frac{\overline{\tau_{rz} W_z}}{r} + \frac{\overline{\tau_{r\theta} W_\theta}}{r} \right. \\
 & \left. + \frac{\partial \{ \overline{\tau_{zr} W_r} + \overline{\tau_{z\theta} W_\theta} \}}{\partial z} \right] \quad (20)
 \end{aligned}$$

$$\text{and } \bar{\Phi}_{app} = - \left\{ \overline{w_r'^2} \frac{\partial \bar{w}_r}{\partial r} + \overline{w_z'^2} \frac{\partial \bar{w}_z}{\partial z} + \overline{w_r' w_\theta'} \frac{\partial \bar{w}_\theta}{\partial r} \right. \\ \left. + \overline{w_r' w_z'} \left(\frac{\partial \bar{w}_z}{\partial z} + \frac{\partial \bar{w}_r}{\partial r} \right) + \overline{w_z' w_\theta'} \frac{\partial \bar{w}_\theta}{\partial z} \right\} \quad (21)$$

For an axisymmetric case $\frac{\bar{D}}{Dt} = \bar{w}_m \frac{\partial}{\partial m}$ and the equation (19) will become

$$\frac{\partial \bar{I}}{\partial m} = - \left[\left\{ \sin \phi \left(\bar{w}_r + \frac{\overline{w_\theta'^2}}{r} \right) + \tan \beta \bar{\Sigma}_\theta + \cos \phi \bar{\Sigma}_z \right\} - \frac{1}{\bar{w}_m} \bar{\Phi}_{app} \right. \\ \left. + \frac{\partial \overline{w'^2/2}}{\partial m} \right] + \frac{1}{\bar{w}_m s} \left\{ - \frac{\bar{D} \bar{p}'}{Dt} + \frac{\bar{p}' w_r'}{s} \frac{\partial \rho}{\partial r} + \frac{\bar{p}' w_z'}{s} \frac{\partial \rho}{\partial z} \right\} \\ + \frac{1}{\bar{w}_m} \left\{ \frac{\bar{D}' \overline{w'^2/2}}{Dt} + \frac{\bar{D}' (\bar{w} w')}{Dt} \right\} + \frac{\tau_{vis}}{\bar{w}_m} \quad (22)$$

We will now examine different terms of equation (19) to get a better understanding of the energy transport processes responsible for the variation of mean rothalpy along the streamline.

$$\text{Term I} = \left[- \left\{ \bar{w}_r \left(\bar{\Sigma}_r + \frac{\overline{w_\theta'^2}}{r} \right) + \bar{w}_\theta \bar{\Sigma}_\theta + \bar{w}_z \bar{\Sigma}_z \right\} - \bar{\Phi}_{app} \right]$$

represents the work associated with normal and shear apparent stresses as given in equations (C-15) and (C-16) of Appendix C. These terms can be interpreted to represent the work done by the forces due to apparent stresses working at the mean velocities.

Term II = $-\frac{D}{Dt} \overline{W'^2}$ represents the rate of change of the kinetic energy of fluctuations along the mean meridional streamline. It is seen that an increase in kinetic energy of fluctuations along the mean streamline will result in a decrease of mean rothalpy, and this is consistent with the physical concept discussed in the preceding paragraphs.

$$\text{Term III} = -\frac{D'p'}{Dt} = \left(\overline{w'_r \frac{\partial p'}{\partial r}} + \overline{w'_z \frac{\partial p'}{\partial z}} \right)$$

can be interpreted as work done by the velocity fluctuations in correlation with pressure fluctuations. It can in fact be compared to acoustic energy transport.

Terms IV and V are interpreted as the production of the energy of fluctuating pressure due to the density gradient.

Term VI can be written as

$$\frac{D'W'^2}{Dt} = \overline{w'_r \frac{\partial W'^2}{\partial r}} + \overline{w'_z \frac{\partial W'^2}{\partial z}}$$

and the individual terms in the right hand side of this equation can be expressed as

$$\overline{w'_k \frac{\partial W'^2}{\partial x_k}} = \frac{\partial}{\partial x_k} (\overline{w'_k W'^2}) - \overline{W'^2} \frac{\partial w'_k}{\partial x_k}$$

Here the first term on the right hand side is interpreted as the spatial transport of the "kinetic energy of fluctuations" due to velocity fluctuations. The second term represents the production of fluctuation energy due to spatial variation of fluctuating velocity.

Term VIII which represents the effect of molecular viscosity is responsible for the spatial transport of kinetic energy due to viscous shear stresses. This spatial transport process is always accompanied by viscous dissipation resulting in loss of mean relative total pressure. It may be noted that in the case of viscous dissipation, the loss of relative total pressure occurs due to the conversion of kinetic and pressure energy to the heat energy. On the other hand the loss associated with fluctuations is due to the conversion of mean flow kinetic energy to the energy of fluctuations.

Equation (19) in its entirety is not tractable presently because Terms III through VIII cannot be estimated from the available experimental data. In order to estimate these terms it is necessary to carry out a local analysis of blade to blade flow variations so that all the three-dimensional effects are properly accounted for. It may be then possible to arrive at a suitable flow model for predicting blade to blade flow distribution required for evaluating Terms III through VIII. For the purpose of the present analysis, these terms will be neglected. That such a neglect is acceptable can be argued since these terms are not as large as Terms I and II. For example, Term VIII, which represents work associated with viscous shear stresses, will be small, at least outside the blade row. If the

spatial derivatives of density are smaller than the spatial derivatives of apparent stresses, Terms IV and V can be neglected. It may be argued that the spatial derivatives of fluctuating quantities are smaller than the spatial derivatives of apparent stresses, terms III and VII can therefore be neglected. Similarly since the fluctuation in velocities is expected to be smaller than the mean velocity, $\frac{D'(w'^2/2)}{Dt}$ will be small as compared to $\frac{D}{Dt}(w'^2/2)$

In view of the above argument, equation (22) becomes

$$\begin{aligned}
 \frac{\partial \bar{I}}{\partial m} = & - \left\{ \sin \phi \left(\frac{\partial \overline{w_r'^2}}{\partial r} + \frac{\partial \overline{w_r' w_z'}}{\partial z} + \frac{\overline{w_r'^2}}{r} \right) \right. \\
 & + \tan \beta \left(\frac{\partial \overline{w_r' w_\theta'}}{\partial r} + \frac{\partial \overline{w_z' w_\theta'}}{\partial z} + 2 \frac{\overline{w_r' w_\theta'}}{r} \right) \\
 & \left. + \cos \phi \left(\frac{\partial \overline{w_r' w_z'}}{\partial r} + \frac{\partial \overline{w_z'^2}}{\partial z} + \frac{\overline{w_r' w_z'}}{r} \right) \right\} \\
 & + \frac{1}{\bar{v}_m} \left\{ \overline{w_r'^2} \frac{\partial \overline{w_r}}{\partial r} + \overline{w_z'^2} \frac{\partial \overline{w_z}}{\partial z} + \overline{w_r' w_\theta'} \frac{\partial \overline{w_\theta}}{\partial r} \right. \\
 & \left. + \overline{w_r' w_z'} \left(\frac{\partial \overline{w_z}}{\partial r} + \frac{\partial \overline{w_r}}{\partial z} \right) + \overline{w_z' w_\theta'} \frac{\partial \overline{w_\theta}}{\partial z} \right\} \\
 & - \frac{\partial}{\partial m} \left(\overline{w_r'^2}/2 + \overline{w_\theta'^2}/2 + \overline{w_z'^2}/2 \right)
 \end{aligned} \tag{23}$$

In a more compact form equation (23) can be written as

$$\frac{\partial \bar{I}}{\partial m} = - \left\{ \sin \phi \left(\Sigma_r + \frac{\overline{W_\theta'^2}}{r} \right) + \tan \beta \Sigma_\theta + \cos \phi \Sigma_z \right\} - \frac{1}{v_m} \bar{\Phi} I_{app} - \frac{\partial \overline{W'^2/2}}{\partial m} \quad (24)$$

3.4 Mean Flow Equations for Entropy Production

An established practice for the inviscid analysis of turbomachine flow field is to write the equation of motion in Crocco form by using the Gibbs relation

$$T \nabla S = \nabla h - \frac{\nabla p}{\rho} \quad (25)$$

The final form of Crocco's equation suitable for flow through the rotor becomes

$$\underline{W} \times (\nabla \times \underline{V}) = \nabla I - T \nabla S \quad (26)$$

where I is rothalpy defined as

$$I = h + \frac{W^2}{2} - \frac{r^2 \Omega^2}{2}$$

It is assumed to remain constant along a streamline.

There is an apparent inconsistency in the Crocco equation since it contains an entropy variation term without including the source of this entropy variation. One way of interpreting such a situation is to consider that viscous effects are negligible at the point where this equation is being applied, but upstream of this point viscous effects do exist as a result of which an entropy

gradient is present at the point of application. Since the viscous effects are ignored in this equation, the entropy gradient is in a direction perpendicular to the streamline. Therefore, the use of this form of Crocco's equation can probably be justified for application to a region outside the blade row if the dissipative process occurs mainly within the blade row. Such a situation is quite unrealistic for a highly loaded machine in which one of the major sources of loss is the dissipation due to turbulent mixing downstream of a blade row.

In order to overcome this inconsistency, Horlock⁴¹ suggested that a dissipative body force term could be introduced into the equation of motion so that the Crocco equation becomes

$$\underline{W} \times (\nabla \times \underline{V}) = \nabla I - T \nabla S - \underline{D} \quad (27)$$

By taking the dot product with \underline{W} , we get

$$T \frac{DS}{Dt} = - \underline{W} \cdot \underline{D} \quad (28)$$

This is a streamwise equation for entropy production and if a simplified loss model is adopted based on the assumption of dissipative forces opposing the relative velocity vector, we can express the dissipative force \underline{D} in terms of a streamwise entropy gradient.

$$D = T \frac{\partial S}{\partial s} \quad (29)$$

Bossman and Marsh⁴² suggested an improvement over Horlock's formulation by writing the equation of motion in a direction normal to the streamlines and thus managed to eliminate the dissipative force term from the equation. Wennerstrom⁷ used equation (27) as a starting point for deriving the equation of motion for a streamline curvature computational scheme. In this scheme also the equation of motion is written in a direction almost normal to the streamlines and therefore the dissipative force term can be neglected. It may, however, be mentioned here that elimination of dissipative force term by writing the momentum equation in a direction perpendicular to the streamlines, does not provide any special advantage because the knowledge of entropy production along the streamline is necessary to evaluate the entropy gradient term in equation (26). This entropy gradient term plays an important role in changing the radial distribution of velocity.

Although computer programs (1,42) based on the above model have been successfully applied to turbomachine flow problems, there is a major discrepancy in this model which renders it unsuitable for application to a highly loaded system. This formulation assumes that the experimental cascade data is an adequate means for estimation of entropy

increase through the rotor, hence no provision exists to account for entropy rise associated with the flow fluctuations.

In the next section the concept of "apparent entropy production" resulting from the flow fluctuations is introduced.

3.4.1 Entropy Production Associated with Flow Fluctuations

In Section 3.3 an expression for the rate of change of mean rothalpy along a streamline was finalized. It was emphasized that the spatial transfer of fluctuation energy and the streamwise rate of change of fluctuation kinetic energy play an important role in changing mean rothalpy (or mean relative total pressure) along the mean meridional streamline. The concept of "apparent entropy production" due to the flow fluctuations will now be introduced.

The increased rate of viscous dissipation due to flow fluctuations is a well known phenomenon. The viscous dissipation from kinetic energy to thermal energy, results in the decrease of relative total pressure and an increase of entropy. Based on this concept it should be expected that a decrease in the mean relative total pressure would result in an increase in the mean entropy, or the conversion of mean flow kinetic energy to the energy of fluctuations will cause the mean entropy to rise. It is proposed here that the production of fluctuations at any point in the flow

field is equivalent to the production of apparent entropy there, the amount of apparent entropy being equal to the kinetic energy of fluctuations divided by the temperature. It is also proposed that the gradient of this apparent entropy plays the same role as the real entropy gradient in reshaping the flow field. The term "apparent entropy production" refers to the conversion of the mean flow energy to the energy of fluctuations, the corresponding loss in the mean relative total pressure can be termed "apparent losses".

It was argued in Section 3.3 that the mean relative total pressure for incompressible flow should be defined by equation (17), reproduced here

$$\bar{P}_{tr} \equiv \bar{p} + \frac{\rho \bar{W}^2}{2} \quad (30)$$

Using the assumption that all the energy of fluctuations ($\frac{\rho}{2} \overline{W'^2}$) comes from the mean flow kinetic energy ($\frac{\rho}{2} \bar{W}^2$), it is seen from the above equation that the rate of drop of mean relative total pressure $\frac{D}{Dt} \bar{P}_{tr}$ goes as $-\rho \frac{D}{Dt} (\bar{W}^2/2)$. And since the increase of entropy $T \frac{DS}{Dt}$ goes as $-\frac{1}{\rho} \frac{Dp}{Dt}$, we postulate that $T \frac{D S_{app}}{Dt}$ goes as $\frac{D}{Dt} (\bar{W}^2/2)$. Apparent entropy production along a streamline also results from the apparent dissipation which is analogous to the viscous dissipation and refers to the irreversible work done by the apparent stresses. Terms of the type $\overline{w'_i w'_k} \frac{\partial w'_i}{\partial x_k}$ represent apparent dissipation.

Based on the above argument, it is now possible to write an expression for the apparent entropy production along a streamline, which is as follows

$$T \frac{\overline{D}(S_{app})}{Dt} = \overline{\Phi}_{app} + \frac{\overline{D}}{Dt} (\overline{W'^2/2}) \quad (31)$$

For the axisymmetric case

$$\frac{\overline{D}}{Dt} = \overline{v}_m \frac{\partial}{\partial m}$$

Equation (31) therefore becomes

$$T \overline{v}_m \frac{\partial S_{app}}{\partial m} = \overline{\Phi}_{app} + \overline{v}_m \frac{\partial (\overline{W'^2/2})}{\partial m} \quad (32)$$

Substituting for $\overline{\Phi}_{app}$, we get

$$T \frac{\partial S_{app}}{\partial m} = - \frac{1}{\overline{v}_m} \left\{ \overline{w_r'^2} \frac{\partial \overline{w_r}}{\partial r} + \overline{w_z'^2} \frac{\partial \overline{w_z}}{\partial z} + \overline{w_r' w_\theta'} \frac{\partial \overline{w_\theta}}{\partial r} \right. \\ \left. + \overline{w_r' w_z'} \left(\frac{\partial \overline{w_z}}{\partial r} + \frac{\partial \overline{w_r}}{\partial z} \right) \right. \\ \left. + \overline{w_z' w_\theta'} \frac{\partial \overline{w_\theta}}{\partial z} \right\} + \frac{\partial (\overline{W'^2/2})}{\partial m} \quad (33)$$

3.4.2 Entropy Production in the Rotor

Current practice for estimation of entropy increase through the rotor is to use the experimental data from two-dimensional cascade tests. But it is well known that the entropy increase across a highly loaded rotor is larger than that estimated from the results of a corresponding cascade

unit. This behavior is more pronounced in regions near the hub and the casing, and at off design operating conditions. Recent experimental studies carried out at MIT have confirmed that the cascade data does not provide an answer to the above problem for a highly loaded axial transonic compressor rotor.

Within the blade row, both viscous dissipation and the apparent entropy production associated with blade to blade flow variations are important. A proper a priori estimate of the change of entropy through the rotor would require a detailed study of blade surface and end wall boundary layers, blade passage shocks, secondary flows due to end wall boundary layers, and other three-dimensional effects discussed in Section I of this report. No such detailed calculation is attempted here. Rather, it is proposed to estimate the entropy increase through the rotor by assuming that the mean flow viscous losses can be found from the experimental cascade data, and the apparent entropy increase associated with blade to blade flow variations with the aid of equation (33) and measured blade to blade flow variations. The entropy increase due to the blade passage shock can be found by the method given in Section 3.4.3.

Thus the total entropy increase through the rotor =
 $(\Delta S)_{app} + (\Delta S)_{cascade} + (\Delta S)_{shock}.$

3.4.3 Entropy Production Due to Blade Passage Shock

In order to arrive at a realistic estimate of entropy production due to blade passage shock, it is necessary to know the exact location and strength of the shock. The problem is made more complex due to shock-boundary layer interaction resulting in the separation of turbulent boundary layer. For the purpose of estimating the entropy production across the shock, it is normally assumed that the shock stands near the entrance of the blade passage (Figure 2), striking the suction surface at the point B, extending in front of the blade at point A, and then bending back similar to a bow wave. It is then assumed that the loss across the shock can be approximated by the normal shock loss taken for the average of Mach numbers at points A and B. The Mach number at point A is assumed to be equal to the inlet relative Mach number. The Mach number at B is estimated by using Prandtl-Meyer expansion on the blade suction surface. This procedure has been suggested by Miller et al.⁴³

In the light of the experimental studies carried out at the MIT Gas Turbine Laboratory, the above procedure does not appear to be realistic. Density measurements made across the blade passage shock using a flow visualization technique⁴⁴ indicated that the flow Mach number at the point B is not higher than that at the point A. Thus the simple Prandtl-Meyer expansion is not applicable for the three-dimensional

flow existing in the actual machine. It is in fact more realistic to assume that the mean relative Mach number at the blade inlet represents the uniform Mach number ahead of the blade passage shock. Entropy rise across the shock can then be estimated by the normal shock relation given in Reference (45).

$$\Delta S = \frac{R}{J} \frac{2\gamma}{(\gamma+1)^2} \frac{(M_i^2 - 1)^3}{3} \quad (34)$$

SECTION IV
MEAN FLOW EQUATIONS FOR STREAMLINE
CURVATURE COMPUTATIONAL MODEL

In order to study the effect of blade to blade flow variations on the mean flow field of a highly loaded transonic compressor, a computational scheme commonly known as the Streamline Curvature technique was adopted. It is a computational scheme based on the assumption of axially symmetric flow field and requires loss distribution as input from external sources such as cascade data. In its most general form the method consists of writing a single equation of motion in the meridional plane along the direction of computation. For a non-bladed region the direction of computation is normally taken as the radial direction, but for flow field computation at the inlet and outlet to a blade row, the direction of computation is made to coincide with the meridional projection of leading and trailing edges respectively. Since most of the cascade data such as flow angles, losses are known at the blade trailing edge and depend on the conditions at the blade leading edge, the above mentioned procedure of writing the equation along the blade leading and trailing edges increases the accuracy of the computational scheme. This single equation of motion is suitably transformed by expressing radial and axial derivatives in terms of the derivatives in the meridional stream-

line direction and the direction of computation. Streamline curvature enters into the equation through the terms containing radius of curvature and the slope of meridional streamlines. The continuity equation is used along with the momentum equation to fix the constant of integration. References (1,3) have given a detailed description of Streamline Curvature Technique. The aim of this chapter is to re-derive the equations of motion for the Computer program of Reference (1) so that the effect of blade to blade flow variations can be accounted for.

4.1 Basic Equation of Motion in l-Direction

In order to derive the mean flow equation of motion in the Streamline Curvature format, the method adopted is to first transform the mean flow equations of motion in r , θ , and z directions (equations D-1, D-2, and D-3 of Appendix D) to equations of motion in terms of the components of vorticity. These equations are then combined to give a single vector equation which is further modified using Gibbs relation to get a mean flow equation of Crocco's type.

Equation (D-16), a detailed derivation of which is included in Appendix D, has the form

$$\begin{aligned} \overline{\underline{W}} \times (\nabla \times \overline{\underline{V}}) &= \nabla \overline{I} - T \nabla \overline{S} \\ &+ (\hat{r} \Sigma_{r\lambda} + \hat{\theta} \Sigma_{\theta\lambda} + \hat{z} \Sigma_{z\lambda}) - \underline{F}_i - \underline{F}_u \end{aligned} \quad (D-16)$$

In this equation, the effect of blade to blade flow variations enters directly through the terms $(\hat{r} \Sigma_{r\lambda} + \hat{\theta} \Sigma_{\theta\lambda} + \hat{z} \Sigma_{z\lambda})$. The term \underline{F}_i which is the blade force vector originating from the inviscid pressure field of the blade, also enters the equation through the pitchwise averaging process as a jump of pressure across the blade from suction to the pressure surface. Although the usual axisymmetric through flow formulation does include this term as the distributed forces representing the effect of blades, it assumes that blade to blade flow variations are small. The term \underline{F}_v represents the mean viscous force in the fluid and is mainly due to the blade surface friction. Outside the blade row \underline{F}_i does not exist and \underline{F}_v is small.

The equation of motion in the l-direction is derived by taking the scalar product of the vector equation (D-16) with a unit vector in l-direction and using transformation relations for radial and axial derivatives. The final form of Streamline Curvature equation as derived in Appendix D

becomes

$$\left(\bar{v}_m \frac{\partial \bar{v}_m}{\partial l} \right) = \left[\bar{v}_m \frac{\partial \bar{v}_m}{\partial m} \sin(\phi + \gamma) + \frac{\bar{v}_m^2}{r_e} \cos(\phi + \gamma) - \frac{\bar{w}_\theta}{r} \frac{\partial(r\bar{w}_\theta)}{\partial l} - 2\bar{w}_\theta \Omega \cos \gamma + \frac{\partial \bar{l}}{\partial l} - T \frac{\partial \bar{s}}{\partial l} + \Sigma_{r\lambda} \cos \gamma + \Sigma_{z\lambda} \sin \gamma - (F_{mi} + \bar{F}_{mv}) \sin(\phi + \gamma) - (F_{ni} + \bar{F}_{nv}) \cos(\phi + \gamma) \right] \quad (35)$$

Before commenting on this equation, the assumptions made in deriving this equation can be summarized as:

- a) Steady state flow with respect to a coordinate system fixed to the blades.
- b) Pitchwise variation of density and temperature are small.

It may be noted that over bars have not been used for quantities which are assumed to be pitchwise invariant, such as

ξ, T, ϕ, γ etc. The mean slope of the streamline is

$$\tan \phi = \frac{\bar{v}_2}{\bar{u}_2}$$

Equation (35) is the 1-direction pitchwise averaged momentum equation for \bar{v}_m^2 . The Streamline Curvature procedure which begins by laying a mesh in the meridional plane formed by the initially assumed streamlines and fixed axial stations, provides information on ϕ and r_c . Information on other unknown quantities is obtained as follows:

- a) If the mean rothalpy distribution is specified at an upstream station, it can be estimated at the desired station by numerically integrating equation (23) along the meridional streamline, when the heat transfer and viscous effects are small.
- b) Entropy distribution at the desired station is estimated by using the procedure given in Section 3.4.2.

- c) For design problem, \overline{W}_0 distribution is specified at the blade trailing edge. In the interblade region it can be assumed to remain constant along the streamline. For analysis problem \overline{W}_0 can be replaced by the relative flow angle β and meridional velocity \overline{V}_m .
- d) If the value of \overline{V}_m is assumed, temperature can be estimated from rothalpy.
- e) Apparent stresses are estimated from experimental data.

It is thus seen that equation (35) can be integrated numerically along l-direction using an iterative technique, provided $\frac{\partial \overline{V}_m}{\partial m}$ and the blade force terms can be expressed in terms of the known quantities. As mentioned earlier, the constant of integration is provided by the use of continuity equation. Further, since this l-direction equation of motion could be derived without using the θ -direction equation of motion, one may be misled to the conclusion that r and z direction apparent stresses are sufficient to get the final form of the equation of motion. This, however, is not true because θ -direction apparent stresses are indirectly introduced through the θ -direction blade force term \overline{F}_θ which is given by pitchwise averaged θ -direction momentum equation

$$\begin{aligned} \overline{F}_\theta &= \overline{F}_{\theta i} + \overline{F}_{\theta v} \\ &= \frac{\overline{V}_m}{r} \frac{\partial (r \overline{V}_\theta)}{\partial m} + \frac{1}{r} \left\{ \frac{\partial (\overline{W}_r' \overline{W}_\theta' r^2)}{\partial r} + \frac{\partial (\overline{W}_z' \overline{W}_\theta' r^2)}{\partial z} + \frac{\partial (\overline{W}_\tau' \overline{W}_\theta' r^2)}{\partial \tau} \right\} \end{aligned} \quad (36)$$

4.2 Equation of Motion for Computer Program

As seen in the previous section, for the application of equation (35), it is necessary to express the term $\frac{\partial \bar{V}_m}{\partial m}$ and blade force terms in terms of the known quantities. This equation may also require further modifications in order to make it applicable to the analysis problem. Hearsay, whose streamline curvature program¹, will be modified for this investigation, arrived at the desired equation by evaluating $\frac{\partial \bar{V}_m}{\partial m}$ with the aid of continuity equation, and for the blade forces, he adopted the formulation given by Wennerstrom⁷. Equations being derived in this section are kept identical to those given in Reference (1), so that the basic logic of Hearsay's program is not changed. Detailed derivation of only those equations which are changed as a result of pitchwise averaging is included.

4.2.1 Blade Forces

In equation (35) mean (or distributed) force terms in the meridional direction and in a direction perpendicular the meridional direction (in the meridional plane) have been separated into the inviscid blade forces (F_{mi} , F_{ni}) and viscous body forces (\bar{F}_{mv} , \bar{F}_{nv}). If the viscous body forces are considered to result from the blade drag force only, the problem of estimating these forces becomes relatively less cumbersome.

The basic method for evaluating the blade force terms was given by Marble¹³, which was later generalized by Wennerstrom⁷ for any arbitrary direction in the meridional plane.

If the blade surface geometry is known, it is possible to fix the directions of \overline{F}_i and \overline{F}_v . \overline{F}_i which arises as a result of inviscid pressure field of the blade, can be taken as perpendicular to the mean blade surface, and if the mean flow velocity is assumed to be approximately tangential to the mean blade surface, the inviscid blade force will be perpendicular to the relative velocity vector. For evaluating the viscous force \overline{F}_v , it is assumed that this represents blade surface friction and it is assumed to be acting in a direction opposite to the mean relative velocity vector. This in fact is not a realistic assumption for a highly loaded rotor in which the boundary layer fluid may have a significant radial component due to the combined action of centrifugal and coriolis forces. However, in the absence of exact knowledge of boundary layer flow and since the viscous force term is not very important in the momentum equation, the above assumption was retained for this analysis.

Blade Force in the Meridional Direction

With the above assumption and for small variation of temperature and entropy in the pitchwise direction, it can be shown that (for example, see Reference 13)

$$T \bar{v}_m \frac{\partial \bar{S}}{\partial m} = - \frac{\bar{F}_\theta}{\rightarrow} \cdot \frac{\bar{W}}{\rightarrow} \quad (37)$$

Equation (37) requires further investigation but in view of the above discussion, this relation has been retained without any alterations.

From Figure 4, we have $\bar{F}_\theta \cos \beta = \bar{F}_{m\theta}$, $\bar{v}_m = \bar{W} \cos \beta$
Therefore, equation (37) becomes (36)

$$\bar{F}_{m\theta} = -T \frac{\partial \bar{S}}{\partial m} \cos^2 \beta \quad (38)$$

We also find from Figure 4

$$\bar{F}_{mi} = -\bar{F}_{\theta i} \tan \beta \quad (39)$$

But from equation (36)

$$\bar{F}_\theta = \bar{F}_{\theta i} + \bar{F}_{\theta \theta} = \frac{\bar{v}_m}{r} \frac{\partial (r \bar{v}_\theta)}{\partial m} + \Sigma_{\theta r}$$

Combining the above equations, we get

$$\bar{F}_m = \bar{F}_{mi} + \bar{F}_{m\theta} = -\frac{\bar{W} \theta}{r} \frac{\partial (r \bar{v}_\theta)}{\partial m} - T \frac{\partial \bar{S}}{\partial m} - \Sigma_{\theta r} \tan \beta \quad (40)$$

Equation (40) is valid in the bladed region only.

For non-bladed region, $\bar{F}_{\theta i} = 0$ and $\bar{F}_m = \bar{F}_{m\theta}$ which can be assumed to represent internal fluid friction.

This is given by

$$\bar{F}_m = -T \frac{\partial \bar{S}}{\partial m} \cos^2 \beta \quad (41)$$

However, if the friction is limited to the blade surface only then in the non-bladed region both \bar{F}_{m_i} and \bar{F}_{m_u} will vanish.

Blade Force in a Direction Perpendicular to the Meridional Direction

Since \bar{F}_r is assumed to be parallel to the meridional streamline, $\bar{F}_{nr} = 0$

$$\therefore \bar{F}_n = \bar{F}_{n_i}$$

A detailed derivation of F_{n_i} is given in Reference (7). Combining equations (25) and (27) of Reference (7), we get

$$\bar{F}_n = \left\{ \frac{\bar{F}_\theta}{\cos \epsilon \cos \beta} + \frac{\sin \beta}{\cos \epsilon} T \frac{\partial \bar{S}}{\partial m} \right\} \times \left\{ \sin \beta \tan(\phi + \gamma) \cos \epsilon + \cos \beta \sin \epsilon \sec(\phi + \gamma) \right\} \quad (42)$$

Here $(\phi - \gamma)$ has been changed to $(\phi + \gamma)$ since γ represents blade trailing edge location in Figure (1) of Reference (7).

Equation (42) can be transformed to the apparent stress format by using equation (36), thus

$$\bar{F}_n = \left\{ \sec \epsilon \sec \beta \left(\frac{\bar{v}_m}{r} \frac{\partial (r \bar{v}_\theta)}{\partial m} + \Sigma_\theta \right) + \sin \beta \sec \epsilon T \frac{\partial \bar{S}}{\partial m} \right\} \times \left\{ \sin \beta \tan(\phi + \gamma) \cos \epsilon + \cos \beta \sin \epsilon \sec(\phi + \gamma) \right\} \quad (43)$$

4.2.2 Equation for Meridional Velocity Gradient

The gradient $\frac{\partial \bar{v}_m}{\partial m}$ is eliminated from equation (35) through the use of continuity equation.

Using the transformation relation

$$\frac{\partial}{\partial z} = \left(\sin \phi \frac{\partial}{\partial l} - \cos r \frac{\partial}{\partial m} \right) / \left(\sin \phi \sin r - \cos \phi \cos r \right) \quad (D-21)$$

and the geometric relationship $\frac{\partial \phi}{\partial m} = -\frac{1}{r_c}$ the following relation can be derived with some algebraic manipulation

$$\begin{aligned} \frac{\partial \bar{v}_m}{\partial m} &= \frac{\sin \phi}{\cos r} \frac{\partial \bar{v}_m}{\partial l} + (1 - \tan \phi \tan r) \frac{\partial \bar{v}_z}{\partial z} \\ &+ \frac{\bar{v}_m \tan \phi}{r_c} - \frac{\bar{v}_m \sin^2 \phi \cos \phi}{\cos r} \frac{\partial (\tan \phi)}{\partial l} \end{aligned} \quad (44)$$

The term $\frac{\partial \bar{v}_z}{\partial z}$ is now eliminated with the aid of continuity equation. Although, the axisymmetric system represents a blade free space, it is expedient to recognize at this point the possibility of blockage due to blades. It is considered as a distributed blockage to avoid a conflict with the condition of axial symmetry.

Denoting blockage by $\bar{\lambda}$, we can write open area as

$$\lambda = (1 - \bar{\lambda})$$

For the axisymmetric model with distributed blockage, the mean flow continuity equation is written as

$$\frac{\partial (r \lambda \bar{v}_r)}{\partial r} + \frac{\partial (r \lambda \bar{v}_z)}{\partial z} = 0 \quad (45)$$

This equation is converted into the following suitable form for $\frac{\partial \bar{v}_z}{\partial z}$, with the aid of transformation relation (D-20)

$$\begin{aligned}
 -\frac{\partial \bar{v}_z}{\partial z} = & \frac{\bar{v}_m}{\rho} \frac{\partial \rho}{\partial m} + \frac{\bar{v}_m \sin \phi}{r} + \frac{\bar{v}_m}{\lambda} \frac{\partial \lambda}{\partial m} + \frac{\sin \phi}{\cos r (1 - \tan \phi \tan r)} \frac{\partial \bar{v}_m}{\partial l} \\
 & - \frac{\tan r \tan \phi}{(1 - \tan \phi \tan r)} \frac{\partial \bar{v}_m}{\partial m} + \frac{\bar{v}_m \cos^3 \phi}{\cos r (1 - \tan \phi \tan r)} \frac{\partial (\tan \phi)}{\partial l} \\
 & - \frac{\tan r \bar{v}_m}{(1 - \tan \phi \tan r) r}
 \end{aligned} \tag{46}$$

It is seen from equation (46) that we have still to eliminate the meridional derivative of density from the first term in the right hand side of equation (46). It may be noted here that although meridional variation of density gradient is permitted, the pitchwise variation of density has been assumed to be small.

The term $\frac{1}{\rho} \frac{\partial \rho}{\partial m}$ is obtained from $\frac{1}{\rho} \frac{\partial \bar{p}}{\partial m}$ by using Second Law of Thermodynamics and the equation of state.

$\frac{1}{\rho} \frac{\partial \bar{p}}{\partial m}$ is obtained by deriving mean flow equation of motion in the meridional direction, a detailed derivation of which is given in Appendix D.

Equation (D-31) of Appendix D is

$$\begin{aligned}
 \frac{1}{\rho} \frac{\partial \rho}{\partial m} = & \frac{M_m^2}{\bar{v}_m^2} \left\{ \frac{\bar{v}_\theta^2}{r} \sin \phi - \bar{v}_m \frac{\partial \bar{v}_m}{\partial m} - \frac{W_\theta}{r} \frac{\partial (r \bar{v}_\theta)}{\partial m} \right\} \\
 & + \frac{M_m^2}{\bar{v}_m^2} \left\{ \sum_{\theta} \tan \beta - (\sum_{r} \sin \phi + \sum_z \cos \phi) \right\} - \frac{J}{R} \frac{\partial S}{\partial m}
 \end{aligned} \tag{47}$$

Substituting $\frac{1}{\rho} \frac{\partial \rho}{\partial m}$ from equation (47) into equation (46), and then substituting $-\frac{\partial \bar{v}_z}{\partial z}$ from (46) into (44), we get after some algebraic manipulation an expression for $\frac{\partial \bar{v}_m}{\partial m}$, given as

$$\begin{aligned}
 \frac{\partial \bar{v}_m}{\partial m} (1 - \bar{M}_m^2) = & \frac{\bar{v}_m (\tan \phi + \tan \tau)}{r (1 - \tan \phi \tan \tau)} - \frac{\bar{v}_m \cos \phi}{\cos \tau (1 - \tan \phi \tan \tau)} \frac{\partial (\tan \phi)}{\partial t} \\
 & - \frac{\bar{v}_m \sin \phi}{r} - \frac{\bar{v}_m}{\lambda} \frac{\partial \lambda}{\partial m} + \frac{\bar{v}_m}{R} \frac{\partial S}{\partial m} \\
 & - \frac{\bar{M}_m^2}{\bar{v}_m} \left\{ \frac{\bar{v}_0^2 \sin \phi}{r} - \frac{\bar{w}_0}{r} \frac{\partial (\tau \bar{v}_0)}{\partial m} \right\} \\
 & - \frac{\bar{M}_m^2}{\bar{v}_m} \left\{ \sum_{\theta, \lambda} \tan \beta - (\sum_{r, \lambda} \sin \phi + \sum_{z, \lambda} \cos \phi) \right\} \quad (48)
 \end{aligned}$$

This is the equation for the meridional velocity gradient.

4.2.3 Analysis-Type Momentum Equation for Computer Program

To get the final form of mean flow equation of motion in 1-direction suitable for computer program, $\frac{\partial \bar{v}_m}{\partial m}$ and the blade force terms are eliminated from equation (35) by using equations (48), (40), and (43).

This gives after some algebraic manipulation

$$\begin{aligned}
\bar{V}_m \frac{\partial \bar{V}_m}{\partial l} = & \frac{\bar{V}_m^2}{r_c} \frac{\left\{ \frac{1 - \cos^2(\phi+r) M_m^2}{\cos(\phi+r)(1-M_m^2)} \right\}}{(1-M_m^2)} - \frac{\bar{V}_0}{r} \frac{\partial(r \bar{V}_0)}{\partial l} - 2 \Omega \bar{V}_0 \cos r + g J T \frac{\partial \bar{S}}{\partial l} \\
& + g J \frac{\partial \bar{I}}{\partial l} + \frac{\bar{V}_m}{r} \frac{\partial(r \bar{V}_0)}{\partial m} \left\{ \frac{M_m}{(1+M_m^2)} \tan \beta \sin(\phi+r) - \tan \xi \right\} \\
& - \frac{\bar{V}_m^2}{(1-M_m^2)} \tan(\phi+r) \frac{\partial \phi}{\partial l} - \frac{\bar{V}_m \sin(\phi+r)}{(1-M_m^2)} \left\{ \frac{\sin \phi (1-M_m^2 \tan^2 \phi)}{r} + \frac{1}{\lambda} \frac{\partial \lambda}{\partial m} \right\} \\
& + g J T \frac{\partial \bar{S}}{\partial m} \left\{ \sin(\phi+r) (\cos^2 \beta + \frac{r M_m^2}{(1-M_m^2)}) - \tan \xi \sin \beta \cos \beta \right\} \\
& + \frac{M_m}{(1-M_m^2)} \sin(\phi+r) \left\{ \sum_{r\lambda} \sin \phi + \sum_{z\lambda} \cos \phi \right\} \\
& - \left(\tan \xi - \frac{M_m}{(1-M_m^2)} \sin \phi \tan \beta \right) \sum_{\theta\lambda} + \sum_{r\lambda} \cos r + \sum_{z\lambda} \sin \lambda
\end{aligned} \tag{49}$$

The final form of this equation in the bladed region, suitable for the analysis problem can now be arrived at. This is given as

$$\begin{aligned}
\frac{\partial \bar{V}_m^2}{\partial l} (1 + \tan^2 \beta) &= \frac{\bar{V}_m^2}{r_c} \frac{(1 - \cos(\phi+r)) \bar{M}_m^2}{\cos(\phi+r)(1 - \bar{M}_m^2)} - \frac{\bar{V}_m^2 \tan \beta}{r_c} \frac{\partial(\tau \tan \beta)}{\partial l} - 2 \Omega \bar{V}_m \tan \beta \cos \tau \\
&- g J \frac{\partial \bar{I}}{\partial l} - g J T \frac{\partial \bar{S}}{\partial l} + g J T \frac{\partial \bar{S}}{\partial m} \left\{ \sin(\phi+r) \left(\cos^2 \beta + r \frac{\bar{M}_m}{\bar{M}_m^2} \right) \right. \\
&- \left. \sin \beta \cos \beta \tan \varepsilon \right\} - \frac{\bar{V}_m^2}{(1 - \bar{M}_m^2)} \sin(\phi+r) \left\{ \frac{\sin \phi}{r} (1 - \bar{M}_m^2) (\tan \beta + \frac{\tau \Omega}{\bar{V}_m}) \right. \\
&+ \left. \frac{1}{\lambda} \frac{\partial \lambda}{\partial l} \right\} + \frac{\bar{V}_m}{r} \frac{\partial(\tau \bar{V}_0)}{\partial m} \left\{ \frac{\bar{M}_m}{(1 - \bar{M}_m^2)} \sin(\phi+r) \tan \beta - \tan \varepsilon \right\} \\
&- \frac{\bar{V}_m}{(1 - \bar{M}_m^2)} \tan(\phi+r) \frac{\partial \phi}{\partial l} + \left(\frac{\bar{M}_m}{1 - \bar{M}_m^2} \right) \sin(\phi+r) \sin \phi + \cos \tau \times \\
&\frac{1}{\lambda} \left(\frac{\partial(\lambda \bar{W}_E^2)}{\partial \tau} + \frac{\partial(\bar{W}_E \bar{W}_E')}{\partial Z} + \frac{\lambda \bar{W}_E^2 - \lambda \bar{W}_E'^2}{r} \right) + \left(\frac{\bar{M}_m}{1 - \bar{M}_m^2} \right) \sin(\phi+r) (\cos \phi + \sin \tau) \times \\
&\frac{1}{\lambda} \left(\frac{\partial(\lambda \bar{W}_E^2)}{\partial \tau} + \frac{\partial(\lambda \bar{W}_E'^2)}{\partial Z} + \frac{\lambda \bar{W}_E \bar{W}_E'}{r} \right) + (\tan \beta \sin(\phi+r)) \frac{\bar{M}_m}{(1 - \bar{M}_m^2)} - \tan \varepsilon \times \\
&\frac{1}{\lambda} \left(\frac{\partial(\bar{W}_E \bar{W}_E')}{\partial \tau} + \frac{\partial(\bar{W}_E' \bar{W}_E')}{\partial Z} + \frac{2 \lambda \bar{W}_E \bar{W}_E'}{r} \right)
\end{aligned} \tag{50}$$

Note: In the actual computation, the terms containing $\frac{\partial \rho}{\partial x_i}$ were neglected as compared to the terms containing $\frac{\partial \bar{W}_E \bar{W}_E'}{\partial x_i}$.

This equation will be used for computing the flow field of the MIT Blowdown Compressor rotor. A few important clarifications about this equation are as follows:

- a) Equation (50) is applicable for the analysis problem within the blade row only. For the unbladed region where the relative flow angles are not specified and where all blade related information such as blade forces, λ , ξ are nonexistent, this equation is suitably modified and it takes the format suitable for design problem.
- b) Although $r \bar{v}_\theta$ is not specified for this equation, it is found from the knowledge of β , blade velocity and the assumed value of \bar{v}_m .
- c) Whereas the mean axial and radial velocities have been expressed in terms of the mean meridional velocity, the velocity correlations (apparent stresses) have been retained as the products of the axial and the radial velocity fluctuations. This is because the experimental data available for testing this formulation could provide velocity fluctuations in the radial, axial and the azimuthal directions only. The radial derivative of the apparent stresses has also been retained for the same reason. The axial derivative of the apparent stresses can, however, be transformed to the radial

and the meridional derivatives by using the relation

$$\frac{\partial}{\partial m} = \sin \phi \frac{\partial}{\partial r} + \cos \phi \frac{\partial}{\partial z} \quad (51)$$

- d) The mean rothalpy gradient $\frac{\partial \bar{I}}{\partial l}$ is estimated with the aid of equation (23).
- e) The entropy gradients $\frac{\partial \bar{s}}{\partial l}$ and $\frac{\partial \bar{s}}{\partial m}$ in this equation are estimated from the cascade data and from the entropy production model as formulated in Section III.
- f) It is also observed that the effect of radial direction apparent stress is greatest because the effect of pitchwise and axial apparent stresses are scaled down due to the small multiplication factor. This is reasonable since the l-direction momentum equation approximately represents an r-direction momentum equation.

SECTION V

CRITICAL ANALYSIS OF THE EXPERIMENTAL DATA

The experimental data adopted for the verification of the flow model formulated in the preceding chapters, was taken from the MIT Blowdown Compressor test facility. Time resolved data on fluctuating pressures had been recorded by Thompkins² behind a highly loaded transonic rotor with the aid of a four diaphragm probe. The data which was digitized every 5 μ secs provided the instantaneous values of the three components of flow Mach number (M_r, M_θ, M_z) and pressure at different radial locations and at two axial stations. These axial stations were situated at 0.1 and 1.0 chords downstream of the rotor blade trailing edge. This data was recorded with respect to an absolute frame of reference.

For the estimation of instantaneous flow velocities from Mach numbers, it is necessary to know static temperature which was not measured. The static temperature was estimated by assuming the Euler Turbine Equation is valid and can be expressed in the following form for the estimation of total temperature ratio across the rotor.

$$\frac{T_{t_2}}{T_{t_1}} = 1 + M_T (r-1) \left(\frac{r}{r_T}\right) M_{\theta_2} \left(1 + \frac{r-1}{2} M_z^2\right)^{-\frac{1}{2}} \left(\frac{T_{t_2}}{T_{t_1}}\right)^{\frac{1}{2}} \quad (52)$$

Here subscripts 1, 2 and T refer to rotor inlet and outlet conditions, and blade tip condition.

In order to make the results representative of usual compressor tests, the inlet conditions were standardized to $T_{t_1} = 520.0^\circ R$, $P_{t_1} = 14.7 \text{ lb}_f \text{ in}^{-2}$, and $R = 53.3 \text{ ft lb}_f / \text{lb}_m \text{ }^\circ R$. The choice of these values at the inlet result only in multiplication of all the terms in the momentum equation by a constant factor, the relative magnitude of these terms remaining unchanged.

The procedure adopted for estimating the distribution of velocity correlations (apparent stresses) $\overline{v_x'^2}$, $\overline{v_\theta'^2}$, $\overline{v_z'^2}$, $\overline{v_x'v_\theta'}$, $\overline{v_x'v_z'}$, $\overline{v_\theta'v_z'}$ involved two steps. These are:

- a) Computation of the time averaged values of each component of velocity.
- b) Computation of the products of fluctuating quantities at each instant and then time averaging the products to obtain the apparent stresses.

Two points may be noted. Firstly, the correlations of the absolute velocity fluctuations are identical to those of the relative velocity fluctuations. Secondly, the time averaged flow with respect to the absolute frame of reference is equivalent to the pitchwise averaged flow with respect to a frame of reference fixed to the blades.

Computations were made of the following quantities, at several different radial locations and at two axial stations

- a) Mean velocity components $\overline{v_r}, \overline{v_\theta}, \overline{v_z}$
- b) Apparent stresses $\overline{v_z' v_z'}, \overline{v_r' v_\theta'}, \overline{v_z' v_\theta'}, \overline{v_z'^2}, \overline{v_\theta'^2}$
and $\overline{v_z'^2}$
- c) Static pressure ratio $\overline{P_{s2}}/P_t$
- d) Mean entropy change across the rotor.

In computing the mean values, a number of different averaging intervals were used. Averages over one blade passing period were first constructed, with the averaging interval beginning at several different points of the blade passing period. If the flow were truly periodic with blade passing, that is steady in rotor coordinates, the mean values should be independent of the averaging interval so long as it covered one complete blade passing period. In fact the averages varied strongly with the location of the interval, indicating that the flow is quite unsteady in the rotor coordinates. Averages were then taken over two and three blade passing periods starting from the first data point.

Finally, averages were taken over five full blade passing periods, the maximum available in digital form, and these values will be interpreted as true means. The scatter from these means will be taken as a measure of the unsteadiness in the rotor coordinates.

5.1 Mean Velocities

The mean velocities $\overline{v_\theta}$, $\overline{v_z}$ and $\overline{v_r}$ at the port 5 location, which is just 0.1 chord downstream of the rotor

trailing edge are shown in Figures 5 and 6. The mean over five blade passing periods is indicated by circular points through which the curve has been drawn. The scatter from this mean, of the values averaged over one, two and three blade passing periods, is also shown. In all the figures from Figure 5 through 21, plus (+), square (\square), triangle (Δ) and circle (o) represent means over one, two, three and five blade passing periods respectively. In some of these figures symbols θ , ψ and $*$ have also been used. These symbols refer to means over one blade passing period but starting at different points of the recorded data. It is seen that the scatter is small in the inner part of the annulus, very large at $r/r_t = 0.87$, decreases for some distance towards the casing and then becomes quite large near the casing. The large scatter near $r/r_t = 0.87$ which was first noted by Thompkins², could be due to a vortex shed from the rotor blade near the termination point of the shock on the suction surface. This view is supported by the fact that the variations in $\overline{v_z}$ are much smaller than those in $\overline{v_\theta}$ and $\overline{v_r}$.

Figures 7 and 8 give the average values of $\overline{v_\theta}$, $\overline{v_z}$ and $\overline{v_r}$ at the port 6 location, which is one chord downstream of the rotor trailing edge. The scatter is comparatively reduced, and the very large $\overline{v_\theta}$ near the tip has decayed. There is also a general upward shift in $\overline{v_\theta}$ in the inner part of the annulus, and a uniform upward shift in $\overline{v_z}$

between port 5 and port 6. The data at the two locations were derived from two separate tests, and this shift is tentatively attributed to a zero shift problem in the pressure transducers. Thus, only the shape of the curves at the two stations should be compared. This radial variation of both \overline{v}_0 and \overline{v}_z does not change very much with distance downstream.

The mean radial velocity \overline{v}_z shows an erratic behavior at port 5 and this is attributed to a possible flow separation near the hub, and shock-boundary layer interaction in the vicinity of radius ratio 0.87. No reasonable explanation can be given for the observed steep rise of \overline{v}_z near the casing. This is attributed to the flow disturbance generated by the cavity which houses the probe. At port 6, however, the erratic behavior of \overline{v}_z has considerably diminished.

5.2 Apparent Stresses

5.2.1 Apparent Stress, $z/c = 0.1$

The apparent shear stresses, $\overline{v_z' v_z'}$, $\overline{v_z' v_\theta'}$, and $\overline{v_\theta' v_\theta'}$ are shown in Figures 9, 10, and 11 for the port 5 location, immediately behind the rotor. Here again the five blade passing period means are shown by the circular points, and the scatter from this mean is shown by other point symbols (listed in Section 5.1). Several points should be noted. First, the scatter is quite small at $r/r_t = 0.78$, very large at $r/r_t = 0.87$, and moderate near the hub and the

casing. Secondly, the apparent shear stresses $-\rho \overline{v_i' u_j'}$ would be of the order of $15 \text{ lb}_f \text{ ft}^{-2}$ if the compressor had operated in ambient air, and hence are fairly small compared to the pressure. On the other hand there appear to be rather steep gradients in the stresses, so their effect may be significant nevertheless.

The apparent normal stresses $\overline{v_i'^2}$, $\overline{v_\theta'^2}$ and $\overline{v_z'^2}$ which are plotted in Figures 12, 13, and 14, are much larger than the apparent shear stresses, and also show larger scatter, particularly near $r/r_t = 0.87$. Taking mean values over five blade passing periods as representative, it is observed that there are very large gradients of $\overline{v_z'^2}$ and $\overline{v_\theta'^2}$ near this radius. For example, the change of $\overline{v_z'^2}$ from nearly zero to $30,000 \text{ ft}^2/\text{sec}^2$ between $r/r_t = 0.8$ and 0.87 yields an effective pressure gradient of the order of $1000 \text{ lb}_f/\text{ft}^2$ per unit radial distance, or in other terms half the static pressure per compressor radius. An alternate way of assessing the order of magnitude of the term $\frac{\partial \overline{v_z'^2}}{\partial r}$ is to compare it with the centrifugal force $\frac{\overline{v_\theta'^2}}{r}$ which approximately balances the radial pressure gradient. A plot of $\frac{\partial \overline{v_z'^2}}{\partial r} / \frac{\overline{v_\theta'^2}}{r}$ vs r/r_t is shown in Figure 12a. From this figure we find that the magnitude of $\frac{\partial \overline{v_z'^2}}{\partial r}$ which is an important apparent stress term in the 1-direction momentum equation, can become four times that of the centrifugal force term $\frac{\overline{v_\theta'^2}}{r}$. Therefore, unless the effect of

the radial normal apparent stress is nullified by the other apparent stresses, it will play a role comparable to the centrifugal force at several radial locations.

5.2.2 Apparent Stresses $z/c = 1.0$

As can be seen from Figures 15, 16, and 17, the apparent shear stresses do not decrease very much between $z/c = 0.1$ and $z/c = 1.0$, but there is a large change in the radial distribution of stresses. This is consistent with the tentative conclusion of Reference (37), that the flow is evolving to a rotor wake structure controlled by the swirl eigen modes of the duct. The apparent normal stresses which are plotted in Figures 18, 19, and 20 are again seen to be much larger than the apparent shear stresses.

5.3 Static Pressure

The distribution of mean static pressure divided by the inlet stagnation pressure $\bar{p}_{s2}/\bar{p}_{t1}$ is shown in Figure 21 for $z/c = 0.1$ and $z/c = 1.0$. The general trend is a decrease in the downstream direction, which is consistent with the increase in \bar{v}_z . A low pressure at $r/r_t = 0.87$ directly behind the rotor is probably associated with the strong vortex which is conjectured at that radius, and which is also considered as an explanation for the large $\bar{v}_z'^2$ and $\bar{v}_\theta'^2$ at that radial location.

5.4 Entropy Distribution

The distribution of mean entropy rise ($\Delta \bar{S}$) was estimated by first finding the instantaneous entropy rise ΔS with the aid of the following equation, and then carrying out the time averaging.

$$\frac{\Delta S}{C_v} = \ln \left\{ \left(\frac{p_{t_2}}{p_{t_1}} \right)^{(1-\gamma)} \left(\frac{T_{t_2}}{T_{t_1}} \right)^\gamma \right\} \quad (53)$$

The value of $\frac{p_{t_2}}{p_{t_1}}$ is known from the experimental data, and $\frac{T_{t_2}}{T_{t_1}}$ is calculated from equation (52).

A plot of $\frac{\Delta \bar{S}}{C_v}$ vs r/r_t for port 5 is shown in Figure 22. The negative values of $\frac{\Delta \bar{S}}{C_v}$ between the radius ratios of 0.7 and 0.85 are confusing since the entropy change being estimated, has been treated as a thermodynamic property which must increase unless heat transfer takes place from the midspan region towards the hub and the casing.

In the absence of any logical explanation, this unrealistic entropy distribution was attributed to the zero shift in the pressure transducer. The corresponding plot for port 6 which is seen in Figure 23, does not show this anomaly, so that the zero shift problem is mainly associated with measurements at port 5. It is also seen that towards the casing the value of $\frac{\Delta \bar{S}}{C_v}$ for port 5 suddenly becomes very large, even larger than that at the corresponding location of port 6. This again conflicts with the concept of entropy change along a streamline and indicates that either the use of Euler Turbine equation is not justified or the experimental data near the casing is not reliable.

SECTION VI
COMPUTER PROGRAM

As mentioned in Section I, one of the objectives of this investigation is to modify a computer program based on the Streamline Curvature Computational technique, so that the effect of blade-to-blade flow variations can be accounted for while computing the mean flow field of an axial flow compressor. The basic computer program chosen for the purpose has been developed by Hearsey,¹ and is one of the most versatile and complete programs for application to a design or an analysis problem. Before describing the modifications introduced in this program, it is considered desirable to outline some of its important features and the computational logic adopted for it. This section gives a general description of the computing routine for an analysis problem, the overall logic of Hearsey's program, and the modifications introduced in the basic program to account for blade-to-blade flow variations. A brief description of the logic used for estimating the experimental flow from the data of Ref. 2 has also been included towards the end of this section.

6.1 General Description of Computing Routine for the Analysis Problem
(Not Including the Effect of Pitchwise Flow Variations)

6.1.1 Input Data

In order to solve an analysis problem by the Streamline Curvature Computational technique the following input data is required for a multistage axial flow compressor.

- a) Axial location and orientation of each computing station: Generally, a number of computing stations

are located at strategic points in the flow and preferably, but not necessarily, close to orthogonal to the local meridional streamline direction.

Typically, several stations are situated upstream of the first blade row. Additionally, stations may be placed within the blade row.

- b) Geometric details in respect of hub, casing and the blading.
- c) Mass flow rate and rpm.
- d) Inlet conditions such as pressure and temperature.
- e) Distribution of losses through the blade row: If the losses are to be specified on the basis of cascade data, their distribution need not be included in the input data. An additional routine can be introduced in the main program which first calculates 'D' factor and then losses from the inbuilt curves. These inbuilt curves give losses as a function of 'D' factor and radial location of the meridional streamline.
- f) The number of streamlines to be used in the computation: Generally, the location of streamlines which is computed by the program, is based on the fixed percentage of the total mass flow through each streamline. However, if it is required to concentrate more streamlines in any particular region, it can be achieved by prespecifying different percentages of the total mass flow through the individual streamtubes.

Hearsey's program has a provision for 30 axial computing stations and 21 streamlines.

6.1.2 The Overall Solution Procedure

The overall solution procedure corresponding to the input data of Section 6.1.1, can be described by the following sequence of steps:

- a) The first step in the computing process is to form a computational mesh by the intersection of the fixed axial stations with the meridional streamlines, henceforth referred to as streamlines. The initial placement of the streamlines is achieved by dividing the annulus area in accordance with the number of streamtubes.
- b) Having chosen the initial locus of each streamline, the program establishes the radius of curvature (r_c) and the slope (ϕ) of each streamline at the computing mesh points by using the standard finite difference format

$$\phi_I = \frac{1}{2} \left\{ \tan^{-1} \left(\frac{r_{I+1} - r_I}{z_{I+1} - z_I} \right) + \tan^{-1} \left(\frac{r_I - r_{I-1}}{z_I - z_{I-1}} \right) \right\} \quad (54)$$

$$\frac{1}{r_c} = \frac{\left\{ \tan^{-1} \left(\frac{r_{I+1} - r_I}{z_{I+1} - z_I} \right) - \tan^{-1} \left(\frac{r_I - r_{I-1}}{z_I - z_{I-1}} \right) \right\} \times 2}{(m_{I+1} - m_{I-1})} \quad (55)$$

- c) Now the first iterative pass begins. During each iterative pass the computation of the flow field is carried out at all the stations, starting at the first computing station and proceeding to the last. The position of streamlines during a pass is not changed. At the end of each pass the streamlines are relocated by iterative process, and the new position of the streamlines is used for the next pass. The details of calculations involved during any computing pass are described in the next few steps. As an example, the computing station will be taken at the exit of the rotor.
- d) Before computing the flow field at the rotor exit during any pass, the flow field at the upstream station is computed. This means that the values of velocities, pressure, entropy, etc. are already known along all the streamlines at the rotor inlet which can be designated as (I-1)th station. To start with, distribution of V_m is assumed at the Ith station. These values are normally taken as those obtained from the previous pass ((n-1)th pass). With the assumed values of V_m and the given values of β at each mesh point, the values of V_θ can be estimated using the relation

$$V_\theta = V_m \tan \beta + r \Omega \quad (56)$$

Now, from the assumption of constant rothalpy along the streamline, the total enthalpy at the rotor exit can be calculated.

$$\underbrace{H(I-1) - r\Omega v_{\theta}(I-1)}_{\text{known at the rotor inlet}} = \underbrace{H(I) - r\Omega v_{\theta}(I)}_{\text{from equation (56)}} \quad (57)$$

- e) With total enthalpy and total velocity known, static enthalpy and thus the flow Mach number can be immediately found. The entropy distribution is found directly from the specified losses, or these losses are calculated by estimating the 'D' factor and then using one of the "loss vs. 'D' factor" curves built into the computer program. Thus all the quantities required for integrating the momentum equation (50) are known.
- f) Using the midstreamline velocity value as a starting point (i.e. as an integration constant), the momentum equation (50) is solved in a stepwise fashion, giving new values of velocities for the inner and the outer halves of the annulus. Once the new values of velocities are known at all the mesh points of the Ith station, it is possible to estimate the new values of static enthalpy and therefore temperature. Finally, the density distribution is estimated by estimating the pressure with the aid of specified losses.

- g) With known density distribution, total mass flow through the annulus is computed and compared with the given value of mass flow. (It may be noted that the mass flow through the individual streamtubes is not compared at this point.) In general the computed mass flow will not equal the actual mass flow. The midstreamline velocity is increased or decreased as required, and the process is repeated until continuity is satisfied. It is thus seen that the simultaneous solution of momentum and continuity equations is an iterative process.
- h) Continuity is now applied for each streamtube. In general the streamtubes will not contain their proper percentages of mass flow. The computer determines, and stores an error function for streamline location.
- i) The information regarding velocities, angles, Mach number, etc., at the rotor exit is now available. The flow field at the next downstream station can therefore be computed. In the interblade region, angular momentum (or total enthalpy) and entropy are assumed to remain constant along the streamlines.
- j) The above process is continued to the last computing station. The previously determined streamline location error functions are now simultaneously applied to redefine the entire streamline pattern

at all the stations, and the next iterative pass begins. Convergence is achieved when the change in the flow field is within a specified limit for two consecutive passes.

The logic of Hearsey's Computer Program is given in Figure 24. Here it has been assumed that the losses have been given as input. A detailed description of the program is given in References (1,3,6).

6.2 Modified Streamline Curvature Program

In order to modify the original Streamline Curvature program to account for blade to blade flow variations, five additional subroutines are introduced. The basic logic of the original program was retained without any alteration. The process of modification is centered around estimating Rothalpy variation and Entropy production along the meridional streamline due to pitchwise flow fluctuations, and introducing apparent stress terms in the l-direction equation of motion. Necessary input variables are introduced to study the effect of the above phenomena individually or in any desired combination. These subroutines can only be called from "overlay UD0308" corresponding to NEQN=0 (Reference 1). No provision is made for calling these subroutines from "overlay UD0326". Terms representing blade thickness ($\frac{\partial \lambda}{\partial x_i}, \frac{\partial \rho}{\partial x_i}$ etc.) appearing in equation (50) were also not introduced in these subroutines. Necessary comment cards giving the basic function of the subroutines, list of variables, and

other relevant details have been introduced. Some of the details in respect of these subroutines are as follows:

a) Subroutine CORDTA

This subroutine reads the velocity correlation data at all the stations and finds the cubic splinefit coefficients with the aid of subroutine SPLINE. These coefficients are stored for estimation of velocity correlations and their derivatives at the mesh points. Velocity correlation data which these subroutines read is generated in a separate program EXPTL FORTRAN from the time resolved experimental data. This subroutine is called by specifying input variable NCOR = 1.

b) Subroutine SPLINE

This subroutine calculates the coefficients for cubic splinefit from the input data on velocity correlations.

c) Subroutine ROEN 1

This subroutine estimates the distributions of Rothalpy and Entropy associated with blade to blade flow fluctuations. This is done by integrating $(\frac{\partial I}{\partial m})_{app}$ and $(T \frac{\partial S}{\partial m})_{app}$ along the meridional streamline, the constant of integration being evaluated from the known value of rothalpy (or apparent Entropy) at the upstream station.

Values of $\frac{\partial I}{\partial l}$, $T \frac{\partial S}{\partial m}$, and $T \frac{\partial S}{\partial l}$ are also estimated for use in the momentum equation (50).

This subroutine is called by specifying input variable NROEN = 1.

d) Subroutine ROEN

This subroutine calculates $(\frac{\partial I}{\partial m})_{app}$ and $(T \frac{\partial S}{\partial m})_{app}$ with the aid of equations (23) and (33) respectively. Apparent stress terms and their radial derivatives are computed by using the cubic splinefit coefficients generated in subroutine CORDTA.

Axial derivatives of apparent stresses are calculated by first estimating the meridional derivatives and then using the relation

$$\frac{\partial F}{\partial z} = \left[\frac{\partial F}{\partial m} - \sin \phi \frac{\partial F}{\partial r} \right] / \cos \phi \quad (58)$$

Meridional derivative of any quantity can be calculated by using the standard finite difference approximation

$$\frac{\partial F}{\partial m} = \left(\frac{F_{I+1} - F_I}{m_{I+1} - m_I} + \frac{F_I - F_{I-1}}{m_I - m_{I-1}} \right) / 2.0 \quad (59)$$

If input variable NROTH = 1, $(\frac{\partial I}{\partial m})_{app}$ is calculated, otherwise $(\frac{\partial I}{\partial m})_{app}$ is taken equal to zero. Similarly, if input variable NENTR is not equal to 1, $(T \frac{\partial S}{\partial m})_{app}$ is taken to be zero.

e) Subroutine WATRAN

This subroutine calculates apparent stress terms appearing in the pitchwise averaged 1-direction momentum equation (50). Cubic splinefit coefficients generated in subroutine CORDTA are used to estimate apparent stresses and their derivatives at various mesh points. The procedure for calculating these derivatives is the same as that described for subroutine ROEN 2. This subroutine is called by specifying input variable NWAT = 1.0 .

The logic of the above subroutines and their interaction with the main program is given in Figure 25.

6.3 Computation of Mean Flow Quantities and the Apparent Stresses from the Experimental Data

The program named EXPTL FORT follows the following sequence of steps for estimating mean flow quantities and the apparent stresses.

- (i) Read experimental data on the instantaneous values of Mach numbers Mr_2 , $M\theta_2$, Mz_2 , at static pressure at different radial locations. Read other input data such as inlet total temperature and pressure.
- (ii) First of all the total temperature ratio is determined by using the Euler Turbine equation in the following form:

AD-A076 204

MASSACHUSETTS INST OF TECH CAMBRIDGE GAS TURBINE AND--ETC F/G 21/5
BOUNDARY LAYER AND WAKE MODIFICATIONS TO COMPRESSOR DESIGN SYST--ETC(U)
MAR 79 A K SEHRA F33615-76-C-2118

UNCLASSIFIED

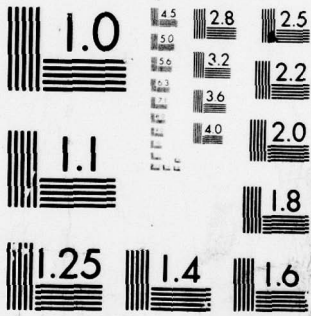
GT/PDL-144

AFAPL-TR-79-2010

NL

2 of 3
AD
A07820b





MICROCOPY RESOLUTION TEST CHART
NATIONAL BUREAU OF STANDARDS-1963-A

$$\frac{T_{t_2}}{T_{t_1}} = 1 + (M_T)(\gamma-1) \left(\frac{r}{r_T}\right) M_{\theta_2} \left(1 + \frac{\gamma-1}{2} M_2^2\right)^{-\frac{1}{2}} \left(\frac{T_{t_2}}{T_{t_1}}\right)^{\frac{1}{2}} \quad (60)$$

where M_T is the rotor tip Mach number and

$$M_2 = \sqrt{M_{\theta_2}^2 + M_{\theta}^2 + M_z^2}$$

(iii) With Tt_1 known, Tt_2 and Ts_2 can be estimated.

Instantaneous values of the velocity of sound and the flow velocities are now estimated at different radial locations.

(iv) Mean velocities and pressure are determined by using the relation

$$\bar{v} = \frac{\sum_{i=1}^N v_i (\Delta t)_i}{\sum_{i=1}^N (\Delta t)_i} \quad (61)$$

(v) Once the mean velocities have been estimated, the fluctuating components of velocities can be estimated $v' = v - \bar{v}$

(vi) Finally, the apparent stresses or mean velocity correlations are estimated by using the relation

$$\overline{v_j v_k} = \frac{\sum_{n=1}^N (v_j' v_k')_n (\Delta t)_n}{\sum_{n=1}^N (\Delta t)_n} \quad (62)$$

SECTION VII

RESULTS OF NUMERICAL CALCULATIONS AND DISCUSSION

The mean flow field of the MIT Blowdown Rotor was computed by using the modified Streamline Curvature Computer Program, described in the preceding chapter. The purpose of this exercise was to verify the validity of flow models for Apparent Stresses, Mean Rothalpy Variation along the streamline, and Apparent Entropy Production. Flow models for these phenomena which are associated with pitchwise flow fluctuations, were formulated in Section III.

First of all, the mean flow field of the MIT Blowdown rotor was computed by only using the cascade losses. This was to confirm that the original Streamline Curvature program is able to accurately predict the design flow field (free vortex). Computations were next carried out to study the effect of the above three phenomena on the mean flow field. Here the effect of individual phenomenon and the combined effect of these phenomena are studied. Computations were also carried out by superimposing the effect of shock losses on the above calculation. Finally, the flow field was calculated by using experimentally estimated losses.

The apparent stress distribution given in Figures 9 through 20 were used as input for estimating $\frac{\partial \bar{I}}{\partial m}$, $\gamma \frac{\partial s}{\partial m}$)_{app} and the Apparent Stress terms appearing in the equation of motion (50).

The negative entropy rise through the rotor as seen around the midspan region (Figure 22), made the problem of specifying the experimental entropy distribution a rather difficult task. In the absence of any reasonable explanation this negative entropy rise was attributed to a zero shift in the pressure transducer. Therefore, for the purpose of specifying the experimental losses, the curve of Figure 22 was shifted up so as to bring the most negative value to zero. This is shown in Figure 26.

7.1 Computational Mesh and Basic Input Data

The computational mesh for application to the MIT Blow-down Compressor was formed by seven nearly radial fixed stations intersecting eleven meridional streamlines. Two stations were located ahead of the rotor, one each at the rotor leading and trailing edges, two within the blade row, and one at a distance of 1.0 chord downstream of the trailing edge. The hub and the casing form two fixed streamlines. The positions of the remaining nine streamlines are fixed during any computational pass but are readjusted at the end of each pass. Figure 27 gives the details of the computational mesh. It may be recalled that the time resolved experimental data was obtained at 0.1 chord (Port 5) and 1.0 chord (Port 6) downstream of the rotor. For this computational study the port 5 location was taken to represent the blade trailing edge projection on the meridional plane.

The basic input data for the analysis problem under investigation consisted of blade exit relative flow angles, geometrical features, mass flow rate, rpm, and the compressor inlet conditions. For all the computational studies, the experimentally determined relative exit flow angles (β) were used. Alternately, the flow angles can be specified by using the deviation angles based on the cascade data. Although this does not alter the basic character of the flow field, the experimental flow angles were used to get better accuracy. Relative flow angles for stations within the blade row were calculated by assuming a sinusoidal distribution of $\frac{d(\tau\bar{v}_a)}{dz}$ along the axial chord. It may be mentioned here that any alternate load distribution within the blade row will have negligible effect on the exit flow field, provided the load distribution at the rotor exit remains unchanged. This is because a change within the blade row can be communicated to the blade exit location only through the change of the slope and the curvature of streamlines which in turn are primarily controlled by the load distribution at the rotor exit. Other basic input data such as the mass flow rate and rpm were reduced to the standard atmospheric conditions at the compressor inlet with air as the fluid. Details of the basic input data and apparent stress data are given in Figures 28a and 28b.

7.2 Mean Flow Field

7.2.1 Computed Flow with Cascade Losses

Mean pitchwise, axial and radial velocity distributions at the rotor exit (Station 6) and at Station 7, as computed by using cascade losses, are shown in Figures 29 through 32. It is seen that the computed flow field is significantly different from that obtained experimentally. The pitchwise velocity $\overline{v_\theta}$ has an almost constant negative slope from the root to the tip and has completely failed to predict the double bucket shaped distribution found experimentally. In fact, the steep downward trend of $\overline{v_\theta}$ near the casing would cause flow instability and is therefore not expected to exist in the actual turbomachine.

The computed distribution of mean axial velocity does not show a steep fall near the casing, which is an important feature of the experimental $\overline{v_z}$ distribution.

The radial velocity distribution which is mainly controlled by the large slope of the hub, is found to decrease steeply from a large value at the hub to zero at the casing in conformity with the casing boundary condition. A reversal of slope at two locations as observed experimentally, has not been predicted by this computation.

It may, however, be noted that the results of this computation show a close resemblance to the flow field predicted

by the three-dimensional inviscid computational scheme of Reference (2). The predicted flow field also gives a good agreement with the design flow field of free vortex type thus showing that the basic program of Reference (1) is reliable for the prediction of mean flow field. Comparison with the 3-D inviscid computation also shows that 3-D inviscid effects per se do not alter the mean flow field of this rotor in a major way. The principal 3-D effects are due to viscous interactions, which are of course strongly controlled by the inviscid 3-D flow.

7.2.2 Computed Flow with Cascade Losses and Apparent Stresses

Figures 33 through 36 give the mean flow field computed with cascade losses and Apparent Stresses. Variations of mean Rothalpy and the production of Apparent Entropy along the meridional streamline are not included in this computation. It is seen from Figure 33 that the mean pitchwise velocity distribution at the rotor exit is similar to that obtained without Apparent Stresses. A slight depression at $r/r_t = 0.87$ and a slight increase in the negative slope near the casing indicate a trend reverse of that observed experimentally. Although the direct effect of Apparent Stresses is negligible on the mean flow field, it is noted from Figure 37 (app. stress/ $\frac{U_0^2}{\epsilon}$ vs r/r_t) that the order of magnitude of Apparent Stresses is comparable to that of the

centrifugal force $\frac{\overline{v_\theta}^2}{r}$. A comparison of Figure 37 with Figure 12a ($\frac{\partial \overline{v_\theta}^2}{\partial r} / \overline{v_\theta}^2 / r$ vs r/r_c) shows that almost all the contribution to the Apparent Stress terms of equation (50) comes from the distribution of the normal radial Apparent Stress $\overline{v_r}^2$.

7.2.3 Computed Flow with Cascade Losses and Apparent Entropy Production

Before computing the mean velocity with cascade losses and Apparent Entropy, the distributions of $T \left(\frac{\partial s}{\partial m} \right)_{app}$ at stations 4 and 5 which are located within the blade row, were estimated. Apparent Entropy rise across the rotor is then computed. These distributions are given in Figures 38 through 40. It is seen from these figures that the apparent entropy production is mainly controlled by the term $\frac{\partial (w^2/2)}{\partial m}$. Since the absolute value of apparent stress and the mean velocity gradients are small, the apparent dissipation term \mathcal{I}_{app} in equation (32) is small.

The computed mean flow field with cascade losses and Apparent Entropy is given in Figures 41 through 44. It is seen from Figure 41 that in the midspan region, $\overline{v_\theta}$ at the rotor exit shows a trend similar to the experimental results. It is, however, noted that the extent of change introduced by Apparent Entropy in the computed flow is considerably less than observed in the experimental distribution.

7.2.4 Computed Flow with Cascade Losses and Rothalpy Variation Along the Streamline

Distributions of $\frac{\partial \bar{I}}{\partial m}$ at stations 4 and 5, and mean Rothalpy variation across the rotor are first computed and these are given in Figures 38, 39, and 45. It is seen from these figures that mean Rothalpy decreases steeply towards the hub and the casing, and it increases slightly in the midspan region. This distribution is due to the spatial transfer of mean flow kinetic energy from the hub and the casing towards the midspan region. Besides towards the casing, conversion of mean flow kinetic energy to the energy of fluctuations becomes quite significant.

The computed mean flow field with cascade losses and Rothalpy variation is given in Figures 46 through 50. The shape of the \bar{v}_θ curve at the rotor exit (station 6) shows good agreement with the experimental distribution up to $r/r_t = 0.9$. It is further seen that a good agreement exists between the predicted and the experimental distributions of \bar{v}_z and \bar{v}_r at station 7. Thus the effect of mean Rothalpy variation along the streamline seems to play an important role in changing the mean velocity field.

7.2.5 Computed Flow with Cascade Losses, Rothalpy Variation, and Apparent Entropy Production Along the Streamline

In order to visualize the combined effect of Apparent Entropy production and mean Rothalpy variation, equivalent entropy change across the rotor defined as

$$\Delta (S_{app} - \frac{\bar{I}}{T})$$

is computed. This is plotted in Figure 51. It is interesting to note that a close resemblance exists between the equivalent entropy rise and the experimental entropy rise.

Figures 52 to 56 give the computed mean velocity field at station 6 and 7. The combined effects of Rothalpy Variation and Apparent Entropy production is found to change the free vortex velocity distribution to a distribution which closely resembles the experimental distribution. The observed difference in the absolute values of \bar{v}_θ at station 6, is attributed to the lower experimental values resulting from a zero shift in the pressure transducer. Therefore, the shape of the curves should only be compared to verify the validity of the flow model.

7.2.6 Computed Flow with Cascade Losses, Rothalpy Variation, Apparent Entropy Production, and Apparent Stresses

Finally, the flow field was computed with all of the above mentioned phenomena, and the results of numerical calculations are given in Figures 57 through 61. It is observed that the effect of adding Apparent Stress to Rothalpy variation and Apparent Entropy production is small, and is localized near the casing. In fact the positive slope of \bar{v}_θ which was obtained by using Rothalpy variation and Entropy production, no longer exists here. Several factors

could be responsible for the disagreement between the experimental and the predicted results near the casing. Error in the experimental data near the casing, assumption of linear distribution of apparent stresses along the meridional streamline, and non-inclusion of shock losses are some of the important factors. The effect of superimposing shock losses on the above computation is given in Figure 62. This is seen to make the slope of \bar{v}_θ positive near the casing.

7.2.7 Computed Flow with Experimental Losses

Mean flow field computed by using the entropy distribution of Figure 26 is given in Figures 63 through 68.

It is observed that \bar{v}_θ predicted at the rotor exit has an excellent agreement with the experimental results.

SECTION VIII

CONCLUSIONS

The primary aim of this research has been to improve the existing turbomachine flow model based on the combination of axisymmetric through flow and 2-D cascade flow, so that it can be applied to highly loaded systems for which the flow field computed by the existing flow model, has shown poor agreement with the experimental results. In order to achieve this goal, the existing flow model has been modified to account for blade to blade flow variations. The major support in verifying the improved flow model came from the time resolved experimental data of the MIT Blowdown Compressor facility. A critical analysis of this data considerably helped in understanding the 3-D viscous effects inherent in a highly loaded axial flow compressor. The computed flow field obtained by modifying the Streamline Curvature program of Reference (1) proved useful in consolidating many of the theoretical concepts and led to several important conclusions. A general discussion on the highlights of this work and the conclusions arising out of it are summarized here.

8.1 In Sections I and III of this report it is shown that the effect of blade to blade flow variations on the mean (circumferentially averaged) flow can be represented by the following phenomena:

- (i) Apparent stresses resulting from the pitchwise averaging of the momentum equation.
- (ii) Mean Rothalpy variation along the streamline due to energy transfer across the stream surfaces by the apparent stresses, and by conversion of mean flow kinetic energy to the energy of fluctuations.
- (iii) Apparent Entropy Production due to dissipation associated with apparent stresses, and due to the production of fluctuation energy.

These phenomena significantly influence the spatial distribution of mean momentum and energy in an axial flow compressor.

8.2 In Section V a critical study of the time resolved experimental data of the MIT Blowdown Compressor is carried out. Some of the important findings of this study are:

- (i) A strong disagreement exists between the mean experimental flow field and the design flow field.
- (ii) Apparent stresses resulting from the pitchwise flow variations are of significant magnitude. In particular, the radial derivative of $\overline{v_r'^2}$ at the rotor exit is found to be of comparable magnitude to the mean specific centrifugal force $\frac{\overline{v_\theta^2}}{r}$. Since the normal radial apparent stress represents the spanwise flows in the blade boundary layer, the above observation indicated that

for a highly loaded system, the radial transport of boundary layer and wakes is an important effect.

- (iii) The radial gradient of the mean entropy rise near the hub and the casing is estimated to be several times larger than that predicted by two-dimensional cascade data.

8.3 A detailed study of the effect of phenomena listed in Section 8.1 has been carried out by using the flow models developed in Section III. A discussion on the flow field computed with the aid of modified streamline curvature computer program (Section VI) is presented in Section VII, and the conclusions arising from this discussion are summarized as follows:

- (i) An axisymmetric computation with entropy distribution based on the cascade data shows an excellent agreement between the predicted flow and the design flow and also agrees well with the results of a 3-D inviscid computation. It is therefore concluded that 3-D inviscid effects such as the blade passage shock and the distortion of stream surfaces due to the inviscid pressure field of the blades, do not produce significant changes in the mean flow for this rotor. Hence, the deviation from the design flow of the experimental results is attributed to 3-D viscous effects which, however, are indirectly controlled by the inviscid blade-to-blade flow.
- (ii) The introduction of apparent stresses into the mean flow 1-direction (nearly radial) momentum

equation does not have a large effect on the mean flow field. It is, however, found that the major contribution to the apparent stress terms in the above momentum equation comes from the radial derivative of $\overline{V_z^2}$. In fact a knowledge of this derivative which represents the distribution of spanwise flow in the blade boundary layers and wakes, will probably be adequate to replace all the apparent stress terms.

(iii) Mean Rothalpy variation and the production of Apparent Entropy along the streamline play the major roles in reshaping the velocity field of a highly loaded axial flow compressor. The flow field computed by accounting for these effects shows a distinct resemblance to the experimental flow. The largest contribution in reshaping the velocity field comes from the variation of mean Rothalpy along the streamline. The effect of Apparent Entropy production, however, is considerably larger than that due to Apparent Stresses and hence, it cannot be ignored. It is thus concluded, if the mean Rothalpy variation and the Apparent Entropy production along the streamline are taken into account, the axisymmetric computational technique will be able to predict the flow field of a highly loaded axial flow compressor with reasonable accuracy.

REFERENCES

1. Hearsey, R. M., "A Revised Computer Program for Axial Compressor Design," Vol. I and II, ARL-TR-75-0001, AD A009157, Aerospace Research Lab., Wright-Patterson Air Force Base, Ohio, 1976.
2. Thompkins, Jr., W. T., "An Experimental and Computational Study of the Flow in a Transonic Compressor Rotor," M.I.T. Gas Turbine Lab. Report No. 129, May 1976.
3. Novak, R. A., "Axisymmetric Computing Systems for Axial Flow Turbomachinery," Lecture 10, ASME Turbomachine Institute, Iowa State University, Ames, Iowa, August 1978.
4. Smith, Jr., L. H., "The Radial-Equilibrium Equation of Turbomachinery," Trans. ASME J. Engineering for Power, Series A, Vol. 88, 1, 1966.
5. Fujii, S., "An Improved Method of the Local Loss Estimate in Axial-Flow Turbomachines," received Nov. 20, 1976, ASME J. Fluids Engineering.
6. Novak, R. A., "Streamline Curvature Computing Procedure for Fluid Flow Problems," Trans. ASME J. Engineering for Power, Series A, Vol. 89, pp. 478-490, 1976.
7. Wennerstrom, A. J., "On the Treatment of Body Forces in the Radial Equilibrium of Turbomachinery," ARL-74-0150, Aerospace Research Lab., Wright-Patterson AFB, Ohio, 1974.
8. Howell, A. R., "Design of Axial Compressors," Proc. Institution Mech. Engrs., London, 153, 1945.
9. Rannie, W. D., Bowen, J. T., and Sabensky, R. H., "Investigation of Axial-Flow Compressors," Trans. ASME, 73, 1951.
10. Bragg, S. L., and Hawthorne, W. R., "Some Exact Solutions of the Flow Through Annular Cascade Actuator Discs," J. Aeronautical Society, April 1950.
11. Ruden, P., "Investigation of Axial-Flow Fans," NACA TM 1062, 1944.
12. Raily, J. W., "The Flow of an Incompressible Fluid Through an Axial Turbomachine with Any Number of Rows," Aeronaut. Quarterly 3, 1951.
13. Marble, F. E., "Three-Dimensional Flow in Turbomachines," High Speed Aerodynamics and Jet Propulsion, Vol. X, Princeton University Press.

REFERENCES (cont'd)

14. Johnson, Bullock, et al., "Aerodynamic Design of Axial-Flow Compressors," NASA SP36, 1965.
15. McCune, J. E., and Hawthorne, W. R., "The Effects of Trailing Vorticity on the Flow Through Highly Loaded Cascade," J. Fluid Mechanics, Vol. 74, 4, pp. 721-740, 1976.
16. Morton, Jr., K. B., "Three-Dimensional Compressible Flow Through a Highly Loaded, Rectilinear Cascade," S.M. Thesis, Aero. & Astro. Dept., M.I.T., September 1974.
17. Cheng, W. K., "A Three-Dimensional Theory for the Velocity Induced by a Heavily Loaded Annular Cascade of Blades," S.M. Thesis, Aero. & Astro. Dept., M.I.T., 1975.
18. Adebayo, A. O., "Three-Dimensional Beltrami Flow Through a Highly Loaded Axial Compressor Rotor Introducing Arbitrary Swirl," Ph.D. Thesis, Aero. & Astro. Dept., M.I.T., 1978.
19. Tan, C. S., "Three-Dimensional Vorticity-Induced Flow Effects in Highly Loaded Axial Compressors," Ph.D. Thesis, Aero. & Astro. Dept., M.I.T., 1978.
20. Wu, C. H., "A General Through Flow Theory of Fluid Flow with Subsonic or Supersonic Velocity in Turbomachines of Arbitrary Hub and Casing Shapes," NACA TN-2302, 1951.
21. Novak, R. A., and Hearsey, R. M., "A Nearly Three-Dimensional Interblade Computing System for Turbomachinery," Part I and Part II, ASME 76-FE-19 and 76-FE-20, 1976.
22. Jenson, W., and Moffat, W. C., "The Off-Design Analysis of Axial Flow Compressors," ASME 66-WA/GT-1, 1966.
23. Marsh, H., "A Digital Computer Program for the Through-Flow Fluid Mechanics in an Arbitrary Turbomachine Using a Matrix Method," Aeronautical Research Council R&M No. 3509, 1968.
24. Oliver, D. A., and Sparis, P., "A Computational Study of Three-Dimensional Shear Flow in Turbomachine Cascades," AIAA Paper No. 71-83.
25. Kerrebrock, J. L., Aircraft Engines and Gas Turbines, The M.I.T. Press, Cambridge, MA, 1977.
26. Hirsch, C., "Unsteady Contributions to Steady Radial Equilibrium Flow Equations," AGARD Conference on Unsteady Phenomena in Turbomachinery, CP-177, Paper No. 13, 1975.

REFERENCES (cont'd)

27. Silverstein, A., Katzoff, S., and Bullivant, W. K., "Downwash and Wake Behind Plain and Flapped Aerofoils," NACA Rep. 651, 1939.
28. Mager, A., "Generalization of Boundary-Layer Momentum-Integral Equations to Three-Dimensional Flow Including Those of Rotating System," NASA Rep. 1067, 1954.
29. Gruschwitz, E., "Turbulente Reibungsschichten mit Sekundärströmung," Ingenieur-Archiv, Bd. VI, pp. 355-365, 1935.
30. Hules, K., "A Theoretical Study of Three-Dimensional Compressible Turbulent Boundary Layers on Rotating Surfaces in Turbomachinery," Sc.D. Thesis, Mech. Engr. Dept., M.I.T., May 1976.
31. Preston, J. H., Sweeting, N. E., and Cox, D. K., "The Experimental Determination of the Boundary Layer and Wake Characteristics of a Piercy Airfoil with Particular Reference to the Trailing Edge Region," Gr. Britain Aero. Res. Council, R&M 2013, 1945.
32. Spence, D. A., "Growth of Turbulent Wake Close Behind an Airfoil at Incidence," Gr. Britain Aero. Res. Council, C.P. No. 125, 1952.
33. Rah, R., and Lakshminarayana, B., "Three-Dimensional Characteristics of Turbulent Wakes Behind Rotors of Axial Flow Turbomachinery," Trans. ASME J. Engineering for Power, Vol. 98, 2, April 1976.
34. Kerrebrock, J. L., "Small Disturbances in Turbomachine Annuli with Swirl," M.I.T. Gas Turbine Lab. Rep. No. 125, October 1975; also AIAA J., Vol. 15, 6, pp. 794-803, June 1977.
35. Kerrebrock, J. L., and Mikolajczak, A. A., "Intra-Stator Transport of Rotor Wakes and its Effect on Compressor Performance," ASME Paper No. 70-GT-39.
36. Kemp, N. H., and Sears, W. R., "The Unsteady Forces Due to Viscous Wakes in Turbomachines," J. Aeronautical Sciences, Vol. 22, 7, pp. 478-483, July 1955.
37. Thompkins, Jr., W. T., and Kerrebrock, J. L., "Exit Flow from a Transonic Compressor Rotor," AGARD Conference on Unsteady Phenomena in Turbomachinery, CP-177, Paper No. 6, 1975.
38. Schlichting, H., Boundary Layer Theory, McGraw-Hill, N.Y., 1968.

REFERENCES (cont'd)

39. Ruden, P., "Investigations of Single-Stage Axial Fans," NACA TM No. 1062, 1944.
40. Horlock, J. H., and Marsh, H., "Flow Models for Turbomachines," J. Mech. Engr. Sci., 13, 5, p. 358, 1971.
41. Horlock, J. H., "On Entropy Production in Adiabatic Flow in Turbomachines," ASME Paper No. 71-FE-3, 1971.
42. Bossman, C., and Marsh, H., "An Improved Method for Calculating the Flow in Turbomachines, Including a Consistent Loss Model," Instit. Mech. Engr., J. Mech. Engr. Sci., Vol. 16, 1, 1974.
43. Miller, G. R., Lewis, Jr., G. W., and Hartmann, M. J., "Shock Losses in Transonic Compressor Blade Rows," ASME J. Engineering for Power, July 1961.
44. Epstein, A. H., "Quantitative Density Visualization in a Transonic Compressor Rotor," M.I.T. Gas Turbine Lab. Report No. 124, September 1975.
45. Liepmann, H. W., and Roshko, A., Elements of Gasdynamics, J. Wiley & Sons, Inc., New York, 1957.

APPENDIX A

DERIVATION OF RADIAL, TANGENTIAL AND AXIAL
EQUATIONS OF MOTION

If we choose a frame of reference fixed to the rotor blades, unsteadiness in the flow exists due to turbulent fluctuations only. Equations of mass and momentum conservations for unsteady flow are:

Mass Conservation

$$\frac{\partial \rho}{\partial t} + \frac{1}{r} \frac{\partial (r \rho W_r)}{\partial r} + \frac{1}{r} \frac{\partial (r \rho W_\theta)}{\partial \theta} + \frac{\partial (\rho W_z)}{\partial z} = 0 \quad (\text{A-1})$$

Momentum Conservation

r-direction

$$\frac{\partial W_r}{\partial t} + W_r \frac{\partial W_r}{\partial r} + \frac{W_\theta}{r} \frac{\partial W_r}{\partial \theta} + W_z \frac{\partial W_r}{\partial z} - 2 W_\theta \Omega - \Omega^2 r - W_\theta^2 / r = -\frac{1}{\rho} \frac{\partial p}{\partial r} + F_{r\theta} \quad (\text{A-2})$$

\theta-direction

$$\frac{\partial W_\theta}{\partial t} + W_r \frac{\partial W_\theta}{\partial r} + \frac{W_\theta}{r} \frac{\partial W_\theta}{\partial \theta} + W_z \frac{\partial W_\theta}{\partial z} + \frac{W_\theta W_z}{r} + 2 \Omega W_r = -\frac{1}{\rho} \frac{\partial p}{\partial \theta} + F_{\theta r} \quad (\text{A-3})$$

z-direction

$$\frac{\partial W_z}{\partial t} + W_r \frac{\partial W_z}{\partial r} + \frac{W_\theta}{r} \frac{\partial W_z}{\partial \theta} = -\frac{1}{\rho} \frac{\partial p}{\partial z} + F_{z\theta} \quad (\text{A-4})$$

In order to make these equations time independent, a time average of these equations will be carried out, which is defined by the following integral:

$$\langle A \rangle = \lim_{T \rightarrow \infty} \frac{1}{T} \int_0^T A dt \quad (\text{A-5})$$

and

$$A = \langle A \rangle + A' \quad (\text{A-5a})$$

Time averaged mass conservation equation becomes

$$\frac{1}{r} \frac{\partial r \langle \rho w_r \rangle}{\partial t} + \frac{1}{r} \frac{\partial \langle \rho w_\theta \rangle}{\partial \theta} + \frac{\partial \langle \rho w_z \rangle}{\partial z} = 0 \quad (\text{A-6})$$

Here $\langle \rho w \rangle$ is the time averaged mass flow defined as

$$\langle \rho w \rangle = \lim_{T \rightarrow \infty} \frac{1}{T} \int_0^T (\rho w) dt \quad (\text{A-7})$$

and

$$\rho w = \langle \rho w \rangle + (\rho w)' \quad (\text{A-7a})$$

For derivation of the time averaged momentum equations, the mass conservation equation is first combined with the momentum conservation equation followed by time averaging of the resulting equation. The time averaged radial momentum equation becomes

$$\begin{aligned} \langle w_r \rangle \frac{\partial \langle w_r \rangle}{\partial t} + \frac{\langle w_\theta \rangle}{r} \frac{\partial \langle w_r \rangle}{\partial \theta} + \langle w_z \rangle \frac{\partial \langle w_r \rangle}{\partial z} - \langle w_\theta \rangle \Omega \\ - r \Omega^2 - \frac{\langle w_\theta^2 \rangle}{r} = - \frac{1}{\langle \rho \rangle} \frac{\partial \langle p \rangle}{\partial r} + \frac{\langle \rho F_{r\theta} \rangle}{\langle \rho \rangle} \\ - \left\{ \frac{1}{\langle \rho \rangle} \frac{\partial \langle (\rho w_r)' w_r' \rangle}{\partial r} + \frac{1}{\langle \rho \rangle r} \frac{\partial \langle (\rho w_\theta)' w_r' \rangle}{\partial \theta} + \frac{1}{\langle \rho \rangle} \frac{\partial \langle (\rho w_z)' w_r' \rangle}{\partial z} \right. \\ \left. + \frac{\langle (\rho w_r)' w_r' \rangle}{\langle \rho \rangle r} - \frac{\langle (\rho w_\theta)' w_\theta' \rangle}{\langle \rho \rangle r} \right\} \quad (\text{A-8}) \end{aligned}$$

In order to account for the blade to blade flow variations, pitchwise averaging of this equation is carried out as per the procedure outlined in Appendix B. Denoting pitchwise average of the time averaged quantities by $\langle \rangle$, and deviation from pitchwise average by $\langle \rangle'$, the mean mass conservation and the radial momentum equations are derived as follows:

Mass Conservation Equation (Pitchwise Averaged)

Following Appendix B, pitchwise average of equation (A-11) is represented as:

$$\frac{1}{(2\pi\lambda/N)} \left\{ \int_{\theta_p}^{\theta_s} \frac{\partial \langle w_r \rangle'}{\partial r} d\theta \right. + \int_{\theta_p}^{\theta_s} \frac{\langle w_r \rangle'}{r} d\theta + \int_{\theta_p}^{\theta_s} \frac{1}{r} \frac{\partial \langle w_\theta \rangle'}{\partial \theta} d\theta + \left. \int_{\theta_p}^{\theta_s} \frac{\partial \langle w_z \rangle'}{\partial z} d\theta \right\} = 0 \quad (A-13)$$

I
II
III
IV

Individual terms can now be evaluated.

From equation (B10) of Appendix B, Term I becomes:

$$\begin{aligned} \text{Term I} &= \frac{\partial \langle w_r \rangle'}{\partial r} = \frac{\partial \langle w_r \rangle'}{\partial r} + \frac{\{ \langle w_r \rangle'_s - \langle w_r \rangle'_p \} (\tan \epsilon_m)'}{2\pi\lambda/N} \frac{1}{r} \\ &\quad + \left(\langle w_r \rangle' - \frac{\langle w_r \rangle'_p + \langle w_r \rangle'_s}{2} \right) \frac{1}{\lambda} \frac{\partial \lambda}{\partial r} \end{aligned} \quad (A-14)$$

Assuming no slip condition on the blade surfaces, equation (A14) becomes

$$\text{Term I} = \frac{\partial \langle w_r \rangle'}{\partial r} + \langle w_r \rangle' \frac{1}{\lambda} \frac{\partial \lambda}{\partial r} \quad (A-15)$$

Here W' (or $(\rho W)'$) represents temporal fluctuations about the time averaged value represented by $\langle W \rangle$ (or $\langle \rho W \rangle$). The third term in the right hand side of equation (A-8) gives the contribution of turbulent stresses.

An alternate method of deriving time averaged equations of motion is to separate density fluctuations from the mass flow fluctuations used in the above derivation. The time averaged mass conservation and radial momentum equations obtained by using this procedure are:

Mass Conservation

$$\left\{ \frac{1}{r} \frac{\partial (r \langle \rho \rangle \langle w_r \rangle)}{\partial r} + \frac{1}{r} \frac{\partial (\langle \rho \rangle \langle w_\theta \rangle)}{\partial \theta} + \frac{\partial (\langle \rho \rangle \langle w_z \rangle)}{\partial z} \right\} + \left\{ \frac{1}{r} \frac{\partial (r \langle \rho' w_r' \rangle)}{\partial r} + \frac{1}{r} \frac{\partial (\langle \rho' w_\theta' \rangle)}{\partial \theta} + \frac{\partial \langle \rho' w_z' \rangle}{\partial z} \right\} = 0 \quad (A-9)$$

Radial Equation of Motion

$$\begin{aligned} & \langle w_r \rangle \frac{\partial \langle w_r \rangle}{\partial r} + \frac{\langle w_\theta \rangle}{r} \frac{\partial \langle w_r \rangle}{\partial \theta} + \langle w_z \rangle \frac{\partial \langle w_r \rangle}{\partial z} - 2 \langle w_\theta \rangle \Omega \\ & - r \Omega^2 - \frac{\langle w_\theta \rangle^2}{r} = - \frac{1}{\langle \rho \rangle} \frac{\partial \langle p \rangle}{\partial r} + \frac{\langle \rho F_{r\theta} \rangle}{\langle \rho \rangle} \\ & - \left\{ \frac{1}{\langle \rho \rangle} \frac{\partial (\langle \rho \rangle \langle w_r'^2 \rangle)}{\partial r} + 2 \langle w_r \rangle \langle \rho' w_r' \rangle + \langle \rho' w_r'^2 \rangle \right. \\ & \quad \left. + \frac{\langle w_r'^2 \rangle}{r} + \frac{\langle \rho' w_r'^2 \rangle}{\langle \rho \rangle r} - \left(\frac{\langle w_\theta'^2 \rangle}{r} + \frac{\langle \rho' w_\theta'^2 \rangle}{\langle \rho \rangle r} \right) \right\} \\ & - \left\{ \frac{1}{\langle \rho \rangle r} \frac{\partial (\langle \rho \rangle \langle w_\theta' w_r' \rangle)}{\partial \theta} + \langle \rho' w_\theta' w_r' \rangle + \langle w_r \rangle \langle \rho' w_\theta' \rangle + \langle w_\theta \rangle \langle \rho' w_r' \rangle \right\} \\ & + 2 \langle \rho' w_\theta' \rangle \Omega - \left\{ \frac{1}{\langle \rho \rangle r} \frac{\partial (r \langle \rho' w_r' \rangle)}{\partial r} + \frac{1}{\langle \rho \rangle r} \frac{\partial \langle \rho' w_\theta' \rangle}{\partial \theta} + \frac{\partial \langle \rho' w_z' \rangle}{\partial z} \right\} \quad (A-10) \end{aligned}$$

The last term in the right hand side of equation (A-10) is the apparent stress contribution from the time averaged mass conservation equation.

Both the equations (A-8) and (A-10) require information on the instantaneous value of density. But since the existing experimental methods cannot provide reliable data on density, it was considered desirable to derive the mean flow equations for the case of small density fluctuations. The time averaged equations of mass conservation and radial momentum now become:

Mass Conservation Equation

$$\frac{1}{r} \frac{\partial (r \langle w_r \rangle \rho)}{\partial r} + \frac{1}{r} \frac{\partial \langle w_\theta \rangle \rho}{\partial \theta} + \frac{\partial \langle w_z \rangle \rho}{\partial z} = 0 \quad (\text{A-11})$$

Radial Momentum Equation

$$\begin{aligned} \langle w_r \rangle \frac{\partial \langle w_r \rangle}{\partial r} + \frac{\langle w_\theta \rangle}{r} \frac{\partial \langle w_r \rangle}{\partial \theta} + \langle w_z \rangle \frac{\partial \langle w_r \rangle}{\partial z} \\ - 2 \langle w_\theta \rangle \Omega - r \Omega^2 - \frac{\langle w_\theta \rangle^2}{r} = \frac{1}{\rho} \left[- \frac{\partial \langle p \rangle}{\partial r} + \rho \langle F_{ru} \rangle \right. \\ \left. - \left\{ \frac{\partial \langle w_r'^2 \rangle \rho}{\partial r} + \frac{1}{r} \frac{\partial \langle w_r' w_\theta' \rangle \rho}{\partial \theta} + \frac{\partial \langle w_r' w_z' \rangle \rho}{\partial z} \right. \right. \\ \left. \left. + \frac{\rho (\langle w_r'^2 \rangle - \langle w_\theta'^2 \rangle)}{r} \right\} \right] \quad (\text{A-12}) \end{aligned}$$

Similarly treatment gives

$$\begin{aligned}
 \text{Term II} &= \frac{\overline{\langle w_r \rangle}}{r} \\
 \text{Term III} &= 0 \\
 \text{Term IV} &= \frac{\partial \overline{\langle w_z \rangle}}{\partial z} + \overline{\langle w_z \rangle} \frac{1}{\lambda} \frac{\partial \lambda}{\partial z}
 \end{aligned}
 \tag{A-16}$$

Thus the pitchwise averaged mass conservation equation becomes:

$$\frac{\partial \overline{\langle w_r \rangle}}{\partial r} + \frac{\overline{\langle w_r \rangle}}{r} + \frac{\overline{\langle w_r \rangle}}{\lambda} \frac{\partial \lambda}{\partial r} + \frac{\partial \overline{\langle w_z \rangle}}{\partial z} + \frac{\overline{\langle w_z \rangle}}{\lambda} \frac{\partial \lambda}{\partial z} = 0
 \tag{A-17}$$

Multiplying equation (A-17) by λ , gives

$$\boxed{\frac{1}{r} \frac{\partial (\lambda \overline{\langle w_r \rangle} r)}{\partial r} + \frac{\partial (\lambda \overline{\langle w_z \rangle})}{\partial z} = 0}
 \tag{A-18}$$

Equation (A-18) represents the axisymmetric form of the mass conservation equation in which the blockage due to the blade thickness has been uniformly distributed.

In deriving the above equation and also for the subsequent derivations, it is assumed that the pitchwise variation of density is small.

Radial Momentum Equation (Pitchwise Averaged)

Multiplying equation (A-11) by $\langle w_r \rangle$ and adding it to equation (A-12), gives

$$\begin{aligned}
& \frac{\partial \langle w_x^2 \rangle}{\partial \tau} + \frac{1}{\tau} \frac{\partial \langle w_\theta \rangle \langle w_x \rangle}{\partial \theta} + \frac{\partial \langle w_x \rangle \langle w_z \rangle}{\partial z} + \rho \frac{\langle w_x^2 \rangle}{\tau} - \rho \frac{\langle w_\theta \rangle^2}{\tau} \\
- 2 \langle w_\theta \rangle \Omega \rho - \rho \Omega^2 \tau = & \left[- \frac{\partial \langle p \rangle}{\partial \tau} + \rho \langle F_{x0} \rangle - \left\{ \frac{\partial \langle w_x^2 \rangle}{\partial \tau} \right. \right. \\
& \left. \left. + \frac{1}{\tau} \frac{\partial \langle w_x' w_\theta' \rangle}{\partial \theta} + \frac{\partial \langle w_x' w_z' \rangle}{\partial z} + \frac{\langle w_x'^2 \rangle - \langle w_\theta'^2 \rangle}{\tau} \right\} \right] \quad (A-19)
\end{aligned}$$

Pitchwise averaging of individual terms can now be carried out using equations (B-11), (B-16), and (B-17)

$$\frac{\partial \langle w_x^2 \rangle}{\partial \tau} = \frac{\partial \langle w_x^2 \rangle}{\partial \tau} + \frac{\rho \langle w_x \rangle}{\lambda} \frac{\partial \lambda}{\partial \tau} + \frac{\partial \langle w_x \rangle}{\partial \tau} + \frac{\rho \langle w_x \rangle}{\lambda} \frac{\partial \lambda}{\partial \tau} \quad (A-19a)$$

$$\frac{1}{\tau} \frac{\partial \langle w_\theta \rangle \langle w_x \rangle}{\partial \theta} = 0 \quad (A-20)$$

$$\begin{aligned}
\frac{\partial \langle w_x \rangle \langle w_z \rangle}{\partial z} = & \frac{\partial \langle w_x \rangle \langle w_z \rangle}{\partial z} + \frac{\rho \langle w_x \rangle \langle w_z \rangle}{\lambda} \frac{\partial \lambda}{\partial z} \\
& + \frac{\partial \langle w_x \rangle \langle w_z \rangle}{\partial z} + \rho \frac{\langle w_x \rangle \langle w_z \rangle}{\lambda} \frac{\partial \lambda}{\partial z} \quad (A-21)
\end{aligned}$$

$$\frac{\rho \langle w_x^2 \rangle}{\tau} = \frac{\rho \langle w_x \rangle^2}{\tau} + \rho \frac{\langle w_x \rangle^2}{\tau} \quad (A-22)$$

$$\frac{\rho \langle w_\theta \rangle^2}{\tau} = \frac{\rho \langle w_\theta \rangle^2}{\tau} + \rho \frac{\langle w_\theta \rangle^2}{\tau} \quad (A-22a)$$

$$- \frac{\partial \langle p \rangle}{\partial \tau} = - \frac{\partial \langle p \rangle}{\partial \tau} + \rho F_{xi} \quad (A-23)$$

where F_{ri} is the inviscid blade force component in the radial direction and is equal to

$$\frac{\{(\langle p \rangle)_p - (\langle p \rangle)_s\}}{2\pi\lambda/N} \cdot \frac{\tan \epsilon_m}{r}$$

We can thus write the pitch averaged form of equation (A-19)

$$\begin{aligned} & \frac{\partial \overline{\langle w_r \rangle^2}}{\partial r} + \frac{\rho \overline{\langle w_r \rangle^2}}{\lambda} \frac{\partial \lambda}{\partial r} + \frac{\partial \overline{\langle w_r \rangle^2}}{\partial r} + \frac{\rho \overline{\langle w_r \rangle^2}}{\lambda} \frac{\partial \lambda}{\partial r} + \frac{\partial (\overline{\langle w_r \rangle \langle w_z \rangle})}{\partial z} \\ & + \frac{\rho \overline{\langle w_r \rangle \langle w_z \rangle}}{\lambda} \frac{\partial \lambda}{\partial z} + \frac{\partial (\overline{\langle w_r \rangle' \langle w_z \rangle'})}{\partial z} + \frac{\rho \overline{\langle w_r \rangle' \langle w_z \rangle'}}{\lambda} \frac{\partial \lambda}{\partial z} \\ & + \frac{\rho \overline{\langle w_r \rangle^2}}{r} + \frac{\rho \overline{\langle w_z \rangle^2}}{r} - 2 \overline{\langle w_\theta \rangle} \Omega r - \Omega^2 r - \frac{\overline{\langle w_\theta \rangle^2}}{r} - \frac{\overline{\langle w_\theta \rangle'^2}}{r} \end{aligned}$$

$$= - \frac{\partial \overline{\langle p \rangle}}{\partial r} + \rho F_{ri} + \rho \overline{\langle F_{rt} \rangle} + \rho F_{rt}$$

(A-24)

Here F_{rt} is the contribution of pitchwise averaged turbulent stresses, given by

$$\overline{F_{rt}} = - \frac{1}{\rho} \left\{ \frac{\partial \overline{\langle w_r \rangle^2}}{\partial r} + \frac{\partial \overline{\langle w_r \rangle' \langle w_z \rangle'}}{\partial z} + \frac{\rho (\overline{\langle w_r \rangle^2} - \overline{\langle w_\theta \rangle'^2})}{r} \right\}$$

(A-25)

Multiplying equation (A-24) by λ and after simple algebraic manipulations, we get

$$\begin{aligned} & \rho \lambda \left\{ \overline{\langle w_r \rangle} \frac{\partial \overline{\langle w_r \rangle}}{\partial r} + \overline{\langle w_z \rangle} \frac{\partial \overline{\langle w_z \rangle}}{\partial z} - \frac{\overline{\langle w_\theta \rangle^2}}{r} - 2 \Omega \overline{\langle w_\theta \rangle} - \Omega^2 r \right\} \\ & + \overline{\langle w_r \rangle} \left\{ \frac{\partial (\lambda \overline{\langle w_r \rangle})}{\partial r} + \frac{\partial (\lambda \overline{\langle w_z \rangle})}{\partial z} \right\} \end{aligned}$$

(A-26)

$$\begin{aligned}
& + \left\{ \frac{\partial (\lambda \overline{\langle w_r \rangle^2})}{\partial r} + \frac{\partial (\lambda \overline{\langle w_r \rangle' \langle w_z \rangle'})}{\partial z} + \lambda \overline{\langle w_r \rangle^2} - \lambda \overline{\langle w_\theta \rangle^2} \right\} \\
& = \lambda \left\{ - \frac{\partial \overline{\langle p \rangle}}{\partial r} + \rho F_{ri} + \rho \overline{\langle F_{rv} \rangle} + \rho \overline{F_{rt}} \right\}
\end{aligned}$$

Using mass conservation equation (A-18) and dividing both sides by λ , we get final form of pitch averaged radial momentum equation

$$\begin{aligned}
\overline{\langle w_r \rangle} \frac{\partial \overline{\langle w_r \rangle}}{\partial r} + \overline{\langle w_z \rangle} \frac{\partial \overline{\langle w_r \rangle}}{\partial z} - \frac{\overline{\langle w_\theta \rangle^2}}{r} - 2\Omega \overline{\langle w_\theta \rangle} \\
- \Omega^2 r = - \frac{1}{\rho} \frac{\partial \overline{\langle p \rangle}}{\partial r} - \frac{1}{\rho \lambda} \left\{ \frac{\partial (\lambda \overline{\langle w_r \rangle^2})}{\partial r} + \frac{\partial (\lambda \overline{\langle w_r \rangle' \langle w_z \rangle'})}{\partial z} - \lambda \overline{\langle w_\theta \rangle^2} \right\} \\
+ F_{ri} + \overline{\langle F_{rv} \rangle} + \overline{F_{rt}} \tag{A-27}
\end{aligned}$$

This is the final form of radial momentum equation which has first been time averaged to make it time independent, and then pitchwise averaged to make it θ -independent.

Equation (A-27) contains two types of velocity correlations, one accounting for turbulent fluctuations (temporal), and the other accounting for the spatial fluctuations of the time averaged quantities. For a highly loaded system where blade to blade flow variations are large, the contribution from turbulent fluctuations is small as compared to that due to the pitchwise fluctuations.

The above procedure can also be applied to the flow fluctuations outside the blade row in the absolute frame of reference to account for pitchwise flow variations. This is done by first taking an ensemble average of the unsteady equation of motion and then taking time average of ensemble averaged quantities.

To simplify equation (A-27), we can either neglect turbulent stresses as compared to the large scale blade to blade fluctuations, or a slightly different averaging procedure can be followed. It is possible to directly carry out pitchwise averaging of unsteady equations of motion by assuming $\frac{\partial \bar{w}}{\partial t}$ to be small. This procedure will give the following radial-direction equation of motion in the apparent stress

$$\begin{aligned} \text{format. } & \bar{w}_r \frac{\partial \bar{w}_r}{\partial t} + \bar{w}_z \frac{\partial \bar{w}_r}{\partial z} - \frac{\bar{w}_\theta^2}{r} - 2\bar{w}_\theta \Omega - \Omega^2 r \\ & = -\frac{1}{\rho} \frac{\partial \bar{p}}{\partial r} - \frac{1}{\lambda \rho} \left\{ \frac{1}{r} \frac{\partial (\tau \lambda \bar{w}_r'^2 \rho)}{\partial r} + \frac{\partial (\lambda \bar{w}_z' \bar{w}_z' \rho)}{\partial z} - \frac{\lambda \bar{w}_\theta'^2 \rho}{r} \right\} \\ & + F_{ri} + \bar{F}_{rv} \end{aligned} \quad (\text{A-28})$$

Corresponding equations in θ and z directions are

θ -direction

$$\begin{aligned} & \bar{w}_r \frac{\partial \bar{w}_\theta}{\partial t} + \bar{w}_z \frac{\partial \bar{w}_\theta}{\partial z} + \frac{\bar{w}_\theta \bar{w}_r}{r} + 2\Omega \bar{w}_r \\ & = -\frac{1}{\lambda \rho} \left(\frac{\partial (\lambda \bar{w}_r' \bar{w}_\theta' \rho)}{\partial r} + \frac{\partial (\lambda \bar{w}_z' \bar{w}_\theta' \rho)}{\partial z} + \frac{2\lambda \bar{w}_r' \bar{w}_\theta' \rho}{r} \right) + F_{\theta i} + \bar{F}_{\theta v} \end{aligned} \quad (\text{A-29})$$

z -direction

$$\begin{aligned} & \bar{w}_r \frac{\partial \bar{w}_z}{\partial t} + \bar{w}_z \frac{\partial \bar{w}_z}{\partial z} = \left\{ -\frac{1}{\rho} \frac{\partial \bar{p}}{\partial z} + F_{zi} + \bar{F}_{zv} \right. \\ & \quad \left. - \frac{1}{\lambda \rho} \left(\frac{\partial (\lambda \bar{w}_r' \bar{w}_z' \rho)}{\partial r} + \frac{\partial (\lambda \bar{w}_z'^2 \rho)}{\partial z} + \frac{\lambda \bar{w}_z' \bar{w}_z' \rho}{r} \right) \right\} \end{aligned} \quad (\text{A-30})$$

APPENDIX B

PITCHWISE AVERAGING

Pitchwise average of any flow property A within the blade row is defined as

$$\bar{A} = \frac{1}{\theta_s - \theta_p} \int_{\theta_p}^{\theta_s} A d\theta \quad (B-1)$$

Here the integration has been carried out from the pressure side of one blade to the suction side of the adjacent blade. This is consistent with the direction of rotation for an axial compressor rotor. For a turbine rotor the integration would be carried out from the suction side of one blade to the pressure side of the adjacent blade.

Following Smith⁴, the mean blade surface and the blade lean angle ξ_m is defined in Figure (3.1). If the blade blockage factor λ is now defined as $\lambda = 1 - \frac{t}{s}$, equation (B1) becomes

$$\bar{A} = \frac{1}{2\pi\lambda/N} \int_{\theta_p}^{\theta_s} A d\theta \quad (B-2)$$

Here $(1-\lambda)$ represents the blockage to the flow due to the blade thickness.

In order to carry out pitchwise average of derivative the flow property we adopt Liebnitz Rule for expressing the derivative of an integral.

Thus

$$\frac{\partial}{\partial x} \int_{\theta_p}^{\theta_s} A d\theta = \int_{\theta_p}^{\theta_s} \frac{\partial A}{\partial x} d\theta + A_s \frac{\partial \theta_s}{\partial x} - A_p \frac{\partial \theta_p}{\partial x} \quad (\text{B-3})$$

Pitchwise Averaging of $\partial p / \partial x$

Equation (B-3) will now be used to carry out pitchwise averaging of $\frac{\partial p}{\partial x}$

$$\begin{aligned} \overline{\frac{\partial p}{\partial x}} &= \frac{1}{(2\pi\lambda/N)} \int_{\theta_p}^{\theta_s} \frac{\partial p}{\partial x} d\theta \\ &= \frac{1}{(2\pi\lambda/N)} \left\{ \underbrace{\frac{\partial}{\partial x} \int_{\theta_p}^{\theta_s} p d\theta}_I - \underbrace{\left(p_s \frac{\partial \theta_s}{\partial x} - p_p \frac{\partial \theta_p}{\partial x} \right)}_{II} \right\} \quad (\text{B-4}) \end{aligned}$$

$$\begin{aligned} \text{Term I} &= \frac{N}{2\pi\lambda} \frac{\partial}{\partial x} \int_{\theta_p}^{\theta_s} p d\theta = \frac{\partial}{\partial x} \left(\frac{1}{2\pi\lambda/N} \int_{\theta_p}^{\theta_s} p d\theta \right) - \left(\int_{\theta_p}^{\theta_s} p d\theta \right) \frac{\partial}{\partial x} \left(\frac{1}{2\pi\lambda/N} \right) \\ &= \frac{\partial \bar{p}}{\partial x} + \left(\frac{1}{2\pi\lambda/N} \int_{\theta_p}^{\theta_s} p d\theta \right) \cdot \frac{1}{\lambda} \frac{\partial \lambda}{\partial x} \end{aligned}$$

$$\text{Term I} = \frac{\partial \bar{p}}{\partial x} + \frac{\bar{p}}{\lambda} \frac{\partial \lambda}{\partial x} \quad (\text{B-5})$$

For evaluating Term II, θ_s and θ_p are expressed as follows

$$\theta_s = \theta_m - \frac{\pi}{N} (1-\lambda) + \frac{2\pi}{N} \quad (\text{B-6})$$

$$\theta_p = \theta_m - \frac{\pi}{N} (1-\lambda) \quad (\text{B-7})$$

here θ_m is the angular location of the mean blade surface.

From Figure (3.1) the blade lean angle is given by

$$\tan \epsilon_m = -r \frac{\partial \theta_m}{\partial r} \quad (\text{B-8})$$

Using equations (B-6), (B-7) and (B-8), Term II becomes

$$\begin{aligned} \text{Term II} &= - \left(p_s \frac{\partial \theta_s}{\partial r} - p_p \frac{\partial \theta_p}{\partial r} \right) \\ &= - \frac{(p_p + p_s)}{2} \frac{1}{\lambda} \frac{\partial \lambda}{\partial r} + \frac{(p_s - p_p)}{(\theta_s - \theta_p)} \frac{\tan \epsilon_m}{r} \end{aligned} \quad (\text{B-9})$$

Therefore equation (B-4) becomes

$$\overline{\frac{\partial p}{\partial r}} = \frac{\partial \bar{p}}{\partial r} + \frac{(p_s - p_p)}{2\pi r/N} \frac{\tan \epsilon_m}{r} + \left(\bar{p} - \frac{(p_p + p_s)}{2} \right) \frac{1}{\lambda} \frac{\partial \lambda}{\partial r} \quad (\text{B-10})$$

The term $\frac{(p_s - p_p)}{2\pi r/N} \frac{\tan \epsilon_m}{r}$ defines the radial component of the inviscid blade force.

The term $\left[\bar{p} - \frac{(p_p + p_s)}{2} \right] \frac{1}{\lambda} \frac{\partial \lambda}{\partial r}$ will be small unless $\frac{\partial \lambda}{\partial r}$ is very large. For the practical blade geometries $\frac{\partial \lambda}{\partial r}$ is small; $\left\{ \bar{p} - \frac{(p_p + p_s)}{2} \right\} / \lambda$ is also small. Hence, the last term of equation (B-10) can be neglected, giving

$$\boxed{\overline{\frac{\partial p}{\partial r}} = \frac{\partial \bar{p}}{\partial r} + F_{rci}} \quad (\text{B-11})$$

$$\text{where } F_{ri} = \frac{(P_s - P_p)}{(2\pi\lambda/N)} \frac{\tan \epsilon_m}{r}$$

Similarly

$$\overline{\frac{\partial p}{\partial z}} = \frac{\partial \bar{p}}{\partial z} + F_{zi} \quad (\text{B-12})$$

and

$$\overline{\frac{1}{r} \frac{\partial p}{\partial \theta}} = F_{\theta i} \quad (\text{B-13})$$

Pitchwise Averaging of $\frac{\partial(w_j w_k)}{\partial x_j}$

The above pitchwise averaging procedure will now be applied to $\frac{\partial w_r^2}{\partial r}$

w_r can be expressed as the sum of the pitchwise quantity and the deviation from the pitchwise value.

$$w_r = \bar{w}_r + w_r' \quad (\text{B-14})$$

$$\overline{\frac{\partial w_r^2}{\partial r}} = \overline{\frac{\partial (\bar{w}_r + w_r')^2}{\partial r}} = \overline{\frac{\partial (\bar{w}_r^2 + w_r'^2)}{\partial r}} \quad (\text{B-15})$$

Here, terms linear in the fluctuating quantities have not been retained since these will vanish on pitchwise averaging.

Following the pitchwise averaging procedure for and noting that velocities at the blade surface will vanish

(no slip condition), we get

$$\frac{\partial \overline{W_e^2}}{\partial z} = \frac{\partial \overline{W_e^2}}{\partial z} + \frac{\overline{W^2}}{\lambda} \frac{\partial \lambda}{\partial z} + \frac{\partial \overline{W_e'^2}}{\partial z} + \frac{\overline{W_e'^2}}{\lambda} \frac{\partial \lambda}{\partial z} \quad (\text{B-16})$$

Similarly

$$\frac{\partial \overline{(W_e W_z)}}{\partial z} = \frac{\partial \overline{W_e W_z}}{\partial z} + \frac{\overline{W_e W_z}}{\lambda} \frac{\partial \lambda}{\partial z} + \frac{\partial \overline{(W_e' W_z')}}{\partial z} + \frac{\overline{W_e' W_z'}}{\lambda} \frac{\partial \lambda}{\partial z} \quad (\text{B-17})$$

APPENDIX C

MEAN FLOW ENERGY EQUATION

(Frame of Reference Fixed to the Blades)

Assumptions:

- (i) Adiabatic flow
- (ii) Blade to blade variations in density and internal energy are small
- (iii) Work done by viscous stresses \ll work done by apparent stresses
- (iv) Mean flow is invariant in time

1. Rate of Gain of Internal Energy per Unit Volume

$$= \frac{\partial(\rho E W_r)}{\partial t} + \frac{\rho E W_r}{r} + \frac{1}{r} \frac{\partial(\rho E W_\theta)}{\partial \theta} + \frac{\partial(\rho E W_z)}{\partial z} \quad (C-1)$$

Where E is the internal energy per unit mass. Taking pitchwise average of equation (C-1) gives:

Rate of gain of mean Internal Energy/vol

$$= \rho \frac{\overline{D} E}{Dt} \quad (C-2)$$

where $\frac{\overline{D}}{Dt} = \overline{W_r} \frac{\partial}{\partial r} + \overline{W_z} \frac{\partial}{\partial z}$ (C-3)

2. Rate of Gain of Kinetic Energy per Unit Volume

$$= \frac{\partial(\rho W_r W_r^2/2)}{\partial t} + \frac{\rho W_r W_r^2/2}{r} + \frac{1}{r} \frac{\partial(\rho W_\theta W_\theta^2/2)}{\partial \theta} + \frac{\partial(\rho W_z W_z^2/2)}{\partial z} \quad (C-4)$$

Where $W^2 = W_r^2 + W_\theta^2 + W_z^2$ (C-5)

Using continuity equation $\nabla \cdot (\rho W) = 0$ gives:

Rate of Gain of K.E/vol

$$= \rho W_r \frac{\partial (W^2/2)}{\partial r} + \frac{\rho}{r} W_\theta \frac{\partial (W^2/2)}{\partial \theta} + \rho W_z \frac{\partial (W^2/2)}{\partial z} \quad (C-6)$$

Taking pitchwise average gives:

Rate of Gain of mean K.E/vol

$$= \rho \left\{ \overline{\frac{D}{Dt} (W^2/2)} + \overline{\frac{D'}{Dt} (W^2/2)} + \overline{\frac{D''}{Dt} (W^2/2)} + \overline{\frac{D'''}{Dt} (W W')} \right\} \quad (C-7)$$

where $\overline{\frac{D'}{Dt}} = \overline{W_r' \frac{\partial}{\partial r}} + \overline{\frac{W_\theta'}{r} \frac{\partial}{\partial \theta}} + \overline{W_z' \frac{\partial}{\partial z}}$ (C-8)

3. Rate of Work Input from Pressure Forces per Unit Volume

$$= - \left(\frac{1}{r} \frac{\partial}{\partial r} (r p W_r) + \frac{1}{r} \frac{\partial}{\partial \theta} (W_\theta p) + \frac{\partial}{\partial z} (W_z p) \right) \quad (C-9)$$

$$= \left\{ \left(W_r \frac{\partial p}{\partial r} + \frac{W_\theta}{r} \frac{\partial p}{\partial \theta} + W_z \frac{\partial p}{\partial z} \right) + p \left(\frac{1}{r} \frac{\partial}{\partial r} (r W_r) + \frac{1}{r} \frac{\partial W_\theta}{\partial \theta} + \frac{\partial W_z}{\partial z} \right) \right\} \quad (C-10)$$

The second term in the right hand side of equation (C-10) can be written as $p \nabla \cdot W$ and using continuity equation, we have

$$\rho \nabla \cdot \vec{W} = -\rho \frac{D\rho}{Dt} \quad (C-11)$$

where

$$\frac{D\rho}{Dt} = w_r \frac{\partial \rho}{\partial r} + \frac{w_\theta}{r} \frac{\partial \rho}{\partial \theta} + w_z \frac{\partial \rho}{\partial z} \quad (C-12)$$

Therefore,

Rate of work input by pressure force/vol

$$= -\frac{Dp}{Dt} + \frac{p}{\rho} \frac{D\rho}{Dt} \quad (C-13)$$

Taking a pitchwise average of equation (C-13):

Rate of mean work input by pressure forces/vol

$$= -\left\{ \frac{D\bar{p}}{Dt} + \frac{D\bar{p}'}{Dt} \right\} + \left\{ \frac{\bar{p}}{\rho} \frac{D\rho}{Dt} + \frac{\bar{p}'w_r'}{\rho} \frac{\partial \rho}{\partial r} + \frac{\bar{p}'w_z'}{\rho} \frac{\partial \rho}{\partial z} \right\} \quad (C-14)$$

4. We can find the work done per unit volume by the normal and shear stresses. Here we will assume that the apparent stresses introduced due to the pitchwise averaging of equations of motion dominate and the viscous stresses are small.

Work done by apparent normal stresses per unit volume

$$= -\rho \left\{ \bar{w}_r \frac{\partial \bar{w}_r'^2}{\partial r} + \bar{w}_r'^2 \frac{\partial \bar{w}_r}{\partial r} + \frac{\bar{w}_r \bar{w}_r'^2}{r} + \bar{w}_z \frac{\partial \bar{w}_z'^2}{\partial z} + \bar{w}_z'^2 \frac{\partial \bar{w}_z}{\partial z} \right\} \quad (C-15)$$

Here the terms containing the derivative of density are neglected.

Similarly, work done by apparent shear stresses per unit volume

$$\begin{aligned}
 &= -\rho \left\{ \overline{w_z} \frac{\partial(\overline{w_r' w_z'})}{\partial r} + \overline{w_r' w_z'} \frac{\partial \overline{w_z}}{\partial r} + \overline{w_\theta} \frac{\partial(\overline{w_r' w_\theta'})}{\partial r} + (\overline{w_r' w_\theta'}) \frac{\partial \overline{w_\theta}}{\partial r} \right. \\
 &\quad \left. + \overline{w_z} \left(\frac{\overline{w_r' w_z'}}{r} \right) + \overline{w_\theta} \left(\frac{\overline{w_r' w_\theta'}}{r} \right) \right\} - \rho \left\{ \overline{w_r} \frac{\partial(\overline{w_r' w_z'})}{\partial z} \right. \\
 &\quad \left. + (\overline{w_r' w_z'}) \frac{\partial \overline{w_r}}{\partial z} + \overline{w_\theta} \frac{\partial(\overline{w_r' w_\theta'})}{\partial z} + (\overline{w_r' w_\theta'}) \frac{\partial \overline{w_\theta}}{\partial z} \right\} \quad (C-16)
 \end{aligned}$$

If $-\Sigma_r$, $-\Sigma_\theta$ and $-\Sigma_z$ represent the apparent stress terms appearing in the radial, pitchwise and axial momentum equations respectively, and if Φ_{app} denotes the production or apparent dissipation term, the rate of work done by apparent stresses per unit volume can be written as:

Rate (work done by apparent stresses)

$$= -\rho \left\{ \overline{w_r} \left(\Sigma_r + \frac{\overline{w_\theta'^2}}{r} \right) + \overline{w_\theta} \Sigma_\theta + \overline{w_z} \Sigma_z \right\} + \rho \Phi_{app} \quad (C-17)$$

$$\text{where } \Phi_{app} = - \left\{ \overline{w_r'^2} \frac{\partial \overline{w_r}}{\partial r} + \overline{w_z'^2} \frac{\partial \overline{w_z}}{\partial z} + \overline{w_r' w_\theta'} \frac{\partial \overline{w_\theta}}{\partial r} \right. \\
 \left. + \overline{w_r' w_z'} \left(\frac{\partial \overline{w_r}}{\partial r} + \frac{\partial \overline{w_r}}{\partial z} \right) + \overline{w_z' w_\theta'} \frac{\partial \overline{w_\theta}}{\partial z} \right\}$$

5. Rate of Work Done by Centrifugal Force

As we are using the relative frame of reference, it is necessary to account for the work done by the centrifugal force. It may be mentioned here that no work is done by the Coriolis forces since both the radial and the tangential

components of coriolis forces are associated with velocities normal to them.

Centrifugal force only has a radial component and therefore work done by it per unit volume

$$= \int w_r \Omega^2 r \quad (C-18)$$

Pitchwise averaging gives the mean rate of work done by the centrifugal force

$$= \int \overline{w_r} r \Omega^2 = \int \frac{D}{Dt} (\overline{r^2} \Omega^2 / 2) \quad (C-19)$$

The energy equation can now be written by equating the rate of gain of mean internal and kinetic energies to the mean work input rate from the pressure and centrifugal forces, and the apparent stresses. This gives, after rearranging

$$\begin{aligned} & \int \frac{D E}{Dt} + \frac{D}{Dt} (\overline{w^2} / 2) + \frac{D \overline{p}}{Dt} - \frac{\overline{p}}{\rho} \frac{D \rho}{Dt} - \int \frac{D}{Dt} (\overline{r^2} \Omega^2 / 2) \\ &= - \int \left\{ \overline{w_r} (\Sigma_r + \frac{\overline{w_\theta^2}}{r}) + \overline{w_\theta} \Sigma_\theta + \overline{w_z} \Sigma_z \right\} - \int \overline{\Phi}_{app} \\ &+ \left\{ - \frac{D \overline{p'}}{Dt} + \frac{\overline{p' w_r}}{\rho} \frac{\partial \rho}{\partial r} + \frac{\overline{p' w_z}}{\rho} \frac{\partial \rho}{\partial z} \right\} \\ &+ \int \left\{ \frac{D \overline{w'^2}}{Dt} + \frac{D (\overline{w w'})}{Dt} \right\} - \frac{D}{Dt} (\overline{w'^2} / 2) \end{aligned} \quad (C-20)$$

Now, consistent with the discussion presented in Section 3.3, mean rothalpy is defined as

$$\overline{I} \equiv \overline{E} + \frac{\overline{p}}{\rho} + \frac{\overline{w^2}}{2} - \frac{r^2 \Omega^2}{2} \quad (C-21)$$

Equation (C-20) then becomes

$$\begin{aligned} \frac{\overline{D\bar{I}}}{Dt} = & - \left[\left\{ \overline{W_r} \left(\Sigma_r + \frac{\overline{W_\theta^2}}{r} \right) + \overline{W_\theta} \Sigma_\theta + \overline{W_z} \Sigma_z \right\} + \overline{\Phi}_{app} + \frac{\overline{D(W'^2/2)}}{Dt} \right] \\ & + \frac{1}{s} \left\{ - \frac{\overline{D'p'}}{Dt} + \frac{\overline{p'W_r'}}{s} \frac{\partial s}{\partial r} + \frac{\overline{p'W_z'}}{s} \frac{\partial s}{\partial z} \right\} \\ & + \left\{ \frac{\overline{D'W'^2/2}}{Dt} + \frac{\overline{D'(\overline{W}W')}}{Dt} \right\} \end{aligned} \quad (C-22)$$

Equation (C-22) gives the rate of mean Rothalpy variation along the mean meridional streamline

$$\text{For the axisymmetric case, } \frac{\overline{D\bar{I}}}{Dt} = \overline{W_m} \frac{\partial \bar{I}}{\partial m}$$

and according to the definitions

$$\frac{\overline{W_\theta}}{\overline{W_m}} = \tan \beta, \quad \frac{\overline{W_z}}{\overline{W_m}} = \cos \phi, \quad \frac{\overline{W_r}}{\overline{W_m}} = \sin \phi \quad (C-23)$$

Substituting these relations in equation (C-22), we get

$$\begin{aligned} \frac{\partial \bar{I}}{\partial m} = & - \left[\left\{ \sin \phi \left(\Sigma_r + \frac{\overline{W_\theta^2}}{r} \right) + \tan \beta \Sigma_\theta + \cos \phi \Sigma_z \right\} + \overline{\Phi}_{app} + \frac{\partial \overline{W'^2/2}}{\partial m} \right] \\ & + \frac{1}{\overline{W_m} s} \left\{ - \frac{\overline{D'p'}}{Dt} + \frac{\overline{p'W_r'}}{s} \frac{\partial s}{\partial r} + \frac{\overline{p'W_z'}}{s} \frac{\partial s}{\partial z} \right\} \\ & + \frac{1}{\overline{W_m}} \left\{ \frac{\overline{D'W'^2/2}}{Dt} + \frac{\overline{D'(\overline{W}W')}}{Dt} \right\} \end{aligned} \quad (C-24)$$

APPENDIX D

DERIVATION OF MEAN FLOW EQUATIONS OF MOTION FOR STREAMLINE CURVATURE TECHNIQUE

Equation of Motion in l-direction

In deriving the mean flow (pitchwise averaged) equation of motion, it is assumed that pitchwise variation of density is small. Hence the mean flow equations of motion derived in Appendix A are considered valid here. Variation of density in the streamwise direction is taken into account through the continuity equation.

For Streamline Curvature technique, a single equation of motion is derived in the meridional plan (or r-z plane). The mean flow equation of motion will be derived in a direction inclined at an angle γ to the radial direction. Figure (4.1) gives the details of various directions and angles to be used in the derivation.

The procedure adopted for getting the desired equation is to start with mean flow equations of motion in r, θ , and z directions and derive a single vector mean flow equation in Crocco's form. Equation in any particular direction can then be derived from the Crocco equation by taking its scalar product with the unit vector in the desired direction.

Pitchwise averaged equations of motion in the r, θ , and z directions, in a coordinate system fixed to the blades, were derived in Appendix A.

These are,

r-direction

$$\begin{aligned} \overline{W}_r \frac{\partial \overline{W}_r}{\partial r} + \overline{W}_z \frac{\partial \overline{W}_r}{\partial z} - \frac{\overline{W}_\theta^2}{r} - 2\overline{W}_\theta \Omega - \Omega^2 r \\ = -\frac{1}{\rho} \frac{\partial \overline{P}}{\partial r} - \Sigma_{r\lambda} + F_{ri} + \overline{F}_{rv} \end{aligned} \quad (D-1)$$

θ-direction

$$\begin{aligned} \overline{W}_r \frac{\partial \overline{W}_\theta}{\partial r} + \overline{W}_z \frac{\partial \overline{W}_\theta}{\partial z} + 2\Omega \overline{W}_r + \frac{\overline{W}_\theta \overline{W}_r}{r} \\ = -\Sigma_{\theta\lambda} + F_{\theta i} + \overline{F}_{\theta v} \end{aligned} \quad (D-2)$$

z-direction

$$\overline{W}_r \frac{\partial \overline{W}_z}{\partial r} + \overline{W}_z \frac{\partial \overline{W}_z}{\partial z} = -\frac{1}{\rho} \frac{\partial \overline{P}}{\partial z} - \Sigma_{z\lambda} + F_{zi} + \overline{F}_{zv} \quad (D-3)$$

where $\Sigma_{r\lambda}$, $\Sigma_{\theta\lambda}$ and $\Sigma_{z\lambda}$ are the apparent stress terms

$$\begin{aligned} \Sigma_{r\lambda} &= \frac{1}{\rho \lambda} \left(\frac{\partial (\lambda \overline{W}_r^2 \lambda \rho)}{\partial r} + \frac{\partial (\lambda \overline{W}_r \overline{W}_z \rho)}{\partial z} - \frac{\lambda \overline{W}_\theta^2 \rho}{r} \right) \\ \Sigma_{\theta\lambda} &= \frac{1}{\lambda \rho} \left(\frac{\partial (\lambda \overline{W}_r \overline{W}_\theta \rho)}{\partial r} + \frac{\partial (\lambda \overline{W}_z \overline{W}_\theta \rho)}{\partial z} + \frac{2\lambda \overline{W}_r \overline{W}_\theta \rho}{r} \right) \end{aligned} \quad (D-3a)$$

and
$$\Sigma_{z\lambda} = \frac{1}{\lambda \rho} \left(\frac{\partial (\lambda \overline{W}_r \overline{W}_z \rho)}{\partial r} + \frac{\partial (\lambda \overline{W}_z^2 \rho)}{\partial z} + \frac{\lambda \overline{W}_r \overline{W}_z \rho}{r} \right)$$

F_{ri} , $F_{\theta i}$ and F_{zi} are the r, θ, and z components of the mean inviscid blade force, given by

$$F_{ri} = -\frac{\Delta p}{\rho r \Delta \theta} \tan \epsilon_m, \quad F_{\theta i} = -\frac{\Delta p}{\rho r \Delta \theta} \quad \text{and} \quad F_{zi} = -\frac{\Delta p}{r \Delta \theta} \tan \beta_m$$

where ϵ_m is the mean blade lean angle and β_m is the mean blade angle with respect to z axis in the azimuthal plane.

\bar{F}_{ru} , $\bar{F}_{\theta u}$ and \bar{F}_{zu} are the components of mean viscous drag force in r, θ , and z directions.

By adding and subtracting $\bar{w}_\theta \frac{\partial \bar{w}_\theta}{\partial r} + \bar{w}_z \frac{\partial \bar{w}_z}{\partial r}$ to equation

(D-1) $\bar{w}_r \frac{\partial \bar{w}_r}{\partial z} + \bar{w}_\theta \frac{\partial \bar{w}_\theta}{\partial z}$ to equation (D-3), the equations

(D-1), (D-2), and (D-3) can be rearranged as

$$\begin{aligned} & -\frac{\bar{w}_\theta}{r} \left(\frac{\partial (r \bar{w}_\theta)}{\partial r} \right) + \bar{w}_z \left(\frac{\partial \bar{w}_r}{\partial z} - \frac{\partial \bar{w}_z}{\partial r} \right) - 2 \bar{w}_\theta \Omega - \Omega^2 r + \\ \text{a) } & \frac{\partial}{\partial r} \left(\frac{1}{2} (\bar{w}_r^2 + \bar{w}_\theta^2 + \bar{w}_z^2) \right) = -\frac{1}{s} \frac{\partial \bar{p}}{\partial r} - \Sigma_{r\lambda} + F_{ri} + \bar{F}_{ru} \end{aligned} \quad (\text{D-4})$$

$$\begin{aligned} \text{b) } & -\frac{\bar{w}_z}{r} \left(-\frac{\partial (r \bar{w}_\theta)}{\partial z} \right) + \frac{\bar{w}_r}{r} \left(\frac{\partial (r \bar{w}_\theta)}{\partial r} \right) + 2 \Omega \bar{w}_z \\ & = -\Sigma_{\theta\lambda} + F_{\theta i} + \bar{F}_{\theta u} \end{aligned} \quad (\text{D-5})$$

$$\begin{aligned} \text{c) } & -\bar{w}_r \left(\frac{\partial \bar{w}_r}{\partial z} - \frac{\partial \bar{w}_z}{\partial r} \right) + \frac{\bar{w}_\theta}{r} \left(\frac{\partial (r \bar{w}_\theta)}{\partial z} \right) + \frac{\partial}{\partial z} \left(\frac{1}{2} (\bar{w}_r^2 + \bar{w}_\theta^2 + \bar{w}_z^2) \right) \\ & = -\Sigma_{z\lambda} + F_{zi} + \bar{F}_{zu} \end{aligned} \quad (\text{D-6})$$

Now replacing \bar{w}_θ by $\bar{v}_\theta - r \Omega$ in $r \bar{w}_\theta$ and \bar{w}_θ^2 terms, and since $\bar{w}_r = \bar{v}_r$ and $\bar{w}_z = \bar{v}_z$ these equations become

$$\begin{aligned} \text{a) } & -\frac{\bar{w}_\theta}{r} \left(\frac{\partial (r \bar{v}_\theta)}{\partial r} \right) + \bar{v}_z \left(\frac{\partial \bar{v}_r}{\partial z} - \frac{\partial \bar{v}_z}{\partial r} \right) + \frac{\partial}{\partial r} \left(\frac{1}{2} (\bar{v}_r^2 + \bar{v}_\theta^2 + \bar{v}_z^2) \right) \\ & - \frac{\partial (r \Omega \bar{v}_\theta)}{\partial r} = -\frac{1}{s} \frac{\partial \bar{p}}{\partial r} - \Sigma_{r\lambda} + F_{ri} + \bar{F}_{ru} \end{aligned} \quad (\text{D-7})$$

$$\text{b) } -\frac{\bar{v}_z}{r} \left(-\frac{\partial (r \bar{v}_\theta)}{\partial z} \right) + \frac{\bar{v}_r}{r} \left(\frac{\partial (r \bar{v}_\theta)}{\partial r} \right) = -\Sigma_{\theta\lambda} + F_{\theta i} + \bar{F}_{\theta u} \quad (\text{D-8})$$

$$\begin{aligned} \text{c) } & -\bar{v}_r \left(\frac{\partial \bar{v}_r}{\partial z} - \frac{\partial \bar{v}_z}{\partial r} \right) + \frac{\bar{v}_\theta}{r} \left(\frac{\partial (r \bar{v}_\theta)}{\partial z} \right) + \frac{\partial}{\partial z} \left(\frac{1}{2} (\bar{v}_r^2 + \bar{v}_\theta^2 + \bar{v}_z^2) \right) \\ & - \frac{\partial (r \Omega \bar{v}_\theta)}{\partial z} = -\Sigma_{z\lambda} + F_{zi} + \bar{F}_{zu} \end{aligned} \quad (\text{D-9})$$

The bracketed terms of equations (D-7), (D-8) and (D-9) are the components of vorticity. Thus for pitchwise average flow

$$\begin{aligned}
 \text{a)} \quad & \left(\nabla \times \underline{\bar{V}} \right)_r = \frac{1}{r} \left(- \frac{\partial (r \bar{v}_\theta)}{\partial z} \right) \\
 \text{b)} \quad & \left(\nabla \times \underline{\bar{V}} \right)_\theta = \left(\frac{\partial \bar{v}_r}{\partial z} - \frac{\partial \bar{v}_z}{\partial r} \right) \\
 \text{c)} \quad & \left(\nabla \times \underline{\bar{V}} \right)_z = \frac{1}{r} \left(\frac{\partial (r \bar{v}_\theta)}{\partial r} \right)
 \end{aligned} \tag{D-10}$$

We can now get a single equation in vector form replacing equations (D-7), (D-8) and (D-9)

$$\begin{aligned}
 - \underline{\bar{W}} \times \left(\nabla \times \underline{\bar{V}} \right) + \nabla \left(\frac{1}{2} \bar{v}^2 \right) - \nabla (r \Omega \bar{v}_\theta) \\
 = - \frac{\nabla \bar{p}}{\rho} - \left(\hat{r} \Sigma_{r\lambda} + \hat{\theta} \Sigma_{\theta\lambda} + \hat{z} \Sigma_z \right) + \underline{\bar{F}}_i + \underline{\bar{F}}_v
 \end{aligned} \tag{D-11}$$

where $\underline{\bar{F}}_i$ is the mean inviscid blade force vector and $\underline{\bar{F}}_v$ is the mean viscous force vector.

We know from Gibbs relation that

$$\frac{1}{\rho} \nabla p = \nabla h - T \nabla s \tag{D-12}$$

Taking pitchwise average, this becomes

$$\frac{1}{\rho} \nabla \bar{p} = \nabla \bar{h} - T \nabla \bar{s} \tag{D-13}$$

Here the temperature fluctuations have been assumed to be small

Equation (D-11) then becomes,

$$\begin{aligned} \overrightarrow{W} \times (\nabla \times \overrightarrow{V}) = \nabla \left(\bar{h} + \frac{1}{2} \bar{q}^2 - r \Omega \bar{v}_\theta \right) - T \nabla \bar{s} \\ + \left(\hat{r} \Sigma_{r\lambda} + \hat{\theta} \Sigma_{\theta\lambda} + \hat{z} \Sigma_{z\lambda} \right) - \underline{F}_i - \underline{F}_v \end{aligned} \quad (D-14)$$

From the definition of Rothalpy (relative total enthalpy) I , we know

$$I = h + \frac{q^2}{2} - r \Omega v_\theta \quad (D-15)$$

Using the definition (1.1) for \bar{I} , we have

$$\bar{I} = \bar{h} + \bar{q}^2/2 - r \Omega \bar{v}_\theta$$

Substituting for $(\bar{h} + \bar{q}^2/2 - r \Omega \bar{v}_\theta)$ in (D-14), we get

$$\boxed{\begin{aligned} \overrightarrow{W} \times (\nabla \times \overrightarrow{V}) = \nabla \bar{I} - T \nabla \bar{s} \\ + \left(\hat{r} \Sigma_{r\lambda} + \hat{\theta} \Sigma_{\theta\lambda} + \hat{z} \Sigma_{z\lambda} \right) - \underline{F}_i - \underline{F}_v \end{aligned}} \quad (D-16)$$

Equation (D-16) is the pitchwise averaged counterpart of the steady state Crocco equation modified to include viscous terms.

This is the basic equation for deriving mean flow equation of motion in any desired direction.

In order to arrive at the mean flow equation of motion in 1-direction (Figure 4.1), we will take dot product of equation (D-16) with unit vector \hat{l} .

Let $\underline{A} = \underline{W} \times (\nabla \times \underline{V})$, and let A_r, A_θ and A_z be the components of vector \underline{A} in r, θ and z directions.

Let $\overline{F}_{mi}, \overline{F}_{ni}$ and $\overline{F}_{\theta i}$ be the components of inviscid force \underline{F}_i in m, n and θ directions, and $\overline{F}_{mv}, \overline{F}_{nv}$ and $\overline{F}_{\theta v}$ be the components of viscous force in m, n and θ directions. Writing the equation for dot product $\hat{l} \cdot \underline{A}$

$$\begin{aligned} \hat{l} \cdot \{ \hat{r} A_r + \hat{\theta} A_\theta + \hat{z} A_z \} &= \frac{\partial \overline{I}}{\partial l} - \tau \frac{\partial \overline{S}}{\partial l} \\ &+ \hat{l} \cdot \{ \hat{r} \Sigma_{r\lambda} + \hat{\theta} \Sigma_{\theta\lambda} + \hat{z} \Sigma_{z\lambda} \} \\ &- \hat{l} \cdot \{ \hat{m} \overline{F}_{mi} + \hat{n} \overline{F}_{ni} + \hat{\theta} \overline{F}_{\theta i} \} \\ &- \hat{l} \cdot \{ \hat{m} \overline{F}_{mv} + \hat{n} \overline{F}_{nv} + \hat{\theta} \overline{F}_{\theta v} \} \end{aligned} \quad (D-17)$$

Since \hat{l} lies in the meridional plane which is perpendicular to θ direction $\hat{l} \cdot \hat{\theta} = 0$

$$\begin{aligned} \text{From Figure (4.1) we find } \hat{l} \cdot \hat{r} &= \cos \gamma, \\ \hat{l} \cdot \hat{z} &= \sin \gamma, \quad \hat{l} \cdot \hat{m} = \sin(\phi + \gamma), \quad \hat{l} \cdot \hat{n} = \cos(\phi + \gamma) \end{aligned}$$

Here γ is fixed and ϕ is defined as the angle of mean stream surface.

Substituting these relations in equation (D-17), we get

$$\begin{aligned} &\left\{ \underline{W} \times (\nabla \times \underline{V}) \right\}_r \cos \gamma + \left\{ \underline{W} \times (\nabla \times \underline{V}) \right\}_z \sin \gamma \\ &= \frac{\partial \overline{I}}{\partial l} - \tau \frac{\partial \overline{S}}{\partial l} + \Sigma_{r\lambda} \cos \gamma + \Sigma_{z\lambda} \sin \gamma \\ &- (F_{mi} + \overline{F}_{mv}) \sin(\phi + \gamma) - (F_{ni} + \overline{F}_{nv}) \cos(\phi + \gamma) \end{aligned} \quad (D-18)$$

Simultaneous solution of these two equations gives

$$\frac{\partial(\)}{\partial r} = \frac{\sin r \frac{\partial(\)}{\partial m} - \cos \phi \frac{\partial(\)}{\partial l}}{\sin \phi \sin r - \cos \phi \cos r} \quad (D-20)$$

$$\frac{\partial(\)}{\partial z} = \frac{\sin \phi \frac{\partial(\)}{\partial l} - \cos r \frac{\partial(\)}{\partial m}}{\sin \phi \sin r - \cos \phi \cos r} \quad (D-21)$$

We can now transform Terms I and II in the left hand side of equation (D-19) in terms of derivatives in m and l directions.

Using equations (D-20) and (D-21), Term I becomes,

$$\text{Term I} = \frac{\bar{w}_0}{r} \left\{ - \frac{\cos r \cos \phi \frac{\partial(\tau \bar{v}_0)}{\partial l}}{\sin \phi \sin r - \cos \phi \cos r} + \frac{(\sin r \sin \phi \frac{\partial(\tau \bar{v}_0)}{\partial l})}{\sin \phi \sin r - \cos \phi \cos r} \right\}$$

Simplifying

$$\text{Term I} = \frac{\bar{w}_0}{r} \left\{ \frac{\partial(\tau \bar{v}_0)}{\partial l} \right\}$$

changing \bar{v}_0 to $\bar{w}_0 + r\Omega$, we get

$$\text{Term I} = \frac{\bar{w}_0}{r} \left\{ \frac{\partial(\tau \bar{w}_0)}{\partial l} + 2r\Omega \frac{\partial \tau}{\partial l} \right\}$$

Substituting in (D-18) for $\{\vec{W} \times (\nabla \times \vec{V})\}_r$ and $\{\vec{W} \times (\nabla \times \vec{V})\}_z$ from the following relations

$$\left\{ \vec{W} \times (\nabla \times \vec{V}) \right\}_r = \left\{ \frac{\bar{W}_\theta}{r} \frac{\partial(r\bar{V}_\theta)}{\partial r} - \bar{V}_z \left(\frac{\partial \bar{V}_r}{\partial z} - \frac{\partial \bar{V}_z}{\partial r} \right) \right\}$$

$$\left\{ \vec{W} \times (\nabla \times \vec{V}) \right\}_z = \left\{ \bar{V}_r \left(\frac{\partial \bar{V}_r}{\partial z} - \frac{\partial \bar{V}_z}{\partial r} \right) + \frac{\bar{W}_\theta}{r} \frac{\partial(r\bar{V}_\theta)}{\partial z} \right\}$$

(Note: $\bar{W}_r = \bar{V}_r$ $\bar{W}_z = \bar{V}_z$)

and rearranging, gives

$$\begin{aligned} & \frac{\bar{W}_\theta}{r} \left\{ \underbrace{\cos r \frac{\partial(r\bar{V}_\theta)}{\partial r}}_I + \underbrace{\sin r \frac{\partial(r\bar{V}_\theta)}{\partial z}}_I \right\} \\ & + \left\{ \underbrace{(\bar{V}_r \sin r - \bar{V}_z \cos r)}_{II} \left(\frac{\partial \bar{V}_r}{\partial z} - \frac{\partial \bar{V}_z}{\partial r} \right) \right\} = \frac{\partial I}{\partial t} - \tau \frac{\partial S}{\partial t} \end{aligned} \quad (D-19)$$

$$+ (\cos r) \Sigma_{r\lambda} + (\sin r) \Sigma_{z\lambda} - (F_{mi} + \bar{F}_{mv}) \sin(\phi+r) - (F_{zi} + \bar{F}_{nz}) \cos(\phi+r)$$

In order to get radial and axial derivative in terms of derivatives in m and l directions, following transformation relations are used

$$\frac{\partial(\)}{\partial m} = \frac{\partial(\)}{\partial z} \frac{\partial z}{\partial m} + \frac{\partial(\)}{\partial r} \frac{\partial r}{\partial m}$$

$$\frac{\partial(\)}{\partial l} = \frac{\partial(\)}{\partial z} \frac{\partial z}{\partial l} + \frac{\partial(\)}{\partial r} \frac{\partial r}{\partial l}$$

OR

$$\frac{\partial(\)}{\partial m} = \cos \phi \frac{\partial(\)}{\partial z} + \sin \phi \frac{\partial(\)}{\partial r}$$

$$\frac{\partial(\)}{\partial l} = \sin r \frac{\partial(\)}{\partial z} + \cos r \frac{\partial(\)}{\partial r}$$

(D-19a)

or

$$\text{Term I} = \frac{\bar{w}_\theta}{r} \frac{\partial(r\bar{w}_\theta)}{\partial t} + 2\bar{w}_\theta \Omega \cos r \quad (\text{D-22})$$

For evaluating Term II, we use the relations

$$\bar{v}_r = \bar{v}_m \sin \phi \quad \text{and} \quad \bar{v}_z = \bar{v}_m \cos \phi$$

This gives

$$\text{Term II} = \bar{v}_m (\sin \phi \sin r - \cos \phi \cos r) \left(\frac{\partial \bar{v}_r}{\partial z} - \frac{\partial \bar{v}_z}{\partial r} \right)$$

Using equations (D-20) and (D-21), we get

$$\begin{aligned} \text{Term II} &= \bar{v}_m (\sin \phi \sin r - \cos \phi \cos r) \times \\ &\quad \left\{ \frac{(\sin \phi \frac{\partial \bar{v}_r}{\partial z} - \cos r \frac{\partial \bar{v}_r}{\partial m}) - (\sin r \frac{\partial \bar{v}_z}{\partial m} - \cos \phi \frac{\partial \bar{v}_z}{\partial r})}{(\sin \phi \sin r - \cos \phi \cos r)} \right\} \\ &= \bar{v}_m (\sin \phi \sin r - \cos \phi \cos r) \times \\ &\quad \left\{ \frac{(\frac{\sin \phi}{2\bar{v}_r} \frac{\partial \bar{v}_r^2}{\partial z} + \frac{\cos \phi}{2\bar{v}_z} \frac{\partial \bar{v}_z^2}{\partial r}) - (\cos r \frac{\partial \bar{v}_r}{\partial m} + \sin r \frac{\partial \bar{v}_z}{\partial m})}{(\sin \phi \sin r - \cos \phi \cos r)} \right\} \end{aligned}$$

Simplifying and using the relations $\bar{v}_x^2 + \bar{v}_z^2 = \bar{v}_m^2$ and

$\frac{\partial \phi}{\partial m} = \frac{1}{\tau c}$, we get

$$\text{Term II} = \bar{v}_m \frac{\partial \bar{v}_m}{\partial l} - \bar{v}_m \frac{\partial \bar{v}_m}{\partial m} \sin(\phi + \tau) - \frac{\bar{v}_m^2}{\tau c} \cos(\phi + \tau) \quad (\text{D-23})$$

Substituting Term I and Term II in equation (D-19),

rearranging the equation and using the relation $\frac{\partial}{\partial l} = \cos \tau \frac{\partial}{\partial z} + \sin \tau \frac{\partial}{\partial z}$, equation (D-19) becomes

$$\begin{aligned} \bar{v}_m \frac{\partial \bar{v}_m}{\partial l} &= \bar{v}_m \frac{\partial \bar{v}_m}{\partial m} \sin(\phi + \tau) + \frac{\bar{v}_m^2}{\tau c} \cos(\phi + \tau) - \frac{\bar{w}_0}{\tau} \frac{\partial(\tau \bar{w}_0)}{\partial l} \\ &\quad - \frac{\partial \bar{I}}{\partial l} - 2 \bar{w}_0 \Omega \cos \tau - \tau \frac{\partial \bar{S}}{\partial l} \\ &\quad + \frac{\cos \tau}{\lambda \rho} \left\{ \frac{1}{\tau} \frac{\partial(\tau \lambda \bar{w}_z^2)}{\partial z} + \frac{\partial(\lambda \bar{w}_z^2)}{\partial z} - \frac{\lambda \bar{w}_0^2}{\tau} \right\} \\ &\quad + \frac{\sin \tau}{\lambda \rho} \left\{ \frac{\partial(\lambda \bar{w}_z^2)}{\partial z} + \frac{\partial(\lambda \bar{w}_z^2)}{\partial z} + \frac{\lambda \bar{w}_z^2}{\tau} \right\} \\ &\quad - (F_{mi} + \bar{F}_{miv}) \sin(\phi + \tau) \\ &\quad - (F_{ni} + \bar{F}_{niv}) \cos(\phi + \tau) \end{aligned} \quad (\text{D-24})$$

This is the mean flow equation for Streamline Curvature Computational method. This equation has to be suitably modified for the computer program depending on the type of input data. Inviscid and viscous force terms have also to be expressed in terms of the known input data.

Mean Flow Equation of Motion in the Meridional Direction

Pitchwise averaged equations of motion (D-1) and (D-3) in the radial and axial direction can be written as

$$a) \quad \overline{W}_t \frac{\partial \overline{W}_t}{\partial r} + \overline{W}_z \frac{\partial \overline{W}_r}{\partial z} - \frac{\overline{U_\theta}^2}{r} = -\frac{1}{\rho} \frac{\partial \overline{P}}{\partial r} - \sum_{r\lambda} + \overline{F}_r \quad (D-25)$$

$$b) \quad \overline{W}_r \frac{\partial \overline{W}_z}{\partial r} + \overline{W}_z \frac{\partial \overline{W}_z}{\partial z} = -\frac{1}{\rho} \frac{\partial \overline{P}}{\partial z} - \sum_{z\lambda} + \overline{F}_z \quad (D-26)$$

Here $(\frac{\overline{W_\theta}^2}{r} + 2\overline{W_\theta} \Omega + \Omega^2 r)$ has been replaced by $\frac{\overline{U_\theta}^2}{r}$ and $\overline{F}_r = F_{ri} + \overline{F}_{rv}$; $\overline{F}_z = F_{zi} + F_{zv}$

Using the relations

$$\overline{U_m}^2 = \overline{W_m}^2 = \overline{W_z}^2 + \overline{W_r}^2 ;$$

$$\overline{W}_r = \overline{V_m} \sin \phi ; \quad \overline{W}_z = \overline{V_m} \cos \phi$$

and after some algebraic manipulation, we get

$$\begin{aligned} & \overline{U_m} \frac{\partial \overline{U_m}}{\partial m} - \frac{\overline{U_\theta}^2}{r} \sin \phi \\ & = -\frac{1}{\rho} \frac{\partial \overline{P}}{\partial m} + (\overline{F}_r \sin \phi + \overline{F}_z \cos \phi) - (\sum_{r\lambda} \sin \phi + \sum_{z\lambda} \cos \phi) \quad (D-27) \end{aligned}$$

$$\text{But} \quad \overline{F}_m = \overline{F}_r \sin \phi + \overline{F}_z \cos \phi$$

This reduces equation (D-27) to the following form

$$\frac{1}{s} \frac{\partial \bar{p}}{\partial m} = -\bar{v}_m \frac{\partial \bar{v}_m}{\partial r} + \frac{\bar{v}_\theta^2}{r} \sin \phi - (\Sigma_{r\lambda} \sin \phi + \Sigma_{z\lambda} \cos \phi) + \bar{F}_m \quad (\text{D-28})$$

\bar{F}_m is eliminated from equation (D-28) by using equation (40)

$$\bar{F}_m = -\frac{\bar{w}_\theta}{r} \frac{\partial (r\bar{v}_\theta)}{\partial m} - \Sigma_{\theta\lambda} \tan \beta - T \frac{\partial \bar{s}}{\partial m} \quad (40)$$

Equation (D-28) becomes for the bladed region

$$\begin{aligned} \frac{1}{s} \frac{\partial \bar{p}}{\partial m} = & \frac{\bar{v}_\theta^2}{r} \sin \phi - \frac{\bar{w}_\theta}{r} \frac{\partial (r\bar{v}_\theta)}{\partial m} - \bar{v}_m \frac{\partial \bar{v}_m}{\partial m} \\ & - (\Sigma_{r\lambda} \sin \phi + \Sigma_{z\lambda} \cos \phi) - \Sigma_{\theta\lambda} \tan \beta - T \frac{\partial \bar{s}}{\partial m} \end{aligned} \quad (\text{D-29})$$

Equation (D-29) is the mean flow momentum equation in the meridional direction.

Now using the equation $T ds = C_p dT - \frac{dp}{s}$ (D-30)

From the equation of state $T = \frac{p}{sR}$, we have

$$dT = \frac{1}{R} \left(\frac{dp}{s} - \frac{p}{s} \frac{ds}{s} \right)$$

Using this along with the relation $\frac{R}{C_p} = \frac{r-1}{\gamma}$, in equation (D-30), and taking derivative with respect to m , we get

$$\frac{1}{s} \frac{d\bar{p}}{dm} = \frac{r\bar{p}}{s} \cdot \frac{1}{s} \frac{ds}{dm} + (r-1) T \frac{d\bar{s}}{dm}$$

Taking $\frac{r\bar{p}}{s} = \bar{a}^2 = \frac{\bar{v}_m^2}{\bar{M}_m^2}$

and substituting this for $\frac{1}{s} \frac{d\bar{p}}{dm}$, in equation (D-29), we get the modified form of meridional direction equation of motion:

$$\begin{aligned}
\frac{1}{S} \frac{\partial \mathcal{L}}{\partial m} &= \frac{\bar{M}_m^2}{\bar{U}_m^2} \left\{ \frac{\bar{U}_0^2}{r} - \frac{\bar{W}_0}{r} \frac{\partial (r \bar{U}_0)}{\partial m} - \bar{U}_m \frac{\partial \bar{U}_m}{\partial m} \right\} \\
&\quad - \frac{\bar{M}_m^2}{\bar{U}_m^2} \left\{ \sum_{\theta, \lambda} \tan \beta + (\sum_{z, \lambda} \sin \phi + \sum_{z, \lambda} \cos \phi) \right\} \\
&\quad - \frac{1}{R} \frac{\partial \bar{S}}{\partial m}
\end{aligned}$$

(D-31)

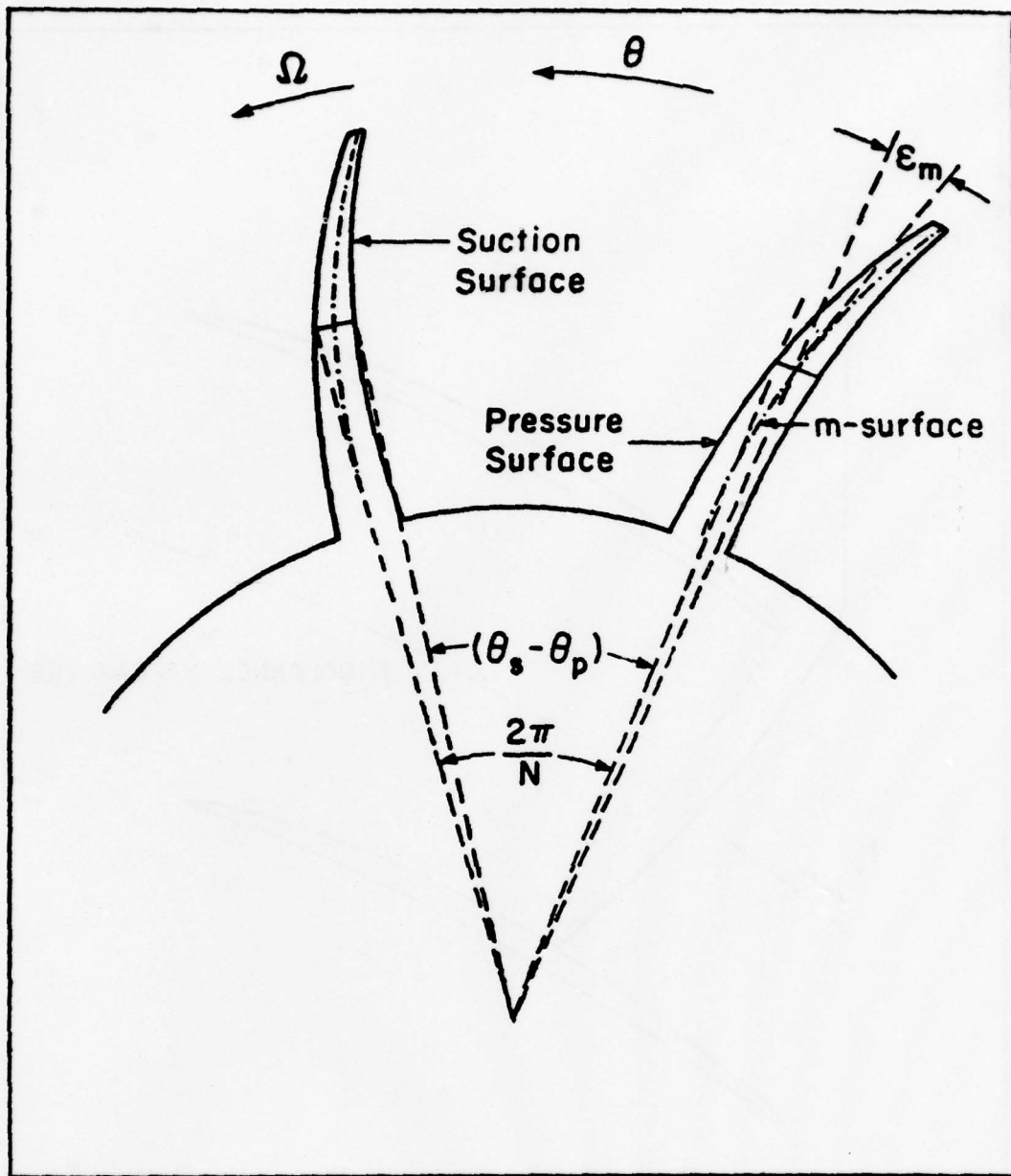


FIGURE 1. ROTOR SECTION CUT AT $z = \text{CONSTANT}$ PLANE.

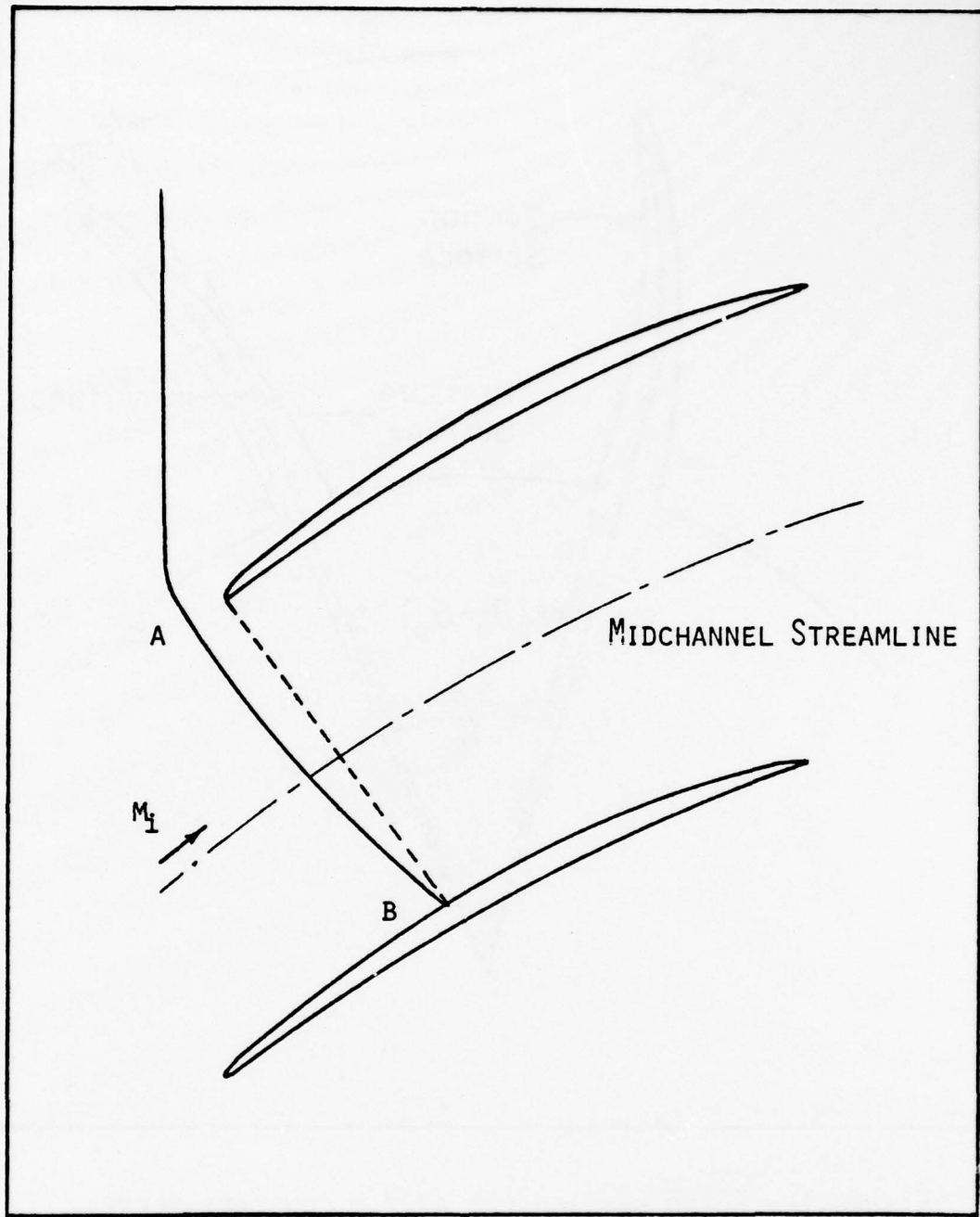


FIGURE 2. PASSAGE SHOCK-WAVE CONFIGURATION.

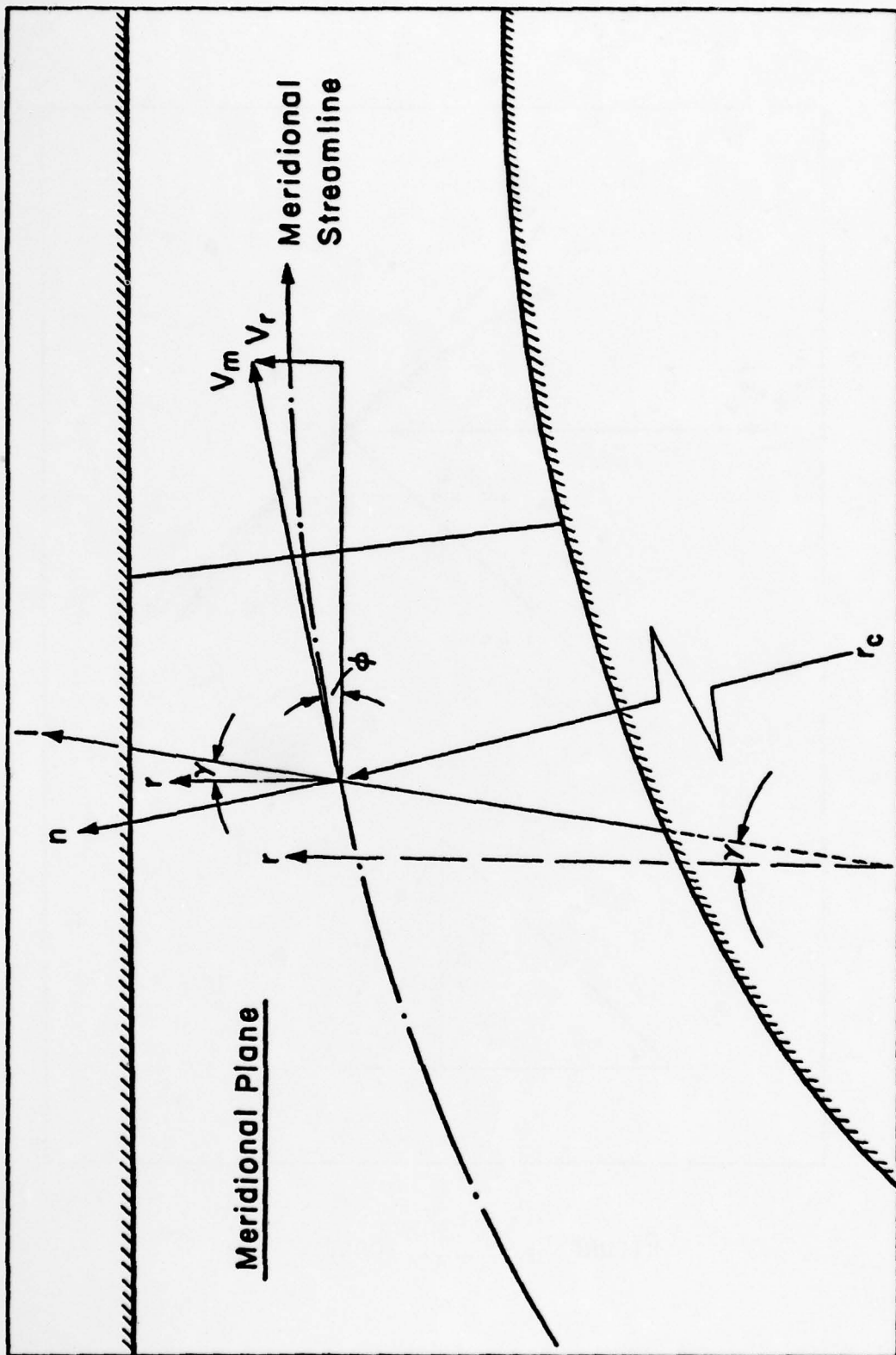


FIGURE 3. MERIDIONAL PLANE PICTURE OF A PASSAGE.

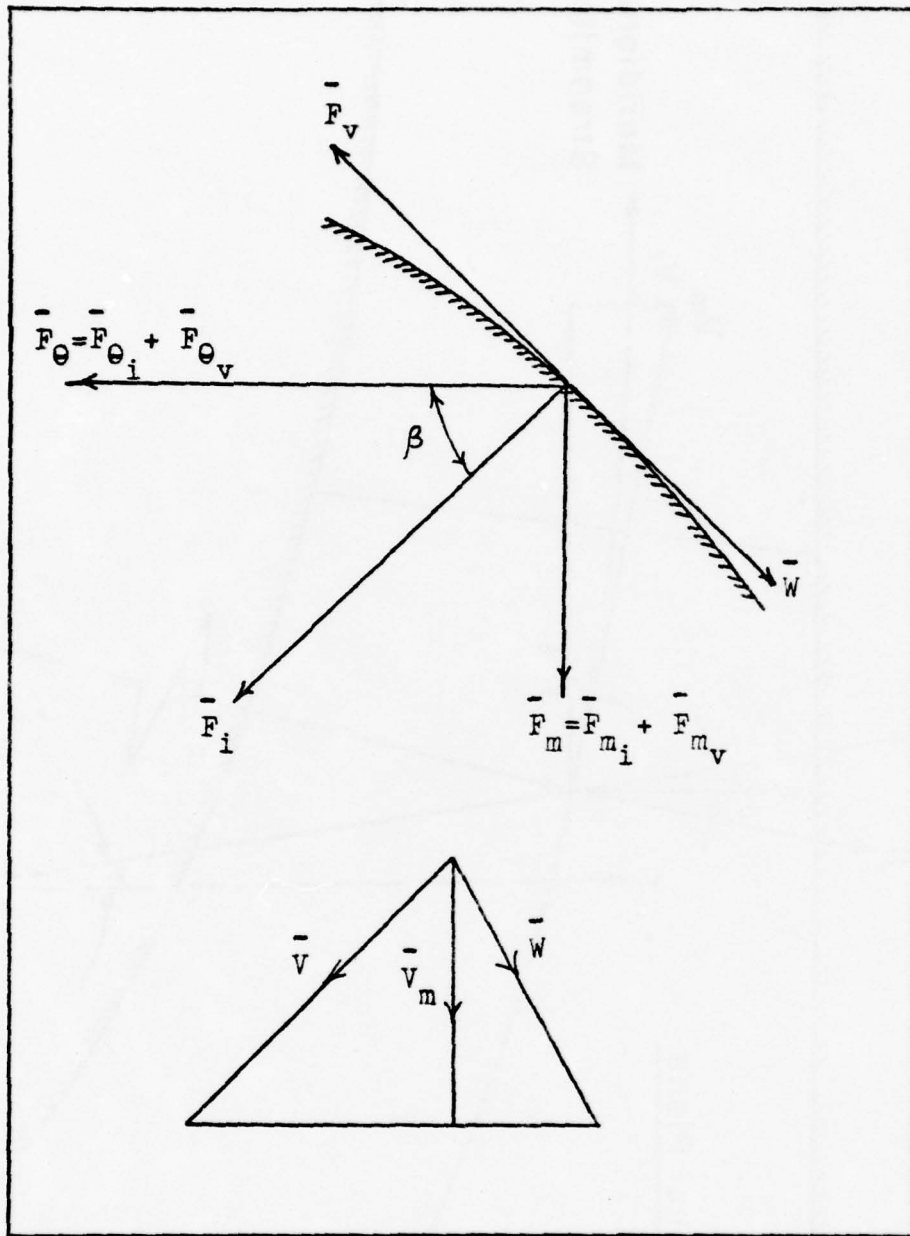


FIGURE 4. BLADE FORCES.

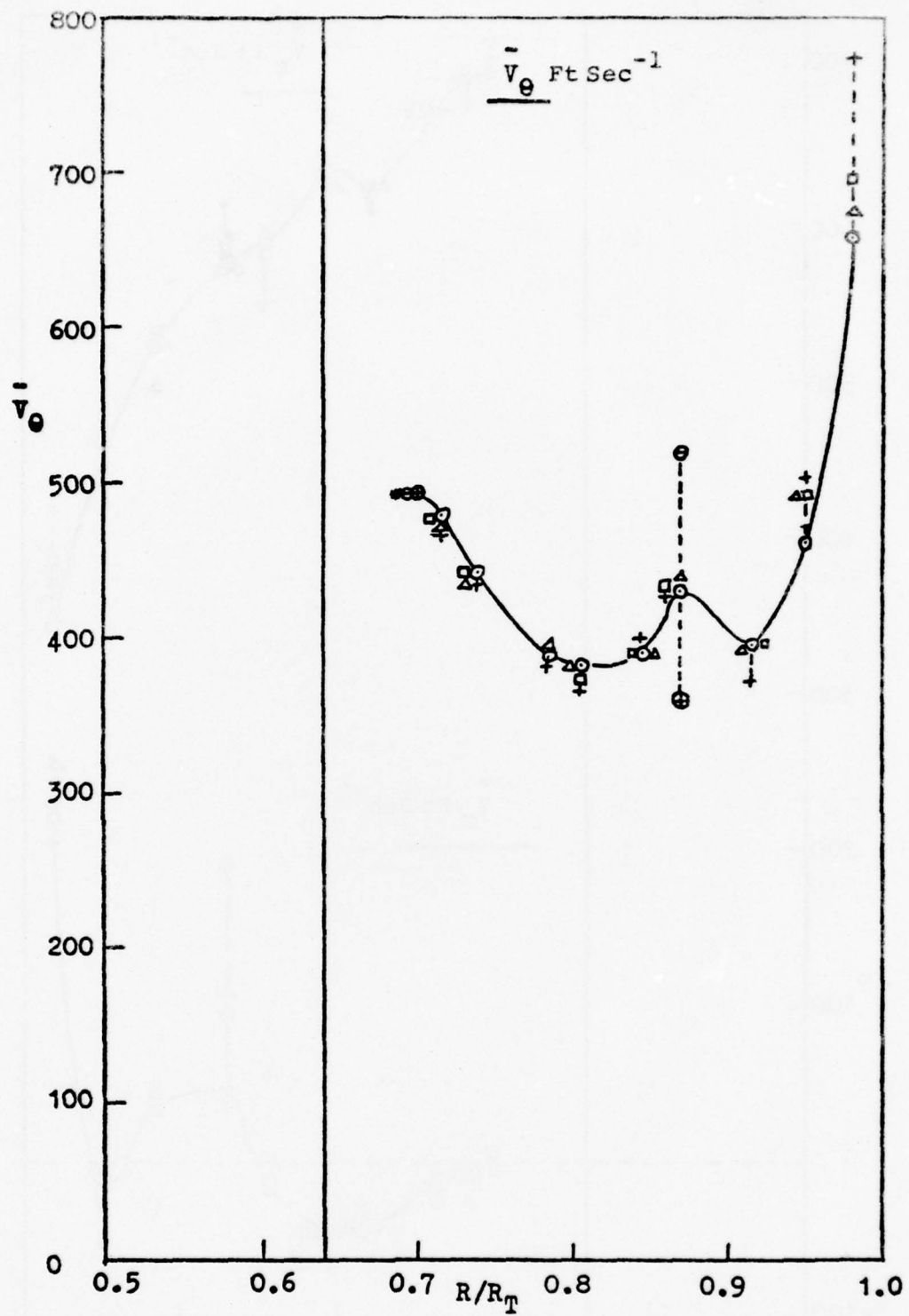


FIGURE 5. EXPERIMENTAL DISTRIBUTION OF MEAN PITCHWISE VELOCITY, 0.1 CHORD DOWNSTREAM OF THE ROTOR.

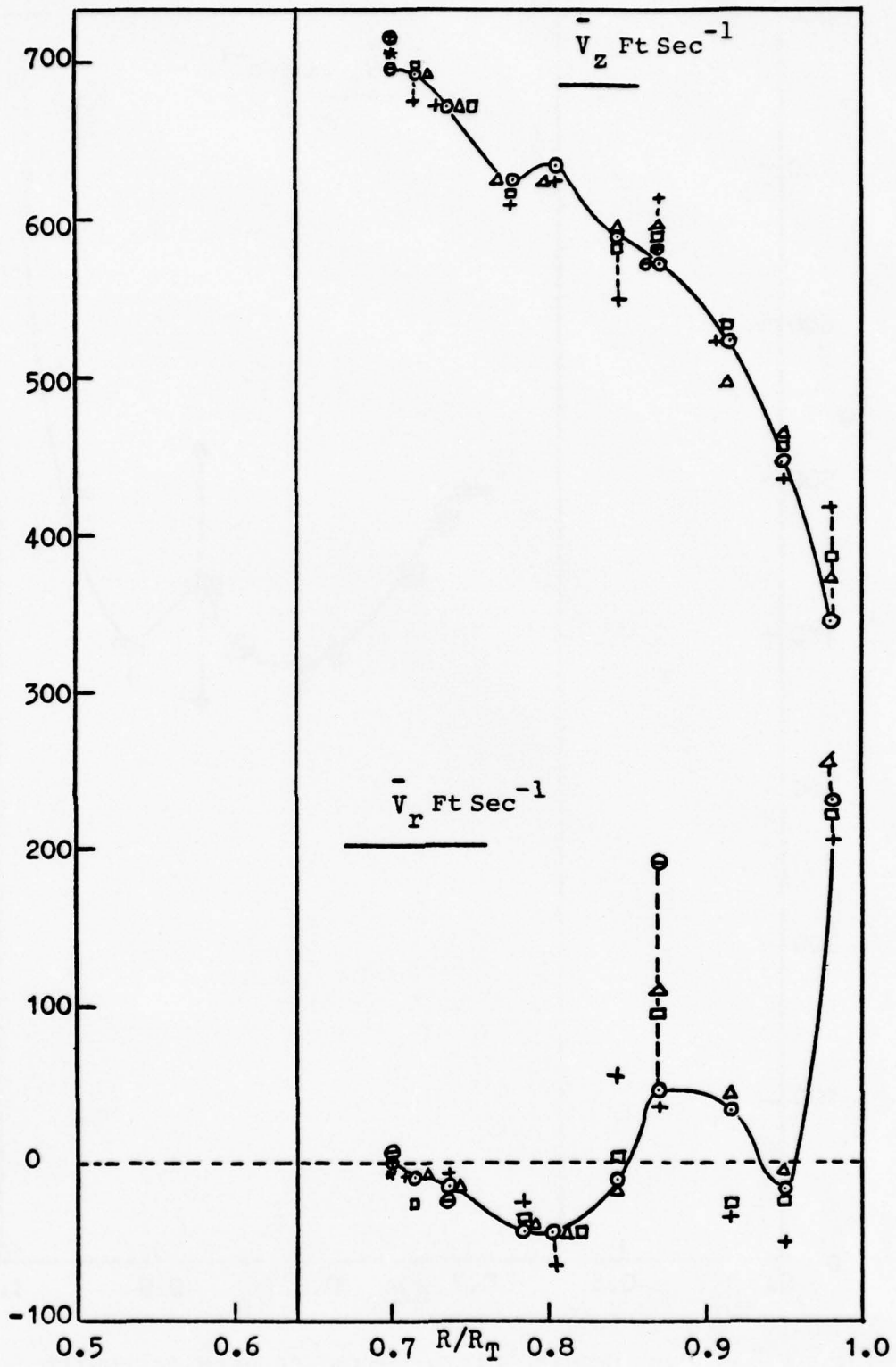


FIGURE 6. EXPERIMENTAL \bar{V}_z AND \bar{V}_r , 0.1 CHORD DOWNSTREAM OF THE ROTOR.

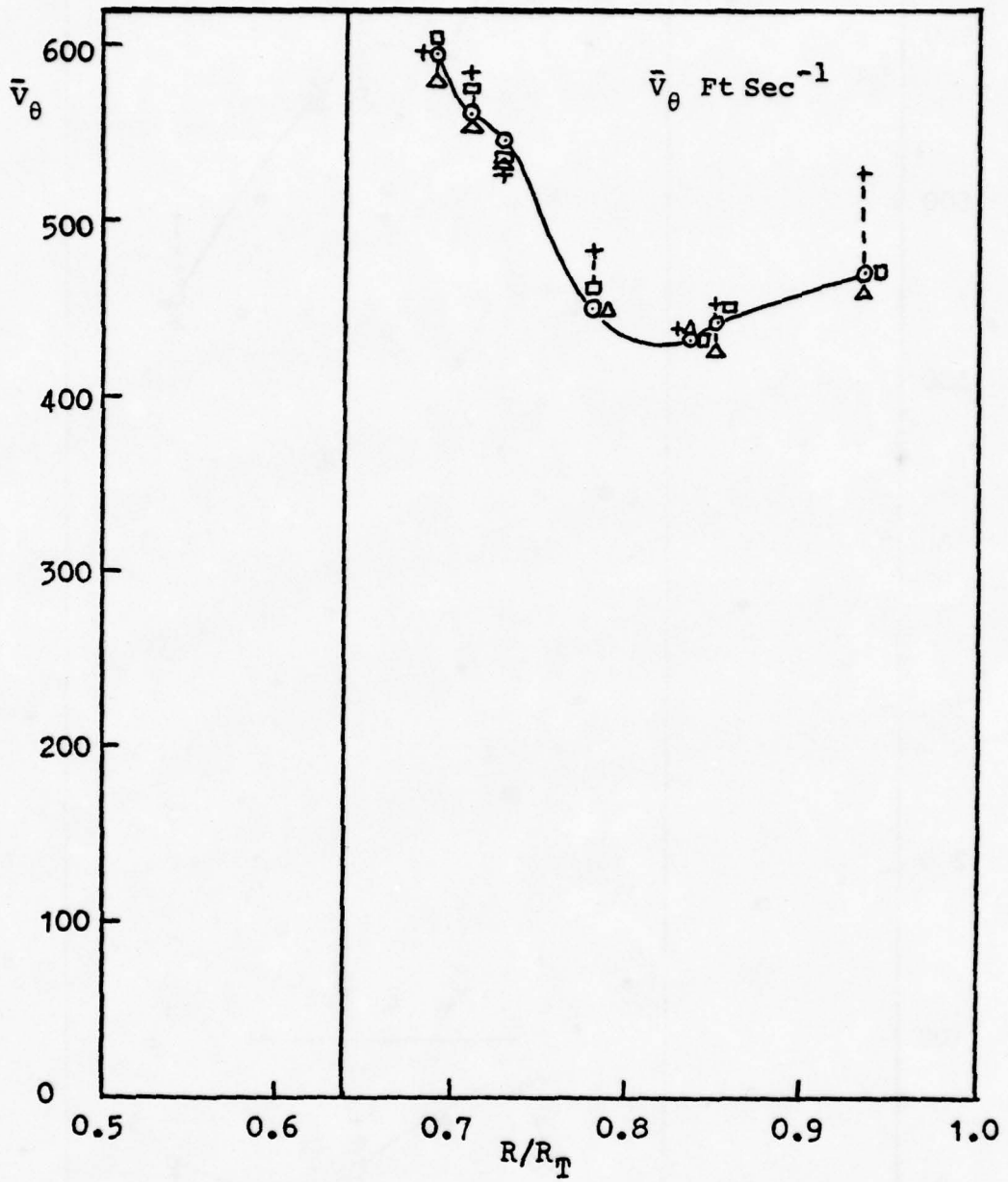


FIGURE 7. EXPERIMENTAL DISTRIBUTION OF MEAN PITCHWISE VELOCITY, 1.0 CHORD DOWNSTREAM OF THE ROTOR.

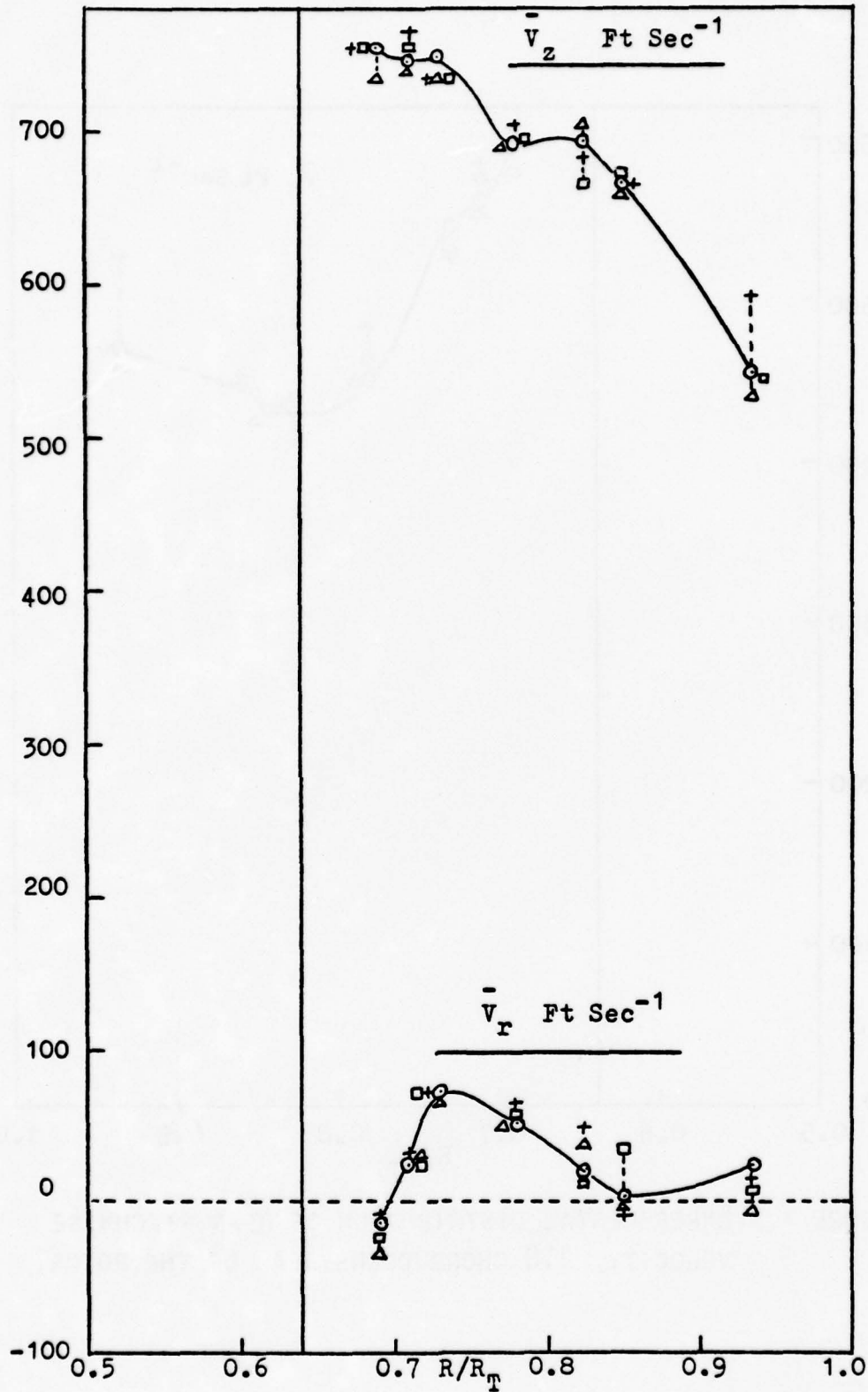


FIGURE 8. EXPERIMENTAL \bar{V}_z AND \bar{V}_r , 1.0 CHORD DOWNSTREAM OF THE ROTOR.

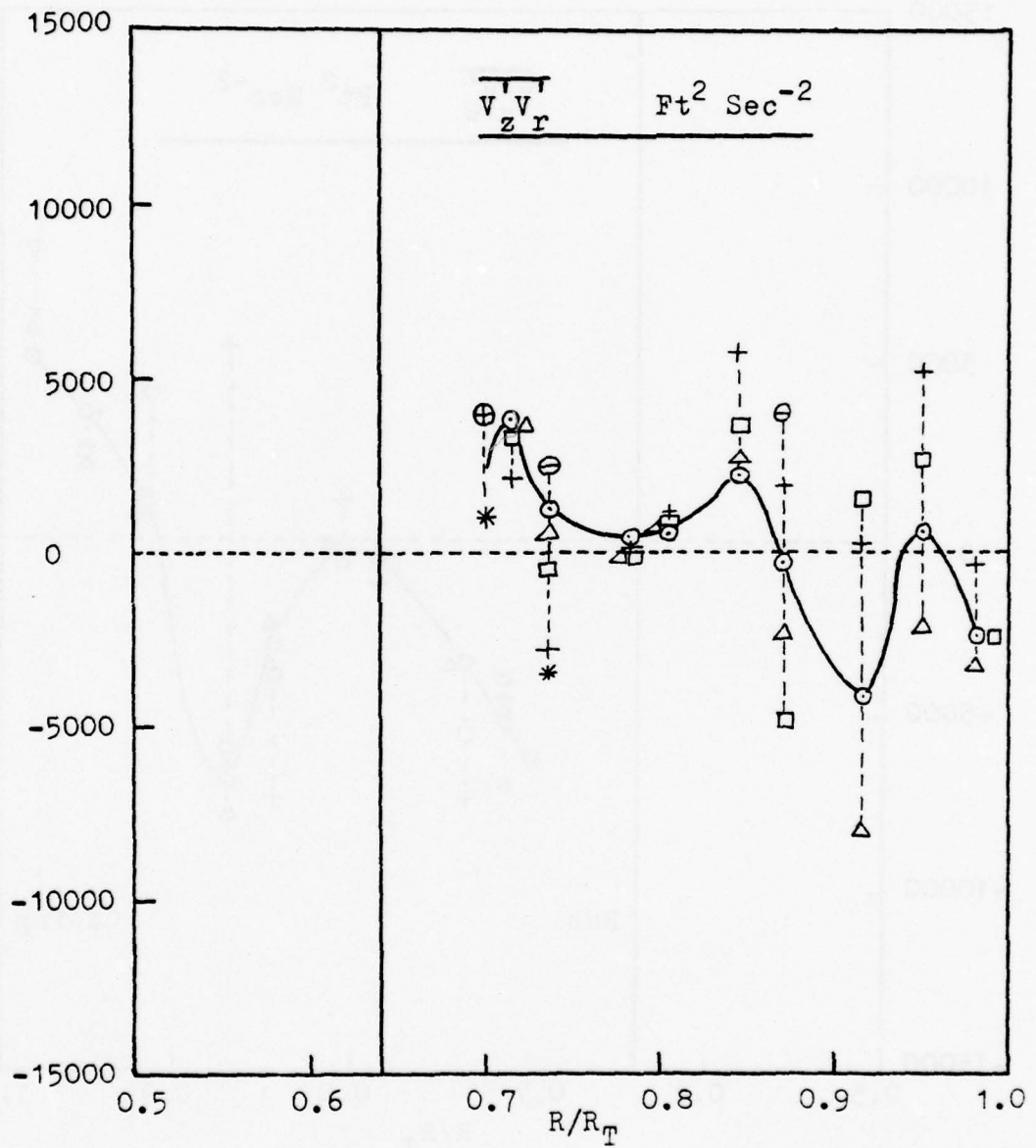


FIGURE 9. APPARENT SHEAR STRESS $\overline{v'_z v'_r}$, 0.1 CHORD DOWNSTREAM OF THE ROTOR.

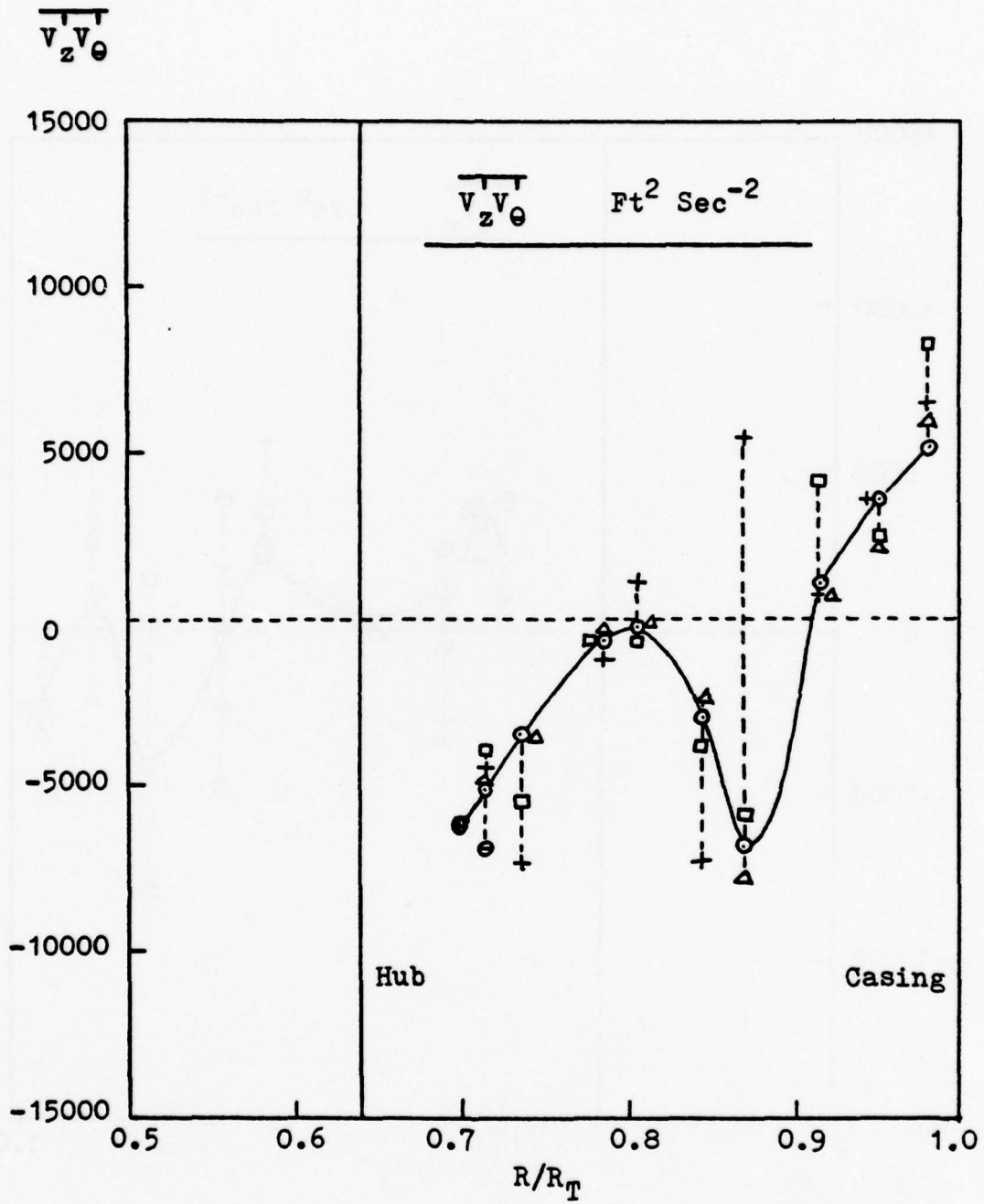


FIGURE 10. APPARENT SHEAR STRESS $\overline{v'_z v'_\theta}$, 0.1 CHORD DOWNSTREAM OF THE ROTOR.

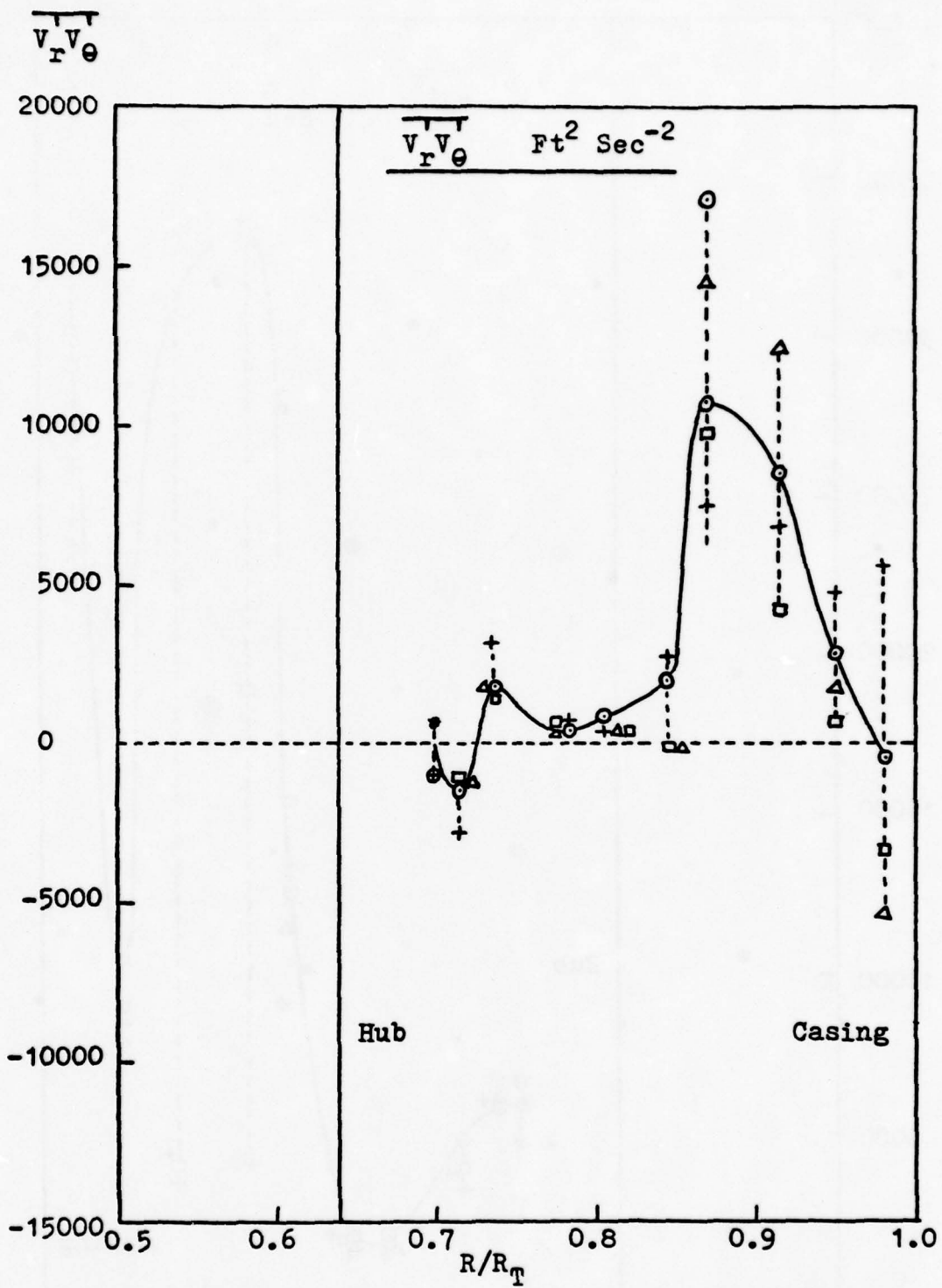


FIGURE 11. APPARENT SHEAR STRESS $\overline{v_r v_\theta}$, 0.1 CHORD DOWNSTREAM OF THE ROTOR.

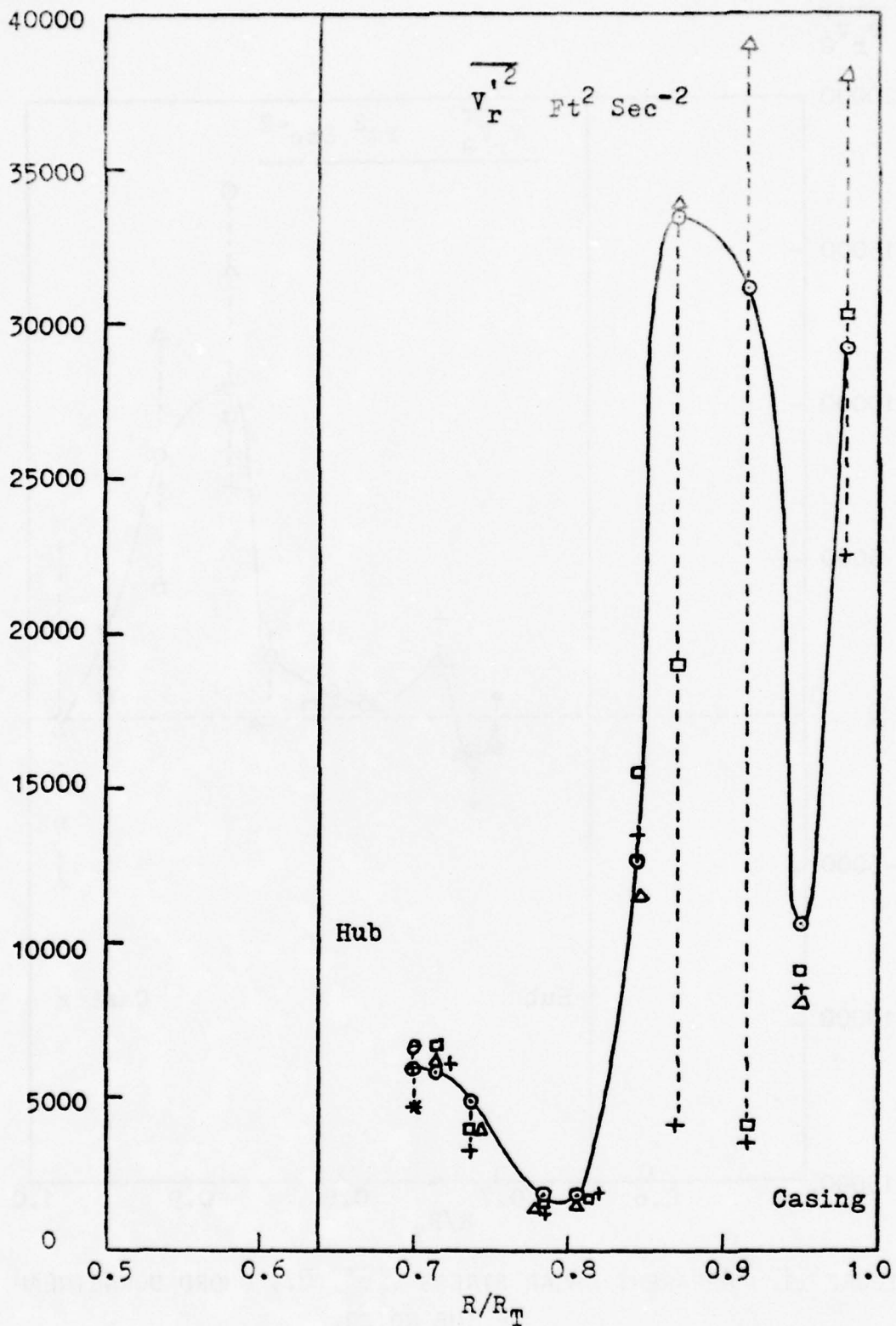


FIGURE 12. $\overline{v_r'^2}$, 0.1 CHORD DOWNSTREAM OF THE ROTOR.

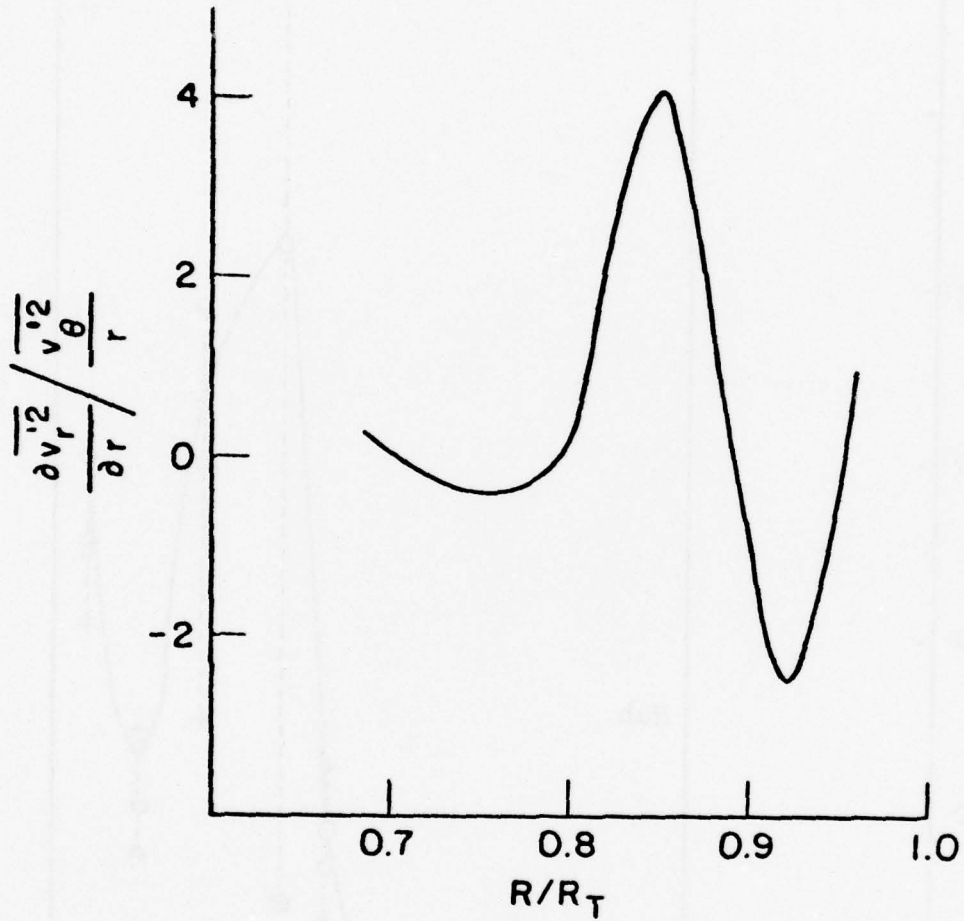


FIGURE 12a. $\frac{\partial \overline{v_r'^2}}{\partial r} / \frac{\overline{v_\theta'^2}}{r}$, 0.1 CHORD DOWNSTREAM
OF THE ROTOR.

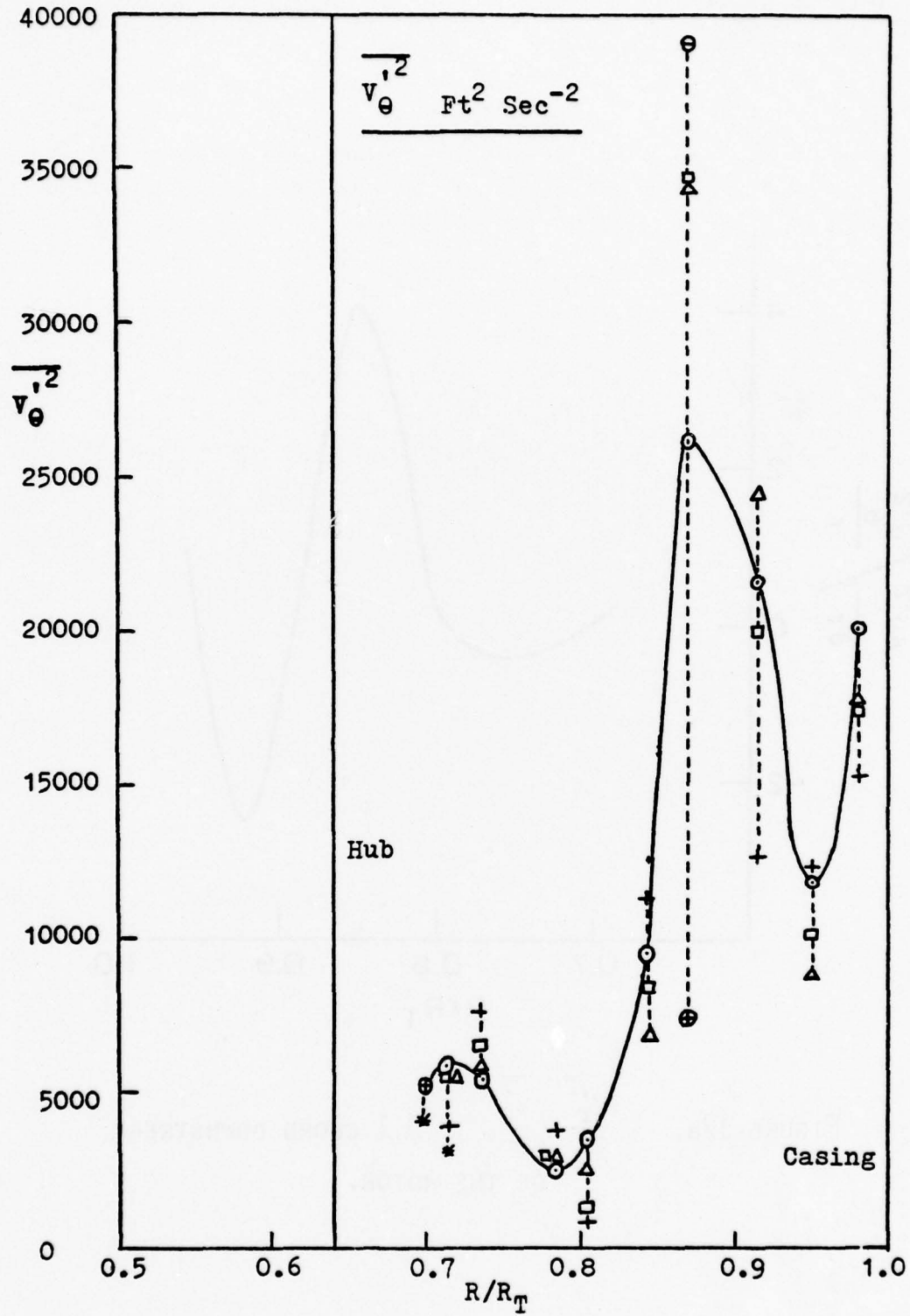


FIGURE 13. APPARENT NORMAL STRESS $\overline{v_{\theta}^{\prime 2}}$, 0.1 CHORD DOWNSTREAM OF THE ROTOR.

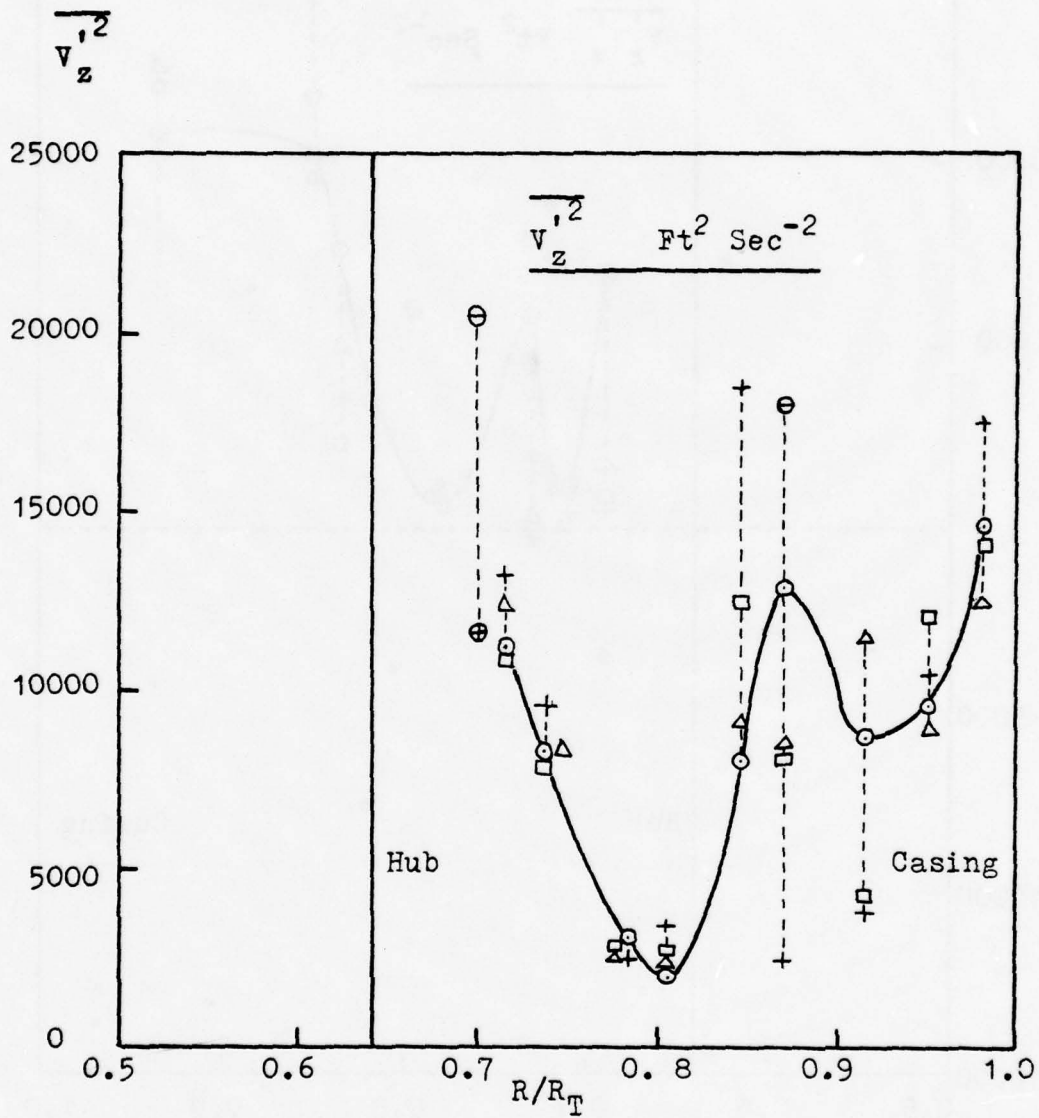


FIGURE 14. APPARENT NORMAL STRESS $\overline{v_z'^2}$, 0.1 CHORD DOWNSTREAM OF THE ROTOR.

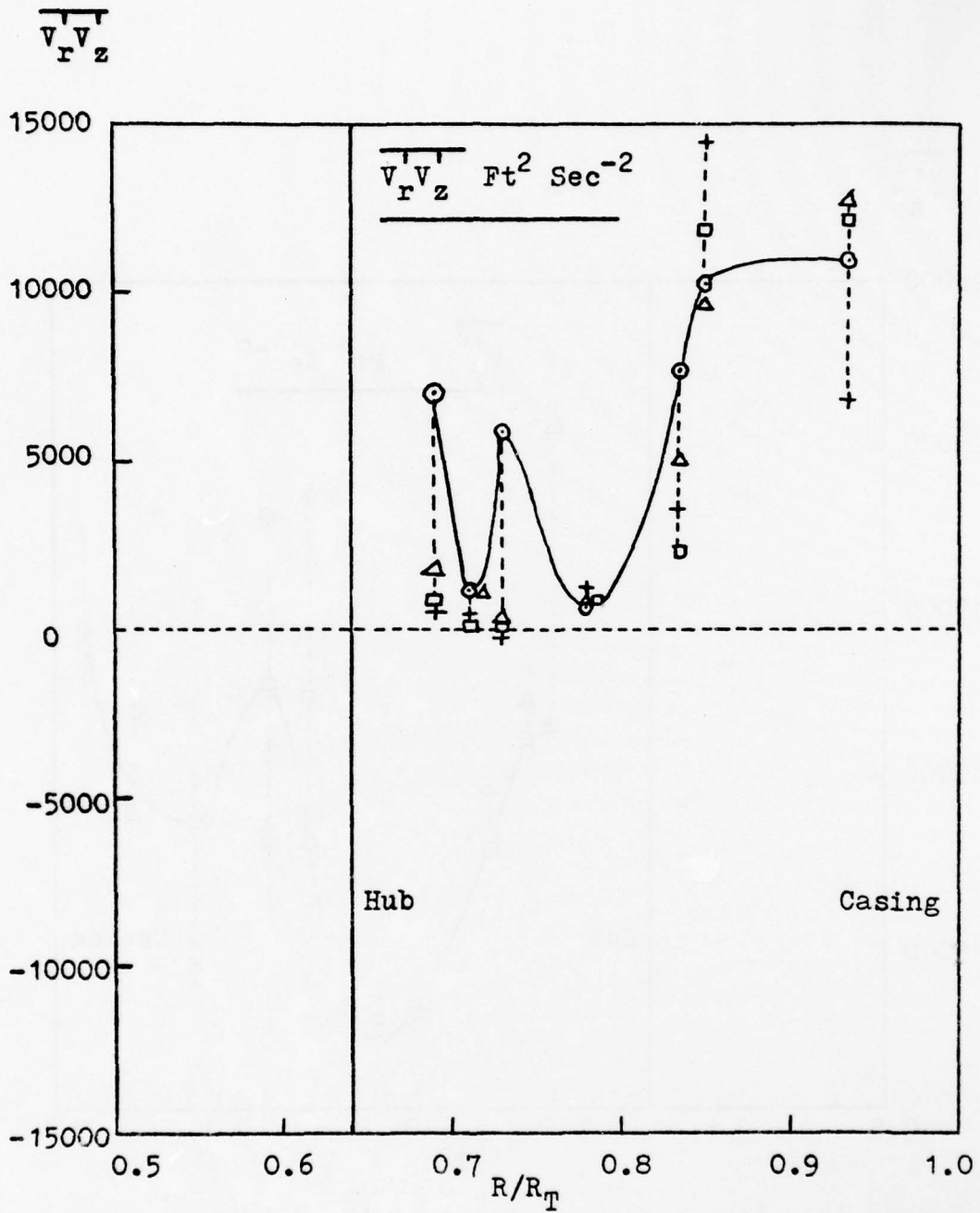


FIGURE 15. APPARENT SHEAR STRESS $\overline{v_r v_z}$, 1.0 CHORD DOWNSTREAM OF THE ROTOR

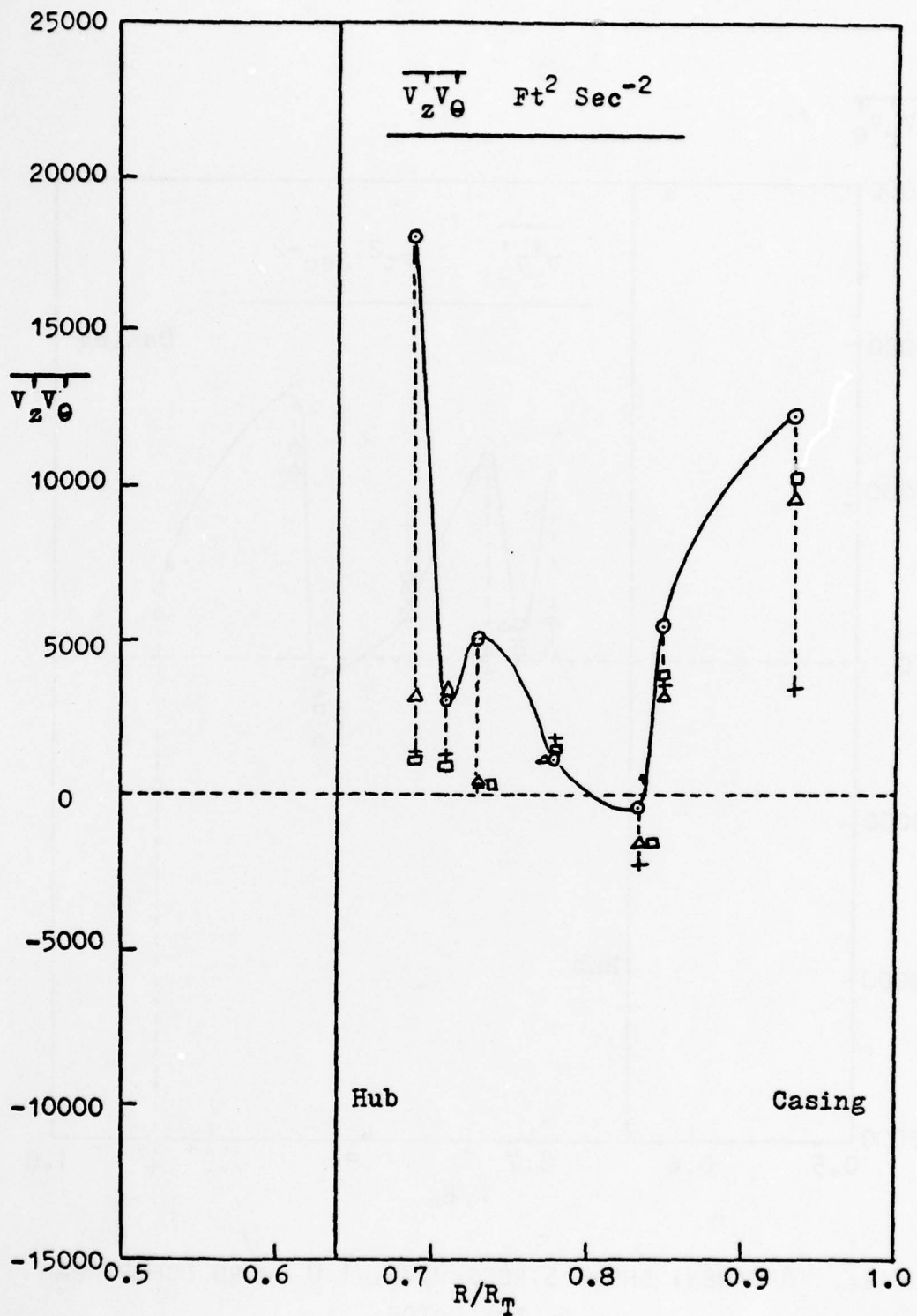


FIGURE 16. APPARENT SHEAR STRESS $\overline{v_z v_\theta}$, 1.0 CHORD DOWNSTREAM OF THE ROTOR.

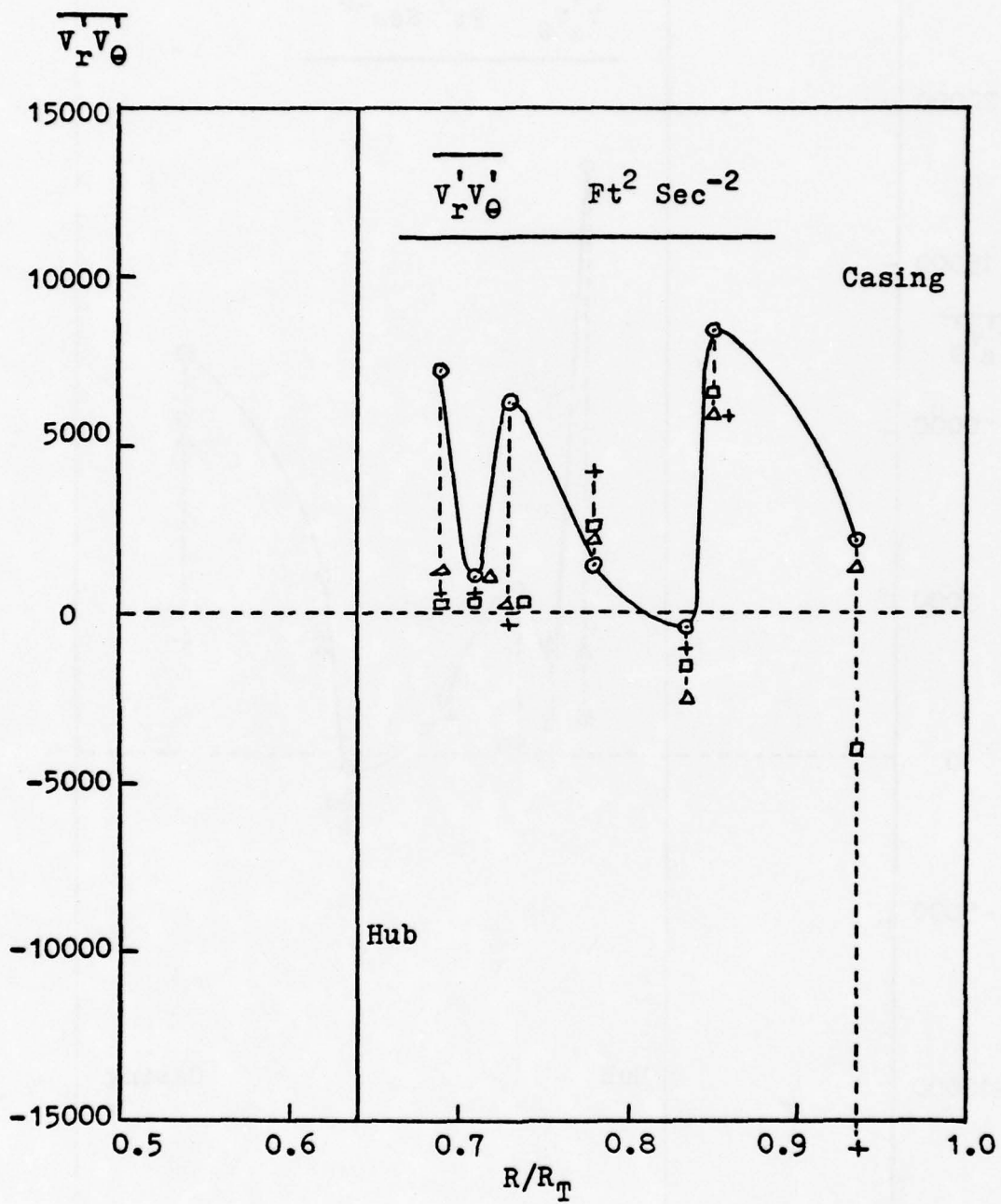


FIGURE 17. APPARENT SHEAR STRESS $\overline{v_r'v_\theta'}$, 1.0 CHORD DOWNSTREAM OF THE ROTOR.

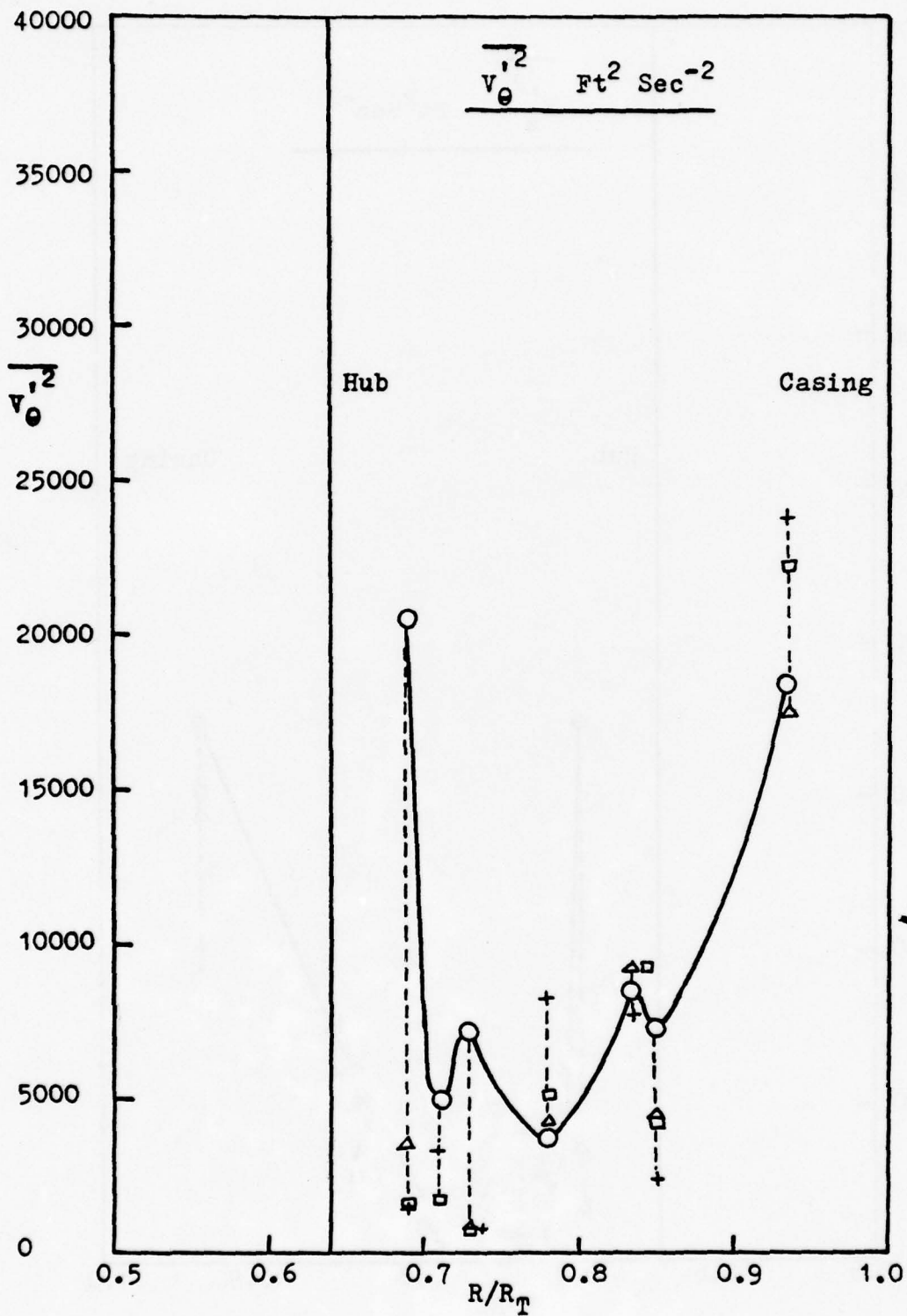


FIGURE 18. APPARENT NORMAL STRESS $\overline{v_\theta'^2}$, 1.0 CHORD DOWNSTREAM OF THE ROTOR.

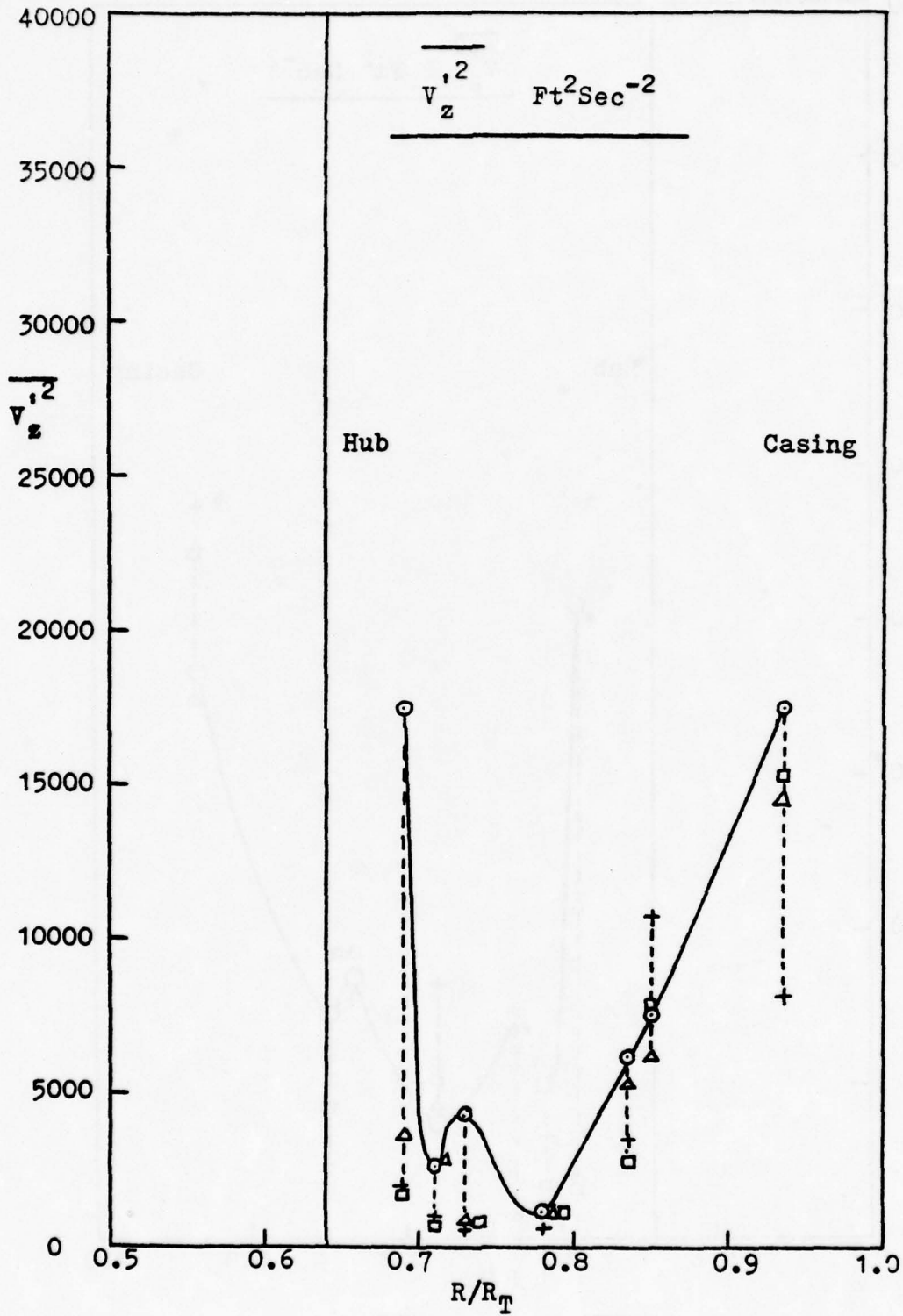


FIGURE 19. APPARENT NORMAL STRESS $\overline{v_z'^2}$, 1.0 CHORD DOWNSTREAM OF THE ROTOR.

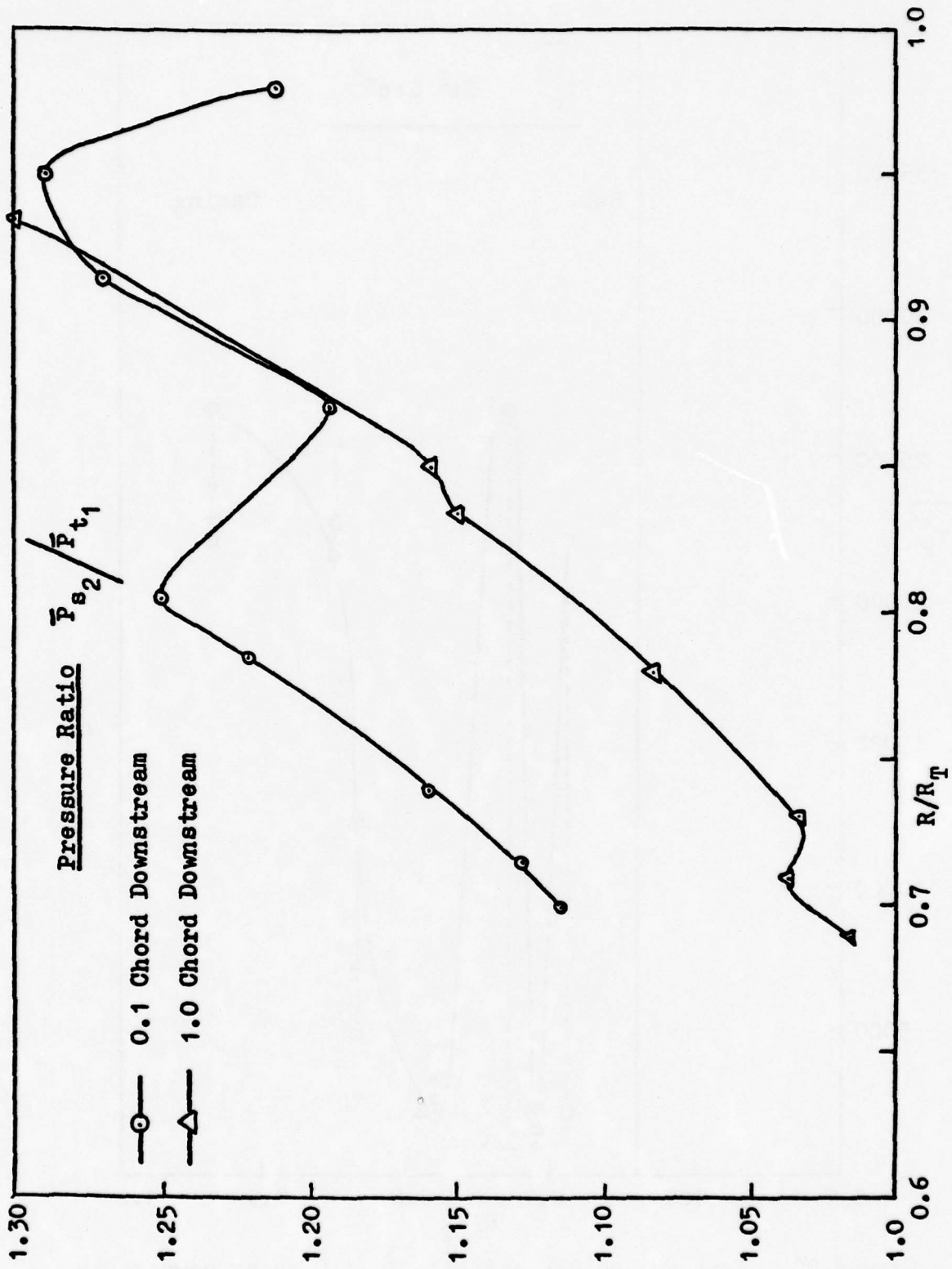


FIGURE 21. $\bar{P}_{s_2} / \bar{P}_{t_1}$, 0.1 AND 1.0 CHORD DOWNSTREAM OF THE ROTOR.

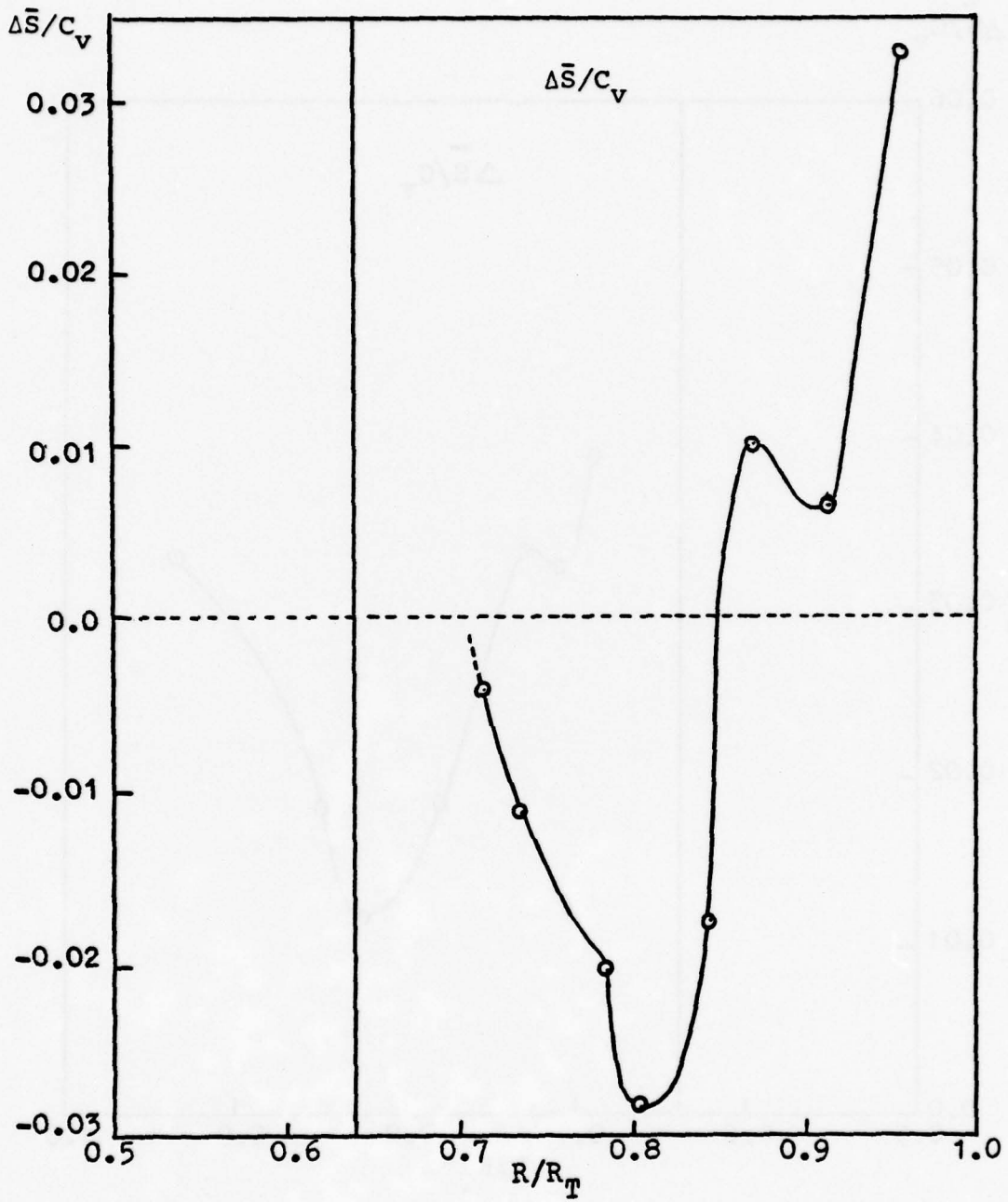


FIGURE 22. MEAN EXPERIMENTAL ENTROPY, 0.1 CHORD
DOWNSTREAM OF THE ROTOR.

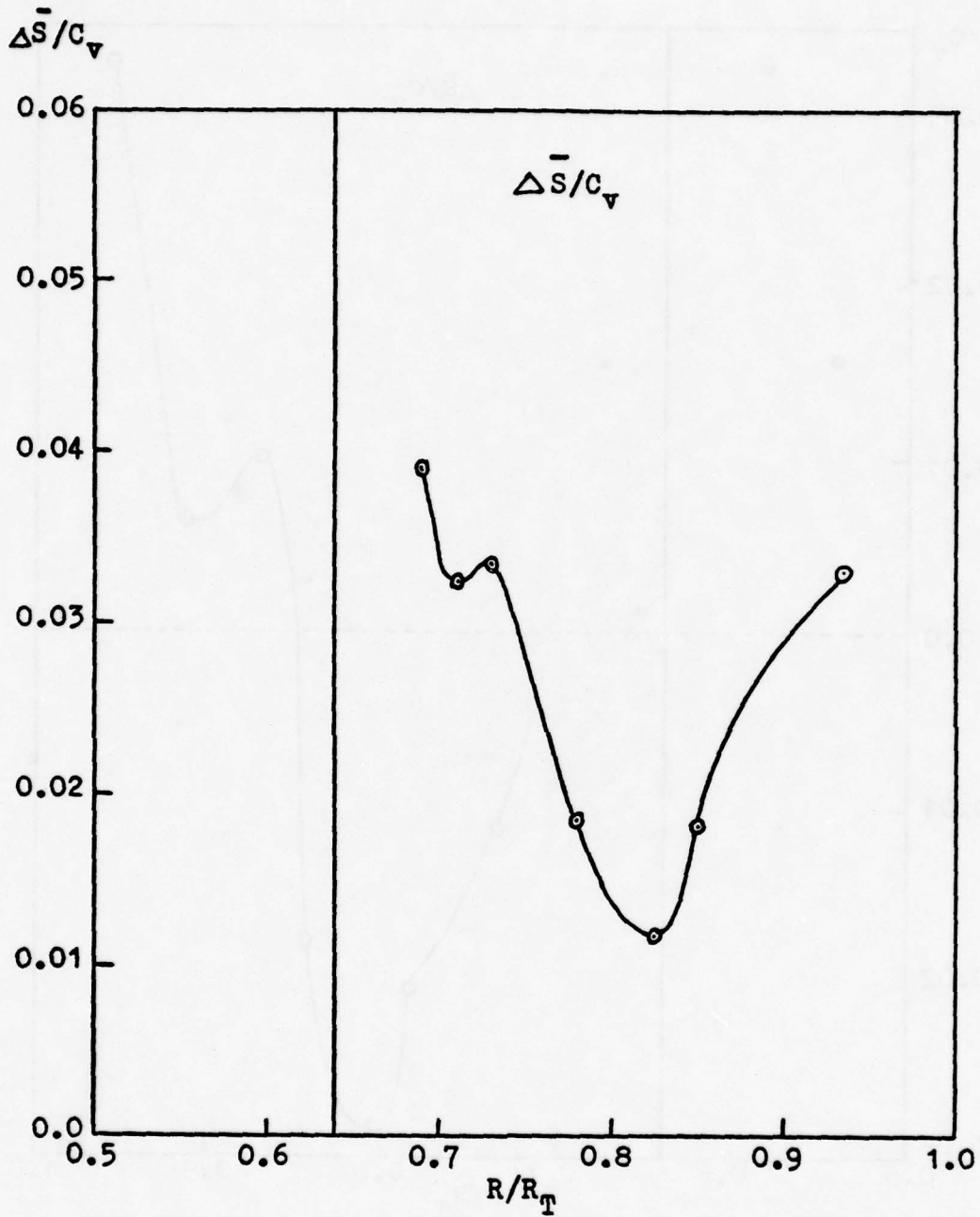
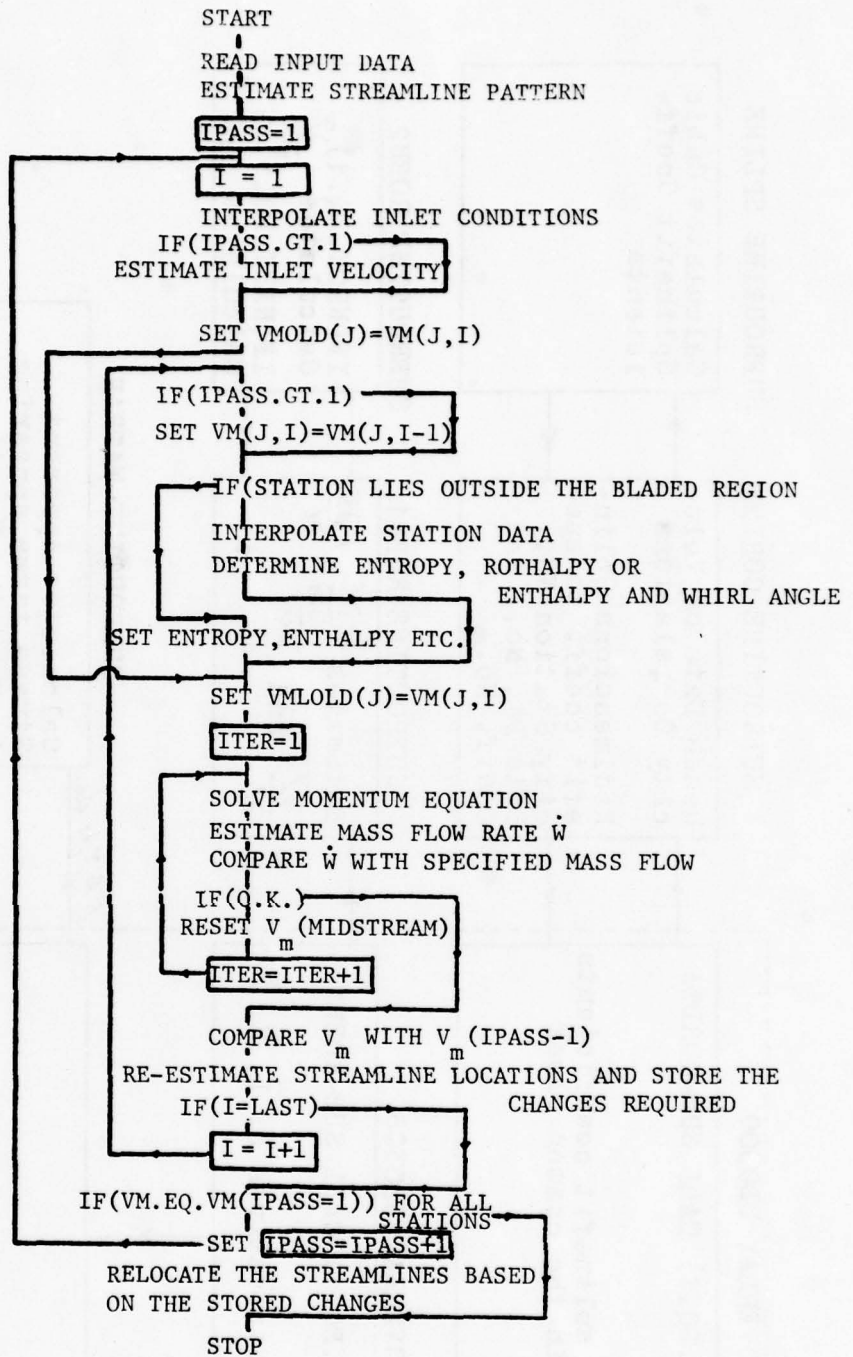
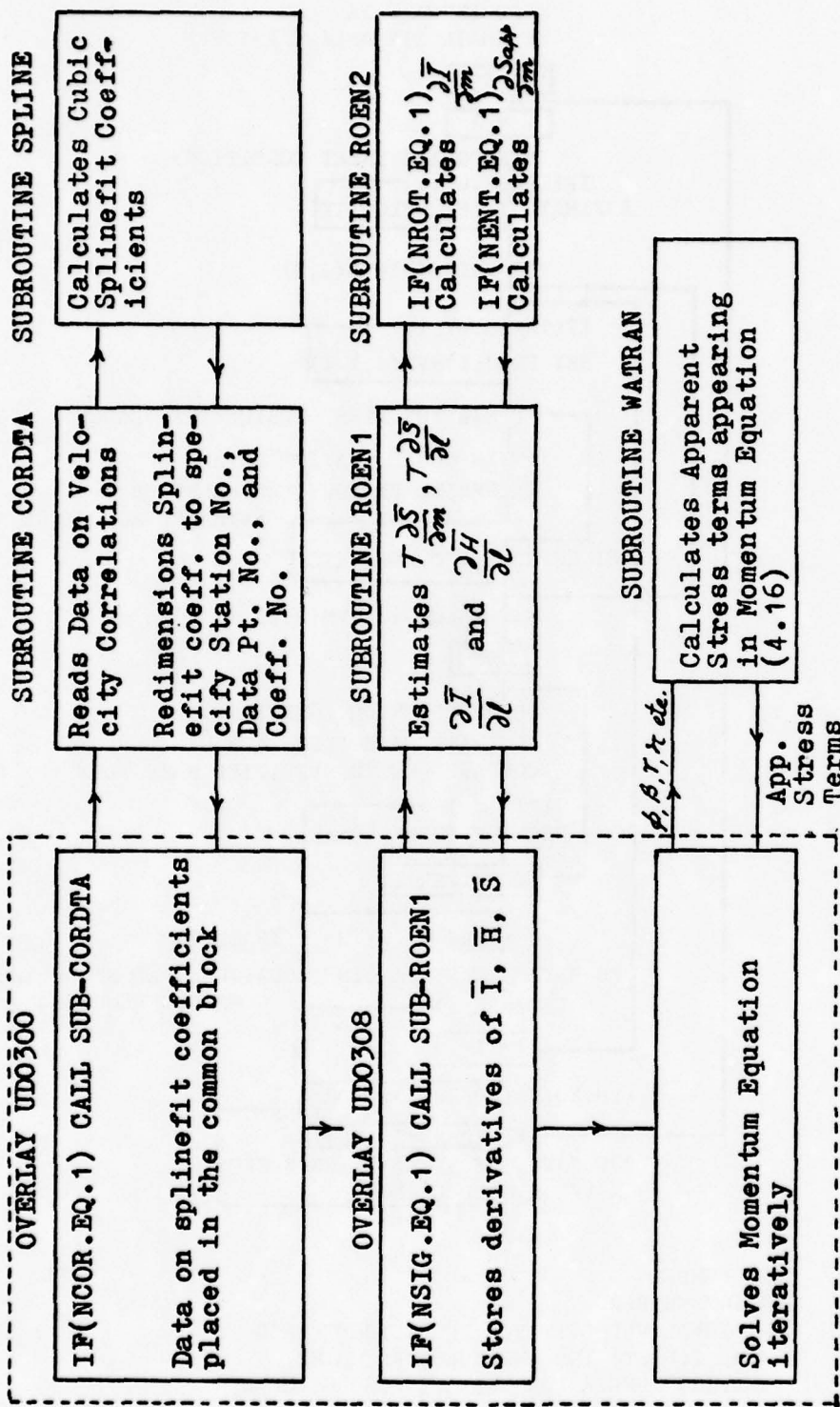


FIGURE 23. MEAN EXPERIMENTAL ENTROPY, 1.0 CHORD
DOWNSTREAM OF THE ROTOR.



IPASS PASS NUMBER
 I STATION NUMBER
 $V_m(J,I)$ MERIDIONAL VELOCITY FOR THE CURRENT PASS
 AT THE Ith STATION AND Jth STREAMLINE
 ITER ITERATION NUMBER FOR ITERATIVE SOLUTION OF
 MOMENTUM AND CONTINUITY EQUATIONS

FIGURE 24. OVERALL LOGIC OF THE ORIGINAL STREAMLINE-CURVATURE PROGRAM.



Interaction of Subroutines CORDTA, SPLINE, ROEN1, ROEN2, and WATRAN with the main program

FIGURE 25.

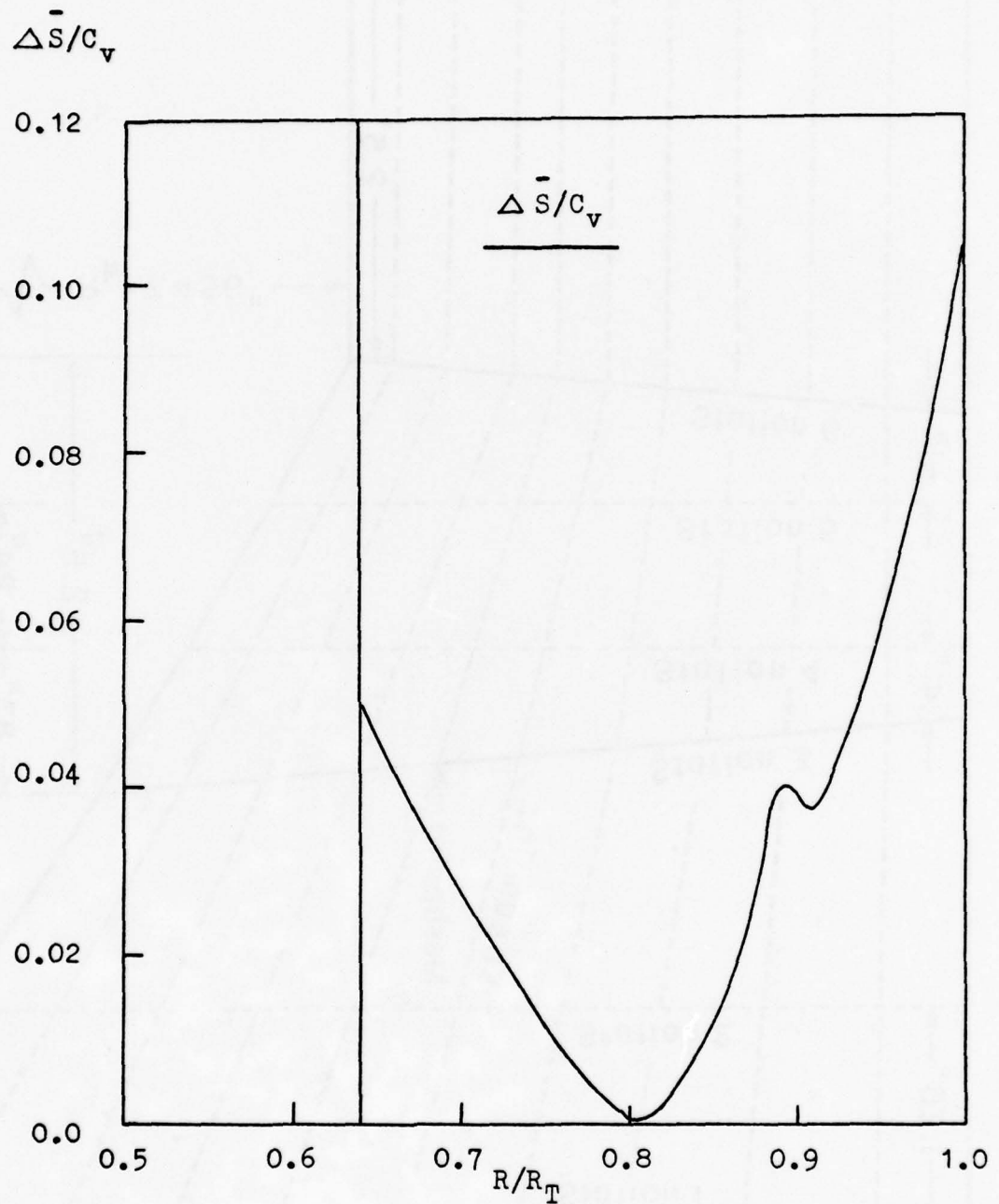


FIGURE 26. ADJUSTED EXPERIMENTAL ENTROPY, 0.1 CHORD DOWNSTREAM OF THE ROTOR.

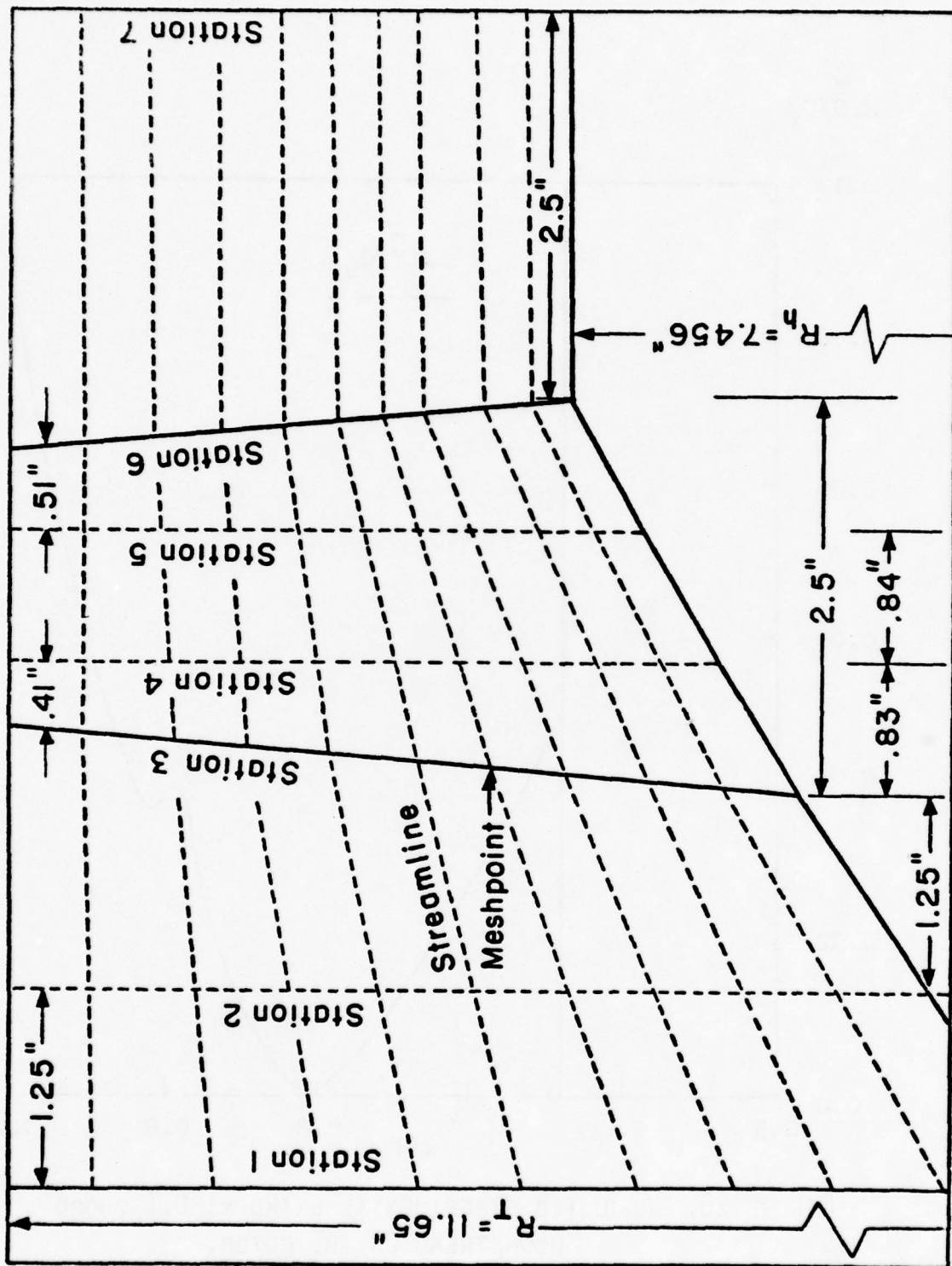


FIGURE 27. LAYOUT OF THE COMPUTATIONAL MESH.

- 1) Mass Flow Rate = 81.88 lb_m/sec
- 2) R.P.M. = 13193
- 3) Total Pressure (P_t) at inlet = 14.7 psia
- 4) Total Temperature (T_t) at inlet = 520.0° R

Relative Flow Angles

Station 4		Station 5		Station 6	
Radial Location (inches)	Relative Flow Angles (degrees)	Radial Location (inches)	Relative Flow Angles (degrees)	Radial Location (inches)	Relative Flow Angles (degrees)
7.4560	-51.700	7.4560	-35.576	7.456	-23.000
7.9818	-54.720	7.9820	-43.441	8.2977	-36.250
9.4365	-59.800	9.4365	-53.500	9.3800	-49.250
10.577	-62.240	10.577	-58.720	10.140	-52.700
11.650	-65.140	11.650	-65.200	11.650	-65.000

FIGURE 28a. BASIC INPUT DATA FOR COMPUTATION.

<u>Station 6</u>							
R/R_T	.640	.715	.8137	.8446	.870	.9497	.9785
$\overline{v_z'^2}$	7000	6000	1200	13000	33500	10500	29000
R/R_T	.640	.715	.790	.8446	.9147	.9497	.9785
$\overline{v_\theta'^2}$	1000	6000	3000	9000	26000	11880	20000
R/R_T	.640	.715	.790	.870	.9147	.9497	.9785
$\overline{v_z' v_\theta'}$	21000	11000	3000	12900	8590	6900	14600
R/R_T	.640	.715	.790	.8446	.9147	.9497	.9785
$\overline{v_z' v_z'}$	4000	3880	500	1500	-3000	0	-2500
R/R_T	.640	.715	.7375	.790	.870	.9147	.9785
$\overline{v_z' v_\theta'}$	7000	-1470	1850	500	10700	9000	0
R/R_T	.640	.70	.790	.87	.9147	.9497	.9785
$\overline{v_z' v_\theta'}$	-9000	-4500	-400	-6760	1160	3630	5000

<u>Station 7</u>							
R/R_T	.640	.690	.71	.73	.78	.896	1.0
$\overline{v_z'^2}$	45000	22200	2000	26000	1930	22000	28000
R/R_T	.640	.690	.720	.78	.85	.935	1.0
$\overline{v_\theta'^2}$	45000	20600	6000	3870	7000	18500	32000
R/R_T	.640	.690	.720	.78	.85	.935	1.0
$\overline{v_z' v_\theta'}$	40000	17700	3000	1170	7600	17800	27000
R/R_T	.640	.690	.720	.78	.85	.935	1.0
$\overline{v_z' v_z'}$	17000	7040	4500	540	10300	11000	12000
R/R_T	.640	.690	.71	.73	.835	.85	1.0
$\overline{v_z' v_\theta'}$	30000	7370	1200	6490	-360	8490	0
R/R_T	.640	.690	.71	.73	.835	.935	1.0
$\overline{v_z' v_\theta'}$	30000	18500	3060	5070	-40	12280	15000

Units for Velocity Correlations Ft²-Sec⁻²

FIGURE 28b. APPARENT STRESS DATA.

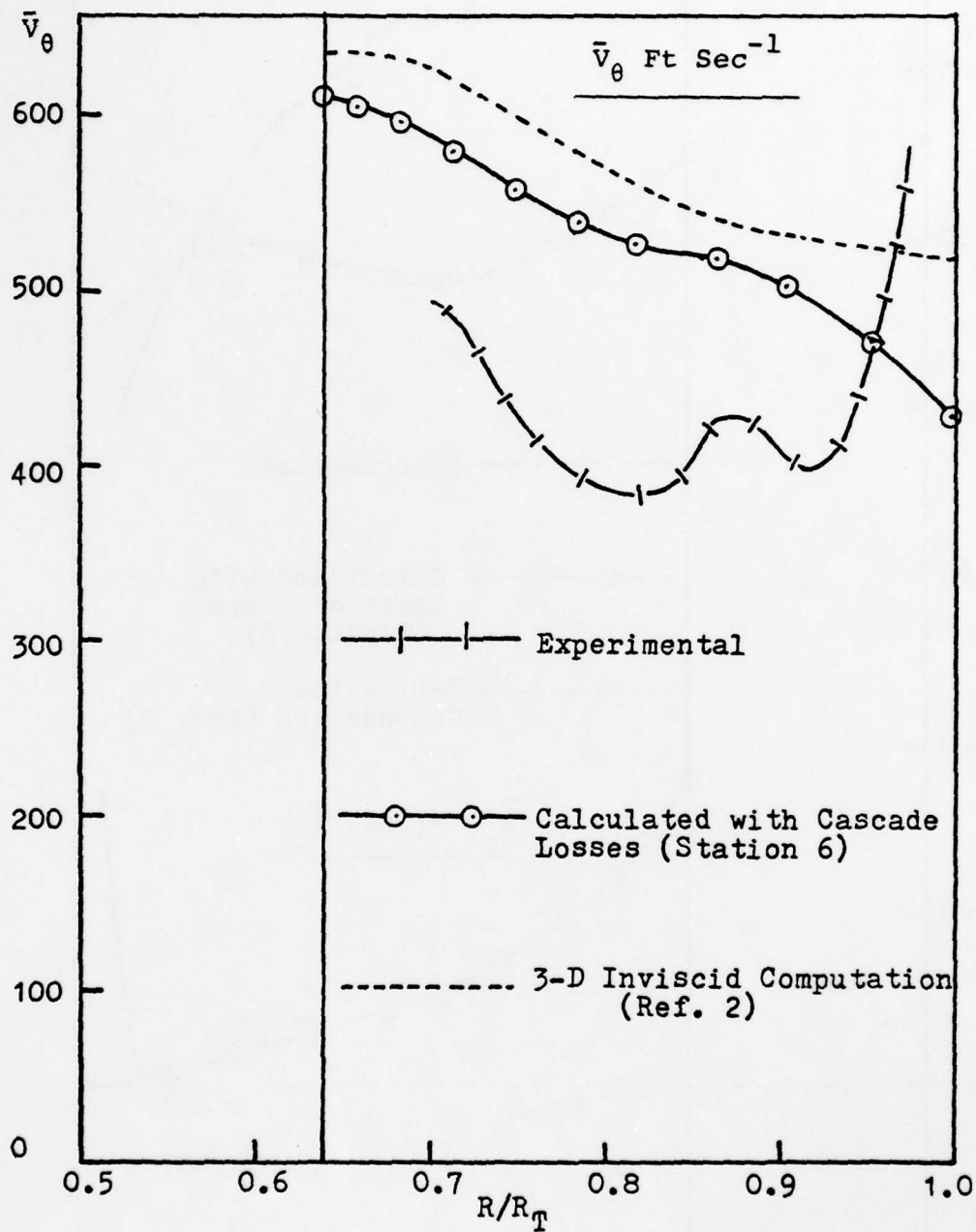


FIGURE 29. MEAN PITCHWISE VELOCITY, 0.1 CHORD DOWNSTREAM OF THE ROTOR.

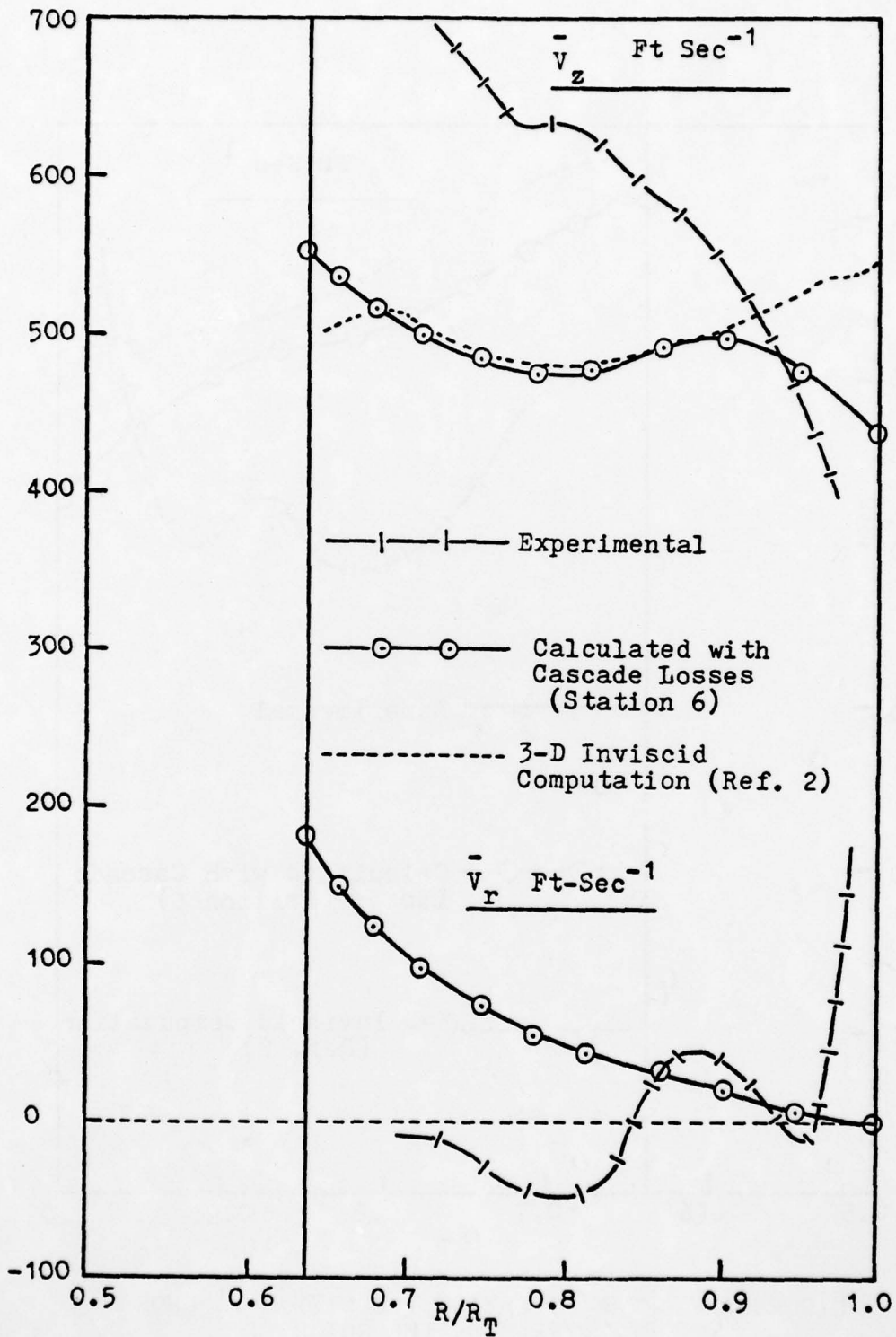


FIGURE 30. MEAN AXIAL AND RADIAL VELOCITIES, 0.1 CHORD DOWNSTREAM OF THE ROTOR.

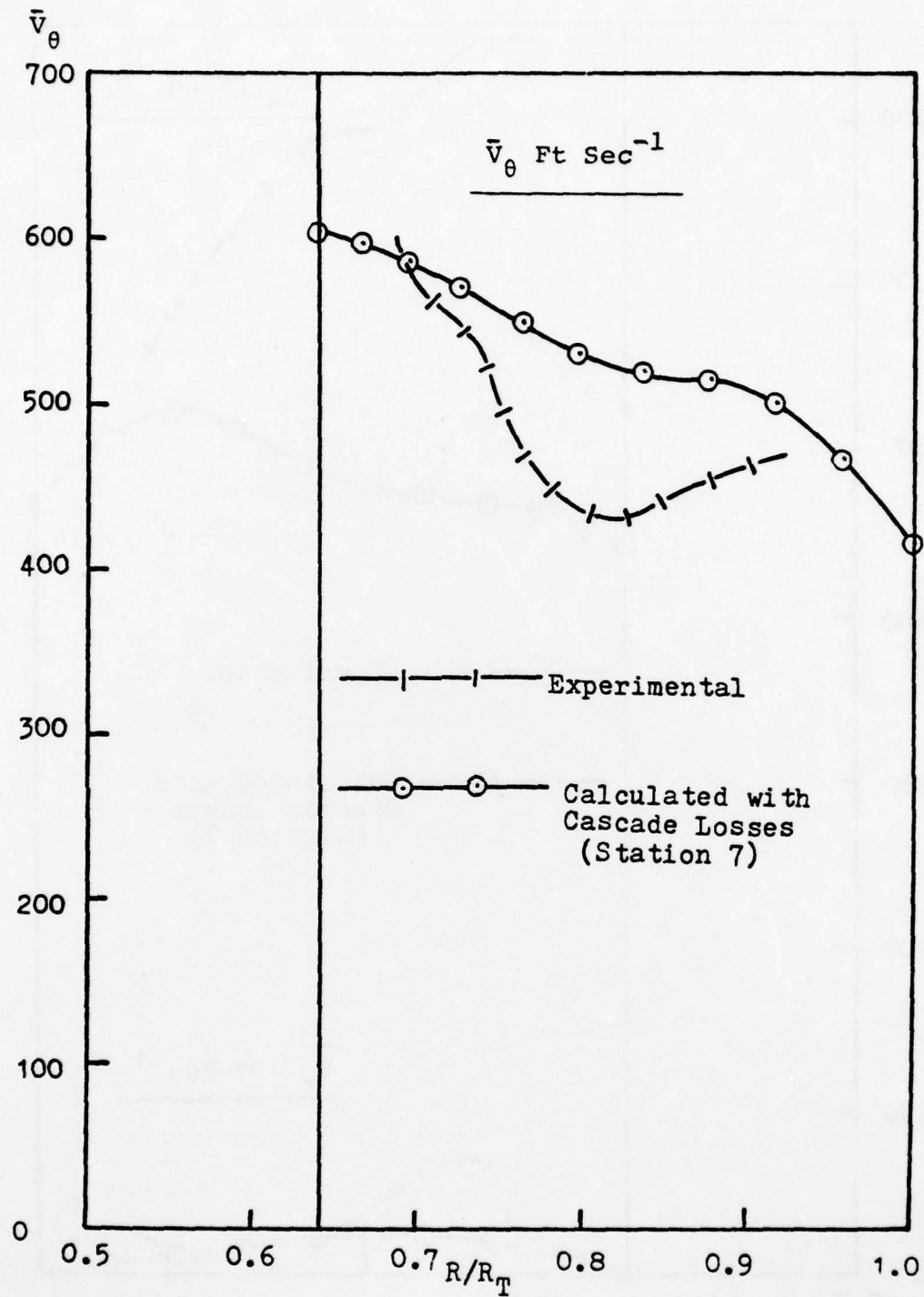


FIGURE 31. MEAN PITCHWISE VELOCITY, 1.0 CHORD DOWNSTREAM OF THE ROTOR.

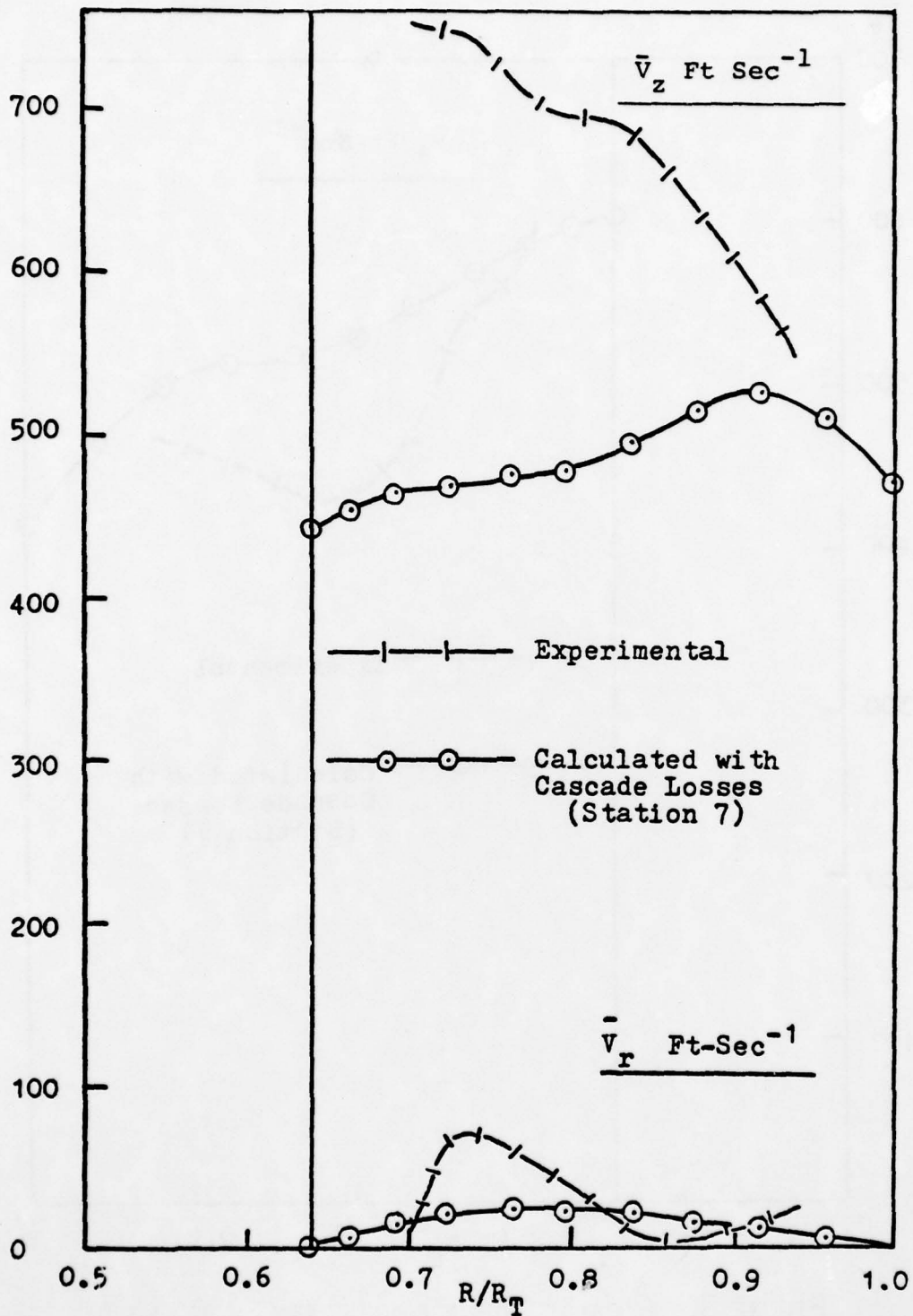


FIGURE 32. MEAN AXIAL AND RADIAL VELOCITIES, 1.0 CHORD DOWNSTREAM OF THE ROTOR.

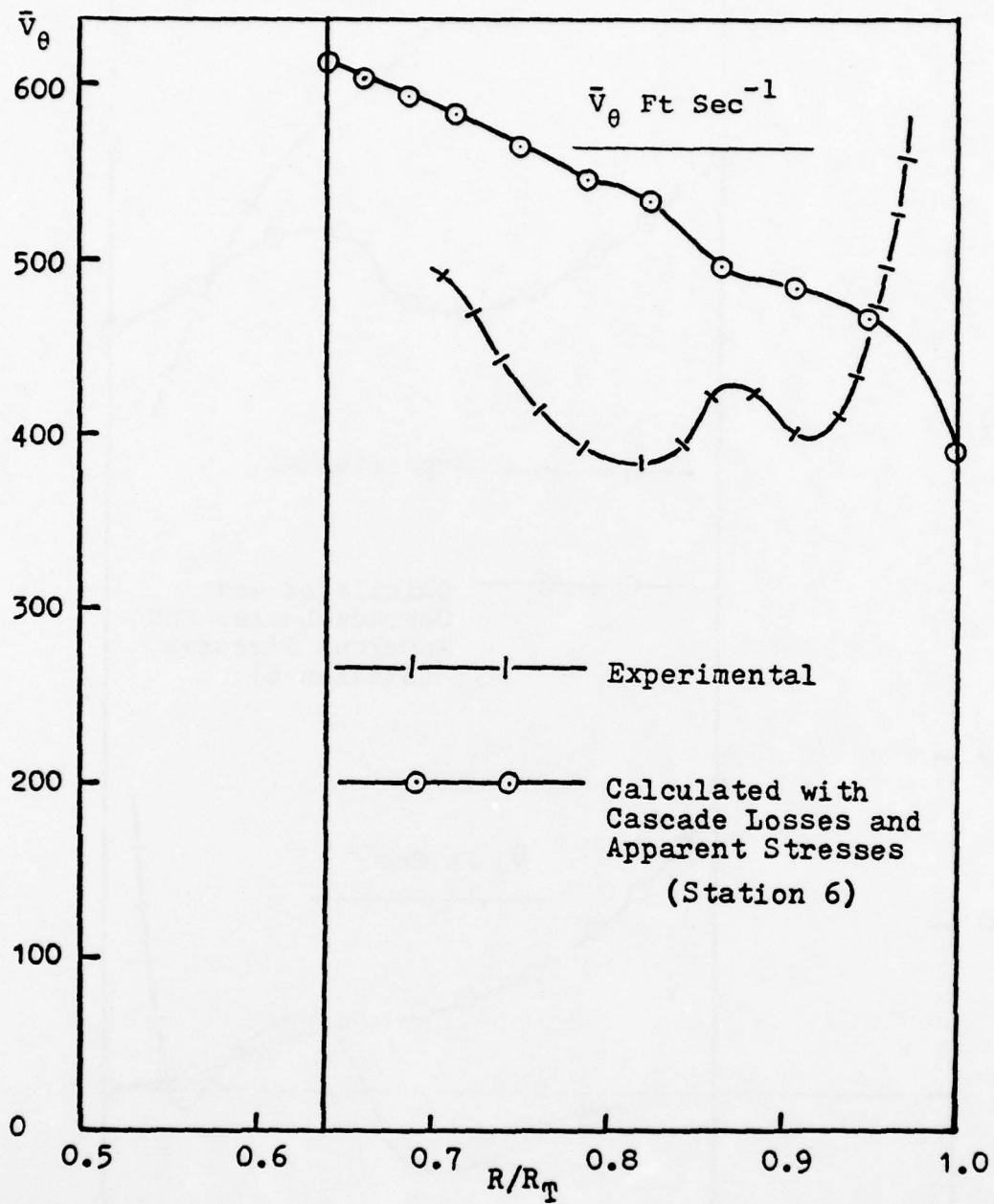


FIGURE 33. MEAN PITCHWISE VELOCITY, 0.1 CHORD DOWNSTREAM OF THE ROTOR.

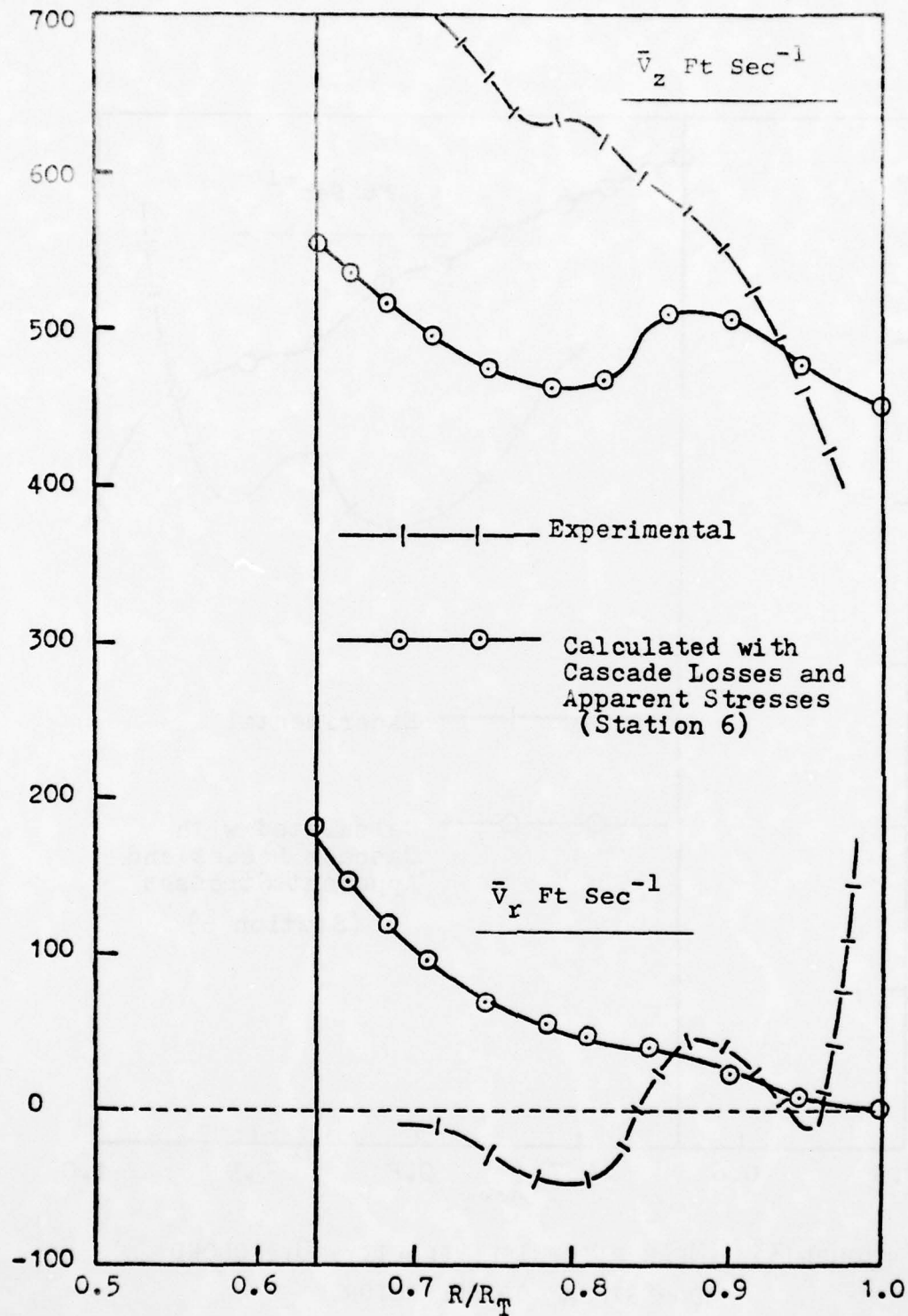


FIGURE 34. MEAN AXIAL AND RADIAL VELOCITIES, 0.1 CHORD DOWNSTREAM OF THE ROTOR.

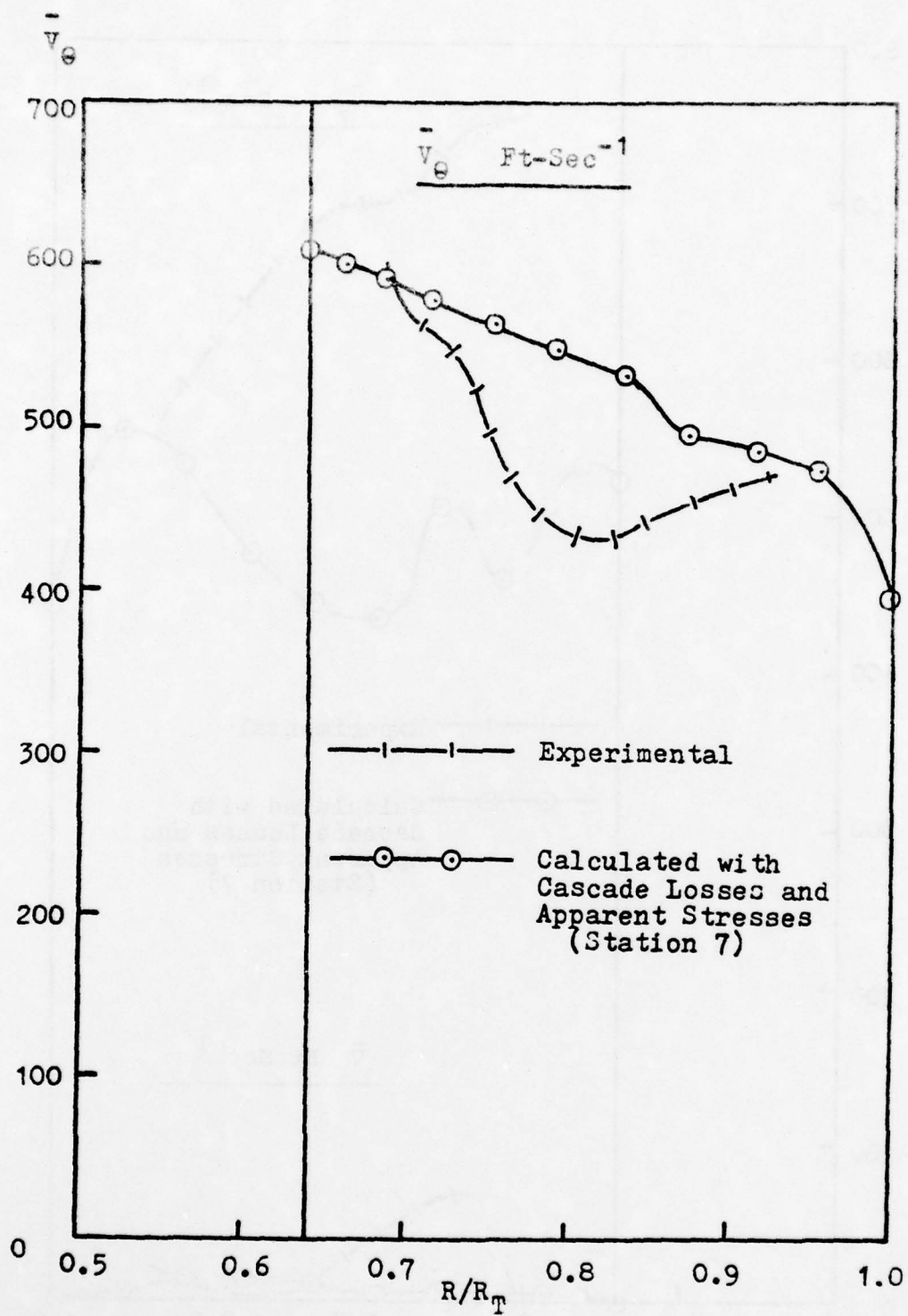


FIGURE 35. MEAN PITCHWISE VELOCITY, 1.0 CHORD DOWNSTREAM OF THE ROTOR.

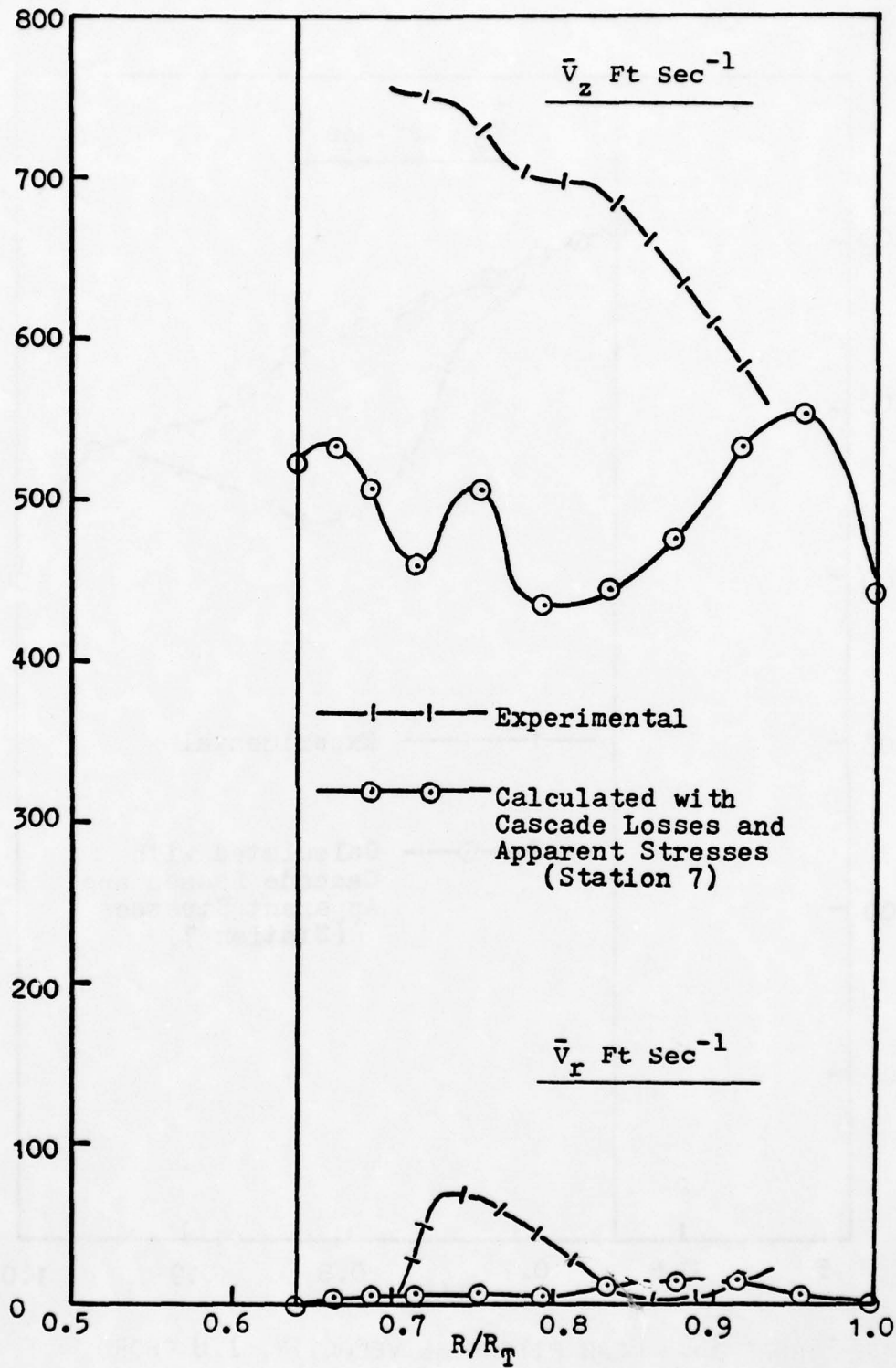


FIGURE 36. MEAN AXIAL AND RADIAL VELOCITIES, 1.0 CHORD DOWNSTREAM OF THE ROTOR.

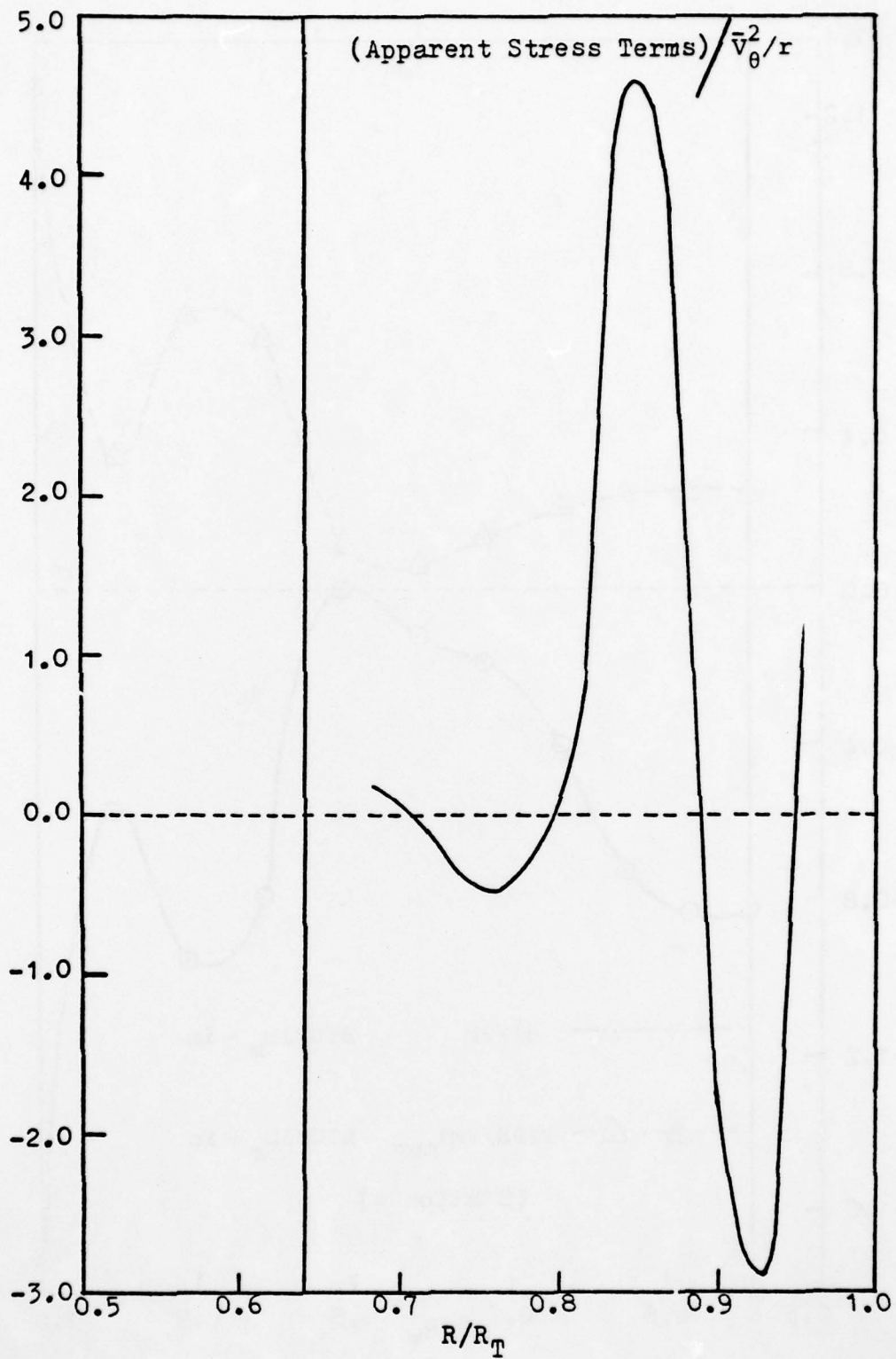


FIGURE 37. APPARENT STRESSES (\bar{v}_θ^2/r), 0.1 CHORD
DOWNSTREAM OF THE ROTOR.

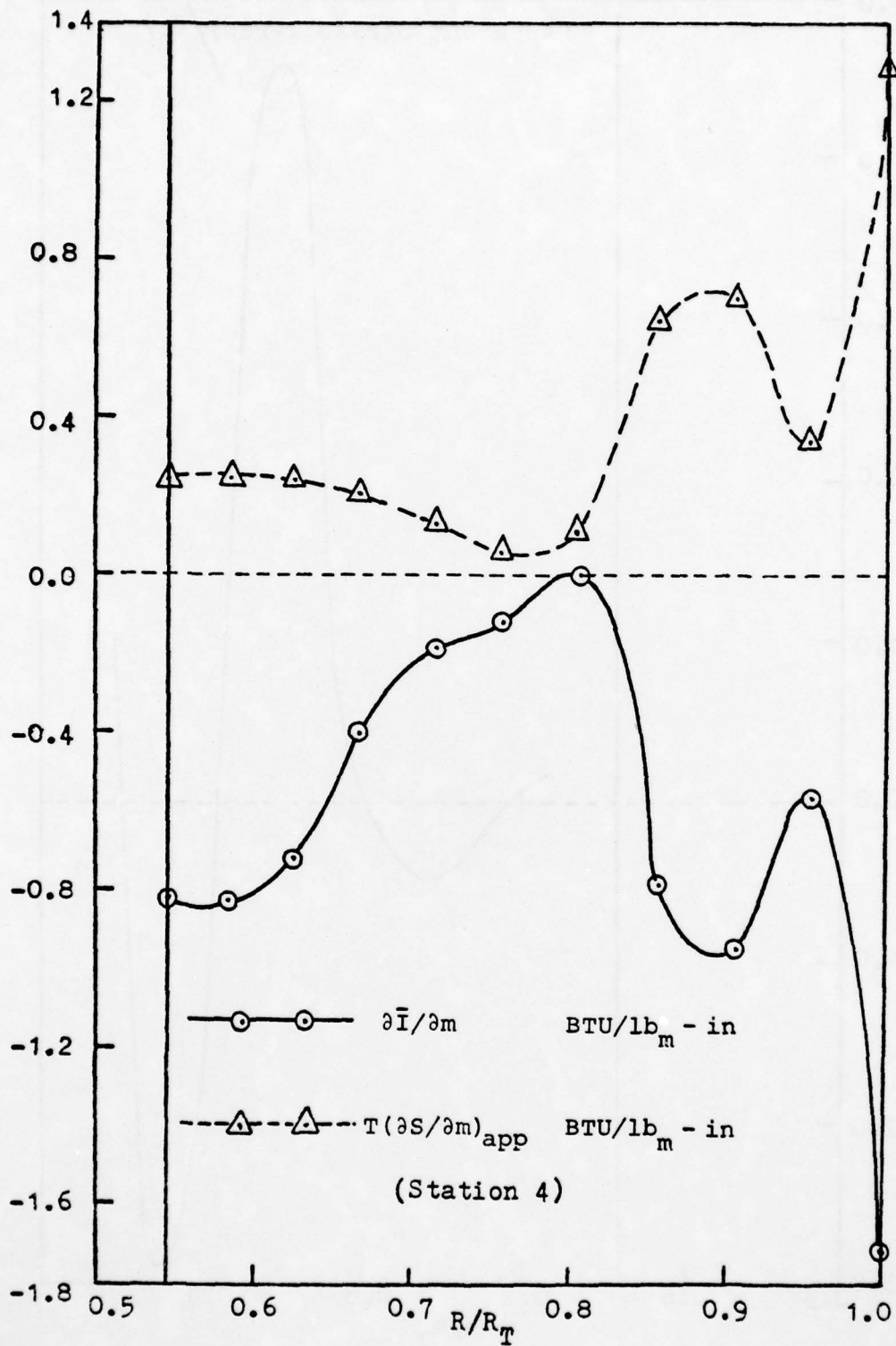


FIGURE 38. COMPUTED $\frac{\partial \bar{I}}{\partial m}$ AND $T \left(\frac{\partial S}{\partial m} \right)_{app}$,
STATION 4.

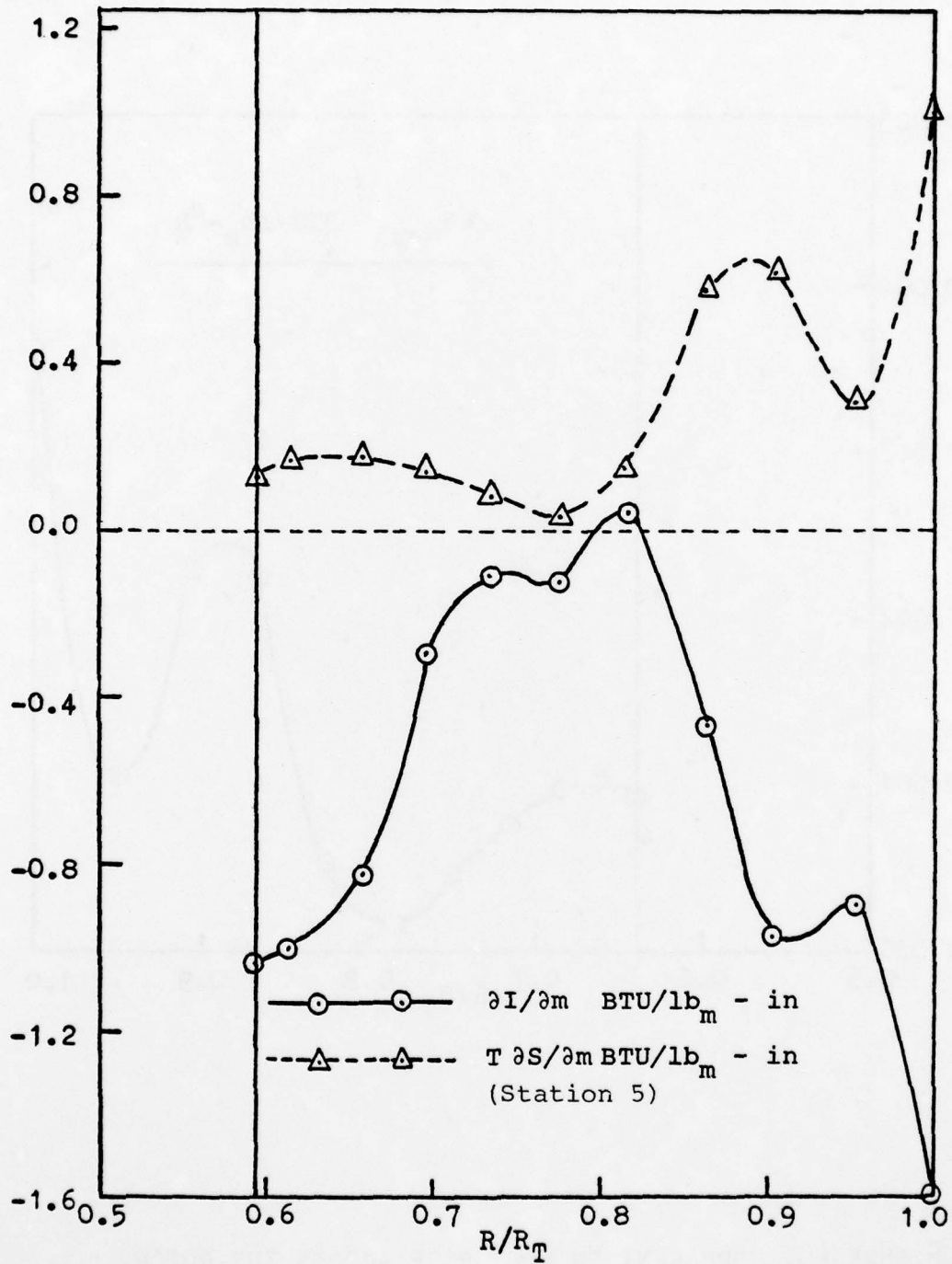


FIGURE 39. CALCULATED DISTRIBUTION OF $\partial I / \partial m$ AND $T \partial S / \partial m$, STATION 5.

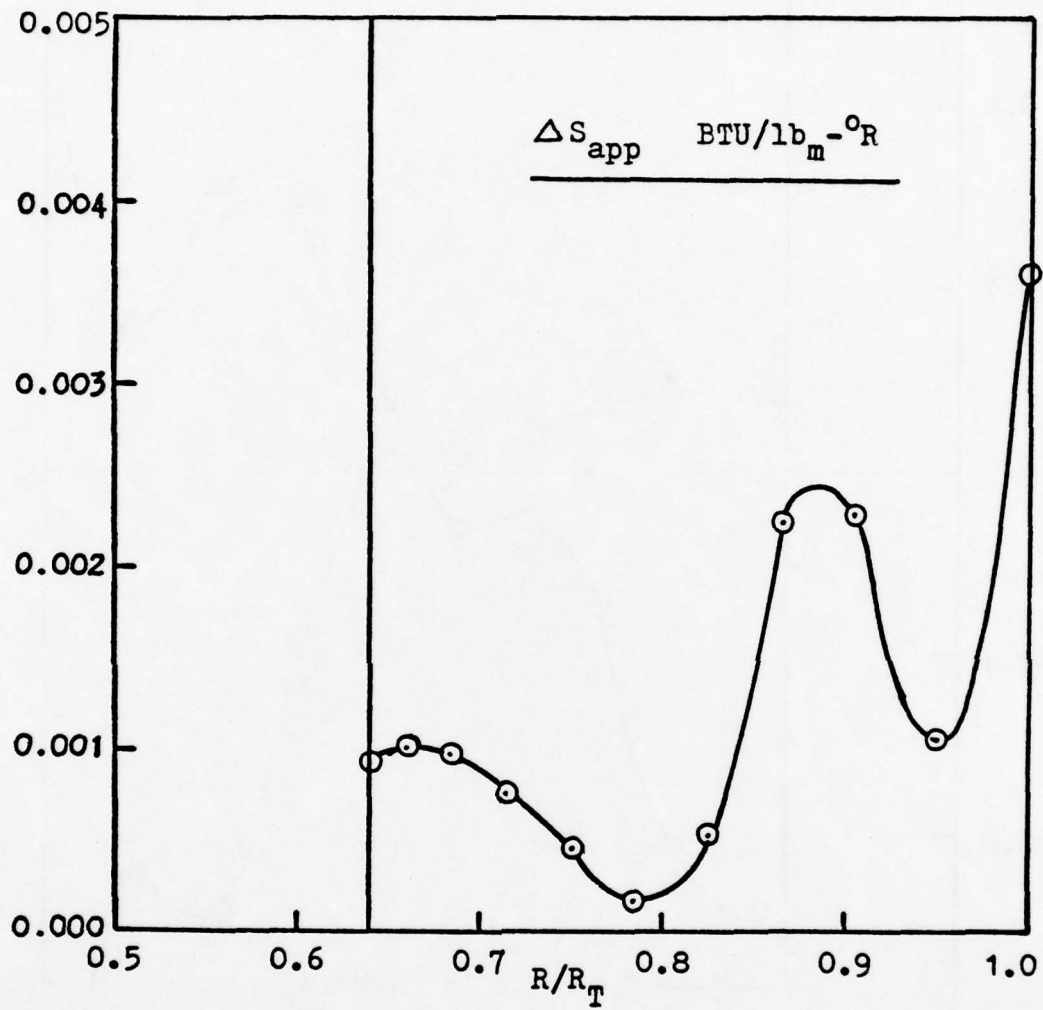


FIGURE 40. APPARENT ENTROPY RISE ACROSS THE ROTOR.

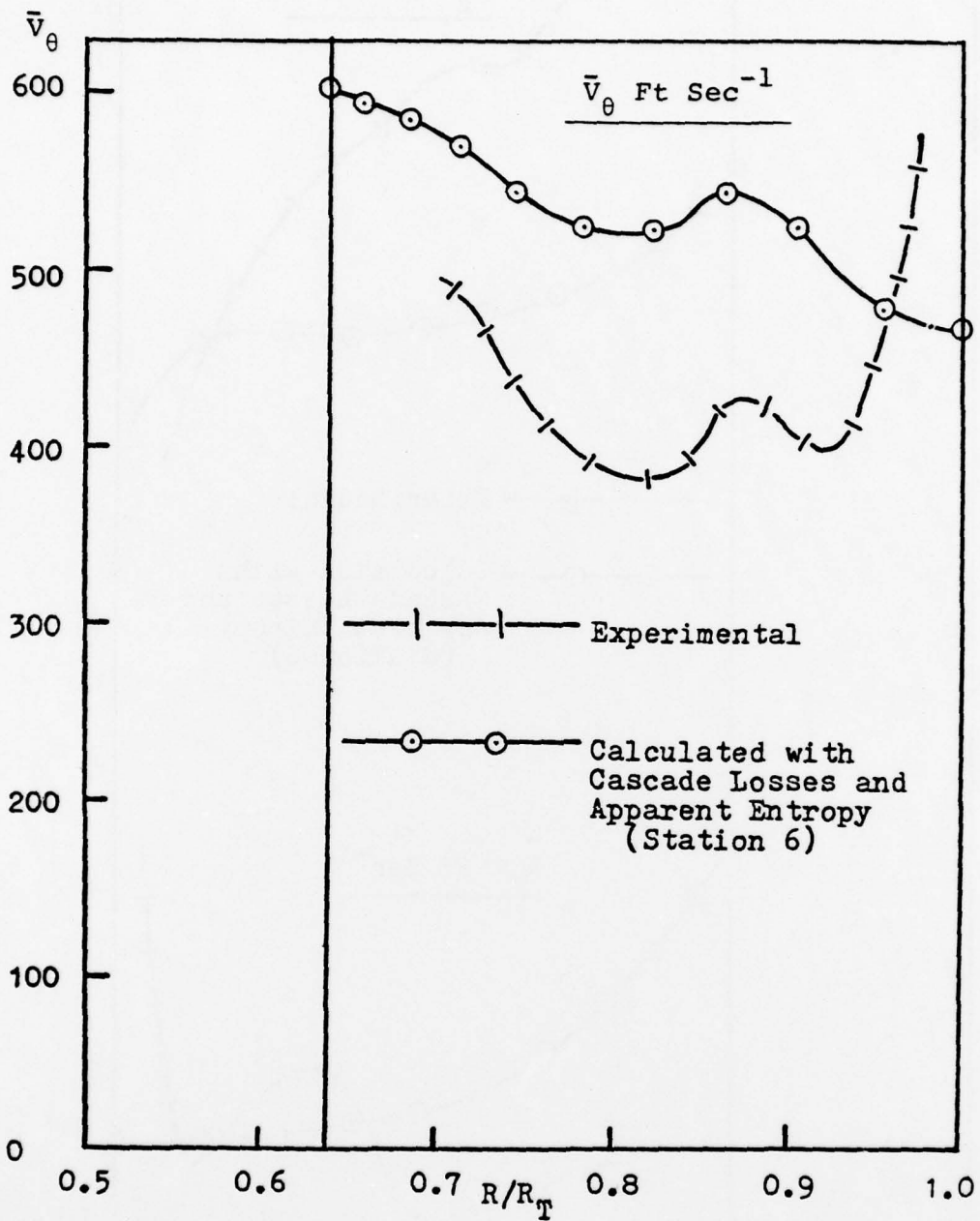


FIGURE 41. MEAN PITCHWISE VELOCITY, 0.1 CHORD DOWNSTREAM OF THE ROTOR.

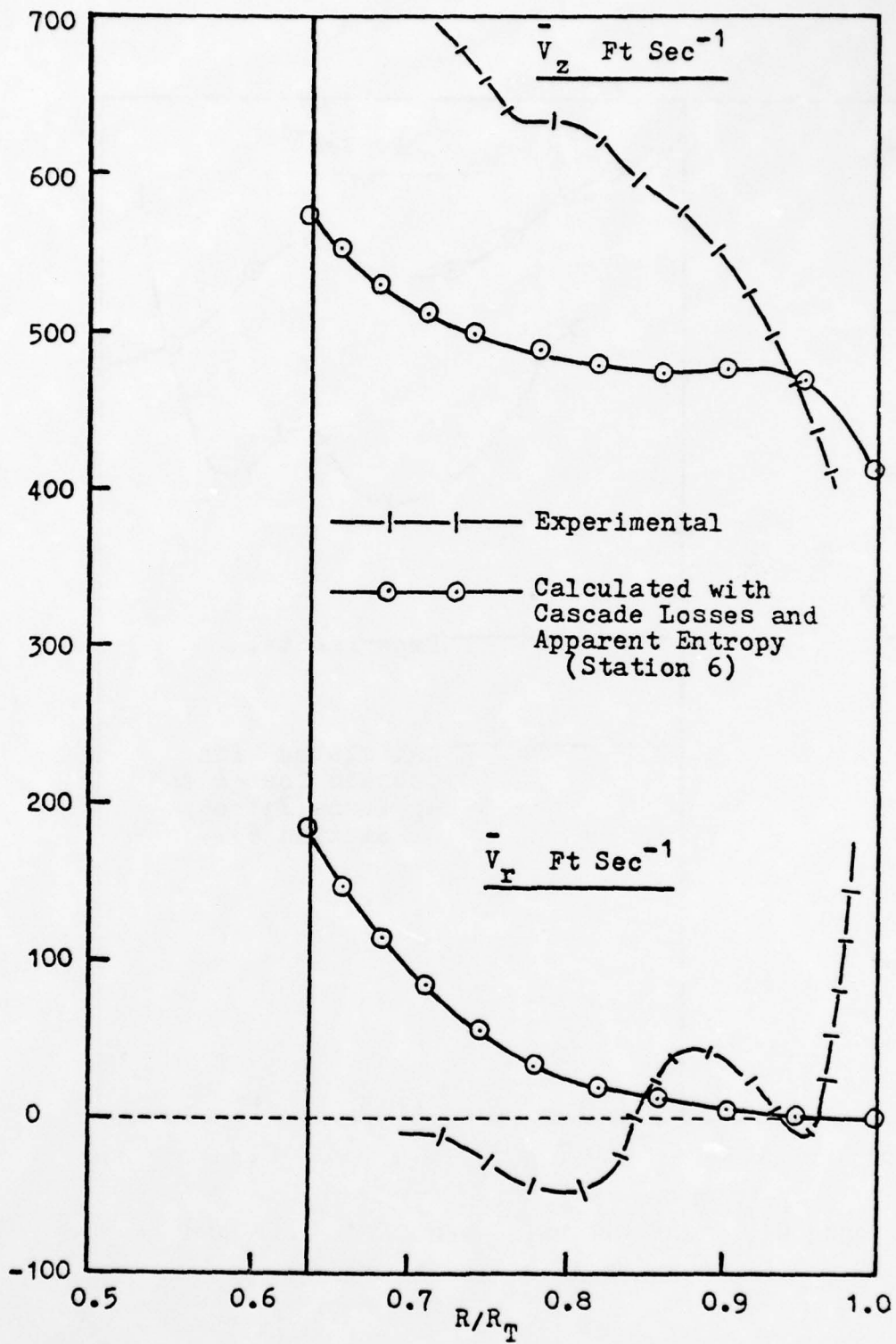


FIGURE 42. MEAN AXIAL AND RADIAL VELOCITIES, 0.1 CHORD DOWNSTREAM OF THE ROTOR.

AD-A076 204

MASSACHUSETTS INST OF TECH CAMBRIDGE GAS TURBINE AND--ETC F/G 21/5
BOUNDARY LAYER AND WAKE MODIFICATIONS TO COMPRESSOR DESIGN SYST--ETC(U)
MAR 79 A K SEHRA F33615-76-C-2118

UNCLASSIFIED

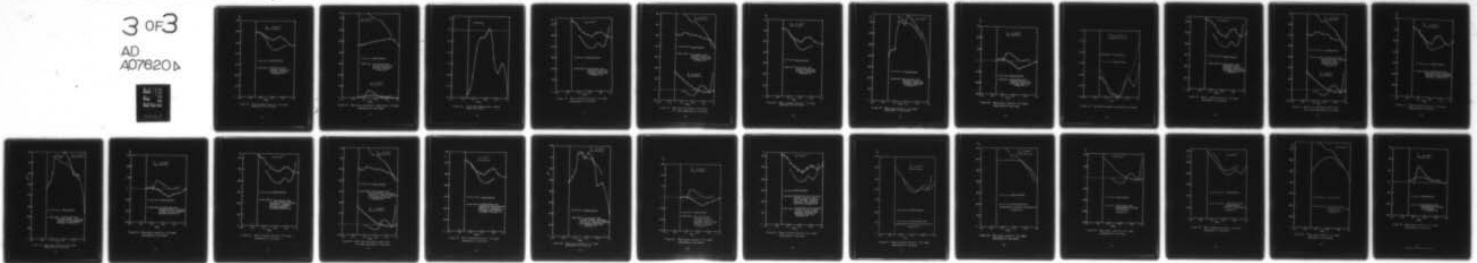
GT/PDL-144

AFAPL-TR-79-2010

NL

3 OF 3

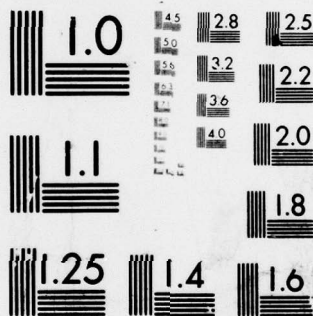
AD
A076204



END
DATE
FILMED

11-79

DDC



MICROCOPY RESOLUTION TEST CHART
NATIONAL BUREAU OF STANDARDS-1963-A

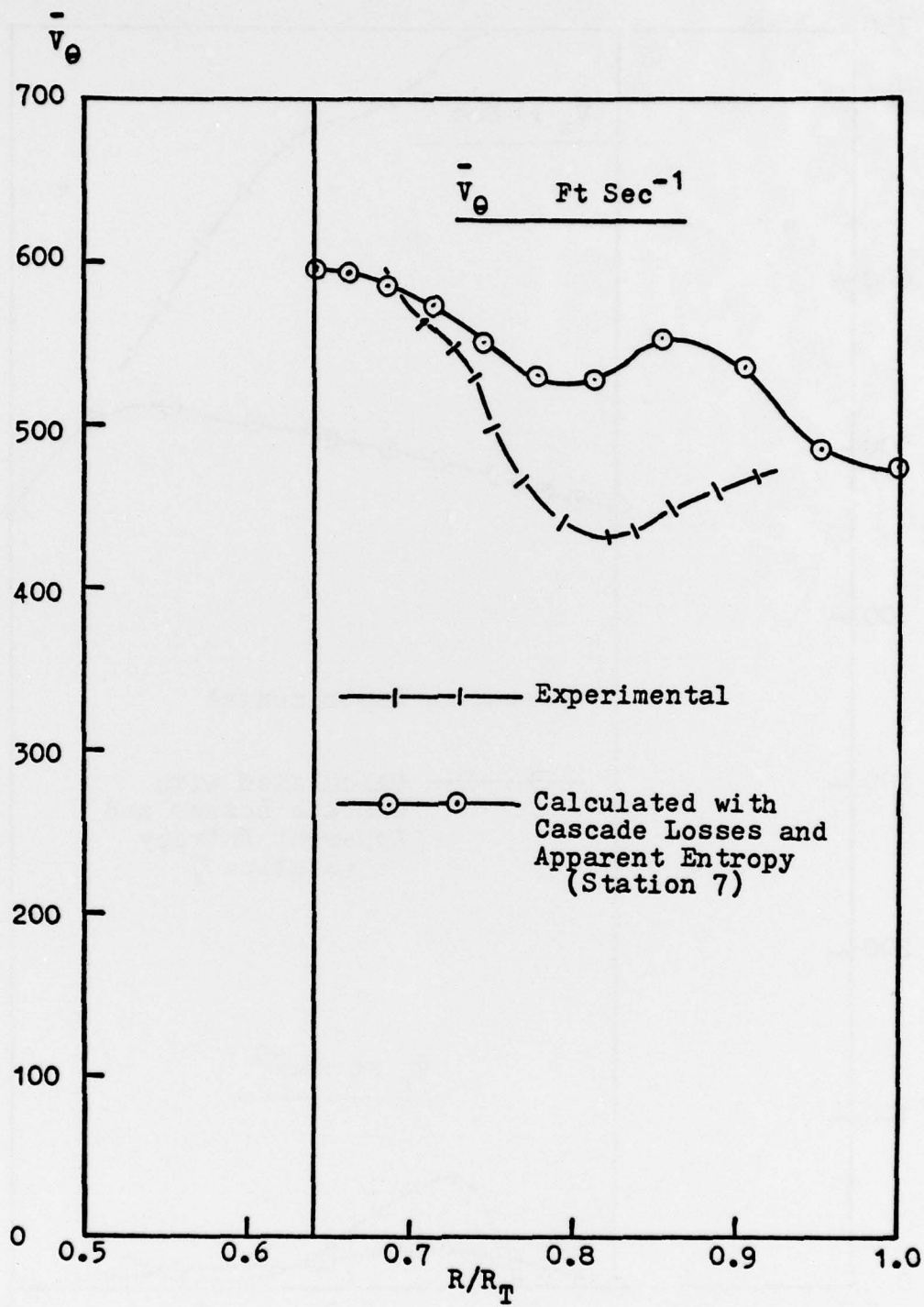


FIGURE 43. MEAN PITCHWISE VELOCITY, 1.0 CHORD DOWNSTREAM OF THE ROTOR.

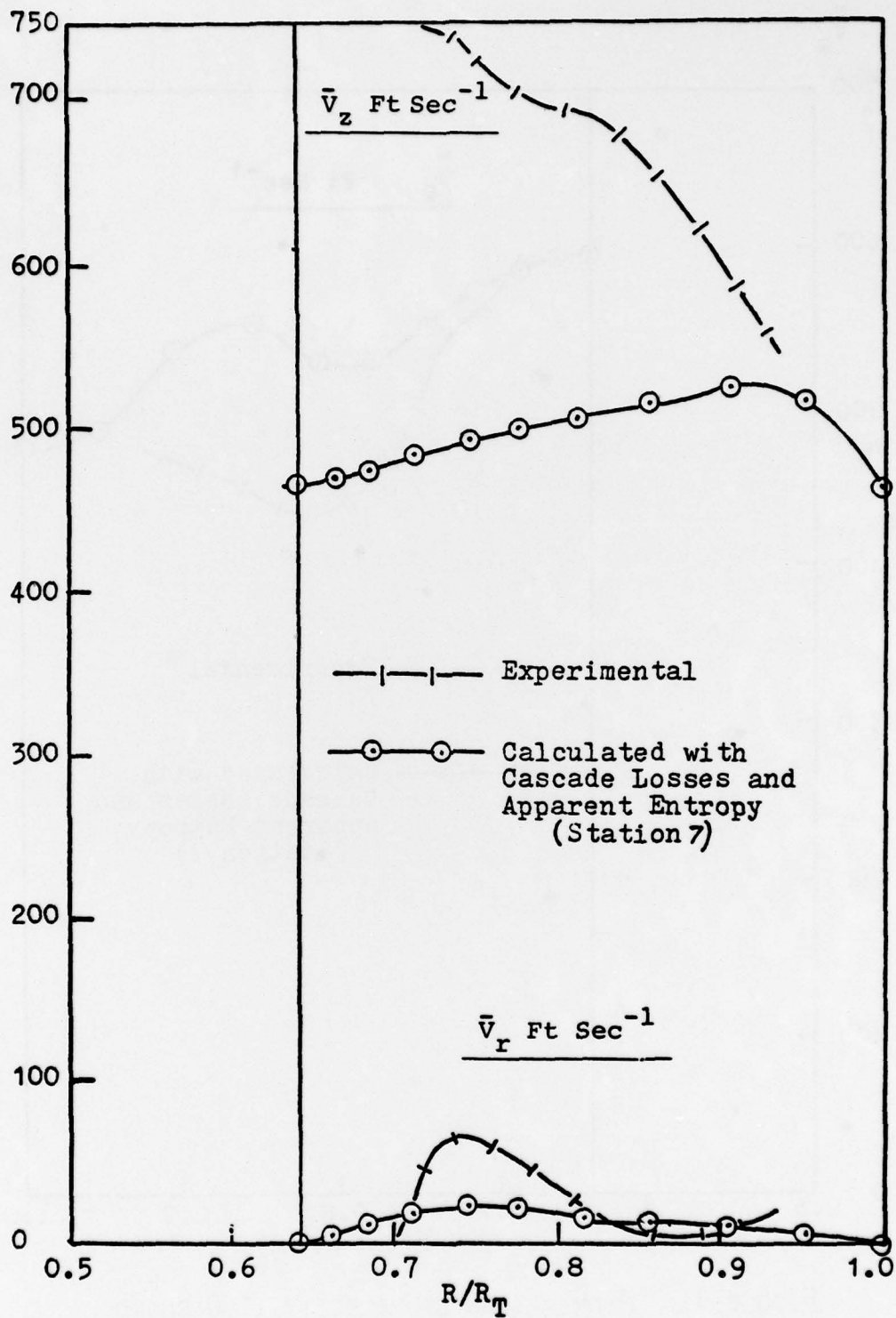


FIGURE 44. MEAN AXIAL AND RADIAL VELOCITIES, 1.0 CHORD DOWNSTREAM OF THE ROTOR.

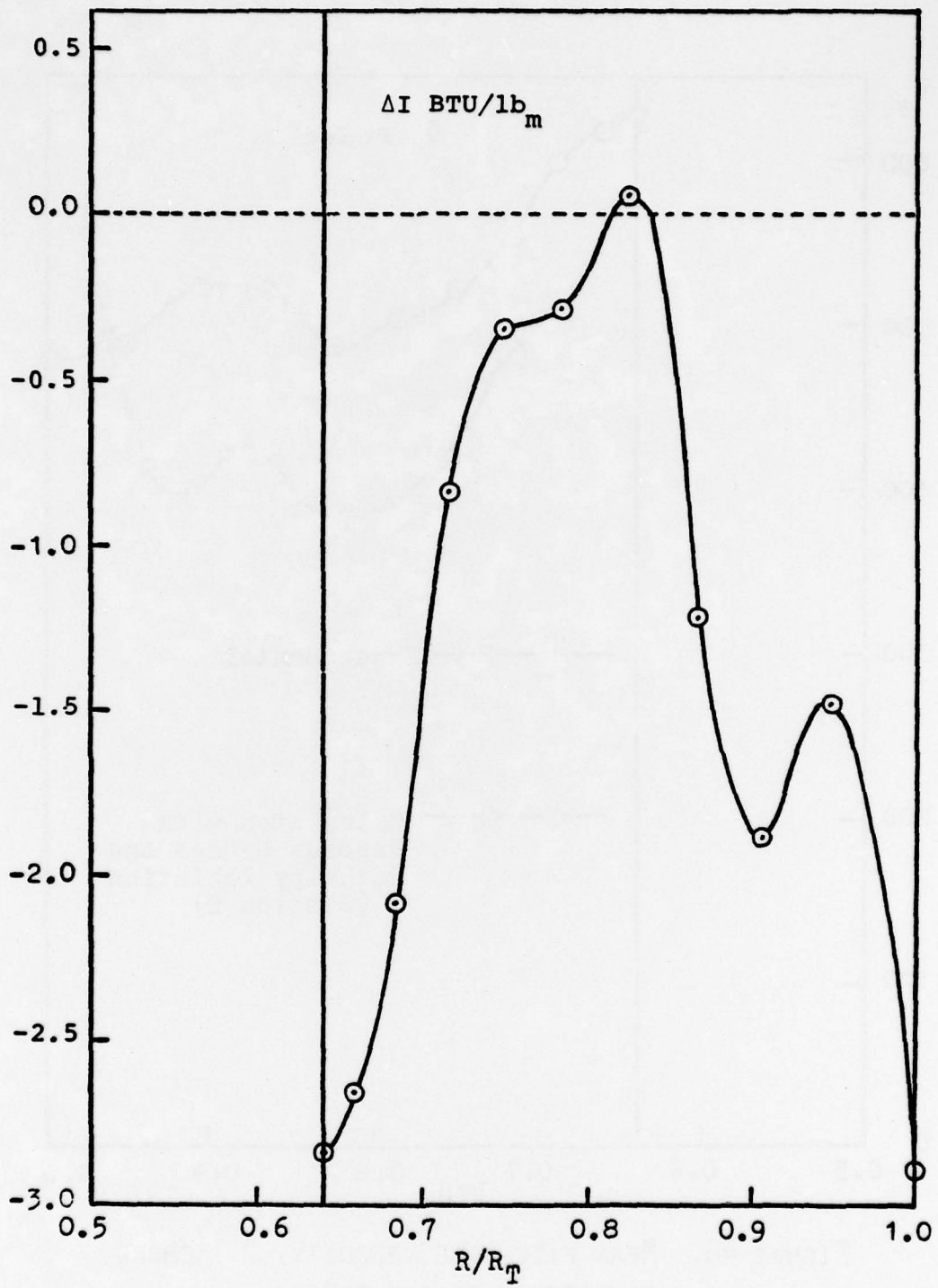


FIGURE 45. CALCULATED MEAN ROTHALPY CHANGE ACROSS THE ROTOR.

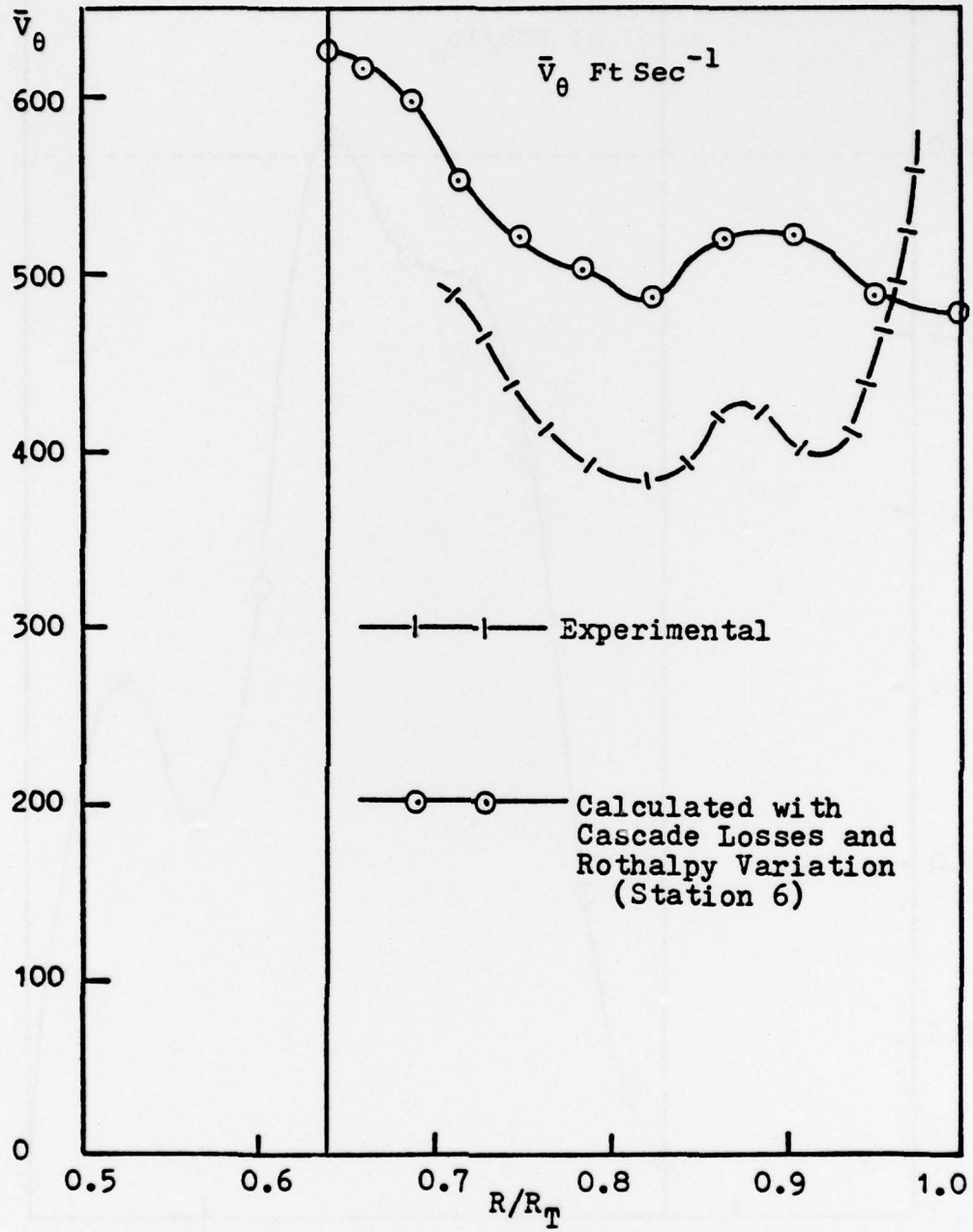


FIGURE 46. MEAN PITCHWISE VELOCITY, 0.1 CHORD DOWNSTREAM OF THE ROTOR.

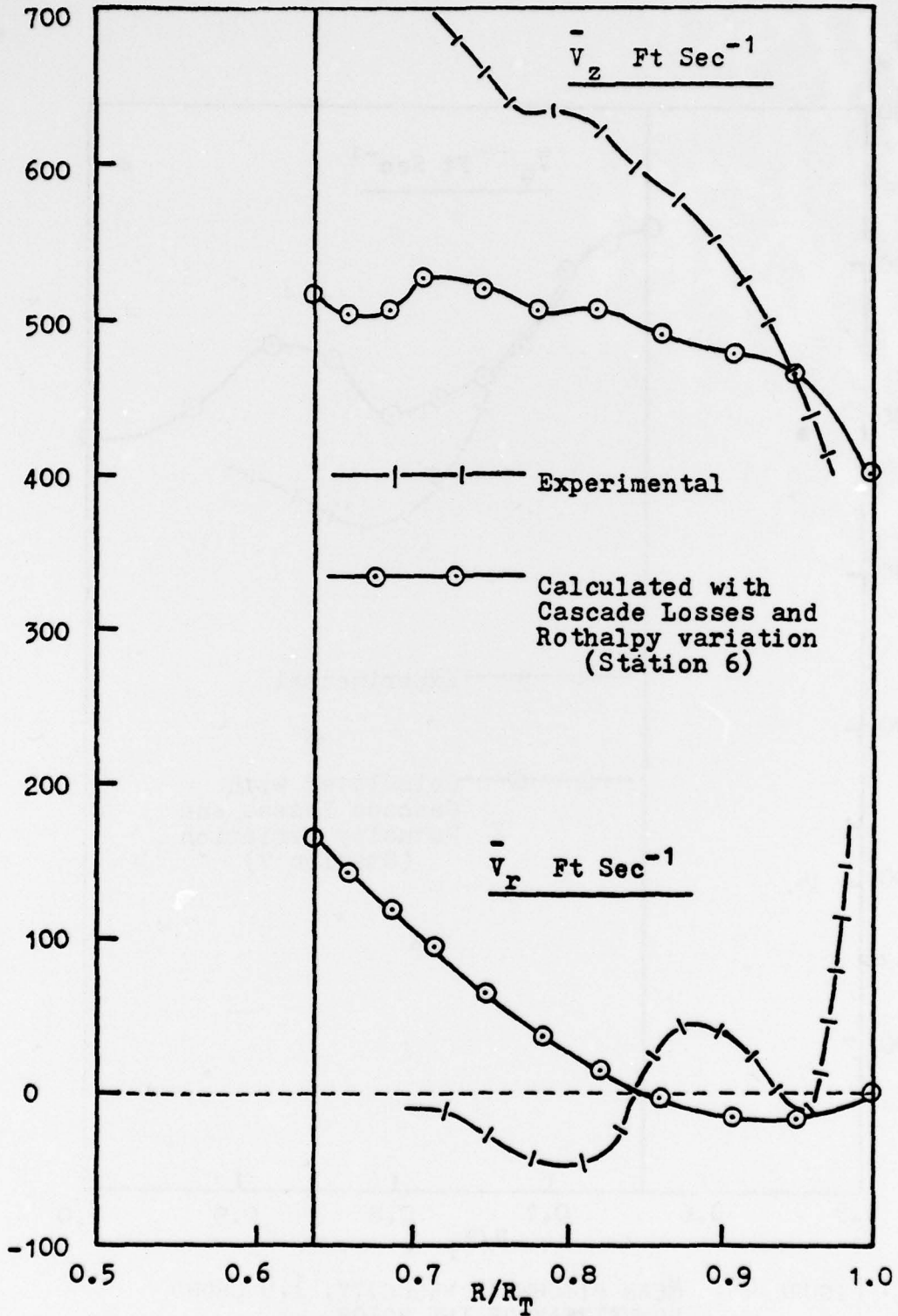


FIGURE 47. MEAN AXIAL AND RADIAL VELOCITIES, 0.1 CHORD DOWNSTREAM OF THE ROTOR.

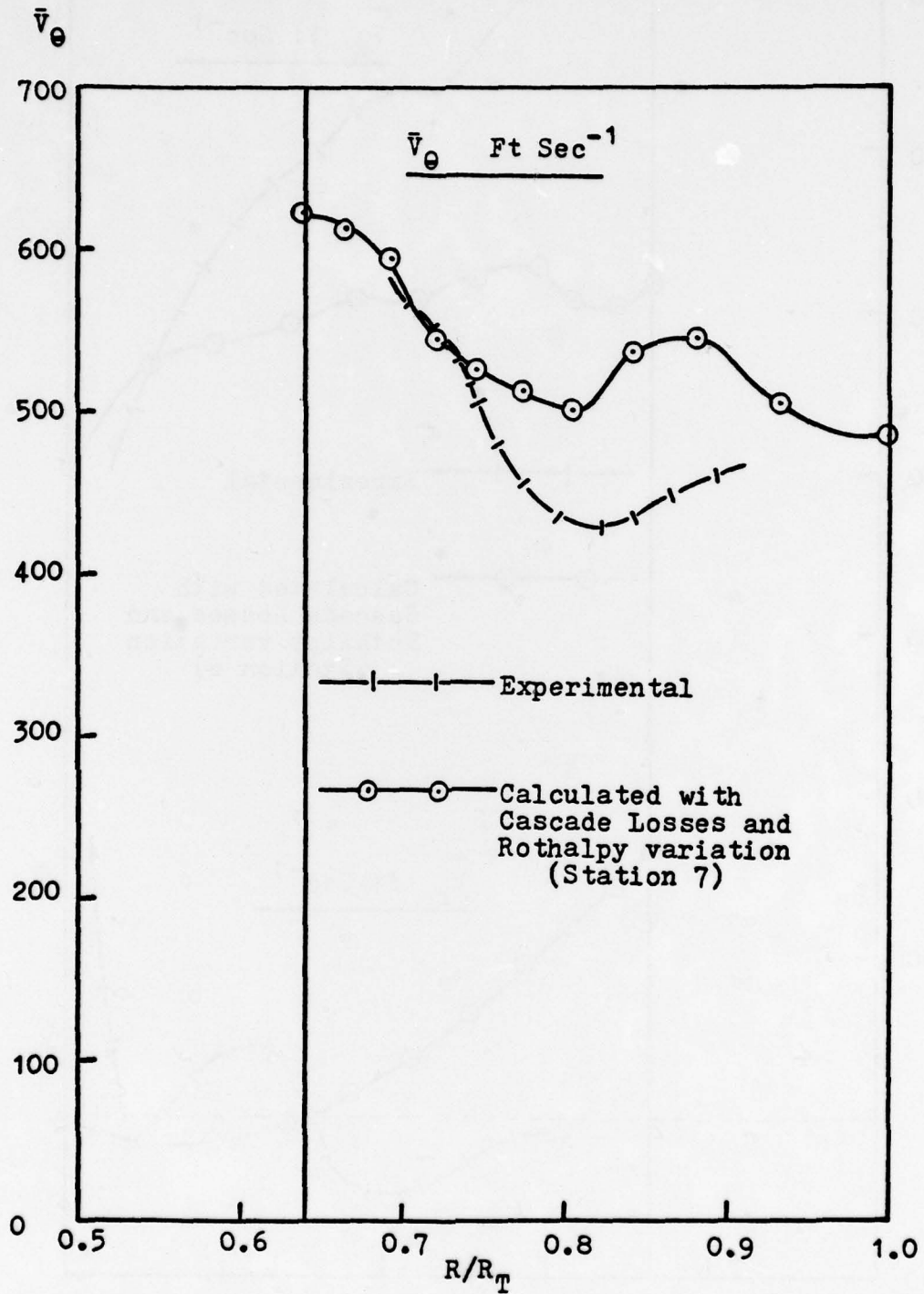


FIGURE 48. MEAN PITCHWISE VELOCITY, 1.0 CHORD DOWNSTREAM OF THE ROTOR.

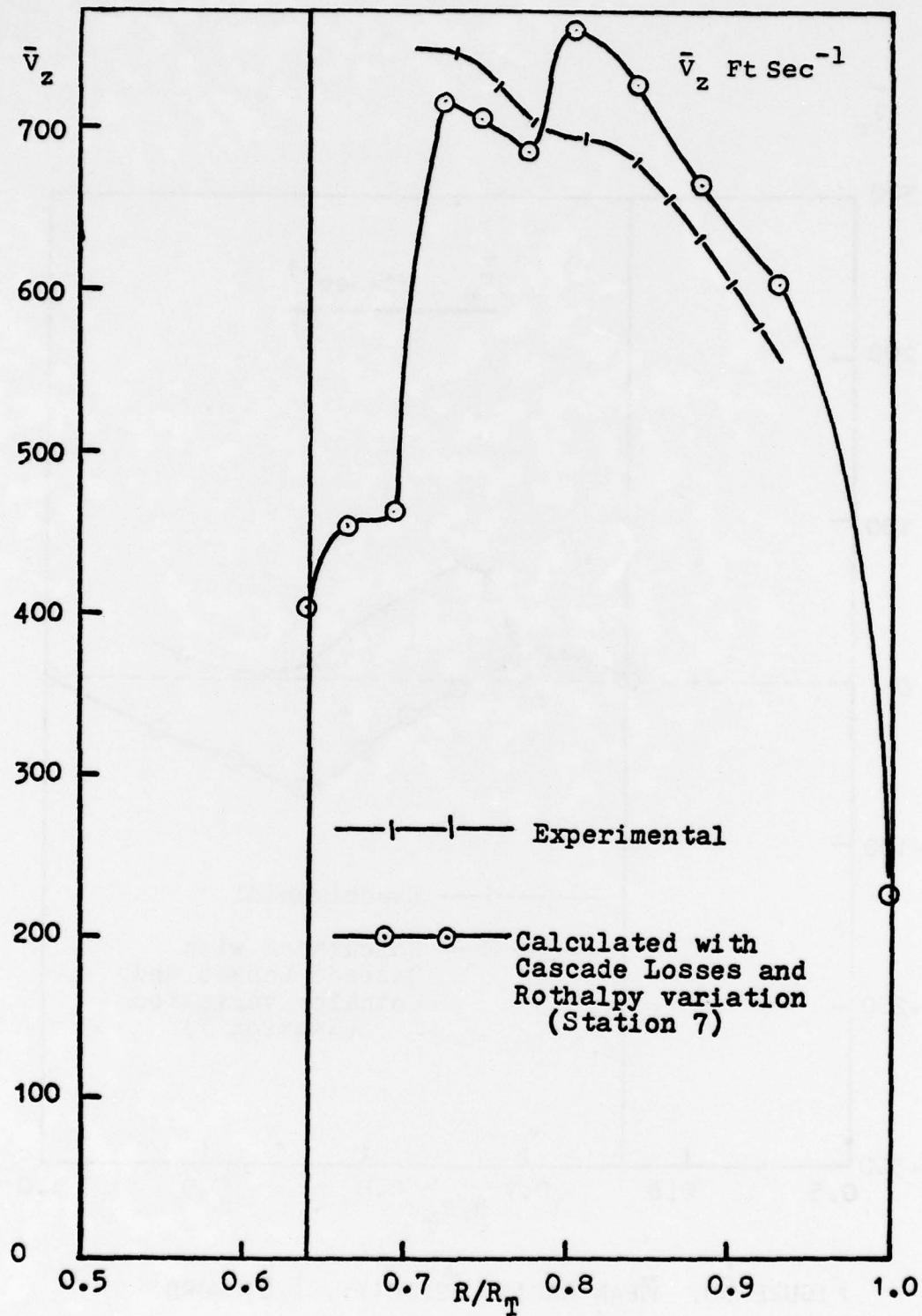


FIGURE 49. MEAN AXIAL VELOCITY, 1.0 CHORD DOWNSTREAM OF THE ROTOR.

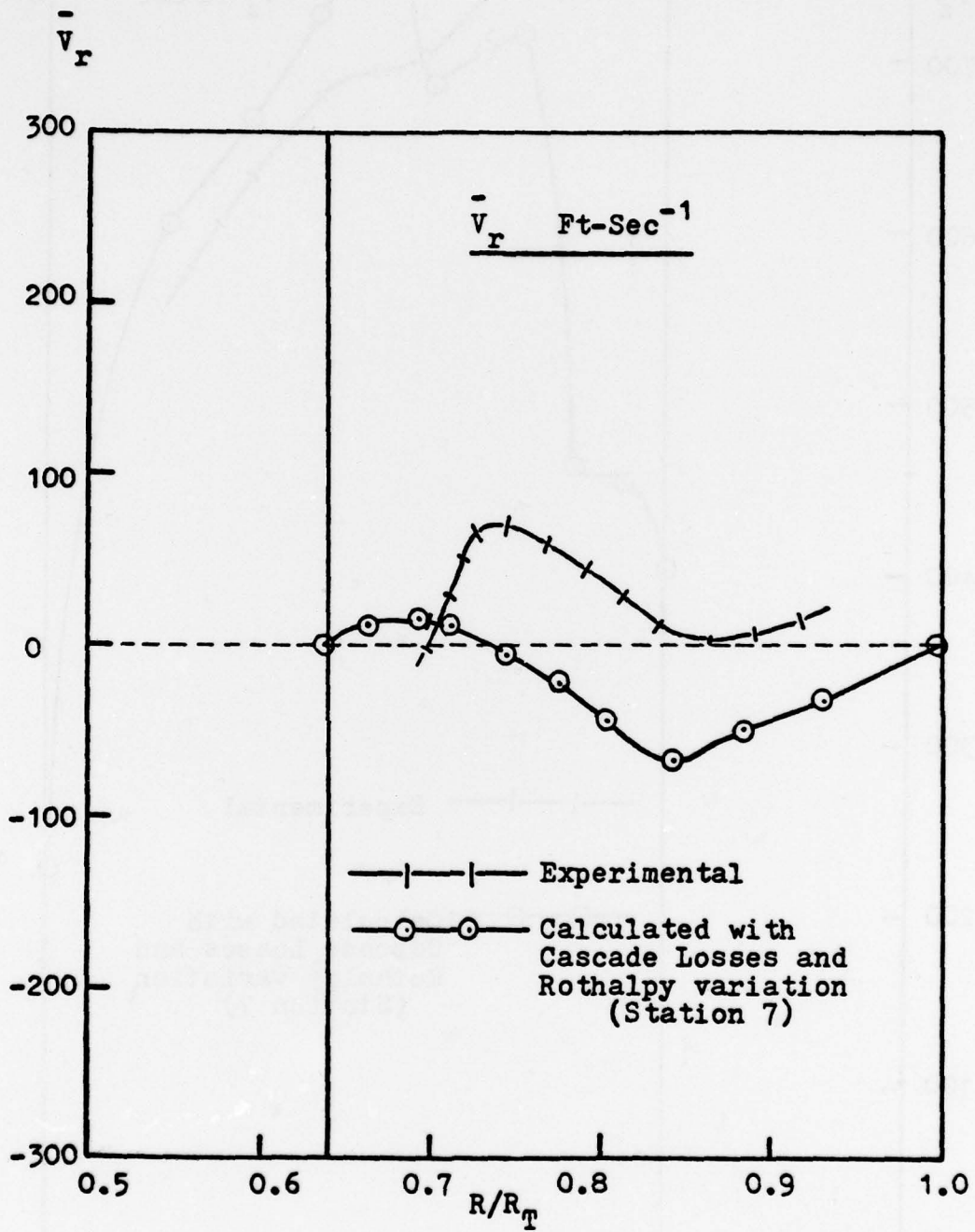


FIGURE 50. MEAN RADIAL VELOCITY, 1.0 CHORD DOWNSTREAM OF THE ROTOR.

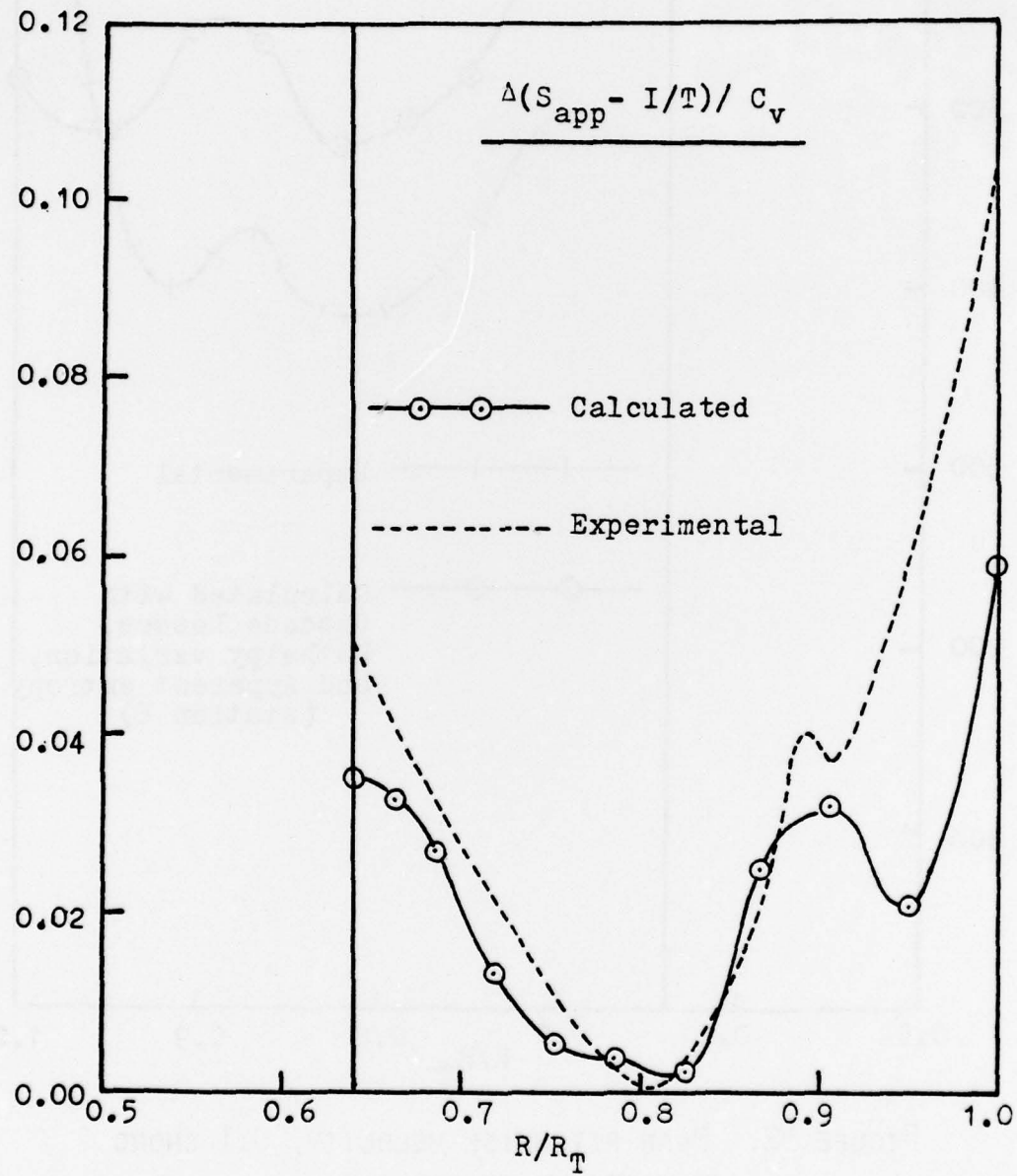


FIGURE 51. EQUIVALENT ENTROPY RISE ACROSS THE ROTOR.

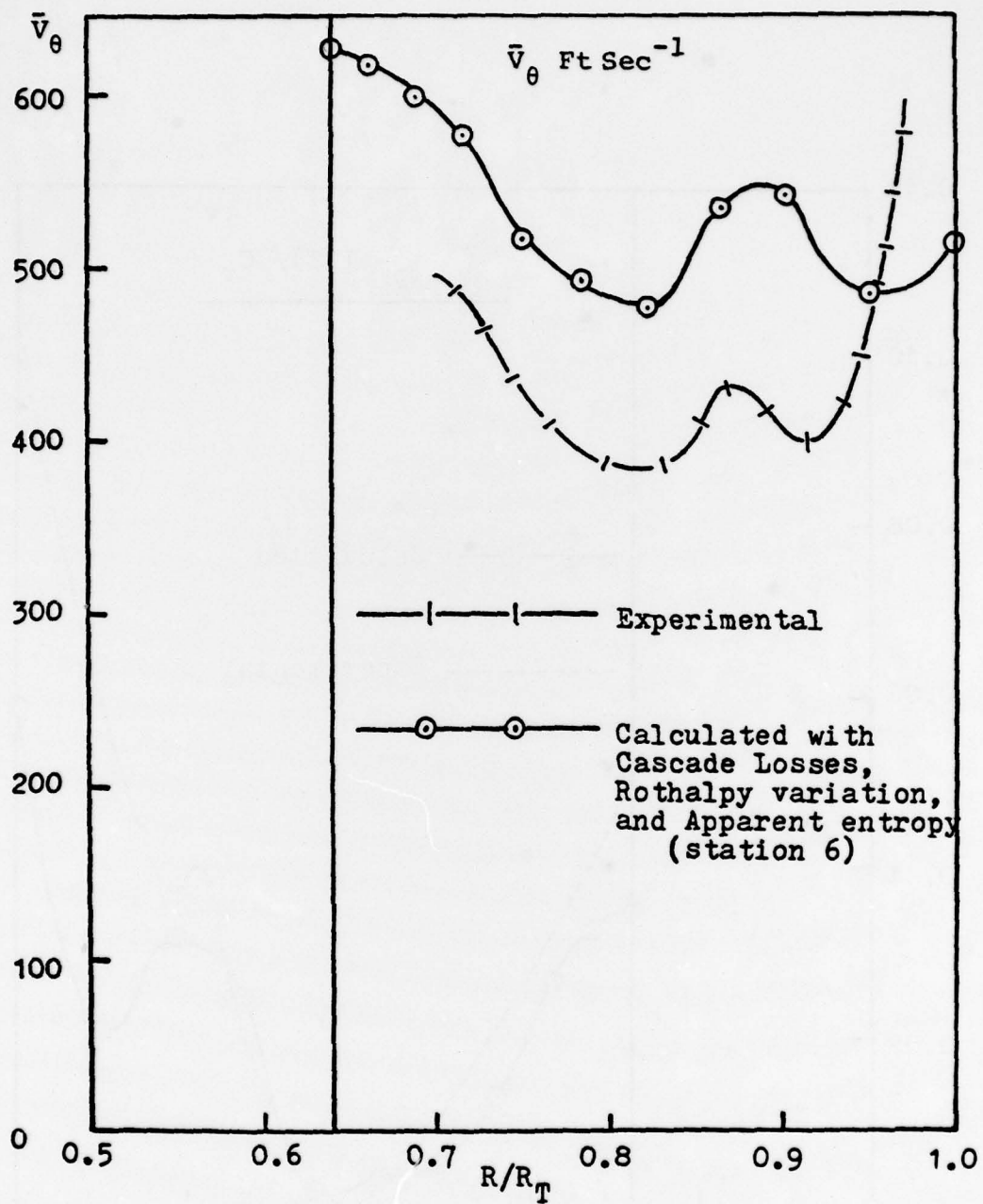


FIGURE 52. MEAN PITCHWISE VELOCITY, 0.1 CHORD DOWNSTREAM OF THE ROTOR.

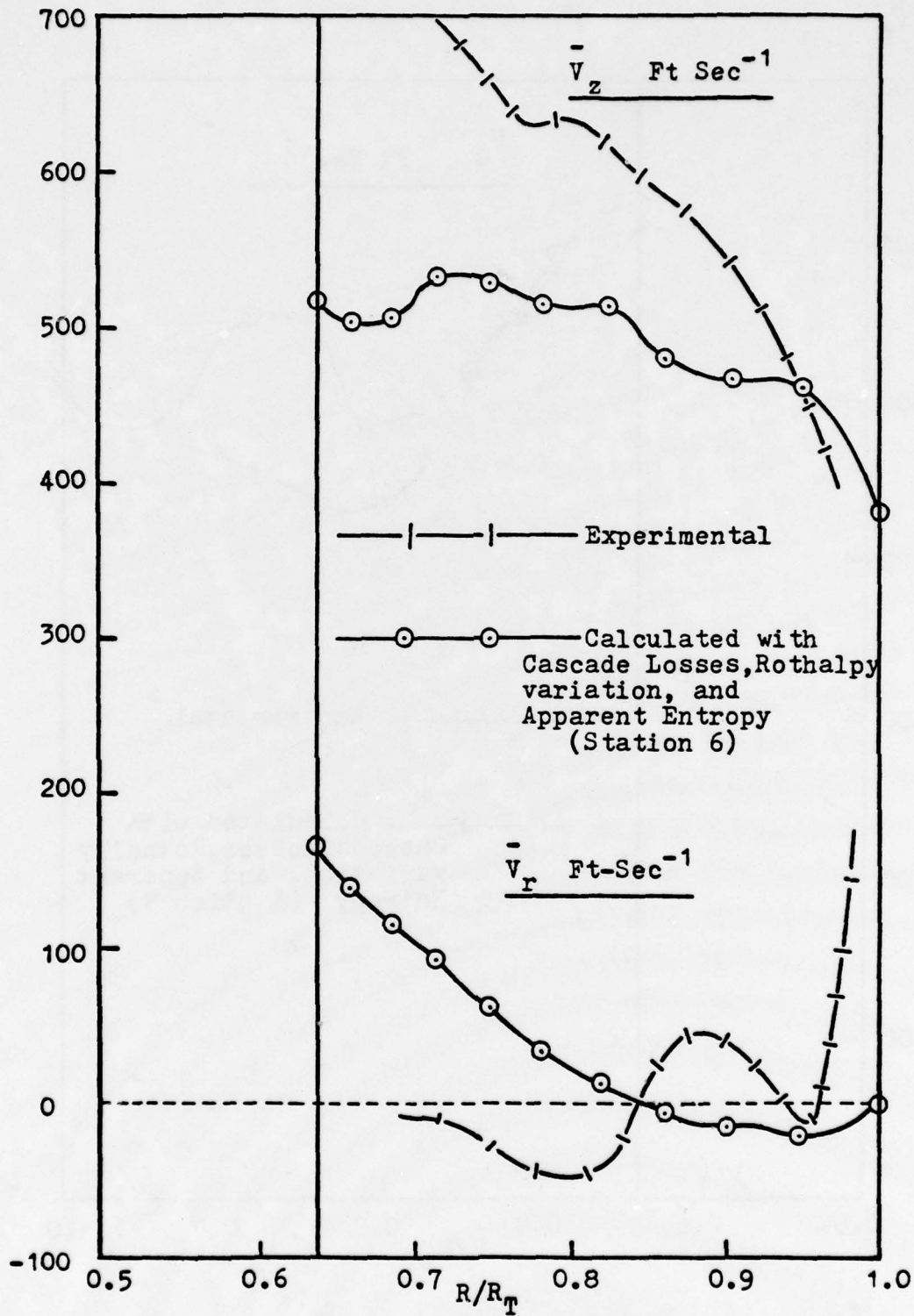


FIGURE 53. MEAN AXIAL AND RADIAL VELOCITIES, 0.1 CHORD DOWNSTREAM OF THE ROTOR.

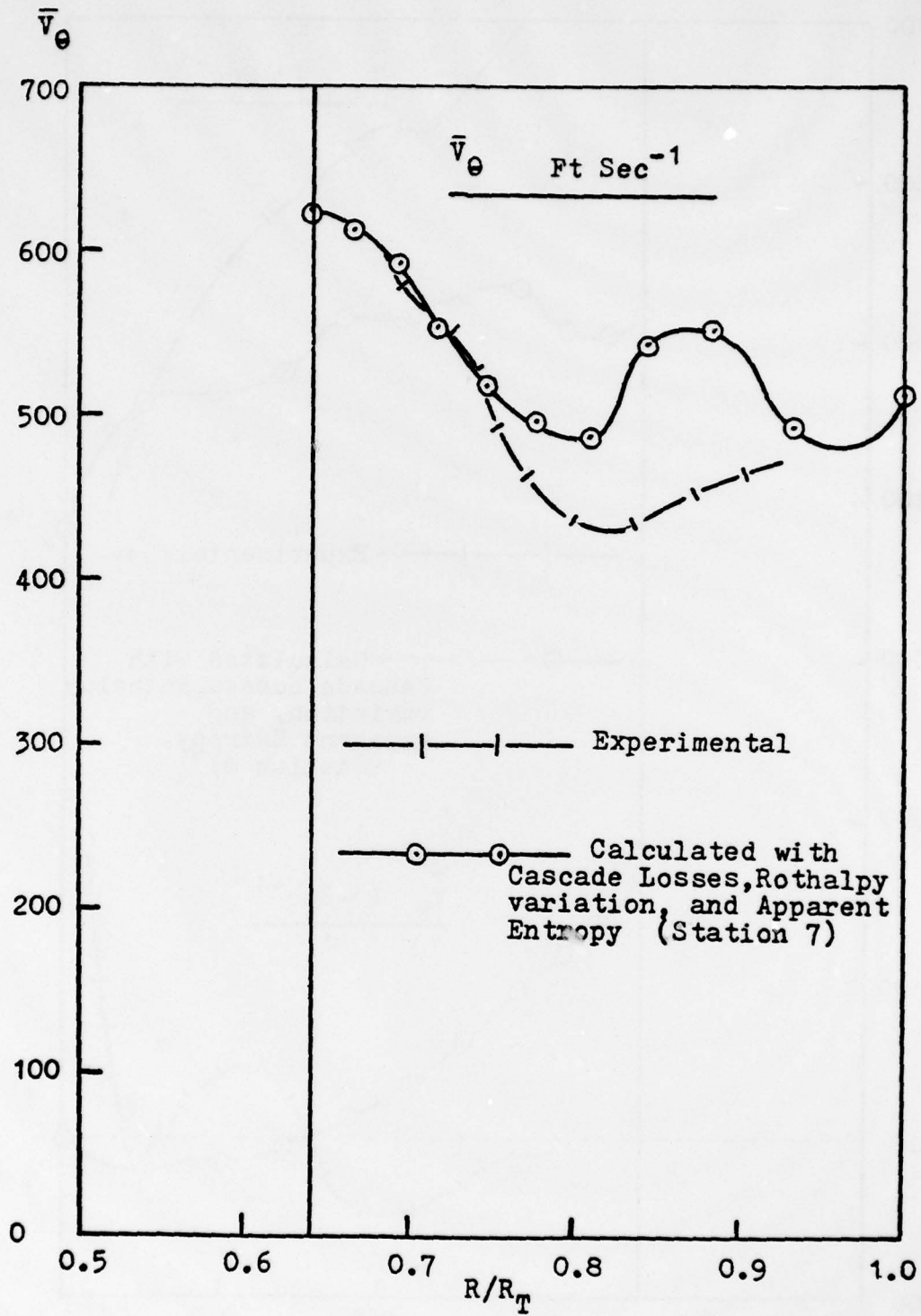


FIGURE 54. MEAN PITCHWISE VELOCITY, 1.0 CHORD DOWNSTREAM OF THE ROTOR.

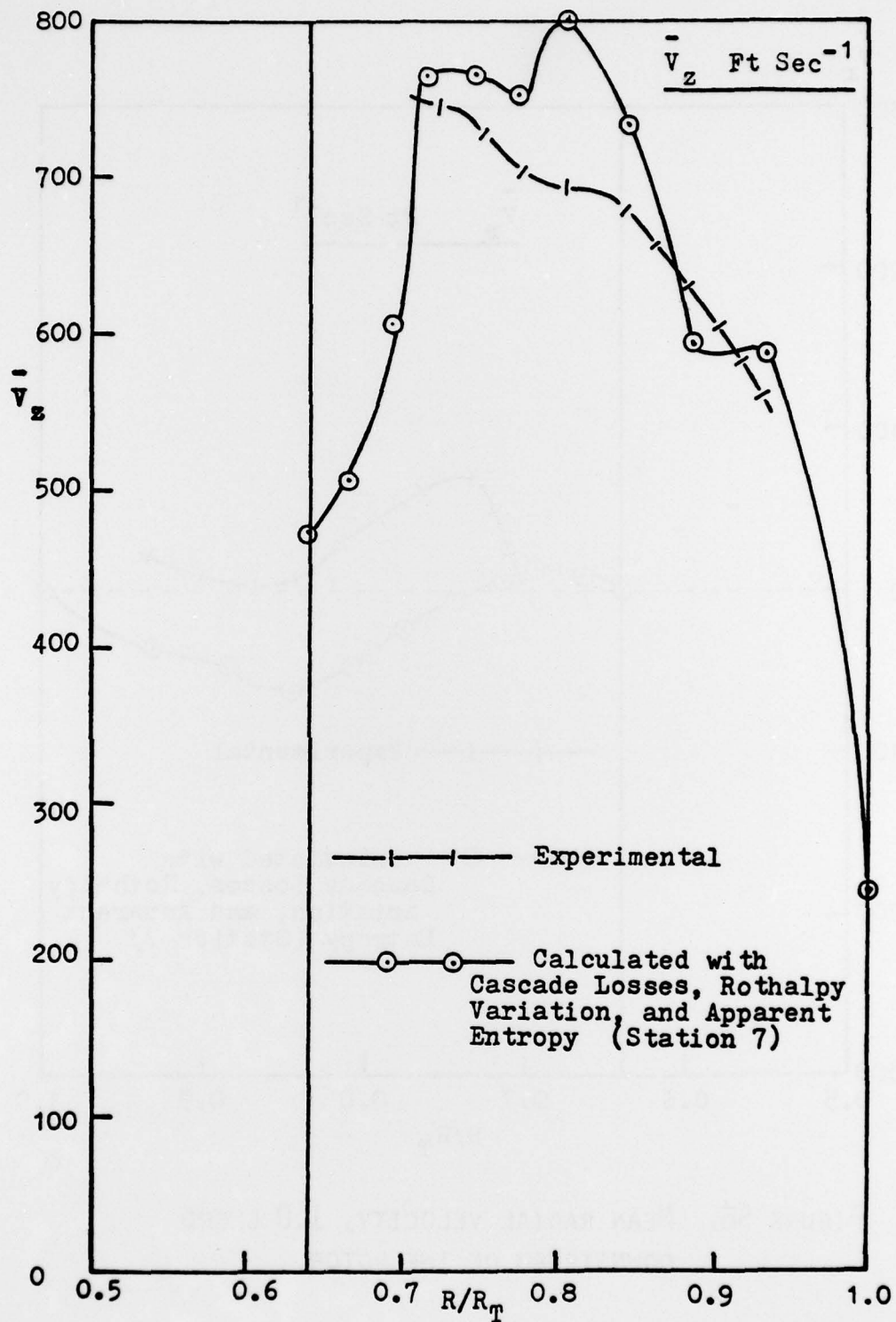


FIGURE 55. MEAN AXIAL VELOCITY, 1.0 CHORD DOWNSTREAM OF THE ROTOR.

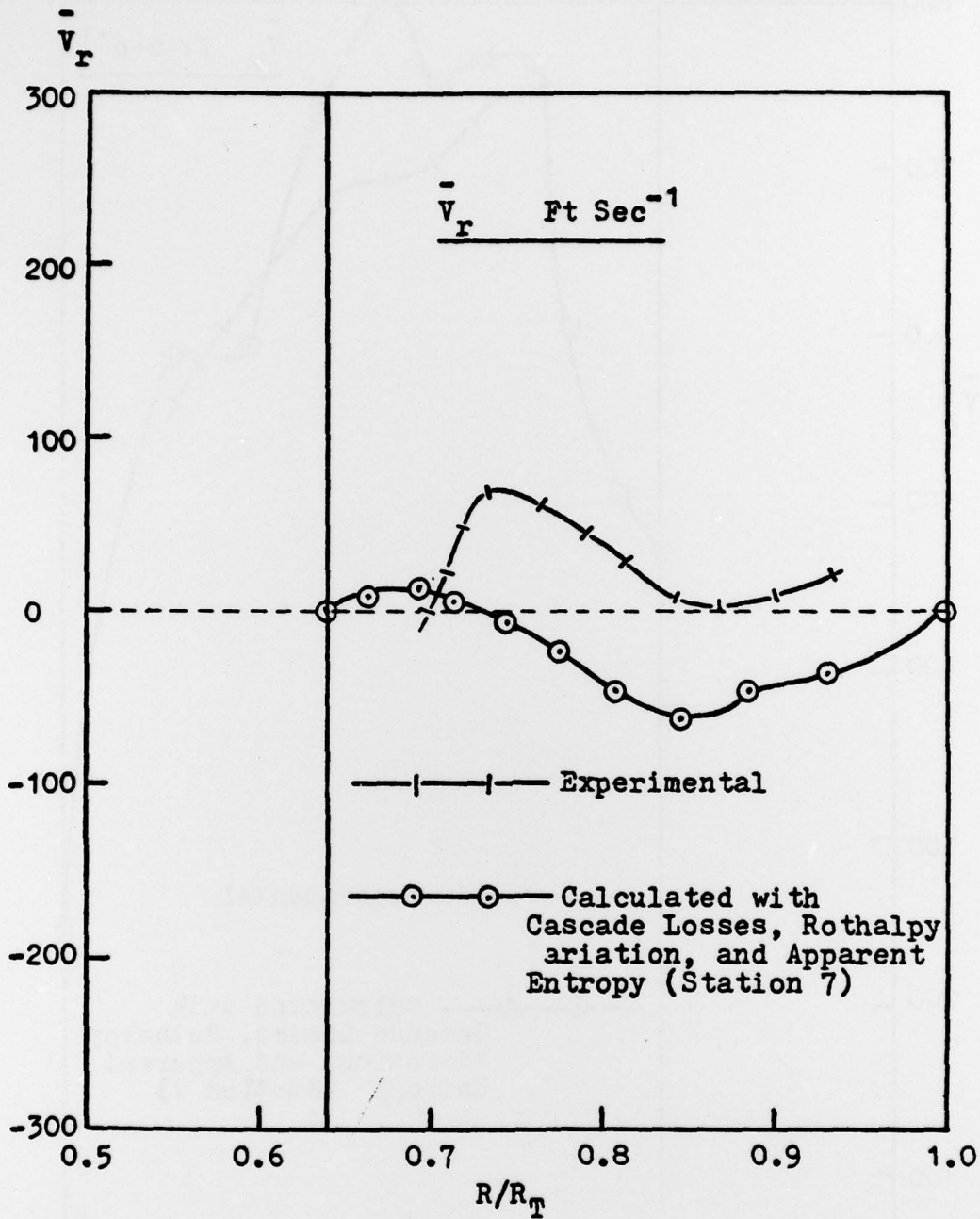


FIGURE 56. MEAN RADIAL VELOCITY, 1.0 CHORD DOWNSTREAM OF THE ROTOR.

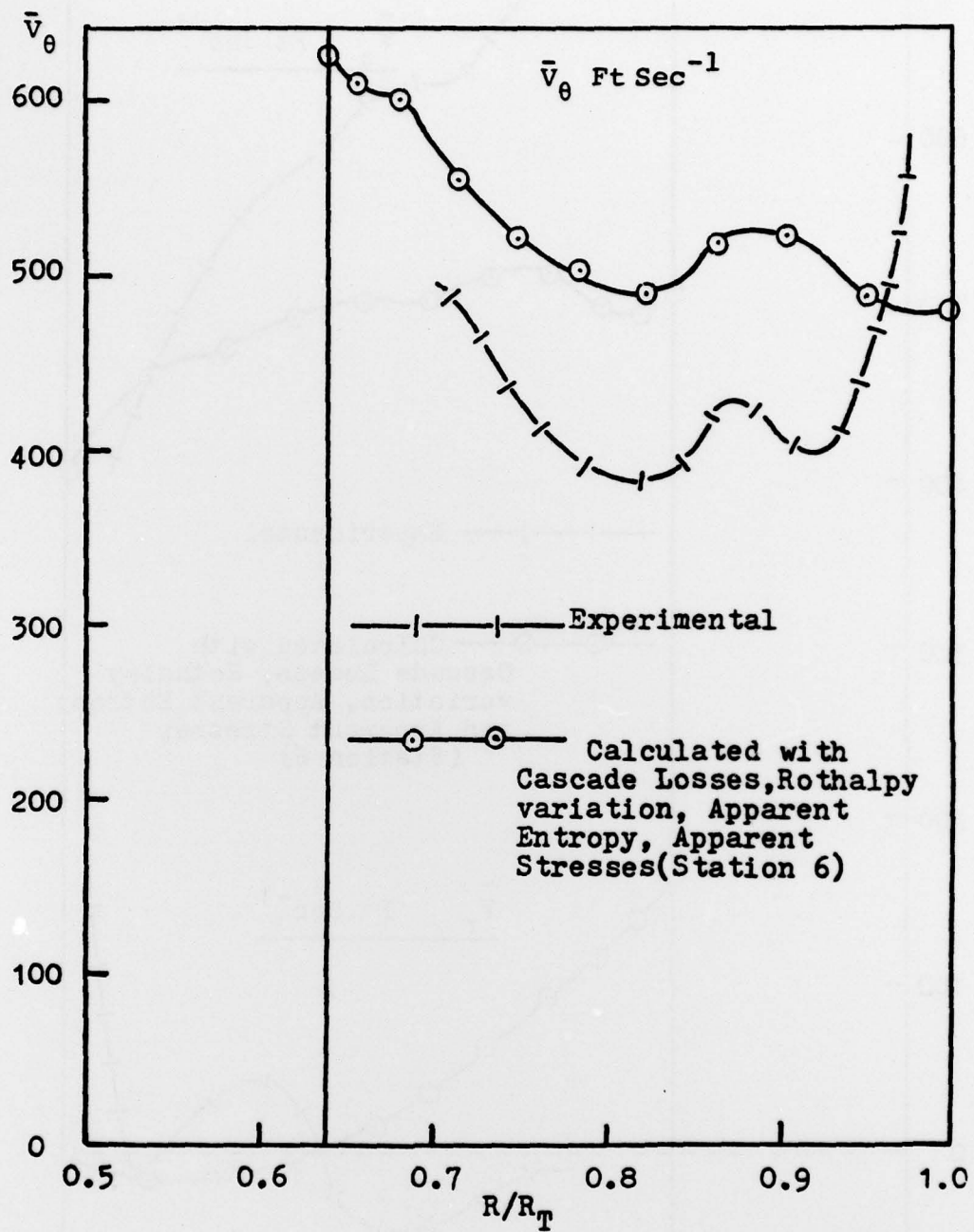


FIGURE 57. MEAN PITCHWISE VELOCITY, 0.1 CHORD
DOWNSTREAM OF THE ROTOR.

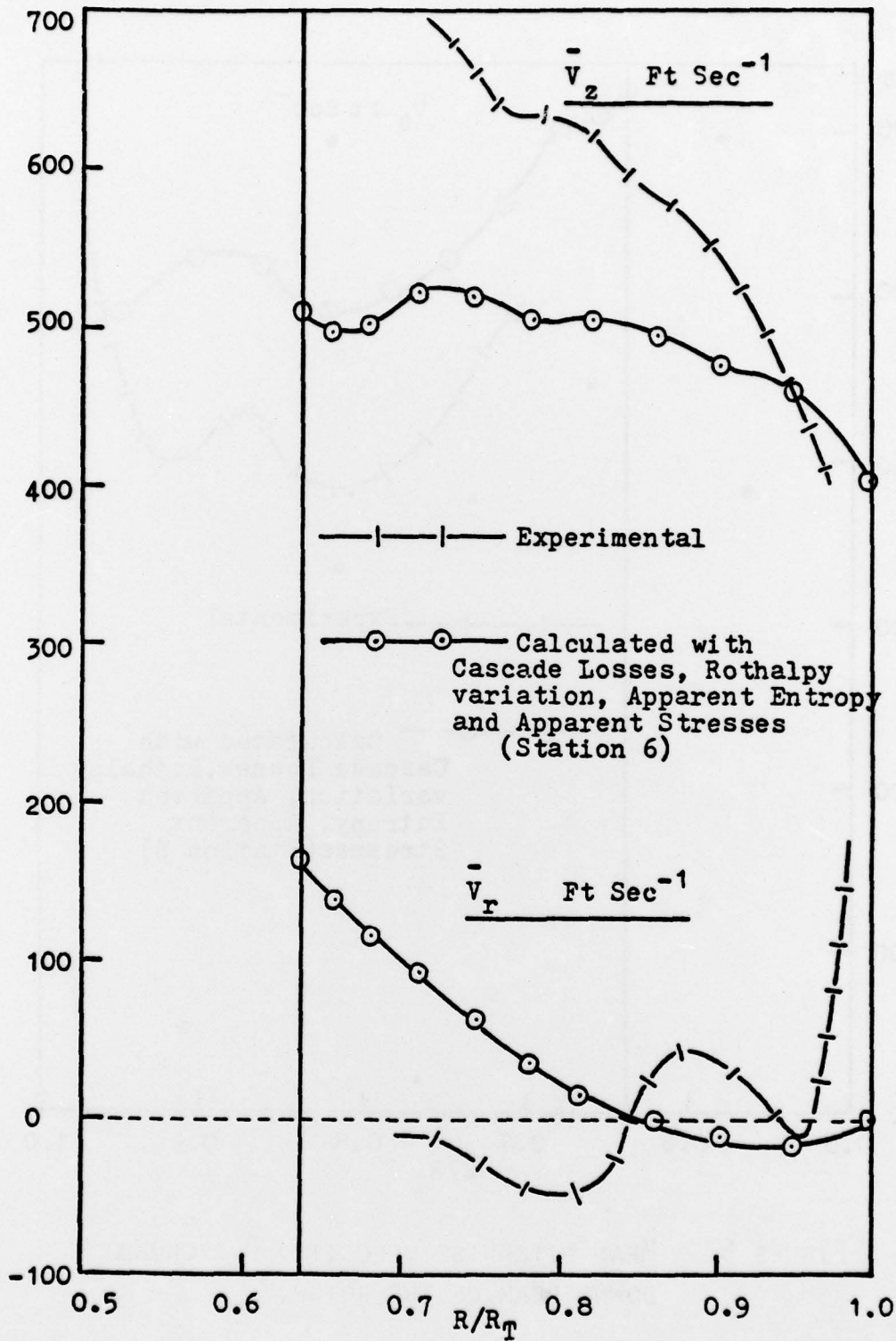


FIGURE 58. MEAN AXIAL AND RADIAL VELOCITIES, 0.1 CHORD DOWNSTREAM OF THE ROTOR.

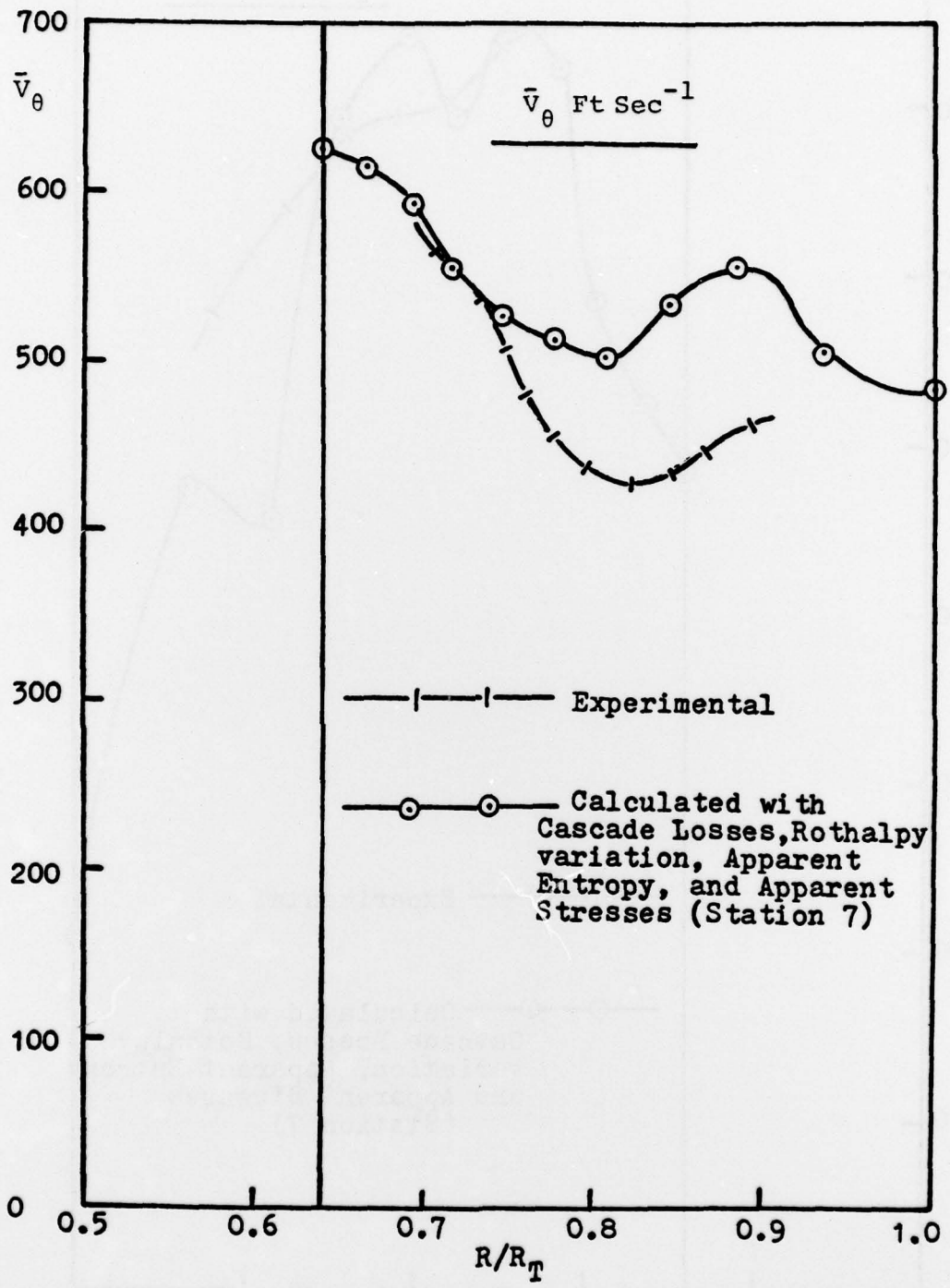


FIGURE 59. MEAN PITCHWISE VELOCITY, 1.0 CHORD DOWNSTREAM OF THE ROTOR.

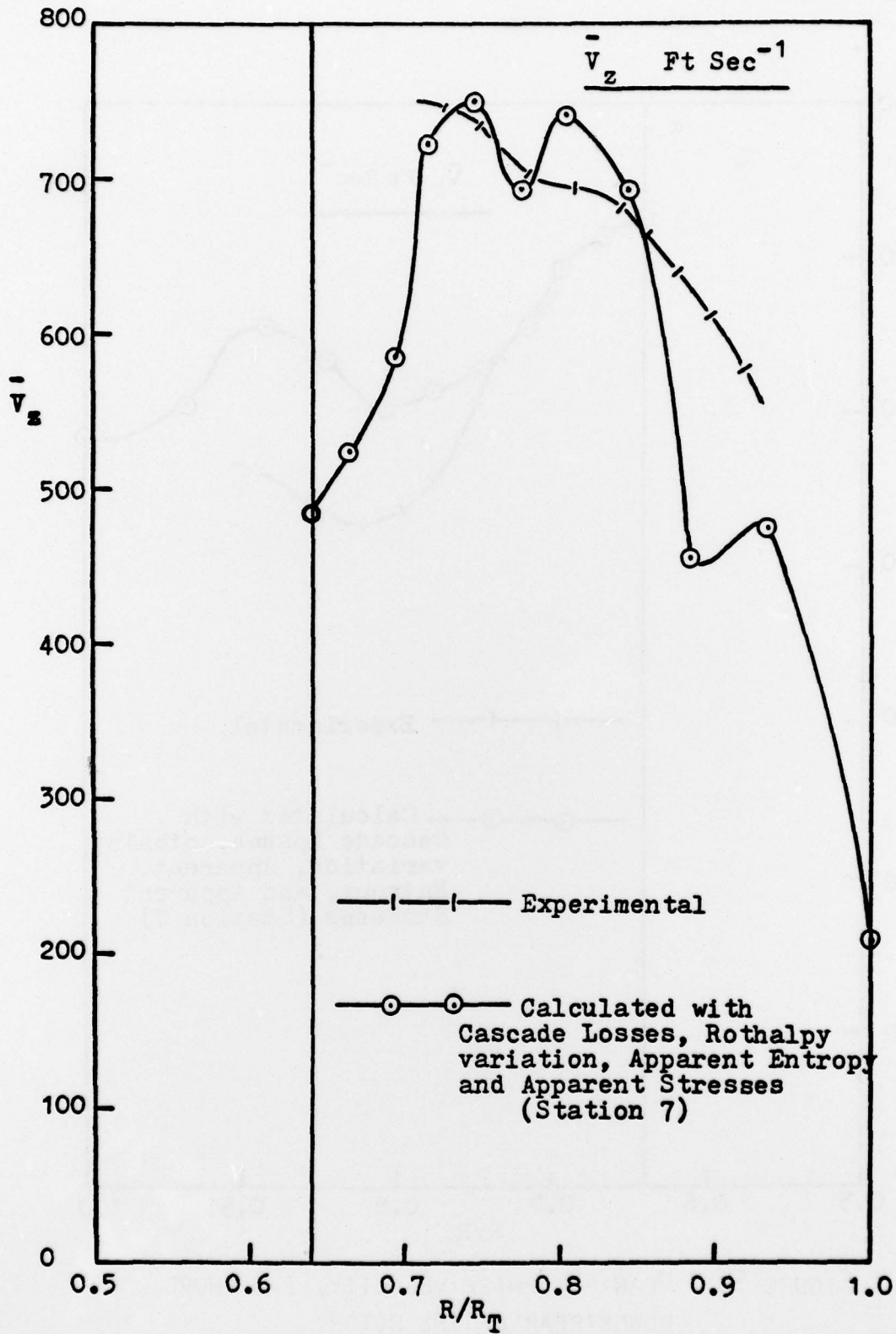


FIGURE 60. MEAN AXIAL VELOCITY, 1.0 CHORD DOWNSTREAM OF THE ROTOR.

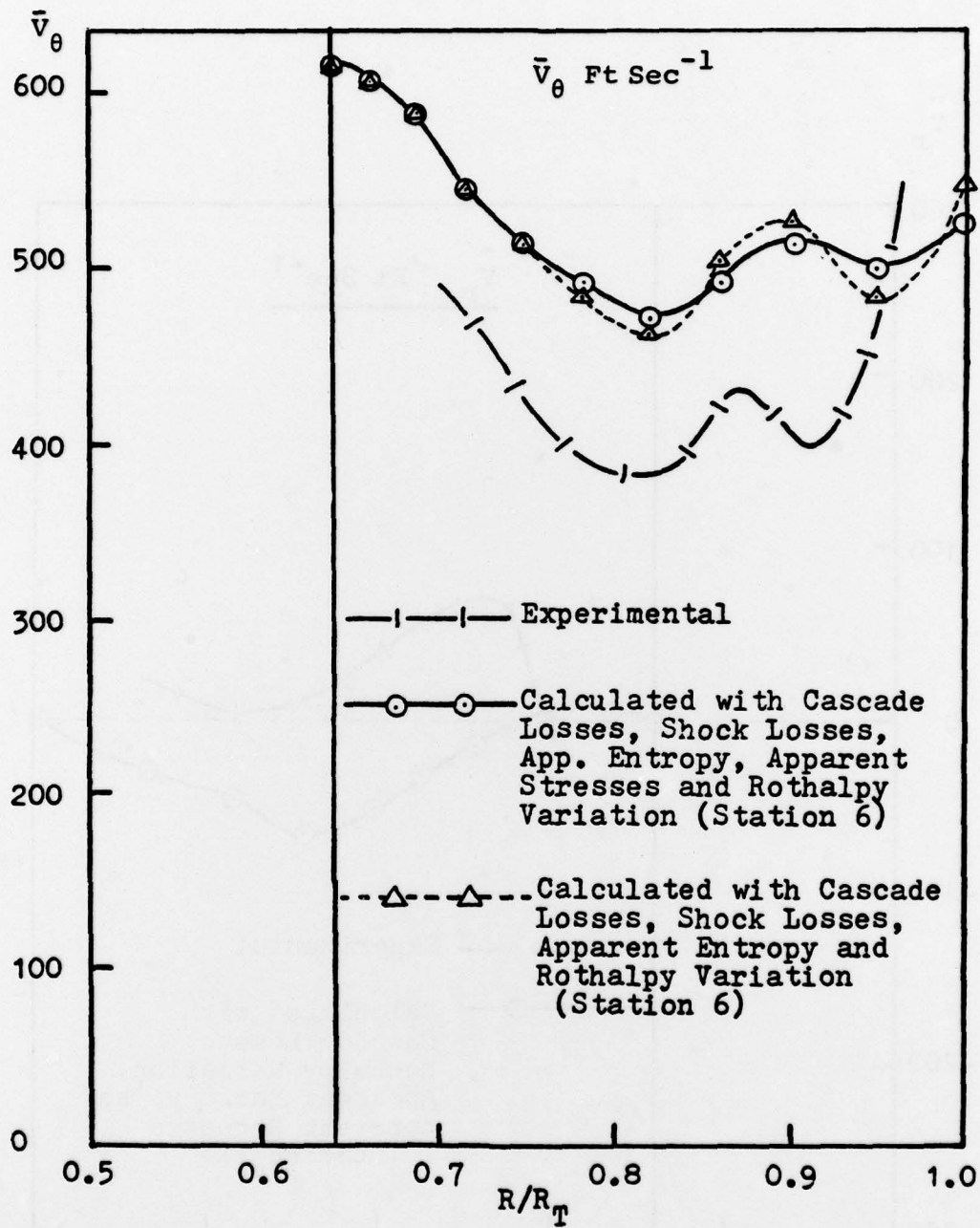


FIGURE 62. MEAN PITCHWISE VELOCITY, 0.1 CHORD DOWNSTREAM OF THE ROTOR.

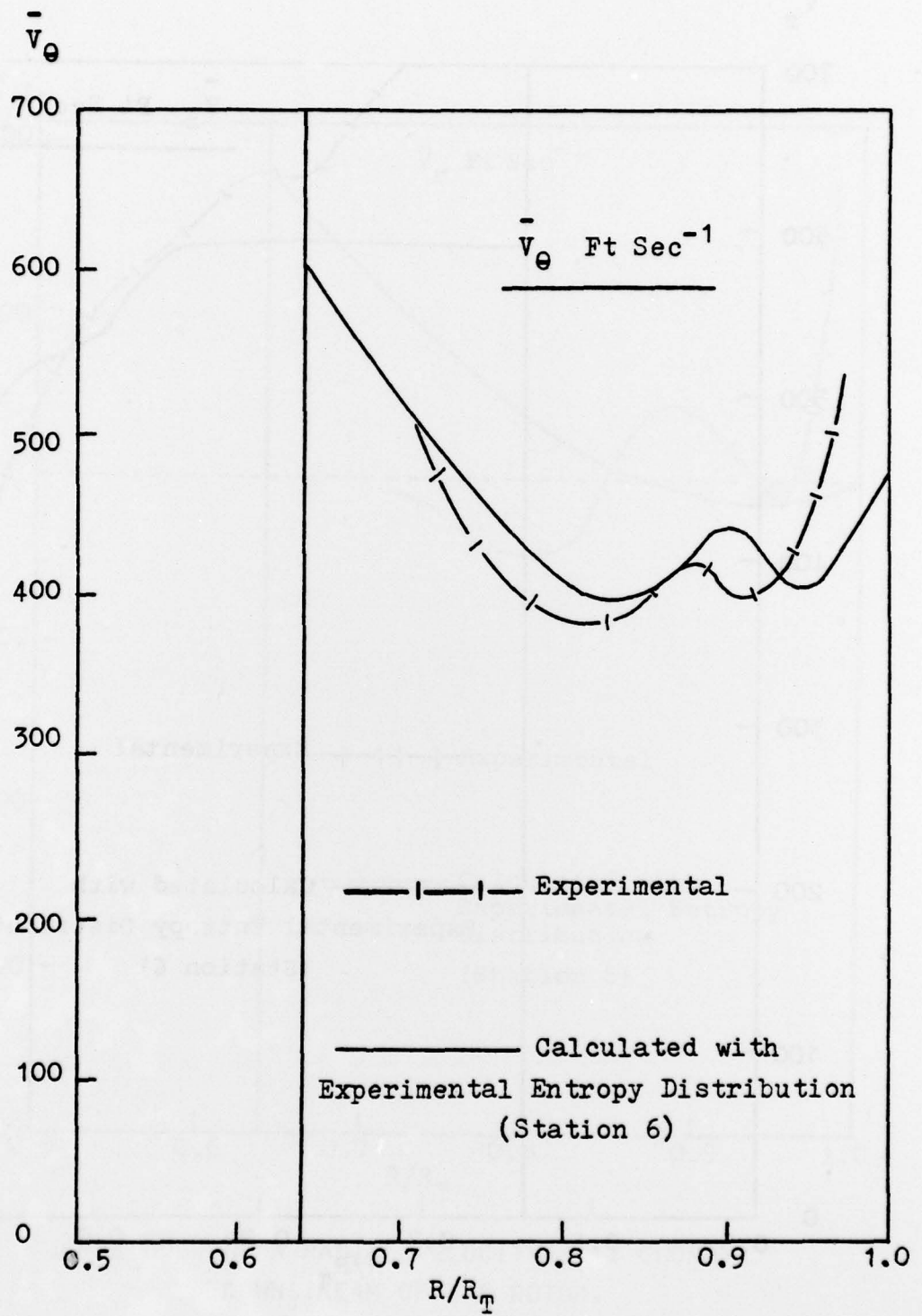


FIGURE 63. MEAN PITCHWISE VELOCITY, 0.1 CHORD DOWNSTREAM OF THE ROTOR.

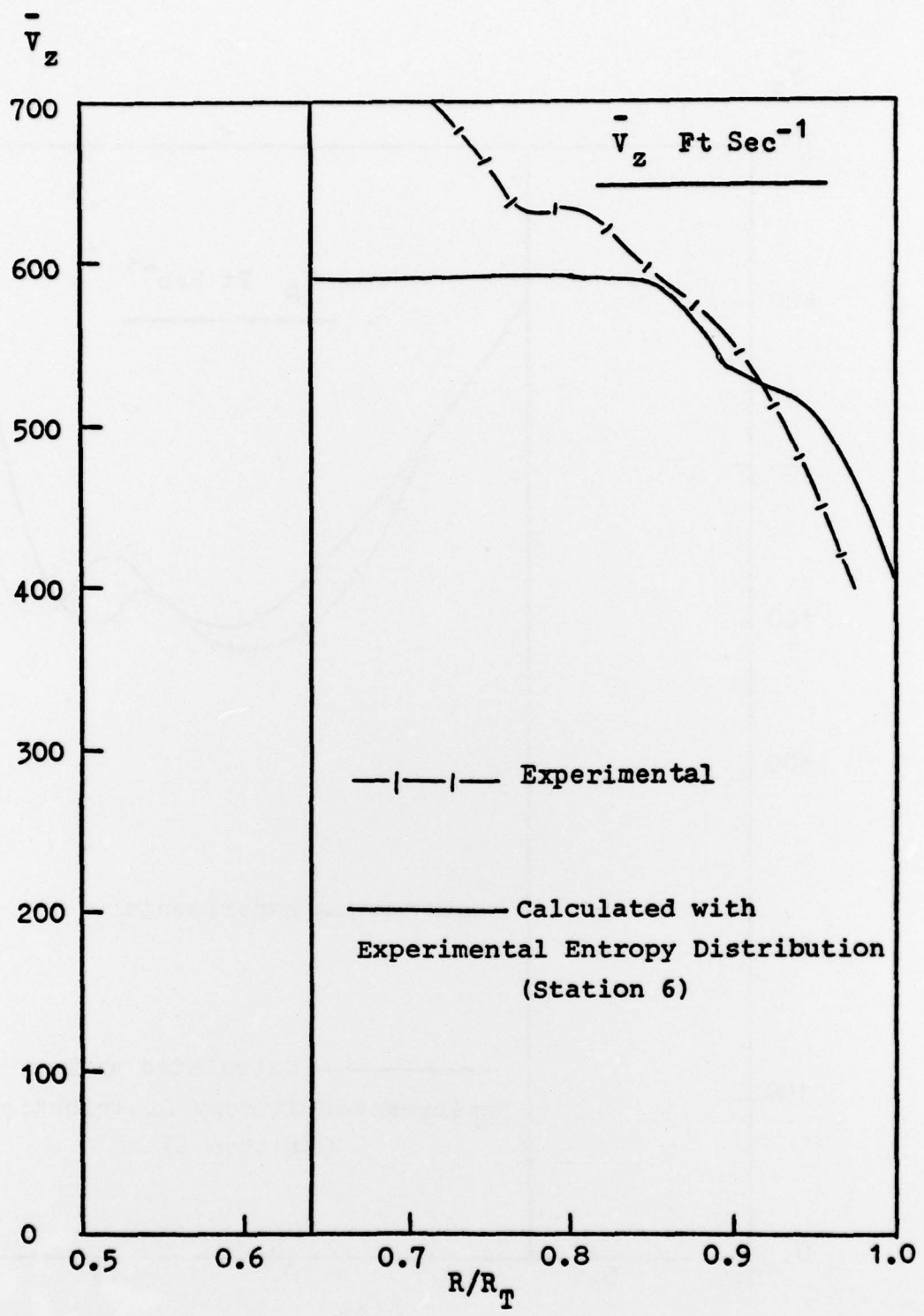


FIGURE 64. MEAN AXIAL VELOCITY, 0.1 CHORD DOWNSTREAM OF THE ROTOR.

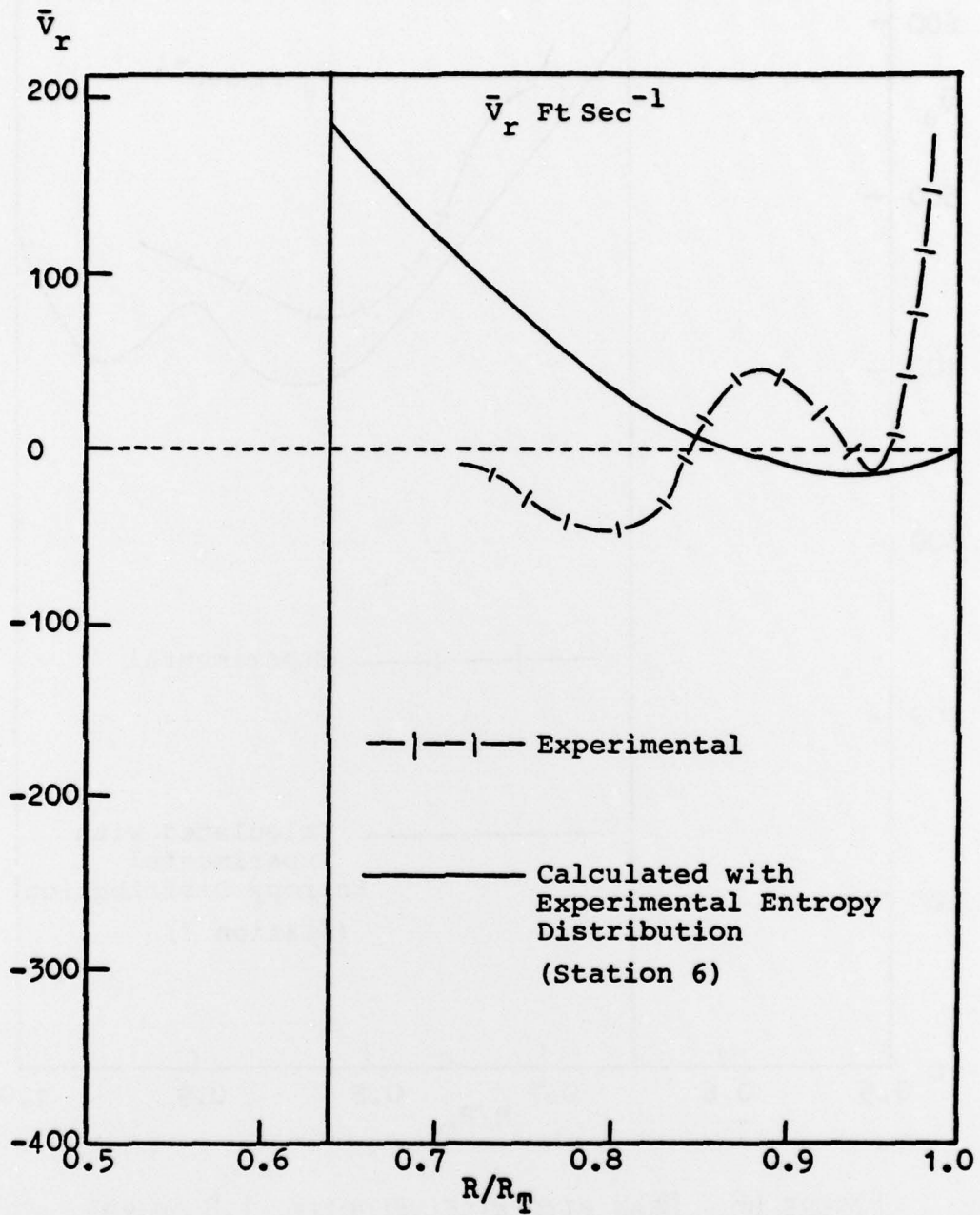


FIGURE 65. MEAN RADIAL VELOCITY, 0.1 CHORD DOWNSTREAM OF THE ROTOR.

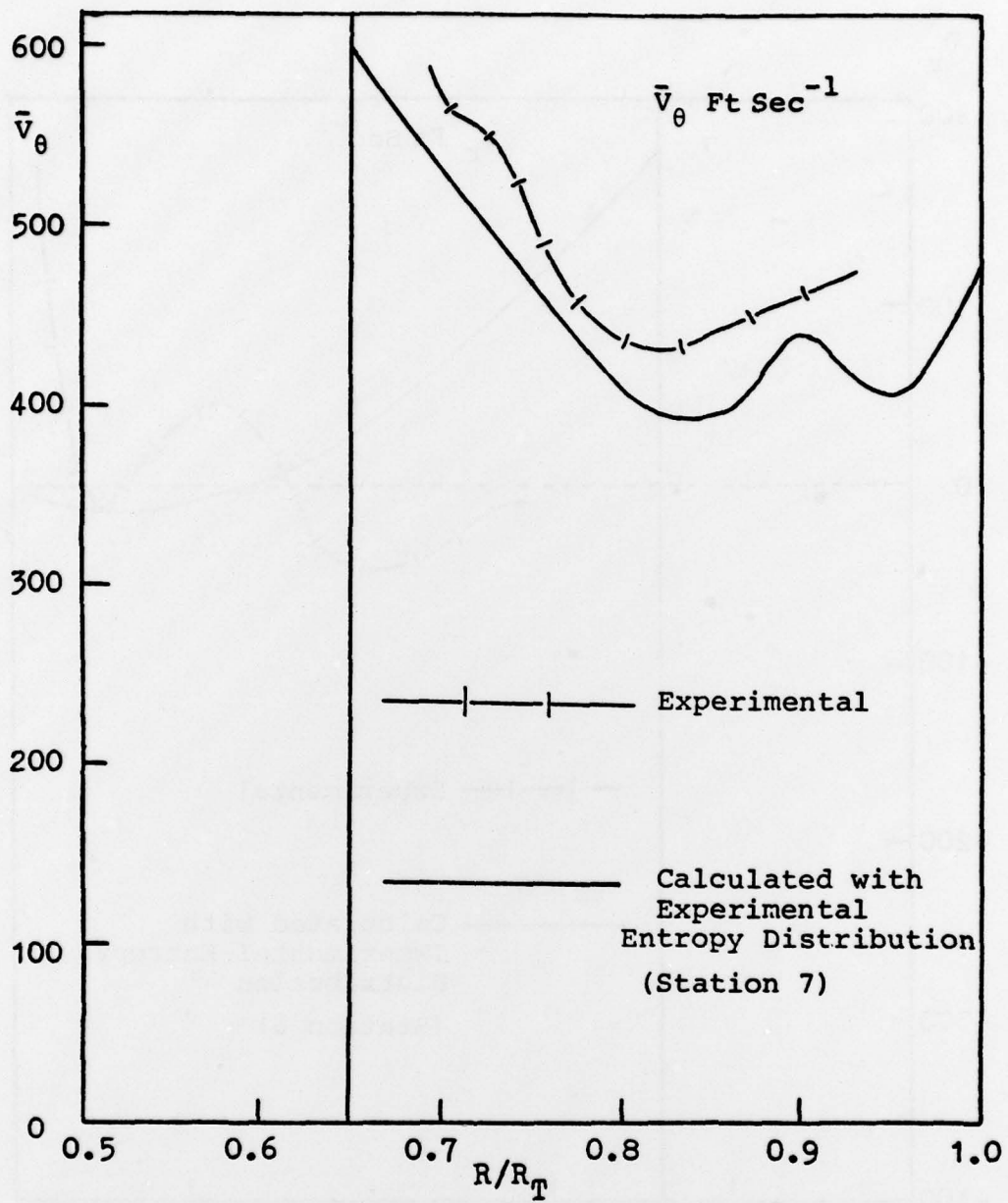


FIGURE 66. MEAN PITCHWISE VELOCITY, 1.0 CHORD
DOWNSTREAM OF THE ROTOR.

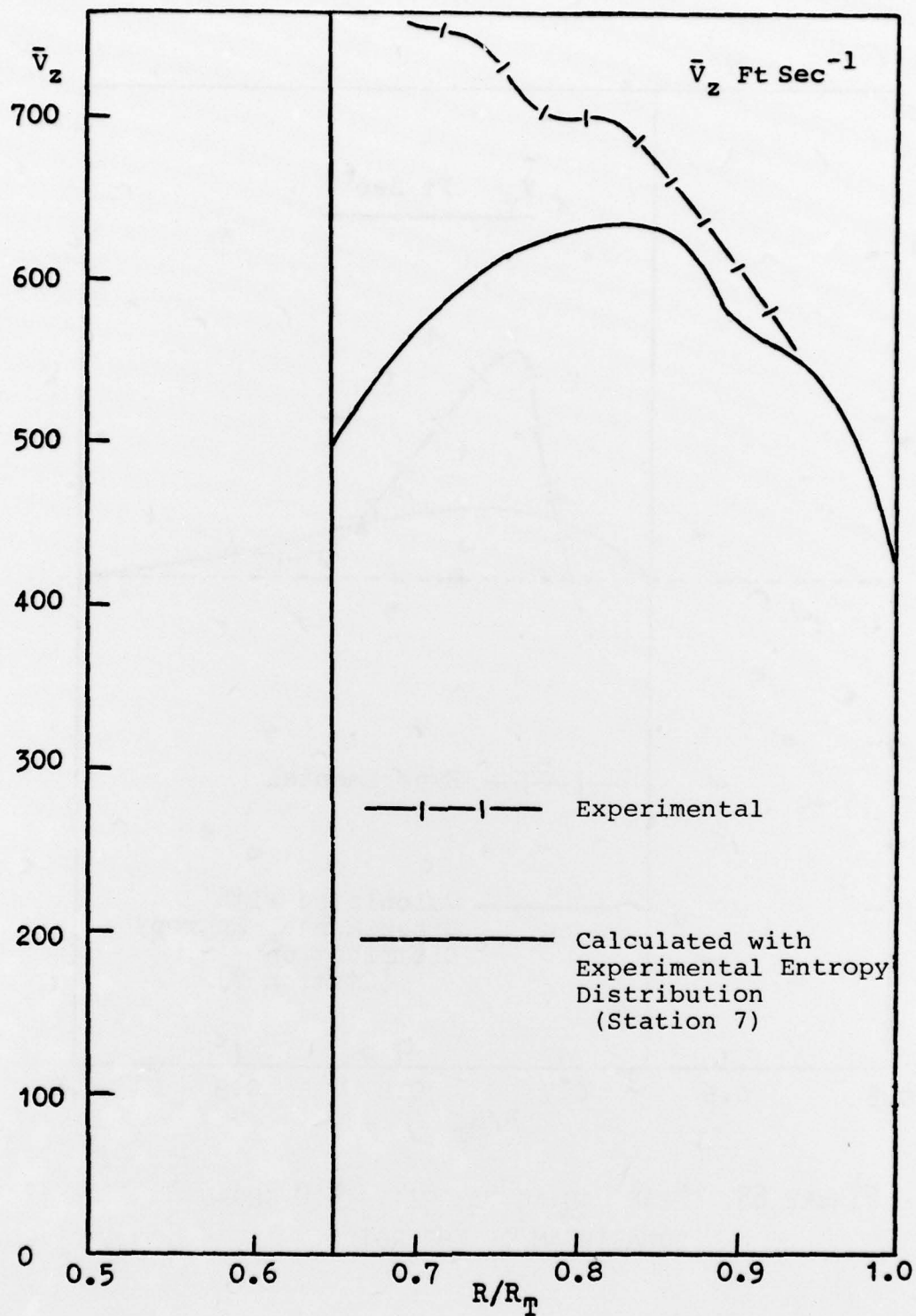


FIGURE 67. MEAN AXIAL VELOCITY, 1.0 CHORD
DOWNSTREAM OF THE ROTOR.

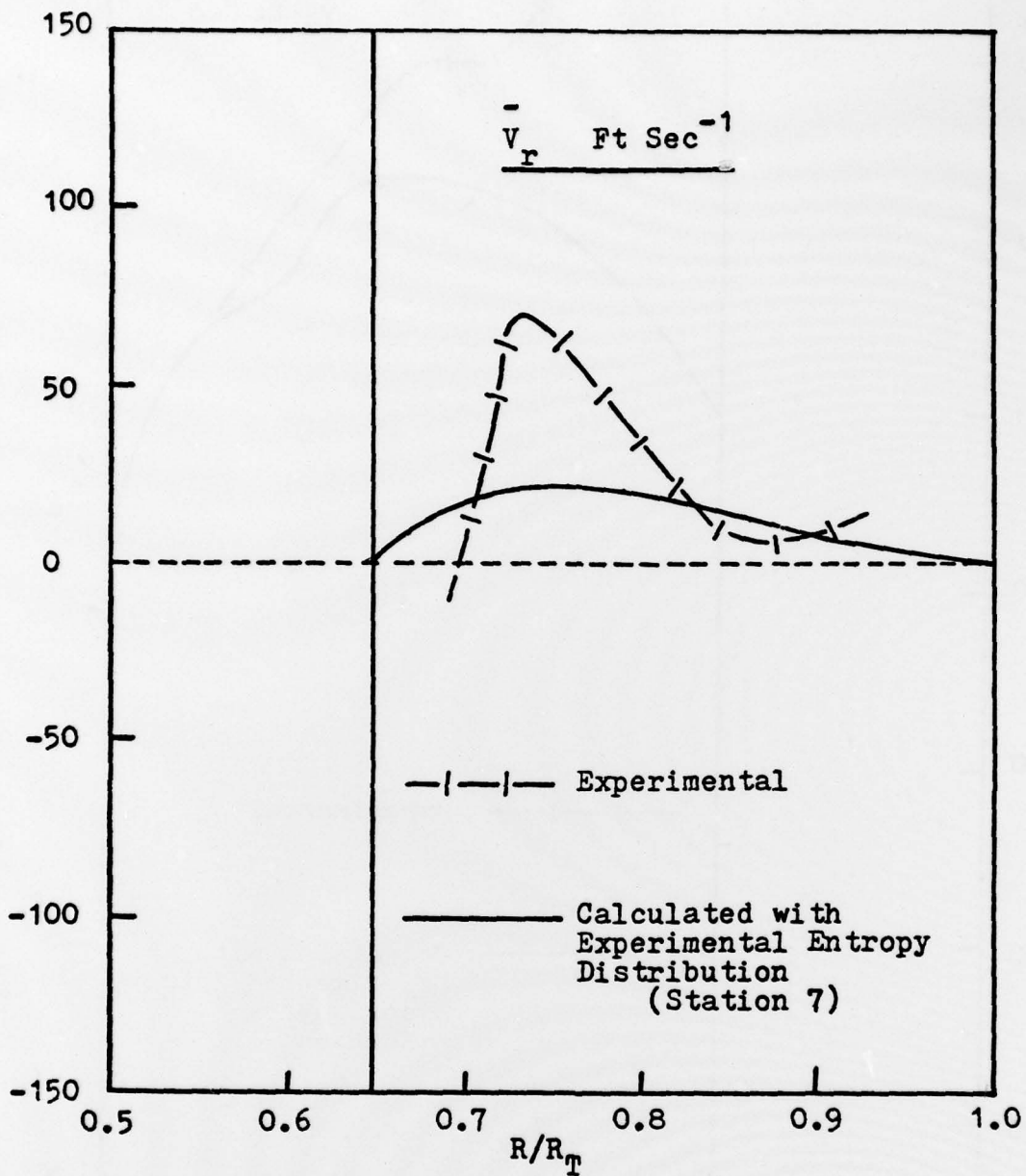


FIGURE 68. MEAN RADIAL VELOCITY, 1.0 CHORD
DOWNSTREAM OF THE ROTOR.